University of Ljubljana

Faculty of Electrical Engineering

Janja Dermol-Černe

Mathematical modelling of molecular transmembrane transport and changes of tissues' dielectric properties due to electroporation

DOCTORAL DISSERTATION

Advisor: Prof. Damijan Miklavčič, Ph.D.

Co-advisor: Prof. Gregor Serša, Ph.D.

Ljubljana, 2018

Univerza v Ljubljani

Fakulteta za elektrotehniko

Janja Dermol-Černe

Matematično modeliranje sprememb električnih lastnosti tkiv in transporta preko celične membrane pri elektroporaciji

DOKTORSKA DISERTACIJA

Mentor: prof. dr. Damijan Miklavčič

Somentor: prof. dr. Gregor Serša

Ljubljana, 2018

"Do. Or do not. There is no try."

Master Yoda

PREFACE

The present doctoral dissertation is a result of experimental work and numerical modeling related to electroporation of single cells, cell suspensions, and tissues. The work was carried out during the Ph.D. study period at the University of Ljubljana, Faculty of Electrical Engineering, Laboratory of Biocybernetics. The results of the research work are present in six papers, five of them published and one submitted to international scientific journals, and in one book chapter.

Paper 1   J. Dermol and D. Miklavčič, "**Predicting electroporation of cells in an inhomogeneous electric field based on mathematical modelling and experimental CHO-cell permeabilization to propidium iodide determination,**" *Bioelectrochemistry*, vol. 100, pp. 52–61, Dec. 2014.

Paper 2   J. Dermol and D. Miklavčič, "**Mathematical Models Describing Chinese Hamster Ovary Cell Death Due to Electroporation In Vitro,**" *Journal of Membrane Biology*, vol. 248, no. 5, pp. 865–881, Oct. 2015.

Paper 3   J. Dermol-Černe, D. Miklavčič, M. Reberšek, P. Mekuč, S.M. Bardet, R. Burke, D. Arnaud-Cormos, P. Leveque, and R. O'Connor, "**Plasma membrane depolarization and permeabilization due to electric pulses in cell lines of different excitability,**" *Bioelectrochemistry*, vol. 122, pp. 103–114, Aug. 2018 .

Paper 4   J. Dermol, O. N. Pakhomova, A. G. Pakhomov, and D. Miklavčič, "**Cell Electrosensitization Exists Only in Certain Electroporation Buffers,**" *PLOS ONE*, vol. 11, no. 7, p. e0159434, Jul. 2016.

Paper 5   J. Dermol-Černe and D. Miklavčič, "**From cell to tissue properties – modeling skin electroporation with pore and local transport region formation,**" *IEEE Transactions on Biomedical Engineering,* vol. 65, no. 2, pp. 458-468, Feb. 2018.

Paper 6   J. Dermol-Černe, J. Vidmar, J. Ščančar, K. Uršič, G. Serša, and D. Miklavčič, "**Connecting the in vitro and in vivo experiments in electrochemotherapy: Modeling cisplatin transport in mouse melanoma by the dual-porosity model,**" *Journal of Controlled Release*, submitted.

Book chapter: J. Dermol and D. Miklavčič, "**Mathematical Models Describing Cell Death Due to Electroporation,**" in *Handbook of Electroporation*, D. Miklavčič, Ed. Cham: Springer International Publishing, 2016, pp. 1–20.

Acknowledgments

I am deeply grateful to my mentor, Prof. Dr. Damijan Miklavčič for his guidance, his continuous support during my Ph. D. study, his patience, motivation, and immense knowledge. Thank you for giving me the option to work in the laboratory already as an undergraduate student, showing me first steps into the scientific world and giving me the opportunity to work on many interesting projects.

I would also like to thank my Co-Advisor, Prof. Dr. Gregor Serša for help with the in vivo experiments and interpretation of the data.

I would like to thank my colleagues, ex-colleagues, and collaborators of the Laboratory for Biocybernetics. I am thankful to Lea and Duša for teaching me how to work with cell cultures and their help with experiments in the cell culture laboratory. I would like to thank Tadeja, Matej R., Matej K., Bor, Lea R., Samo, Tadej, Barbara, Gorazd, Alenka, Dan, Vitalij, Olga, and Andrei for stimulating discussions and insightful comments.

I would like to thank Dr. Janja Vidmar, Dr. Janez Ščančar and members of the Jožef Stefan Institute, Department of environmental physics who measured the cisplatin samples with the inductively coupled plasma – mass spectrometry.

I would like to thank Katja Uršič and members of the Institute of Oncology Ljubljana, Department of Experimental Oncology, who performed the in vivo experiments of electrochemotherapy.

I would like to thank Dr. Rodney O'Connor and Dr. Sylvia Bardet Coste for showing a new universe of excitable cells and ion channels.

I would like to thank Mija Bernik for linguistic proofreading of the abstract in the Slovene language.

And last but not least. I am sincerely grateful to my family for always being there for me and showing me that knowledge is a precious thing and Matevž for his constant support and for reminding me that I can do it.

Table of Contents

Abstract

Electroporation is a phenomenon, which occurs when short high voltage pulses are applied to cells and tissues resulting in a transient increase in membrane permeability or cell death, presumably due to pore formation. If cells recover after pulse application, this is reversible electroporation. If cells die, this is irreversible electroporation. Electroporation is used in biotechnology for biocompound extraction and cryopreservation, in food processing for sterilization and pasteurization of liquid food and in medicine for treating tumors by electrochemotherapy or irreversible electroporation as an ablation technique, for gene electrotransfer, transdermal drug delivery, DNA vaccination, and cell fusion.

In electroporation-based medical treatments, we can treat tumors with predefined electrode geometry and parameters of electric pulses. When we treat larger tumors of irregular shape treatment plan of the position of the electrodes and parameters of the electric pulses has to be calculated before each treatment to assure coverage of the tumor with a sufficient electric field. In treatment plans, currently, 1) we assume that above an experimentally determined critical electric field all cells are affected and below not, although, in reality, the transition between non-electroporated and electroporated state is continuous. 2) We do not take into account the excitability of some tissues. 3) The increase in tissues' conductivity is described phenomenologically and does not include mechanisms of electroporation. 4) Transport of chemotherapeutics into the tumor cells in electrochemotherapy treatments is not included in the treatment plan although it is vital for a successful treatment. We focused on the mathematical and numerical models of electroporation with the aim of including them in the treatment planning of electroporation-based medical treatments.

We aimed to model processes happening during electroporation of tissues, relevant in the clinical procedures, by taking into account processes happening at the single cell level. First, we used mathematical models of cell membrane permeability and cell death which are phenomenological descriptions of experimental data. The models were chosen on the basis of the best fit with the experimental data. However, they did not include mechanisms of electroporation, and their transferability to tissues was questionable. We modeled time dynamics of dye uptake due to increased cell membrane permeability in several electroporation buffers with regard to the electrosensitization, i.e., delayed hypersensitivity to electric pulses caused by pretreating cells with electric pulses. We also modeled the strength-duration depolarization curve and cell membrane permeability curve of excitable and non-excitable cell lines which could be used to optimize pulse parameters to achieve maximal drug uptake at minimal tissue excitation.

Second, we modeled change in dielectric properties of tissues during electroporation. Model of change in dielectric properties of tissues was built for skin and validated with current-voltage measurements. Dielectric properties of separate layers of skin before electroporation were determined by taking into account geometric and dielectric properties of single cells, i.e., keratinocytes, corneocytes. Dielectric properties of separate layers during electroporation were obtained from cell-level models of pore formation on single cells of lower skin layers (keratinocytes in epidermis and lipid spheres in papillary dermis) and local transport region formation in the stratum corneum. Current-voltage measurements of long low-voltage pulses were accurately described taking into account local transport region formation, pore formation in the cells of lower layers and electrode polarization. Voltage measurements of short high-voltage pulses were also accurately described in a similar way

as with long low-voltage pulses; however, the model underestimated the current, probably due to electrochemical reactions taking place at the electrode-electrolyte interface.

Third, we modeled the transport of chemotherapeutics during electrochemotherapy in vivo. In electrochemotherapy treatments, transport of chemotherapeutics in sufficient amounts into the cell is vital for a successful treatment. We performed experiments in vitro and measured the intracellular platinum mass as a function of pulse number and electric field by inductively coupled plasma – mass spectrometry. Using the dual-porosity model, we calculated the in vitro permeability coefficient as a function of electric field and number of applied pulses. The in vitro determined permeability coefficient was then used in the numerical model of mouse melanoma tumor to describe the transport of cisplatin to the tumor cells. We took into account the differences in the transport of cisplatin in vitro and in vivo caused by the decreased mobility of molecules and decreased membrane area available for the uptake in vivo due to the high volume fraction of cells, the presence of cell matrix and close cell connections. Our model accurately described the experimental results obtained in electrochemotherapy of tumors and could be used to predict the efficiency of electrochemotherapy in vitro thus reducing the number of needed animal experiments.

In the thesis, we connected the models at the cell level to the models at the tissue level with respect to cell membrane permeability and depolarization, cell death, change in dielectric properties and transport. Our models offer a step forward in modeling and understanding electroporation at the tissue level. In future, our models could be used to improve treatment planning of electroporation-based medical treatments.

Razširjen povzetek v slovenskem jeziku

Uvod

Elektroporacija

Visokonapetostni električni pulzi povečajo prepustnost celične membrane (Tsong 1991; Weaver 1993; Kotnik et al. 2012) skozi pore (Abidor et al. 1979), ki nastanejo na tistih njenih delih, kjer vsiljena transmembranska napetost preseže kritično vrednost (Towhidi et al. 2008; Kotnik et al. 2010). Elektroporacija je reverzibilna, če si celica po pulzih opomore, in ireverzibilna, če je škoda preobsežna in celica odmre (Pakhomova et al. 2013b; Jiang et al. 2015a). Trenutne optične metode por ne morejo zaznati, zato njihov nastanek zaznavamo posredno, bodisi z meritvami vnosa različnih molekul v celice ali z meritvami električnih lastnosti celic (Napotnik in Miklavčič 2017).

Uporaba elektroporacije

V živilski industriji (Toepfl 2012; Toepfl et al. 2014) uporabljamo elektroporacijo oziroma pulzirajoča električna polja (*angl*. pulsed electric fields), kar je uveljavljen izraz v tej industriji, za uničevanje patogenih organizmov in njihovih produktov (encimov in toksinov). V nasprotju s termično obdelavo hrane električni pulzi ne vplivajo na okus, barvo ali hranilno vrednost. V biotehnologiji uporabljamo elektroporacijo za ekstrakcijo molekul iz mikroorganizmov in rastlin, s čimer se izognemo uporabi kemičnih sredstev in ne uničimo celičnih organelov, torej se izognemo tudi dodatnemu čiščenju končnega produkta (Sack et al. 2010; Haberl et al. 2013a; Mahnič-Kalamiza et al. 2014b; Kotnik et al. 2015). Primeri: ekstrakcija DNK iz bakterij; sladkorja iz sladkorne pese (Haberl et al. 2013b), sokov iz sadja; polifenolov iz grozdja za izboljšanje kvalitete vina (Puértolas et al. 2010); vode pri sušenju zelene biomase, ki služi kot vir za biogorivo (Golberg et al. 2016). Elektroporacija je tudi nova metoda pri zamrzovanju celic in tkiv, *angl*. cryopreservation (Galindo in Dymek 2016; Dovgan et al. 2017).

Elektroporacijo uporabljamo tudi v medicini (Miklavčič et al. 2010; Yarmush et al. 2014), in sicer pri elektrokemoterapiji (Miklavčič et al. 2012; Mali et al. 2013; Cadossi et al. 2014; Miklavčič et al. 2014; Campana et al. 2014; Serša et al. 2015), netermičnem odstranjevanju tkiva z ireverzibilno elektroporacijo (Davalos et al. 2005; Garcia et al. 2010; José et al. 2012; Cannon et al. 2013; Scheffer et al. 2014b; Jiang et al. 2015a; Rossmeisl et al. 2015), genski terapiji (Golzio et al. 2002; Vasan et al. 2011; Gothelf in Gehl 2012; Calvet et al. 2014; Heller in Heller 2015; Trimble et al. 2015) in vnosu učinkovin v kožo in skoznjo (Denet et al. 2004; Zorec et al. 2013b). Pri genski terapiji vnesemo v celice plazmide, v katerih je zapisana sinteza določenega proteina, ki lahko spremeni biološko funkcijo celice (Aihara in Miyazaki 1998; Heller in Heller 2015). Z elektroporacijo povišamo varnost genske terapije, saj se izognemo uporabi virusov in kemikalij. Mehanizmi genske terapije z elektroporacijo še niso popolnoma pojasnjeni, osnovni koraki so opisani v literaturi (Rosazza et al. 2016). Z elektroporacijo lahko zlivamo različne celice, s čimer pridobivamo celice, ki proizvajajo monoklonska protitelesa ali inzulin (Ramos in Teissié 2000; Trontelj et al. 2008; Rems et al. 2013).

V doktorski disertaciji sem se osredotočila na uporabo elektroporacije v medicini, predvsem pri elektrokemoterapiji, netermičnem odstranjevanju tkiva z ireverzibilno elektroporacijo in pri vnosu učinkovin v kožo in skoznjo je, zato so ti trije posegi podrobneje opisani v naslednjem poglavju.

Medicinski posegi z elektroporacijo – elektrokemoterapija, netermično odstranjevanje tkiva z ireverzibilno elektroporacijo in vnos učinkovin v kožo in skoznjo

Elektrokemoterapija je kombinacija kemoterapije in električnih pulzov, dovedenih neposredno na tarčno tkivo. Električni pulzi povečajo prepustnost celične membrane za kemoterapevtike, zato povečamo učinkovitost zdravljenja, obenem pa zmanjšamo dovedeno dozo kemoterapevtika in omilimo stranske učinke. Celoten tumor mora biti pokrit z dovolj visokim električnim poljem, da povečamo prepustnost vseh tumorskih celic (Miklavčič et al. 2006a), zagotoviti pa moramo tudi dovolj visoko koncentracijo kemoterapevtika znotraj tumorja (Miklavčič et al. 2014). Okoliško tkivo ne sme biti uničeno, torej mora biti električno polje okoli tumorja pod mejo za ireverzibilno elektroporacijo. Pri elektrokemoterapiji običajno dovajamo osem pulzov dolžine 100 μs s ponavljalno frekvenco 1 Hz. S poskusi določena meja za povišanje prepustnosti tumorskega tkiva je 0,4 kV/cm (Miklavčič et al. 2010). Osem pulzov je bilo določenih kot optimalno število pulzov (Marty et al. 2006; Mir et al. 2006), večje število dovedenih pulzov namreč že zmanjšuje preživetje (Dermol in Miklavčič 2015). Za zdravljenje tumorjev z elektrokemoterapijo so bili definirani standardni postopki (*angl.* standard operating procedures) (Marty et al. 2006; Mir et al. 2006), kjer so glede na število tumorjev, njihovo velikost in lokacijo (na koži ali pod kožo) določeni tip elektrod, kemoterapevtik, anestezija in način dovajanja kemoterapevtika. Kemoterapevtik lahko dovedemo lokalno ali sistemsko. V elektrokemoterapiji oz. terapiji z električnimi pulzi sta najbolj razširjena kemoterapevtika cisplatin in bleomicin. Z elektrokemoterapijo je možno zdraviti tudi globlje ležeče tumorje (Miklavčič et al. 2010; Pavliha et al. 2013; Edhemović et al. 2014; Miklavčič in Davalos 2015). V zadnjem času se uveljavlja tudi uničevanje tumorskih celic z visokimi koncentracijami kalcija in električnimi pulzi (Frandsen et al. 2015; Frandsen et al. 2016; Frandsen et al. 2017). Pri elektrokemoterapiji se pojavijo še dodatni učinki, ki povišajo učinkovitost elektroporacije. Vazokonstrikcija zmanjša spiranje kemoterapevtika iz tumorja in s tem ohranja visoko koncentracijo kemoterapevtika v tumorju, obenem se zmanjša pretok krvi skozi tumor, kar povzroči hipoksijo in pomanjkanje hranilnih snovi (Mir 2006; Serša et al. 2008). Elektrokemoterapija sproži tudi odziv imunskega sistema, ki nato odstrani preostale tumorske celice (Serša et al. 2015).

Z ireverzibilno elektroporacijo netermično odstranjujemo tumorje brez uporabe kemoterapevtika (Jiang et al. 2015a). Tako se popolnoma izognemo stranskim učinkom kemoterapevtikov, vendar na račun več dovedene energije in posledično Joulovega gretja. Pri ireverzibilni elektroporaciji dovajamo več (okoli 90) električnih pulzov, dolgih od 50 μs do 100 μs, s ponavljalno frekvenco 1 Hz. Dovedeno električno polje je v rangu nekaj kV/cm, kar je dosti več kot pri elektrokemoterapiji. Pri ireverzibilni elektroporaciji lahko z visoko natančnostjo odstranimo želeno tkivo – območje med uničenim in nepoškodovanim tkivom je široko le nekaj premerov celic (Rubinsky et al. 2007). Za odstranjevanje tumorjev tradicionalno uporabljamo termične metode (Hall et al. 2014) – radiofrekvenčno odstranjevanje in odstranjevanje s tekočim dušikom, kjer tkivo uničujemo z visoko oz. z nizko temperaturo. Prednost ireverzibilne elektroporacije pred uveljavljenimi termičnimi metodami je krajši čas zdravljenja, izognemo se učinkom hlajenja oz. gretja tkiva

zaradi bližine žil (Golberg et al. 2015), pri čemer ostanejo okoliške pomembne strukture (žile, živci) nedotaknjene (Jiang et al. 2015a). Tudi pri ireverzibilni elektroporaciji je v dokončno odstranitev tumorskih celic vpleten imunski sistem (Neal et al. 2013).

Pri elektrokemoterapiji in ireverzibilni elektroporaciji se zaradi daljših pulzov in ponavljalne frekvence 1 Hz pojavljajo težave zaradi krčenja mišic (Miklavčič et al. 2005), bolečine med dovajanjem pulzov, heterogenosti električnih lastnosti tkiv v tem frekvenčnem področju ter zaradi možnosti srčnih aritmij (Ball et al. 2010). Bolečini in krčenju mišic se lahko izognemo, če pulze dovajamo z višjo frekvenco, npr. 5 kHz (Županič et al. 2007; Serša et al. 2010). Srčnim aritmijam se izognemo tako, da s sinhroniziramo dovedene električne pulze z električno aktivnostjo srčne mišice (Mali et al. 2008; Deodhar et al. 2011a; Mali et al. 2015). Bolečini, krčenju mišic in heterogenosti električnih lastnosti tkiv se lahko izognemo z dovajanjem 1 μs bipolarnih pulzov (Arena et al. 2011; Arena in Davalos 2012; Sano et al. 2015). V zadnjem času so se pojavile tudi metode, s katerimi so vnos barvil v celico dosegli brezkontaktno s t. i. magnetoporacijo (Chen et al. 2010; Towhidi et al. 2012; Kardos in Rabussay 2012; Novickij et al. 2015; Kranjc et al. 2016; Novickij et al. 2017b; Novickij et al. 2017a).

Elektroporacijo lahko uporabljamo ne le za zdravljenje tumorjev, temveč tudi za vnos učinkovin v kožo in skoznjo. Vnos učinkovin skozi kožo je neinvaziven, poleg tega pa se izognemo degradaciji učinkovin pri prehodu skozi prebavni trakt. Skozi kožo lahko preide le malo molekul, zato uporabljamo različne metode za povečanje prehoda učinkovin – iontoforezo, radiofrekvenčno mikroablacijo, laser, mikroigle, ultrazvok in elektroporacijo (Zorec et al. 2013b). Proces elektroporacije kože je slabo razumljen. Predpostavljamo, da pri dovajanju visokonapetostnih električnih pulzov v roženi plasti nastanejo lokalna transportna območja, kjer sta povišani električna prevodnost in prepustnost (Pliquett et al. 1996; Pliquett et al. 1998; Pliquett et al. 1998; Pavšelj in Miklavčič 2008a). Skozi lokalna transportna območja lahko nato učinkovine še nekaj ur po dovedenih pulzih vstopajo skozi kožo v krvni obtok (Zorec et al. 2013a). Gostota teh območij je odvisna od električnega polja v koži – višje električno polje jih povzroči več. Velikost lokalnih transportnih območij je odvisna od trajanja pulza. Med samim pulzom se zaradi Joulovega gretja topijo lipidi v roženi plasti, kar povzroči njihovo širjenje (Pliquett et al. 1996; Prausnitz et al. 1996; Pliquett et al. 1998; Weaver et al. 1999; Vanbever et al. 1999; Gowrishankar et al. 1999b).

Načrtovanje posegov elektrokemoterapije in netermičnega odstranjevanja tkiva z ireverzibilno elektroporacijo

Pri zdravljenju tumorjev z elektroporacijo lahko uporabimo standardne oblike in postavitve elektrod z že določenimi parametri električnih pulzov (Marty et al. 2006; Mir et al. 2006; Campana et al. 2014). Če zdravimo velike tumorje ali tumorje nepravilnih oblik, ki pogosto ležijo globlje, s standardno postavitvijo elektrod ne moremo zagotoviti ustrezne pokritosti tumorja z dovolj visokim električnim poljem. V tem primeru lahko elektrode med samim posegom večkrat premaknemo ali pa prilagodimo njihovo število in postavitev. Pri tem moramo prej pripraviti načrt posega (Kos et al. 2010; Miklavčič et al. 2010; Pavliha et al. 2012; Linnert et al. 2012; Edhemović et al. 2014). V njem zagotovimo, da bo cel tumor izpostavljen dovolj visokemu električnemu polju (Miklavčič et al. 2006a), obenem pa škoda na okoliškem tkivu minimalna.

Načrtovanje posega poteka v več korakih: 1. zajem medicinskih slik (računalniška tomografija, magnetna resonanca) tumorja in okoliškega tkiva; 2. obdelava slik; 3. razgradnja slik in določitev geometrije tkiva; 4. vzpostavitev tridimenzionalnega modela; 5. optimizacija postavitve elektrod glede na obliko in velikost tumorja; 6. izdelava modela elektroporacije (izračun električnega polja in spremembe električne prevodnosti tkiva); 7. optimizacija napetosti med elektrodami in položaja elektrod (Pavliha et al. 2012). Na sliki 1 lahko vidimo izračunano električno polje v tumorju in okoliškem tkivu pri eni izmed možnih postavitev elektrod.

Med načrtovanjem posega privzamemo naslednje predpostavke.

1.   Pri določanju elektroporiranega in neelektroporiranega območja uporabljamo s poskusi določeno vrednost kritičnega električnega polja (Miklavčič et al. 2000; Šel et al. 2005; Čorović et al. 2012). Za vsako tkivo privzamemo dve kritični vrednosti električnega polja – eno za reverzibilno in drugo za ireverzibilno elektroporacijo. Predpostavljamo, da so celične membrane vseh celic, ki so izpostavljene električnemu polju pod kritično vrednostjo za reverzibilno elektroporacijo, neprepustne. Vse celice, ki so izpostavljene električnemu polju nad kritično vrednostjo za reverzibilno elektroporacijo, imajo prepustne membrane. Tiste, ki so izpostavljene električnemu polju nad kritično vrednostjo za ireverzibilno elektroporacijo, pa so mrtve. Vendar v resnici kritično električne polje za elektroporacijo ni enako za vse celice v tkivu, temveč je statistično porazdeljeno. Če pri načrtovanju posegov predpostavljamo, da imajo vse celice enak prag za reverzibilno in ireverzibilno elektroporacijo, je lahko tumor izpostavljen prenizkemu električnemu polju in tumorske celice preživijo. Če tkivo izpostavimo previsokemu električnemu polju, lahko poškodujemo pomembne bližnje strukture.

2.   Z elektroporacijo lahko vplivamo tudi na vzdražna tkiva, kot so nevroni in mišice. Zdravimo jih pri netermičnem odstranjevanju tumorjev v možganih z ireverzibilno elektroporacijo (Garcia et al. 2012; Rossmeisl et al. 2015; Sharabi et al. 2016), pri genski terapiji (Hargrave et al. 2013; Hargrave et al. 2014; Bulysheva et al. 2016) ali netermičnem odstranjevanju tkiva srčne mišice z ireverzibilno elektroporacijo (Neven et al. 2014b; Neven et al. 2014a) in pri genski terapiji skeletnih mišic (Aihara in Miyazaki 1998). Lahko pa vzdražna tkiva električnemu polju izpostavimo nenamerno, ko so v bližini tarčnega območja. Vplivamo na živčno-žilni snop pri zdravljenju raka na prostati (Neal et al. 2014; Ting et al. 2016), na nevrone pri zdravljenju kostnih metastaz (Tschon et al. 2015; Gasbarrini et al. 2015) ali na hrbtenjačo pri zdravljenju tumorjev v hrbtenici (Tschon et al. 2015). Električna stimulacija živcev in mišic povzroči nelagodje in bolečino (Miklavčič et al. 2005; Županič et al. 2007; Arena in Davalos 2012; Golberg in Rubinsky 2012). Pokazali so, da lahko električni pulzi povzročijo stimulacijo receptorjev za bolečino (nociceptorjev) (Nene et al. 2006; Jiang in Cooper 2011). Pomemben napredek pri zdravljenju vzdražnih tkiv ali tkiv v njihovi bližini bi bila določitev optimalnih parametrov električnega polja, kjer dosežemo najvišjo prepustnost celične membrane, obenem pa ne vzdražimo tkiva.

3.   Elektroporacija poviša električno prevodnost tkiva zaradi povišane električne prevodnosti celičnih membran in zaradi Joulovega gretja (Šel et al. 2005; Ivorra et al. 2009; Essone Mezeme et al. 2012a; Neal et al. 2012). Spremenjena električna prevodnost vpliva na porazdelitev električnega polja (Šel et al. 2005). Pri načrtovanju posegov predpostavljamo, da se prevodnost tkiva poviša za približno štirikrat (Neal et al. 2012). Tkiva imajo različne električne lastnosti, ki se spremenijo in vplivajo na porazdelitev električnega

polja. Vrednosti električnih lastnosti tkiv po elektroporaciji lahko izračunamo z ekvivalentnim vezjem (Neal et al. 2012), lahko pa bi v izračune vključili tudi mehanizme elektroporacije.

4. Pri elektrokemoterapiji je za učinkovitost zdravljenja najpomembnejši zadosten vnos kemoterapevtika v celice (Miklavčič et al. 2014). Pri nizki znotrajcelični koncentraciji kemoterapevtika bleomicina pride do mitotske smrti, pri visoki pa do procesa, podobnega apoptozi (programirani celični smrti) (Tounekti et al. 1993; Tounekti et al. 2001). V načrtovanju zdravljenja predpostavljamo, da je električno polje nad kritično vrednostjo za reverzibilno elektroporacijo tkiva dovolj za zadosten vnos kemoterapevtika v celice. Lahko se zgodi, da kemoterapevtika kljub dovolj visokemu električnemu polju v celice ne pride dovolj, če je njegova začetna prostorska porazdelitev v tumorju nehomogena in ga v zunajceličnem prostoru zmanjka.
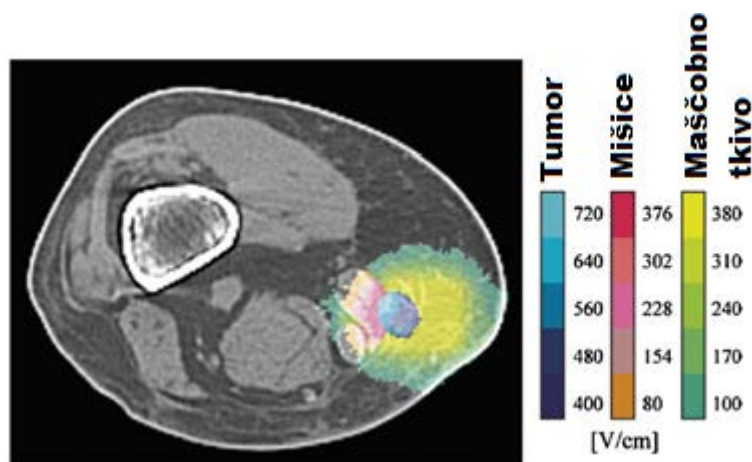
Slika 1: Primer izračunanega električnega polja v različnih tkivih (tumorju, mišicah, maščobnem tkivu) pri zdravljenju tumorja z elektroporacijo. Tumor je označen z modro barvo in je cel izpostavljen električnemu polju nad kritično vrednostjo za reverzibilno elektroporacijo. Povzeto po (Županič et al. 2012).

Električne lastnosti celic in tkiv

Elektroporacija poveča električno prevodnost celične membrane, kar so merili v več raziskavah z dielektrično impedančno spektroskopijo (Abidor et al. 1993; Schmeer et al. 2004), s tokovnonapetostnimi meritvami (Pliquett in Wunderlich 1983; Pavlin et al. 2005; Pavlin in Miklavčič 2008; Suzuki et al. 2011), z optičnimi metodami (Hibino et al. 1991; Griese et al. 2002) ali z metodo vpete krpice, *angl*. patch clamp (Pakhomov et al. 2007; Wegner 2015; Yoon et al. 2016; Napotnik in Miklavčič 2017). Zaradi elektroporacije se poveča tudi električna prevodnost sloja celic (Ghosh et al. 1993; Müller et al. 2003; Stolwijk et al. 2011; García-Sánchez et al. 2015). Elektroporacija spremeni električne lastnosti človeških, živalskih in rastlinskih tkiv, kar lahko merimo s podobnimi metodami kot pri celicah – z dielektrično impedančno spektroskopijo (Barnes in Greenebaum 2006; Ivorra in Rubinsky 2007; Grimnes in Martinsen 2008; Dean et al. 2008; Zhuang et al. 2012; Dymek et al. 2014; Trainito et al. 2015; Zhuang in Kolb 2015), s tokovnonapetostnimi meritvami (Pavlin et al. 2005; Cukjati et al. 2007; Ivorra in Rubinsky 2007; Pavlin in Miklavčič 2008; Ivorra et al. 2009; Chalermchat et al. 2010; Neal et al. 2012; Becker et al. 2014; Dymek et al. 2015), z električno impedančno tomografijo (Davalos et al. 2002; Davalos et al. 2004; Granot in Rubinsky 2007; Meir in Rubinsky 2014) ali z magnetno resonančno električno impedančno tomografijo (Kranjc et al. 2014; Kranjc et al. 2015; Kranjc et al. 2017). Elektroporacija spremeni specifično prevodnost

tkiva predvsem v območju β-disperzije (Pliquett et al. 1995; Ivorra in Rubinsky 2007; Garner et al. 2007; Oblak et al. 2007; Ivorra et al. 2009; Neal et al. 2012; Zhuang et al. 2012; Salimi et al. 2013). Ta nastane zaradi polarizacije celične membrane, na katero elektroporacija najbolj vpliva zaradi por v njej in posledično povečane prevodnosti. Iz spremembe elektičnih lastnosti tkiv lahko sklepamo na odziv tkiva na zdravljenje (Cukjati et al. 2007; Ivorra et al. 2009; Neal et al. 2012). Pri meritvah električnih lastnosti po elektroporaciji moramo biti pozorni na sekundarne učinke elektroporacije, ki lahko vplivajo na rezultate meritev: spremembo velikosti celic (Serša et al. 2008; Sano et al. 2010; Deodhar et al. 2011b; Calmels et al. 2012), nastanek edema (Ivorra et al. 2009), izpust ionov iz celic (Pavlin et al. 2005) in vaskularno okluzijo (Ivorra in Rubinsky 2007; Serša et al. 2008).

Specifična prevodnost tkiv s frekvenco narašča, dielektričnost pa pada. Obe lahko razdelimo na več značilnih disperzijskih območij (Pethig 1984; Pethig in Kell 1987; Gabriel et al. 1996a; Miklavčič et al. 2006b; Barnes in Greenebaum 2006; Grimnes in Martinsen 2008), kar lahko vidimo na sliki 2. Pri nizkih frekvencah (pod 100 kHz) je prisotna α disperzija zaradi interakcij v bližini celične membrane, znotrajceličnih struktur, ionske difuzije in polarizacije elektrod. β disperzija je prisotna v območju megahertzov in nastane zaradi polarizacije celičnih membran in odzivov proteinov. γ disperzija nastane nad 1 GHz zaradi dipolarnih mehanizmov v polarnih medijih, kot je voda. Obstaja tudi manjša δ disperzija pri nekaj 100 MHz, ki nastane zaradi sprostitve vezane vode in manjših polarnih delov bioloških molekul ter zaradi ionske difuzije ob nabiti površini (Barnes in Greenebaum 2006). Električne lastnosti tkiv so prikazane na sliki 2, vendar so absolutne vrednosti različne od tkiva do tkiva (Gabriel et al. 1996a; Gabriel et al. 1996b; Gabriel et al. 1996c; Grimnes in Martinsen 2008). Obenem so lahko tkiva tudi anizotropna, kar pomeni, da je tkivo različno električno prevodno v različne smeri. Tipičen primer anizotropnega tkiva so mišice (Čorović et al. 2010).
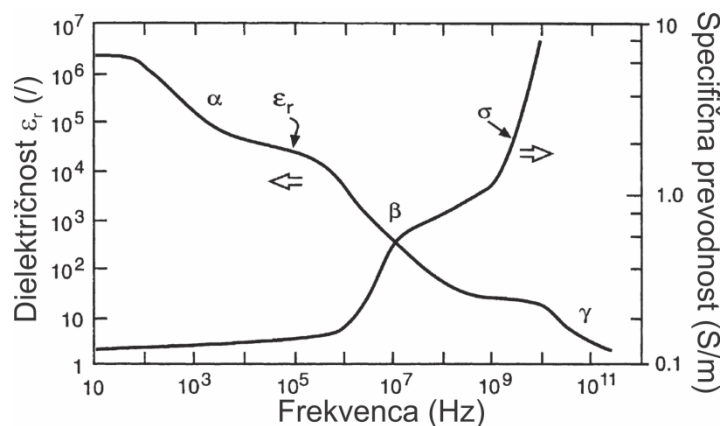
Slika 2: *Frekvenčna odvisnost električne prevodnosti (σ) in relativne dielektričnosti (ε_r). Vidimo lahko, da dielektričnost s frekvenco pada, specifična prevodnost pa narašča. Povzeto po (Miklavčič et al. 2006b).*

Transport majhnih molekul v celice in v tkivo

Transport molekul skozi celično membrano zaradi elektroporacije je posledica treh različnih mehanizmov – difuzije, elektroforeze in endocitoze. Med samimi pulzi je transport elektroforetski in difuzijski (Li in Lin 2011; Sadik et al. 2013), po pulzih pa predvsem difuzijski (Pucihar et al. 2008). Endocitozo so opazili po dovajanju daljših pulzov pri nižjih električnih poljih (Rols et al. 1995; Antov et al. 2005).

In vitro lahko transport določamo z različnimi tehnikami (Napotnik in Miklavčič 2017), kot so fluorescentna mikroskopija, pretočna citometrija, vnos citotoksičnih molekul (Maček Lebar in Miklavčič 2001), vnos plazmidov (Golzio et al. 2002), vnos magnetnih nanodelcev, masna spektrometrija (Čemažar et al. 2001) ali barvanje z barvili. Pri tehnikah in vivo je merjenje transporta zahtevnejše, saj je treba tkivo pred analizo večinoma izrezati in razgraditi. Uporabljamo metode, kot so radioaktivno označevanje z molekulami [57]Co-bleomicin (Belehradek et al. 1994), ^{111}In-bleomicin (Engström et al. 1998), ^{99m}Tc-DTPA (Grafström et al. 2006), ^{51}Cr-EDTA (Batiuškaitė et al. 2003), magnetna resonanca z gadolinijem (Garcia et al. 2012; Kranjc et al. 2015), masna spektrometrija (Melvik et al. 1986; Čemažar et al. 1998; Čemažar et al. 1999; Ogihara in Yamaguchi 2000; Čemažar et al. 2001; Serša et al. 2010; Hudej et al. 2014; Čemažar et al. 2015) in barvanje z barvilom lucifer rumeno (Kranjc et al. 2015).

Pri elektrokemoterapiji je transport ključen za učinkovitost zdravljenja (Miklavčič et al. 2014). Primerjava transporta in vitro ter in vivo je težavna. Celice v celični suspenziji so obdane s topljencem, ki lahko vanje vstopi z vseh strani. Transport poteka večinoma z difuzijo. Če je topljenca dovolj, se transport ustavi, ko je membrana zaceljena. Difuzija po zunajcelični tekočini ni omejena in transport topljenca skozi celično membrano lahko neposredno povežemo z njeno prepustnostjo (Mahnič-Kalamiza et al. 2014a). In vivo je začetna koncentracija topljenca prostorsko nehomogena, celice imajo na voljo različno začetno koncentracijo topljenca, ki ga lahko zmanjka, še preden je membrana zaceljena. Transport topljenca z difuzijo in konvekcijo (Canatella et al. 2004; Pucihar et al. 2008) poteka z določeno časovno konstanto. Električni pulzi povzročijo vazokonstrikcijo (Serša et al. 2008), ki omeji izpiranje in pritok topljenca. Tesen stik med celicami zmanjšuje površino membrane, skozi katero lahko poteka transport. Zunajcelični matriks ovira transport topljenca. Že pri elektroporaciji sferoidov (preprost približek tkiva) v fluorescentnem barvilu so ugotovili, da je transport majhnih molekul po sferoidu nehomogen – najvišji vnos so dosegli na robu sferoida, nato pa se je zmanjševal proti njegovemu središču (Canatella et al. 2004; Gibot et al. 2013). Vazokonstrikcija po električnih pulzih zmanjša pretok krvi v tumor in iz njega, kar podaljša izpostavljenost kemoterapevtiku. V tumorju je transport še dodatno otežen zaradi povišanega intersticijskega tlaka, heterogene prekrvavitve, vezave aktivnih molekul na netarčne molekule v tumorju, okvarjenega limfnega sistema in metabolizma (Baxter in Jain 1989; Baxter in Jain 1990; Baxter in Jain 1991; Jain 1999).

Modeliranje elektroporacije
Z uporabo matematičnih in fizikalnih zakonov pri modeliranju strnjeno opišemo biološke pojave ter omogočimo razumevanje in napovedovanje odziva ter zmanjšamo število poskusov. Elektroporacijo modeliramo na različnih prostorskih ravneh: molekule lipidov, lipidni dvosloj, celice in tkiva. Trenutno so modeli večinoma omejeni na eno prostorsko raven, povezovalnih modelov med njimi pa je malo.

Modeli na ravni molekul
Osnovni gradniki celične membrane so fosfolipidi. Obnašanje lipidov in drugih molekul pod vplivom električnega polja lahko ugotavljamo s simulacijami molekularne dinamike (Tieleman 2006; Böckmann et al. 2008; Delemotte in Tarek 2012; Reigada 2014; Casciola et al. 2014; Kirsch in Böckmann 2015), ki so zaradi računske zahtevnosti časovno omejene nekaj 100 do 1000 nanosekund. Raziskave molekularne dinamike predvidevajo, da zaradi električnega polja v lipidnem dvosloju nastanejo hidrofobne pore, ki se

razvijejo v hidrofilne pore. Simulacije numerične dinamike so primerjali s poskusi. Ugotovili so, da lahko mala interferenčna RNA (siRNA) v nekaj nanosekundah prečka celično membrano (Breton et al. 2012).

Modeli na ravni lipidnih dvoslojev

V polarnem topilu, kot je voda, se lipidi spontano uredijo v lipidni dvosloj. Modele elektroporacije lipidnih dvoslojev lahko razdelimo v dve skupini (Chen et al. 2006a; Pavlin et al. 2008; Rems in Miklavčič 2014). V prvi so deterministični elektromehanski (hidrodinamični, elastični, hidroelastični, viskoelastični) modeli, kjer dvosloj obravnavamo kot elastično telo in ga opisujemo z zakoni elektrostatike. Druga skupina so stohastični modeli nastanka por. Temeljijo na energijskih enačbah (Abidor et al. 1979), združuje pa jih enačba Smoluchowskega, ki opiše nastanek in dinamiko razvoja por. Neu in Krassowska sta jo poenostavila in omogočila njen relativno preprost numerični izračun (Neu in Krassowska 1999; Neu in Neu 2009), vendar pa v njej predvidevata, da se velikost por med pulzom ne spreminja. Asimptotski model elektroporacije je torej primeren le za kratke nanosekundne pulze, pri daljših pulzih namreč že pride do širjenja por v celični membrani. Tudi širjenje por med elektroporacijo lahko modeliramo, a je računsko bolj zahtevno, ker za vsako poro posebej rešujemo diferencialno enačbo spremembe premera v vsaki časovni točki (Smith et al. 2004). Med energijske modele spada tudi model, ki nastanek por opiše s kinetično shemo prehajanja membrane (Neumann et al. 1998; Miklavčič in Towhidi 2010) med prepustnimi in neprepustnimi stanji (Böckmann et al. 2008). Transport majhnih molekul skozi poro lahko opišemo z elektrodifuzijsko enačbo (Granot in Rubinsky 2008; Li in Lin 2011; Smith in Weaver 2011; Movahed in Li 2012; Movahed in Li 2013). Pri primerjavi zveznih modelov elektroporacije lipidnih dvoslojev in modelov molekularne dinamike so ugotovili, da se rezultati obojih dobro ujemajo (Casciola et al. 2016; Rems et al. 2016).

Modeli na ravni posameznih celic

Lipidni dvosloj je skupaj z membranskimi proteini osnova za nastanek biološke celice. Biološka celica je v približku električno slabo prevodna membrana (dielektrik), ki je na obeh straneh obdana z elektrolitom (prevodnik). Na ravni celic obstajajo modeli različnih pojavov: vsiljene transmembranske napetosti, nastanka por, transporta, prepustnosti celične membrane, smrti, spremembe prevodnosti. Časovna in prostorska dinamika vsiljene transmembranske napetosti sta analitično rešljivi za preproste oblike osamljenih celic (Kotnik et al. 1998; Kotnik in Miklavčič 2000a; Kotnik in Miklavčič 2000b; Valič et al. 2003; Kotnik in Miklavčič 2006), v splošnem pa zahtevata numerični izračun (Pucihar et al. 2006). Ko je vsiljena transmembranska napetost znana, lahko opišemo nastanek por (Neu in Krassowska 1999; Smith et al. 2004; Neu in Neu 2009). Celice lahko modeliramo tudi z ekvivalentnim električnim vezjem (Pethig 1984; Gowrishankar in Weaver 2003). Smrt in prepustnost celic v suspenziji lahko opišemo s statističnimi modeli (Peleg 1995; Huang et al. 2012; Dermol 2014; Dermol in Miklavčič 2014; Dermol in Miklavčič 2015; Dermol in Miklavčič 2016). V literaturi se pojavljajo štirje modeli prepustnosti celične membrane – simetrična in asimetrična sigmoida, Gompertzova krivulja in hiperbolični tangens (Laird 1964; Puc et al. 2003; Essone Mezeme et al. 2012b; Dermol in Miklavčič 2014). Modelov celične smrti je več (Hülsheger in Niemann 1980; Hülsheger et al. 1981; Geeraerd et al. 2000; Peleg in Penchina 2000; Huang et al. 2012), večinoma izhajajo iz živilske industrije, kjer z njimi napovedujejo učinkovitost uničevanja patogenih organizmov v živilih z namenom pasterizacije in sterilizacije (Peleg 2006; Huang et al. 2012; Dermol in

Miklavčič 2016). Električno prevodnost in prepustnost celične membrane lahko modeliramo ločeno (Miklavčič in Towhidi 2010; Leguèbe et al. 2014). Transport molekul v posamezno celico lahko opišemo z elektrodifuzijsko enačbo skozi prepustno membrano (Zaharoff et al. 2008; Pucihar et al. 2008; Leguèbe et al. 2014; Blumrosen et al. 2016).

Modeli na ravni tkiv in skupkov celic

Skupek po obliki in funkciji podobnih celic tvori tkivo (Alberts et al. 2009). Modele tkiv delimo v dve skupini – tkivo jemljejo kot homogeno enoto (Šel et al. 2005; Čorović et al. 2007; Pavšelj et al. 2007; Pavšelj in Miklavčič 2008b; Golberg in Rubinsky 2010; Neal et al. 2012; Čorović et al. 2012; Garcia et al. 2014) ali pa vključujejo tudi mikrostrukturo tkiva (Gowrishankar in Weaver 2003; Stewart Jr. et al. 2005; Gowrishankar in Weaver 2006; Esser et al. 2007; Joshi et al. 2008; Esser et al. 2009; Essone Mezeme et al. 2012b; Dymek et al. 2015).

Modeli homogenega tkiva obravnavajo električno polje v odvisnosti od oblike in števila elektrod, parametrov električnih pulzov ter lastnosti tkiva in sprememb njegove prevodnosti (Šel et al. 2005; Čorović et al. 2007; Pavšelj et al. 2007; Pavšelj in Miklavčič 2008b). Za vsak tip tkiva privzamemo s poskusi določeno kritično vrednost električnega polja, kjer pride do povišane prepustnosti membrane ali do smrti (Šel et al. 2005; Čorović et al. 2012), kar uporabimo za optimizacijo parametrov električnega polja. Z matematičnimi modeli lahko napovemo verjetnost za povišano prepustnosti celične membrane ali celično smrt (Golberg in Rubinsky 2010; Garcia et al. 2014; Garcia et al. 2014; Sharabi et al. 2016; Kranjc et al. 2017). S fenomenološkimi modeli, ki temeljijo na različnih porazdelitvah relaksacijskih časov molekul v tkivu, opišemo frekvenčno odvisnost električnih lastnosti različnih tkiv (Debyev, Cole-Colejev, Cole-Davidsonov, Havriliak-Negamijev, Raicujev model (Barnes in Greenebaum 2006)).

Pri elektroporaciji kože modeli opisujejo električno polje ali transport v koži kot organu iz posameznih homogenih slojev (Chizmadzhev et al. 1998; Weaver et al. 1999; Becker in Kuznetsov 2007; Pavšelj et al. 2007; Pavšelj in Miklavčič 2008a; Becker 2012; Becker et al. 2014). Električne lastnosti slojev pred elektroporacijo in po njej so večinoma približki, obenem lahko več slojem pripišemo enake lastnosti (Pavšelj et al. 2007). Nekaj modelov vključuje tudi nastanek lokalnih transportnih območij (Becker in Kuznetsov 2007; Pavšelj in Miklavčič 2008a; Becker 2012), ampak so omejeni le na procese v roženi plasti in ne zajemajo elektroporacije celic v spodnjih slojih kože.

Transport snovi po tkivu (Becker in Kuznetsov 2013) lahko dobro opišemo s statističnimi modeli, ki pa ne vključujejo mehanizmov transporta (Canatella in Prausnitz 2001), s kinetično shemo elektroporacije (Neumann et al. 1998; Miklavčič in Towhidi 2010), s farmakološkim modelom (Puc et al. 2003; Agarwal et al. 2009), z elektrodifuzijsko enačbo ali z modelom dvojne poroznosti (Mahnič-Kalamiza et al. 2014a; Mahnič-Kalamiza et al. 2015). Model dvojne poroznosti temelji na difuzijski enačbi, povezuje nastanek por s prepustnostjo celične membrane in omogoča modeliranje transporta med več razdelki, npr. celicami, intersticijsko tekočino in sosednjimi tkivi. V ta model lahko vključimo termične procese (Mahnič-Kalamiza et al. 2017) ali pa ga povežemo z enačbami za stopnjo elektroporacije, spremembo električne prevodnosti tkiv in celjenje por (Boyd in Becker 2015; Argus et al. 2017) ter celostno opišemo proces elektroporacije in transporta.

Druga večja skupina modelov tkiv upošteva mikrostrukturo tkiv. Iz električnih lastnosti posameznih okroglih celic v nizkih prostorninskih deležih lahko izračunamo ekvivalentne lastnosti z enačbami mešanja, kjer upoštevamo električne lastnosti in prostorninske deleže celic (Asami 2002). Uporabimo enačbe Maxwell-Wagnerja, Hanaija, Böttcherja, Bruggemana, Looyenge (Pavlin in Miklavčič 2009). V dveh dimenzijah lahko presek tkiva vzorčimo s kartezijskimi transportnimi mrežami in s Kirchoffovimi zakoni izračunamo tok, napetost in električni naboj po celi mreži (Gowrishankar in Weaver 2003; Stewart ml. et al. 2005; Gowrishankar in Weaver 2006; Esser et al. 2007; Esser et al. 2009). Podobno metodo ekvivalentnega vezja so uporabili v literaturi (Ramos et al. 2003; Ramos 2005), kjer so najprej analizirali učinke elektroporacije na ravni celic, nato pa preko ekvivalentnih električnih lastnosti celic prešli na tkiva. V dveh dimenzijah odziv tkiva ponazorimo z modeliranjem celic z Voronojevim diagramom in izračunom vsiljene transmembranske napetosti znotraj vsakega poligona oz. celice (Joshi et al. 2008). Slabost zgornjih modelov je, da so v dveh dimenzijah, kjer je obnašanje celic drugačno kot v tridimenzionalnih pogojih in vivo. V tkivu so celice namreč gosto skupaj, so povezane, pride do zastiranja električnega polja in nižanja vsiljene transmembranske napetosti (Susil et al. 1998; Pucihar et al. 2007; Pavlin in Miklavčič 2009), prisotna sta krvni obtok in imunski sistem. Povezavo med celicami in tkivom lahko ponazorimo s tridimenzionalnimi numeričnimi modeli mrež okroglih celic (Pavlin et al. 2002; Ramos 2010). Simulacije so bile narejene za enako velike, popolnoma okrogle, pravilno razporejene in električno nepovezane celice, kar ni v skladu z dejanskimi razmerami v tkivu (Pucihar in Miklavčič 2009), obenem pa je bil največji prostorninski delež celic omejen na vrednosti, nižje od tistih v tkivih. Z numeričnim modeliranjem tridimenzionalnih okroglih različno velikih celic, naključno razporejenih po prostoru, lahko opišemo spremembo električne prevodnosti celične membrane in delež prepustnih celic (Essone Mezeme et al. 2012b). S tridimenzionalnim modelom skupka posameznih celic različnih oblik lahko opišemo obnašanje lista špinače pri elektroporaciji (Dymek et al. 2015). V literaturi (Huclova et al. 2010; Huclova et al. 2011; Huclova et al. 2012) so celice in tkivo tudi modelirali v treh dimenzijah, model pa je opisal celice različnih oblik, velikosti in prostorninskih deležev. Lastnosti posameznih celic so nato posplošili na tkiva. V okviru doktorske disertacije smo model nadgradili z elektroporacijo, ki je že v nelinearnem območju odziva celic (Dermol-Černe in Miklavčič 2018).

Namen

Namen doktorske disertacije lahko povzamemo v dveh točkah:

1. optimizacija (fenomenoloških) matematičnih modelov, ki opisujejo prepustnost celične membrane, depolarizacijo in celično smrt;
2. vključitev mehanizmov elektroporacije v modele sprememb električnih lastnosti tkiv in transporta v tkivih pri elektrokemoterapiji.

V prvi točki smo prilegali različne obstoječe matematične modele povišane prepustnosti celične membrane in celične smrti na rezultate poskusov in vitro. Najprej smo se osredotočili na vprašanje, ali lahko iz deleža celic s prepustnimi membranami v homogenem električnem polju napovemo delež celic s prepustnimi membranami v nehomogenem električnem polju. Modelirali smo časovno dinamiko vnosa barvila v celice in ovrednotili povezavo med celjenjem celične membrane in vnosom barvila. Nato smo prešli na modele celične smrti. Naredili smo pregled obstoječih modelov celične smrti, pri čemer večina izhaja iz živilske industrije. Obstoječe modele celične smrti smo nato prilegali na rezultate poskusov, ki smo jih pridobili pri ireverzibilni elektroporaciji celic. Primerjali smo prepustnost in depolarizacijo vzdražnih in nevzdražnih celic ter oba pojava modelirali.

V drugi točki smo se osredotočili na spremembe električnih lastnosti celic in tkiv ter povečanje vnosa snovi v celice. Modelirali smo spremembe električnih lastnosti kože pri elektroporaciji z dolgimi nizkonapetostnimi pulzi ali s kratkimi visokonapetostnimi pulzi. Ovrednotili smo prispevek nastanka in širjenja lokalnih transportnih območij v roženi plasti in nastanka por v membranah celic spodnjih plasti kože k povišanju električne prevodnosti kože. Preverili smo, ali lahko nastanek por na membranah celic v spodnjih plasteh kože izračunamo z asimptotskim modelom nastanka por in ali lahko nastanek lokalnih transportnih območij povežemo z obliko tokovnonapetostnih meritev. Modelirali smo transport cisplatina v podkožne tumorje na miših. Poskusi na živalih so zamudni, dragi, zaradi etičnih pomislekov pa lahko preizkusimo le omejeno število parametrov. Preverili smo, ali bi lahko rezultate poskusov in vitro uporabili za napoved odziva tkiv ter možnosti kasnejše uporabe pri načrtovanju posegov elektrokemoterapije. Ocenili smo, kako bližina celic, prisotnost celičnega matriksa in zmanjšana površina celične membrane, ki je na voljo za transport, vplivajo na vnos cisplatina v celice.

Rezultati in razprava

V tem podpoglavju so na kratko povzeti vsi rezultati, pridobljeni v okviru doktorske disertacije. Razdeljeni so skladno s tremi izvirnimi znanstvenimi prispevki: 1. Matematično modeliranje prepustnosti celične membrane in celične smrti; 2. Prehod modeliranja z nivoja ene same celice na nivo tkiv, pri čemer je predstavljen realističen tridimenzionalen model kože nadgrajen z modelom elektroporacije vseh sestavnih delov in bistvenih plasti in 3. Matematično modeliranje transporta molekul (kemoterapevtika) skozi celično membrano na osnovi modela dvojne poroznosti. O rezultatih tudi razpravljam, na kratko pa so pri vsakem prispevku opisane še metode.

Želimo si, da bi lahko celostno predstavili pojav elektroporacije ter z modeli opisali dogajanje na več ravneh (lipidni dvosloj, celice, tkiva) pri več procesih (spremembi električnih lastnost, transportu). Začeli smo z matematičnimi modeli prepustnosti celične membrane in celične smrti, časovne dinamike vnosa barvila v celice in intenzivnostno-časovne krivulje vzdražnih tkiv. Modeli so sicer dobro opisali rezultate, niso pa vključevali mehanizmov elektroporacije. Zato smo se namesto na fenomenološke modele osredotočili na vključevanje mehanizmov elektroporacije v modele tkiv pri spremembi njihovih električnih lastnosti ter pri transportu majhnih molekul v tkivu in skozi celične membrane po elektroporaciji.

Matematični modeli prepustnosti celične membrane, celične smrti in depolarizacije

V okviru doktorske disertacije smo se ukvarjali z matematičnimi modeli prepustnosti celične membrane (Dermol 2014; Dermol in Miklavčič 2014; Dermol et al. 2016), celične smrti (Dermol in Miklavčič 2015; Dermol in Miklavčič 2016) in depolarizacije (Dermol-Černe et al. 2018). V literaturi smo poiskali že obstoječe matematične modele in jih prilegali na rezultate poskusov.

Matematični modeli prepustnosti celične membrane

Povišanje prepustnosti celične membrane smo modelirali s štirimi različnimi modeli. Simetrična sigmoida (Puc et al. 2003) in hiperbolični tangens (Essone Mezeme et al. 2012b) sta bila v literaturi že uporabljena, na podlagi primerne sigmoidne oblike pa smo dodali asimetrično sigmoido in Gompertzovo krivuljo (Laird 1964; Dermol in Miklavčič 2014). Matematične modele prepustnosti celične membrane smo optimizirali in primerjali z rezultati poskusov. Poskuse smo izvajali na celični liniji CHO-K1 (jajčne celice samice kitajskega hrčka). Uporabili smo dva tipa elektrod – paralelne žične (slika 3a) pri poskusih v homogenem električnem polju in igelne (slika 3b) pri poskusih v nehomogenem električnem polju. Električno polje med paralelnimi žičnimi elektrodami smo v približku izračunali kot dovedeno napetost, deljeno z razdaljo med elektrodami (Sweeney et al. 2016), električno polje okoli igelnih elektrod pa smo izračunali numerično.

Pritrjene celice različnih gostot smo v rastnem mediju v prisotnosti fluorescentnega barvila propidijev jodid izpostavili enemu 1 ms pulzu pri različnih napetostih. Pet minut po dovedenih električnih pulzih smo rastni medij s propidijevim jodidom zamenjali z rastnim medijem brez propidijevega jodida, s tem zaustavili vnos barvila v celice in zajeli slike pod mikroskopom.
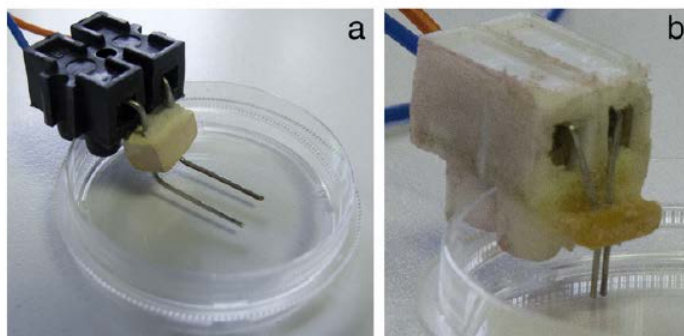
Slika 3: a) Paralelne žične elektrode, med katerimi je električno polje približno homogeno in b) igelne elektrode, okoli katerih smo električno polje izračunali numerično. Povzeto po (Dermol in Miklavčič 2014).

Najprej smo določili delež celic s prepustnimi membranami, izpostavljenih homogenemu električnemu polju. Na rezultate poskusov smo z metodo najmanjših kvadratov prilegali štiri matematične modele prepustnosti celične membrane v odvisnosti od električnega polja. Optimizirane modele smo vstavili v numerični model igelnih elektrod in z numerično izračunanim električnim poljem okoli igelnih elektrod določili deleže prepustnih celic v posameznih območjih (slika 4). Predvidene deleže prepustnih celic v posameznih območjih smo primerjali s preštetimi deleži. Ugotovili smo, da se mora za pravilno napoved deleža prepustnih celic gostota celic v nehomogenem in v homogenem električnem polju ujemati - gostota celic mora biti torej enaka v poskusih, na katerih model optimiziramo, in v poskusih, kjer odziv napovedujemo. Primer prostorsko odvisne verjetnosti za prepustnost celic okoli igelnih elektrod lahko vidimo na sliki 5. Matematične modele prepustnosti celične membrane bi torej lahko uporabili v načrtovanju posegov, kjer bi namesto električnega polja v tkivu predstavili verjetnost za prepustnost tkiva v odvisnosti od geometrije elektrod in parametrov električnih pulzov.
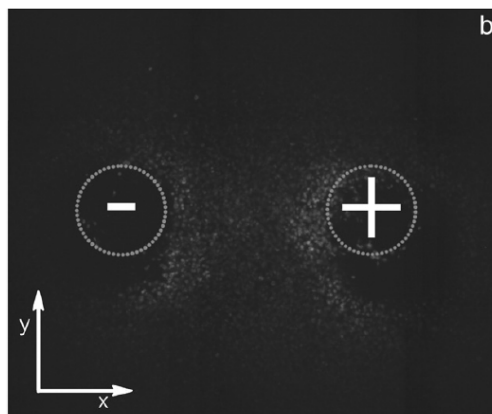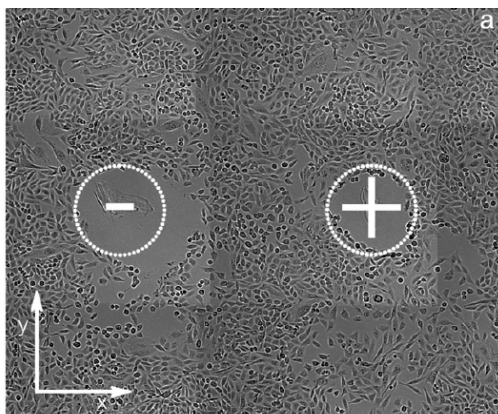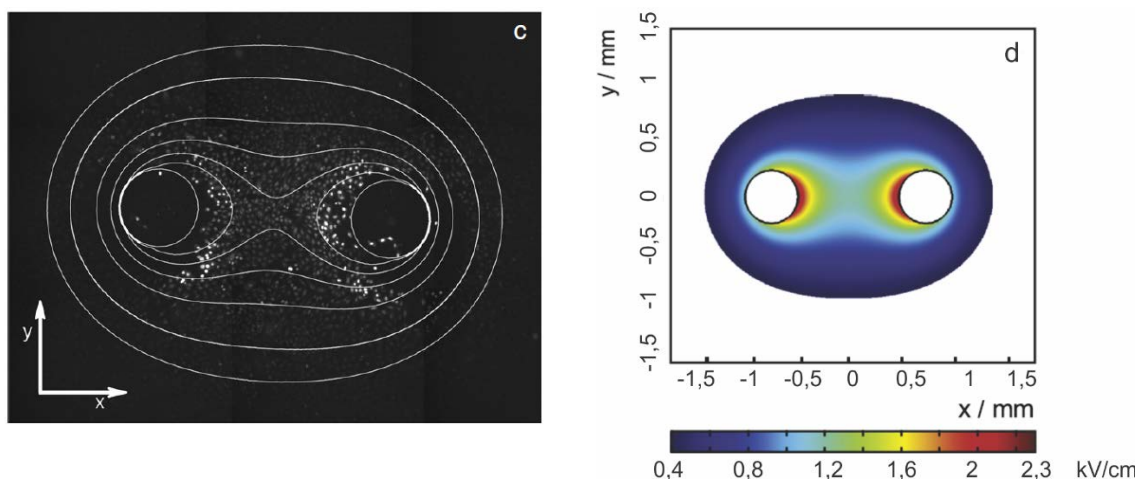
Slika 4: a) Fazno-kontrastna in b) fluorescentna slika območja okoli igelnih elektrod, kjer so bile celice izpostavljene nehomogenemu električnemu polju. Območje okoli elektrod smo primerjali z c in d) numerično izračunanim električnim poljem in določili število prepustnih celic znotraj določenih območij električnega polja. Povzeto po (Dermol in Miklavčič 2014).
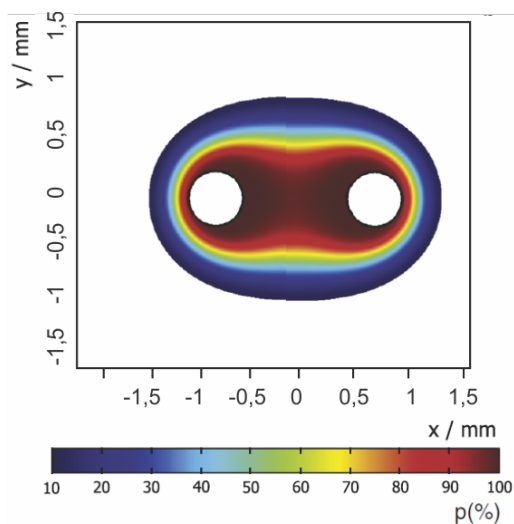
Slika 5: Verjetnost za prepustnost (p) okoli igelnih elektrod pri izpostavitvi celice enemu 1 ms pulzu pri napetosti 120 V. Prehod iz numerično izračunanega električnega polja v verjetnost za prepustnost celične membrane je bil narejen z Gompertzovo krivuljo. Povzeto po (Dermol in Miklavčič 2014).

V drugi študiji (Dermol et al. 2016) smo se ukvarjali z modeliranjem vnosa barvila v celice v odvisnosti od časa. Osredotočili smo se na pojav povišanja občutljivosti celic na električne pulze (*angl.* electrosensitization). V literaturi lahko zasledimo opažanja, da obstaja razlika v celični smrti, če dovedemo električne pulze v enem vlaku ali če vlak razdelimo na več delov, med njimi pa počakamo več minut (Pakhomova et al. 2011; Pakhomova et al. 2013a; Jiang et al. 2014; Jiang et al. 2015b; Muratori et al. 2016; Muratori et al. 2017). Shema dovajanja pulzov v obliki enotnega ali razdeljenega vlaka je prikazana na sliki 6. Premor med posameznimi vlaki pulzov je po poročilih v literaturi bistveno povišal celično smrt pri enaki dovedeni energiji. S tem se je povišala učinkovitost zdravljenja, kar bi lahko imelo pozitivne učinke tudi pri medicinskih posegih z elektroporacijo.
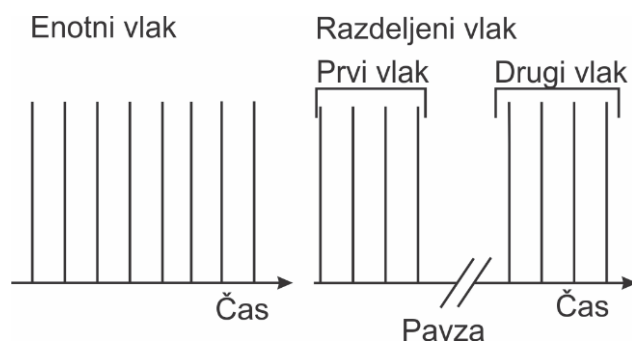
Slika 6: *Shema dovajanja pulzov. Levo je enotni vlak, kjer so bili naenkrat dovedeni vsi pulzi. Desno je razdeljeni vlak, kjer so bili najprej dovedeni štirje pulzi, po 1 do 3 minutnem premoru pa še štirje pulzi. Povzeto po (Dermol et al. 2016).*

Preverjali smo, če je pojav povišanja občutljivosti celic odvisen tudi od sestave elektroporacijskega pufra, t. j. tekočine, v kateri so elektroporirane celice. Poskuse smo izvajali na suspenziji celic CHO-K1. Pod mikroskopom smo zajemali slike pred dovedenimi električnimi pulzi in 8 minut za njimi. Uporabili smo paralelne žične elektrode, prikazane na sliki 3a. Celice smo električnim pulzom izpostavili v štirih različnih elektroporacijskih pufrih, ki so se razlikovali v električni prevodnosti, osmolalnosti, koncentraciji saharoze in kalcija. Dovedli smo enotni ali razdeljeni vlak električnih pulzov ter analizirali prispevek prvega in drugega vlaka električnih pulzov. Časovno dinamiko smo modelirali s fenomenološkim modelom prvega reda. Časovni potek vnosa barvila je shematično prikazan na sliki 7, kjer so napisane tudi enačbe, ki smo jih uporabljali za opis dinamike vnosa barvila v celice, obenem pa so na sliki razloženi tudi parametri enačb. Ugotovili smo, da lahko iz rezultatov vnosa barvil v molekule sklepamo tudi na celjenje celične membrane. S pomočjo merjenja časovne dinamike vstopa fluorescentnega barvila propidijev jodid smo ugotovili, da ima pufer, v katerem celice izpostavimo električnim pulzom, velik vpliv. Sklepali smo, da je povišanje občutljivosti celic posledica skupnega delovanja več procesov ter ni splošno prisoten pojav. Za točno določitev mehanizmov povišanja občutljivosti celic so potrebne nadaljnje študije.
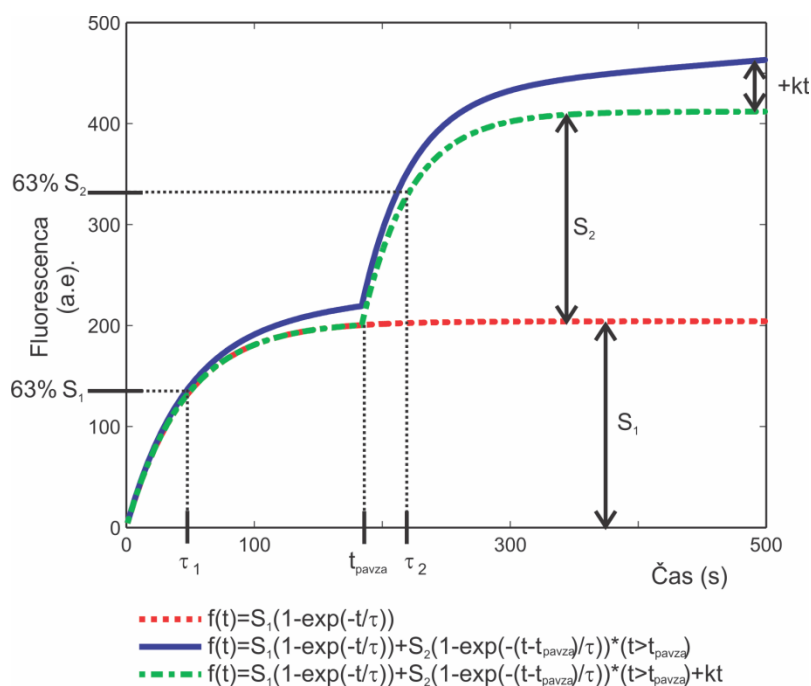
Slika 7: Dinamika zapiranja por je bila modelirana s kinetičnim modelom prvega reda. Na sliki lahko vidimo, kako sta bila posebej analizirana prispevek prvega in drugega vlaka pulzov. Povzeto po (Dermol et al. 2016).

Matematični modeli preživetja celic

Ukvarjali smo se tudi z matematičnimi modeli celične smrti. Matematičnih modelov celične smrti poznamo veliko, saj jih rutinsko uporabljajo za napoved učinkovitosti pasterizacije in sterilizacije v živilski industriji. Pri načrtovanju medicinskih posegov elektroporacije matematični modeli niso razširjeni – trenutno uporabljamo deterministično kritično vrednost za določanje meje med uničenim in nedotaknjenim tkivom.

Modele smo prilegali na rezultate poskusov. Naredili smo poskuse na celični suspenziji CHO-K1 v nizko prevodnem kalijevem pufru. Kapljico celične suspenzije smo prenesli med jeklene paralelne elektrode (slika 8) in jih izpostavili električnim pulzom podobnih parametrov, kot jih uporabljajo pri zdravljenju tkiv z ireverzibilno elektroporacijo (do 90 pulzov dolžine 100 µs, dovedenih s ponavljalno frekvenco 1 Hz pri električnih poljih do 4 kV/cm). Celično smrt smo ovrednotili s testom klonogenosti (Franken et al. 2006), kjer smo po elektroporaciji v petrijevke nasadili celice v nizki gostoti. V šestih dneh so celice ustvarile kolonije, ki smo jih nato fiksirali, obarvali, prešteli ter določili delež preživelih celic.

Slika 8: Jeklene paralelne elektrode, ki so bile uporabljene v poskusih. Med elektrode smo prenesli kapljico celične suspenzije ter jo izpostavili električnim pulzom.

Ovrednotili smo več modelov celične smrti – kinetični model prvega reda, Hülshgerjev, Peleg-Fermijev, Weibullov, logistični, prilagojen Gompertzov in Geeraerdov model. Ugotovili smo, da je najbolj primeren Peleg-Fermijev model, ki je dobro opisal rezultate poskusov in vključeval dve neodvisni spremenljivki – električno polje in število pulzov. V nasprotju z njim so ostali modeli vključevali le eno neodvisno spremenljivko – ali čas izpostavitve (število pulzov zmnoženo z njihovim trajanjem) ali električno polje med elektrodami. Na sliki 9 lahko vidimo rezultate poskusov in modele, ki smo jih prilegali na te podatke. Vidimo lahko, da se uporabljeni modeli različno približajo rezultatom poskusov, parameter R^2, napisan poleg modela, pa nam pove še, kako dober je model v opisu podatkov. Bolj kot se vrednost R^2 približa 1, boljše je prileganje.
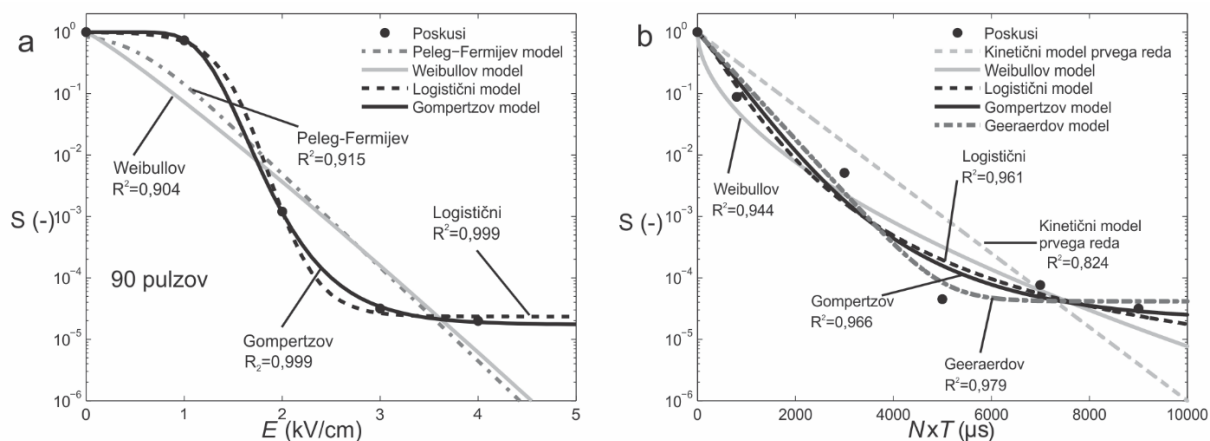
Slika 9: *Modeli celične smrti (Weibullov, Peleg-Fermijev, prilagojen Gompertzov, logistični, kinetični model prvega reda, Geeraerdov), s katerimi smo opisali rezultate poskusov celične smrti. Na sliki a so modeli v odvisnosti od dovedenega električnega polja, na sliki b pa od zmnožka števila pulzov in njihovega trajanja. Povzeto po (Dermol in Miklavčič 2015).*

Ugotovili smo, da bi bili matematični modeli prepustnosti celične membrane in celične smrti lahko uporabni v načrtovanju posegov. Dobra lastnost teh modelov je, da jih hitro prilegamo na rezultate poskusov, vrednosti med točkami lahko interpoliramo. Slabost modelov je, da jih je potrebno optimizirati za vsak tip celic posebej, prenosljivost na tkiva pa je vprašljiva.

Modeliranje depolarizacije celic

Pri načrtovanju medicinskih posegov z elektroporacijo je smiselno upoštevali tudi vzdražnost tkiv. V primeru proženja akcijskega potenciala mišic in živcev pride do neželenega krčenja mišic in bolečine. Ugotavljali smo: 1. ali se vzdražna in nevzdražna tkiva na elektroporacijo odzivajo enako, 2. ali lahko z elektroporacijo zdravimo tumorje osrednjega živčnega sistema in 3. ali so lastnosti vzdražnih tkiv po elektroporaciji spremenjene. Več študij je sicer pokazalo, da so bili učinki elektroporacije na vzdražna tkiva le kratkoročni – tkiva so si opomogla fiziološko, histološko in funkcionalno (Onik et al. 2007; Li et al. 2011; Schoellnast et al. 2011; Jiang et al. 2014; Tschon et al. 2015; Casciola et al. 2017).

S poskusi in modeliranjem smo ovrednotili depolarizacijo in elektroporacijo štirih različnih celičnih linij – nevzdražne celične linije CHO-K1, nevzdražne celične linije U-87 MG (človeški glioblastom), nevzdražne nediferencirane celične linije HT22 (mišji nevroni iz hipokampusa) in vzdražne diferencirane celične linije HT22. Depolarizacija pomeni povišanje transmembranske napetosti, do katere lahko pride tako na vzdražnih kot na nevzdražnih celicah, ko jih izpostavimo zunanjemu električnemu polju. Če presežemo pragovno vrednost transmembranske napetosti, pri vzdražnih celicah pride do proženja akcijskega potenciala.

Najprej smo s poskusi določili depolarizacijsko (za nevzdražne) oz. vzdražnostno (za vzdražne celice) intenzivnostno-časovno krivuljo za en pulz dolžine od 10 ns do 10 ms. Za določanje depolarizacije smo uporabljali fluorescentno barvilo (Baxter et al. 2002). Barvilo je v začetku v zunajceličnem prostoru, po povišanju transmembranske napetosti pa lahko preide v notranjost celice in povzroči v njej dvig signala.

Intenzivnostno-časovno krivuljo vzdražnih celic smo opisali z dvema modeloma – s fenomenološko Lapicquevo krivuljo (Boinagrov et al. 2010) in Hodgkin-Huxleyjevim modelom (Santamaria in Bower 2009; Boinagrov et al. 2010). Hodgkin-Huxleyjev model je sistem diferencialnih enačb, ki opisuje dinamiko odpiranja in zapiranja napetostno odvisnih kanalov. Akcijski potencial, modeliran s Hodgkin-Huxleyjevim modelom, lahko vidimo na sliki 10. Ugotovili smo, da je primernejši Hodgkin-Huxleyjev model, čeprav bi morali za najboljši opis naših rezultatov njegove parametre optimizirati, kar bi bilo zaradi njihovega visokega števila težavno.

Intenzivnostno-časovno krivuljo (slika 11) smo primerjali z rezultati poskusov elektroporacije po enem pulzu različnih dolžin (Pucihar et al. 2011). V isti študiji so rezultate poskusov modelirali s Saulisovim modelom (Pucihar et al. 2011). Dodali smo še modeliranje s časovno odvisno Schwannovo enačbo za eliptične celice v električnem polju (Kotnik et al. 1998; Kotnik in Miklavčič 2000b; Valič et al. 2003). Pri Schwannovi enačbi smo predpostavljali, da je kritična vsiljena transmembranska napetost enaka pri vseh dolžinah pulzov, kar ni nujno pravilno. Ugotovili smo, da elektroporacijo boljše opiše Saulisov model.
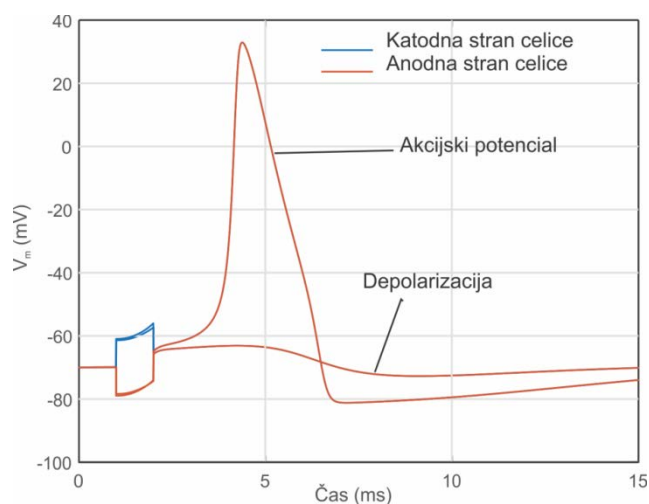
Slika 10: *Primer depolarizacije z akcijskim potencialom in brez njega pri modeliranju s Hodgkin-Huxleyjevim modelom (Boinagrov et al. 2010). Modre in oranžne črte opisujejo napetost na katodnem in na anodnem polu celice. Po dovedenem pulzu se vidi le še oranžna črta, saj se z modro prekrivata. V primeru na sliki smo simulirali en 1 ms pulz tik pod pragom za proženje akcijskega potenciala in nad njim.*
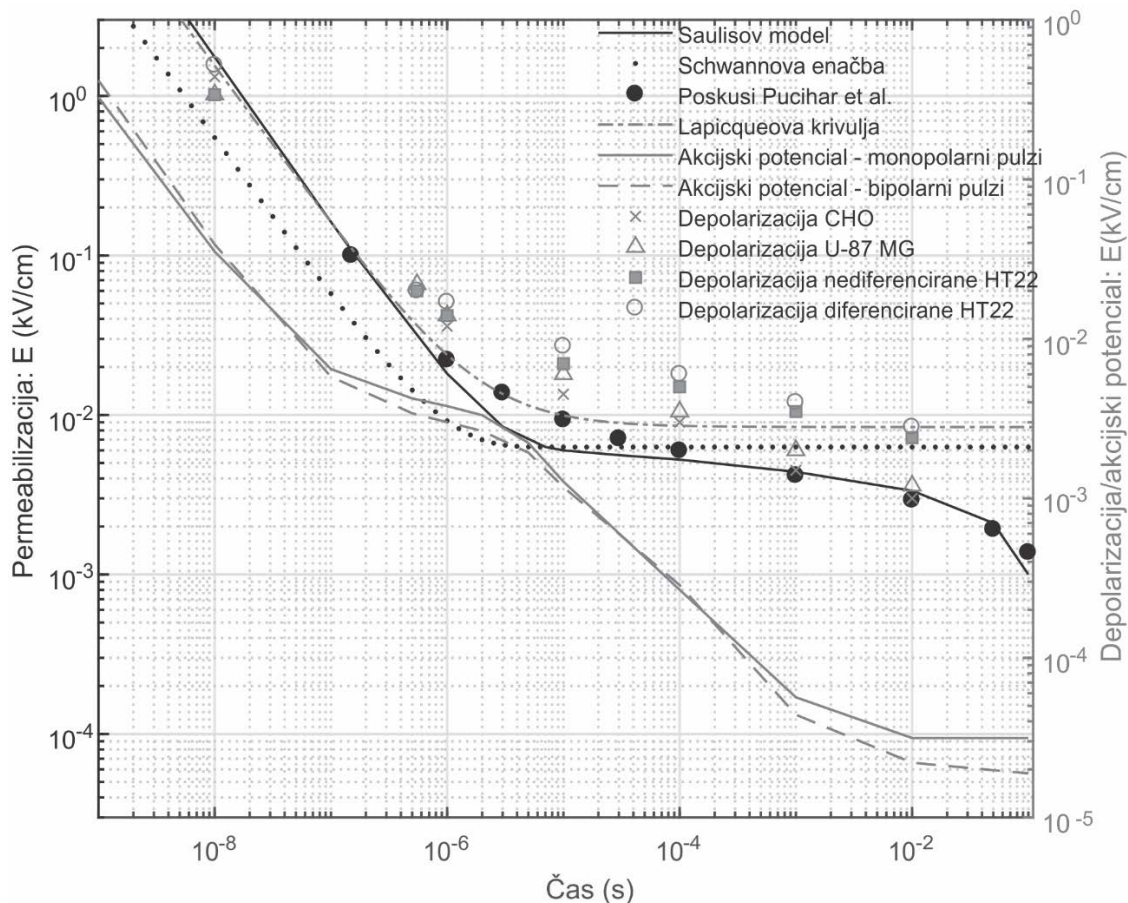
Slika 11: *Intenzivnostno-časovna krivulja CHO, U-87 MG, nediferenciranih in diferenciranih HT22 celic.*
Intenzivnostno-časovno krivuljo smo modelirali z Lapicqueovo krivuljo in s Hodgkin-Huxleyjevim
modelom. Prikazana je tudi prepustnostna krivulja CHO celic, pridobljena v okviru študije (Pucihar et al.
2011) in modelirana s Saulisovim modelom in Schwannovo enačbo. Črne črte in y-os kažejo prepustnost
celične membrane po enem pulzu. Sive črte in desna y-os kažejo depolarizacijo oz. akcijski potencial po
enem pulzu.

Zanimala nas je tudi elektroporacija nevzdražnih in vzdražnih celičnih linij, zato smo vse štiri celične linije izpostavili pulzom podobnih parametrov, kot se običajno uporabljajo pri elektrokemoterapiji – osem pulzov dolžine 100 µs, dovedenih s ponavljalno frekvenco 1 Hz. Vnos smo določali s fluorescentnim barvilom Yo-Pro-1®. Merili smo časovno dinamiko vnosa barvila v celice, kot lahko vidimo na sliki 12. Iz časovne dinamike smo nato določili prepustnostno krivuljo, ki je prikazana na sliki 13a. S poskusi določene prepustnostne krivulje smo modelirali s simetrično sigmoido (Dermol in Miklavčič 2014), kar je prikazano na sliki 13b.
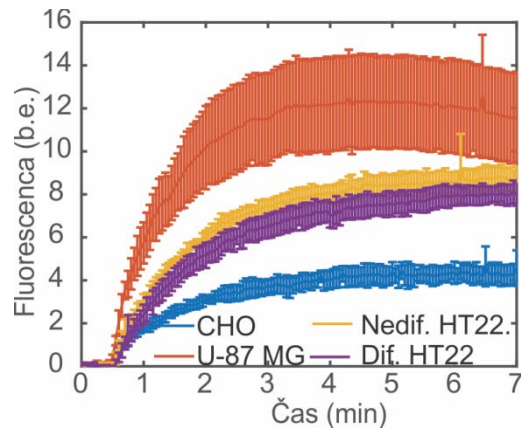
Slika 12: Časovna dinamika vnosa barvila Yo-Pro-1® v celice štirih celičnih linij. Dinamiko smo lahko opisali z modelom prvega reda.
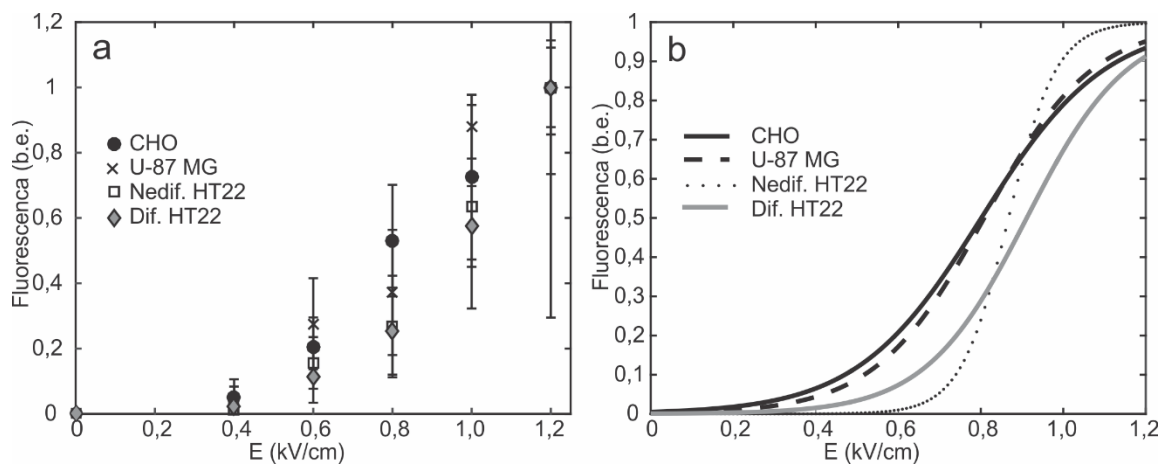
Slika 13: Povišanje prepustnosti membran štirih celičnih linij po dovedenih pulzih podobnih parametrov, kot se uporabljajo pri elektrokemoterapiji. S poskusi določene točke so na sliki a, optimizirana simetrična sigmoida pa na sliki b.

Ugotovili smo, da je prag za depolarizacijo nevzdražnih celic nižji kot prag za depolarizacijo vzdražnih celic, kar lahko pojasnimo s tem, da imajo diferencirane celice, ki se ne delijo, nižjo mirovno transmembransko napetost (Levin in Stevenson 2012). Vse štiri celične linije so se podobno odzvale na elektroporacijo s pulzi podobnih parametrov, kot so uporabljeni pri elektrokemoterapiji. To nakazuje, da je elektroporacija primerna za zdravljenje vzdražnih tkiv. Naši rezultati kažejo, da je možno optimizirati parametre električnih pulzov tako, da dobimo čim višji vnos molekul v celice, obenem pa se izognemo proženju akcijskega potenciala. V prihodnosti bo potrebno določiti, če depolarizacija in vitro in vzdražnost korelirata s krčenjem mišic in bolečino in vivo.

Prehod modeliranja z ravni ene same celice na raven tkiv z upoštevanjem njegove strukture

Zaradi elektroporacije se spremenijo električne lastnosti celic in posledično tudi tkiv. Zgradili smo model kože, ki temelji na geometriji celic (keratinocitov, korneocitov) in lahko opiše spremembe električnih lastnosti kože med elektroporacijo. Elektroporacijo smo modelirali s spremembo prevodnosti kože z nastankom lokalnih transportnih območij v roženi plasti ter nastankom por na membranah celic spodnjih plasti kože.

Model je temeljil na rezultatih poskusov, pridobljenih v okviru že objavljene študije (Zorec et al. 2013a). Na kratko: v Franzevih difuzijskih celicah so pulzom izpostavili 350 μm debele kose prašičje kože z ušes. Elektrode so bile postavljene 0,2 cm nad kožo in 0,5 cm pod njo. Dovedli so dva različna protokola: dolge nizkonapetostne pulze (3x45 V dolžine 250 ms in 100 ms pavze med njimi) ali kratke visokonapetostne pulze (3x500 V dolžine 500 μs, 500 μs pavze med njimi). 350 μm debela koža je glede na model (Huclova et al. 2012) sestavljena iz štirih slojev – rožene plasti, epidermisa, papilarnega dermisa in žilne plasti.

Naš model smo osnovali na že obstoječem modelu (Huclova et al. 2012), kjer so lastnosti posameznih slojev kože izračunane s pomočjo električnih in geometrijskih lastnosti posameznih celic. Tako kot v študiji (Huclova et al. 2012) smo električne lastnosti slojev z nizkim prostorninskim deležem celic izračunali s Hanai-Bruggemanovo formulo, ki sicer spada med t. i. enačbe mešanja. Lastnosti slojev z višjim prostorninskim deležem celic (nad 80%) smo izračunali z modelom enotske celice. Enotska celica je s kvadrom zunajcelične tekočine obdana biološka celica. Tri enotske celice, ki smo jih zgradili v okviru naše študije, so prikazane na sliki 14. Oblika biološke celice je bila opisana s pomočjo t. i. 'superformule' (Gielis 2003). Biološki celici smo pripisali ustrezne električne lastnosti. Z velikostjo enotske celice smo spreminjali prostorninski delež celic v tkivu. Enotsko celico smo izpostavili sinusni napetosti različnih frekvenc v vseh treh smereh (x, y, z) in preko admitance izračunali frekvenčno odvisen kompleksni tenzor električnih lastnosti enotske celice ($\bar{\bar{\varepsilon}}^*$). Posameznim plastem v homogenem modelu kože smo pripisali izračunane električne lastnosti enotske celice in numerične izračune poenostavili na raven homogenih modelov tkiva. V primeru rožene plasti smo električne lastnosti izračunali preko korneocitov v enotski celici, pri epidermisu pa preko keratinocitov v enotski celici. Z izbranim modelom lahko modeliramo realistične oblike celic v visokih prostorninskih deležih, anizotropijo in heterogenost tkiv. V naši študiji smo v model vključili spremembe električnih lastnosti kože med elektroporacijo in model primerjali s tokovnonapetostnimi meritvami.

(a)   (b)   (c)
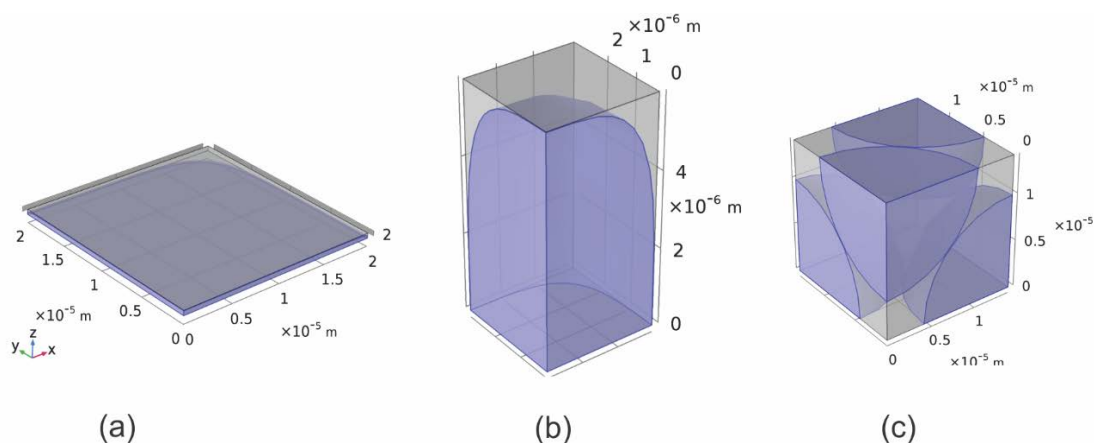
Slika 14: Enotske celice, s katerimi smo predstavili (a) keratinocit, iz katerega smo nato izračunali lastnosti rožene plasti, (b) korneocit, iz katerega smo izračunali lastnosti epidermisa in (c) krogle lipidov v zunajcelični tekočini, iz katerih smo nato izračunali lastnosti papilarnega dermisa. Geometrija keratinocita in korneocita je bila zgrajena s 'superformulo' (Gielis 2003; Huclova et al. 2012), zaradi simetrije pa smo modelirali le eno osmino celice. Geometrija papilarnega dermisa so krogle v ploskovno centrirani mreži. Povzeto po (Dermol-Černe in Miklavčič 2018).

Pri elektroporaciji kože pride do dveh pojavov – v roženi plasti nastanejo lokalna transportna območja, na membranah celic spodnjih plasti pa pride do elektroporacije oz. nastanka por. Pri elektroporaciji kože z dolgimi nizkonapetostnimi pulzi se spreminja velikost lokalnih transportnih območij, saj okoli njih prihaja do topljenja lipidov zaradi Joulovega gretja. Spremembo velikosti lokalnih transportnih območij med nizkonapetostnimi pulzi smo prevzeli iz literature (Zorec et al. 2013a). Pri elektroporaciji s kratkimi visokonapetostnimi pulzi se poviša gostota lokalnih transportnih območij, njihova velikost pa se ne spreminja. Spremembo gostote lokalnih transportnih območij smo določili na podlagi najboljšega ujemanja s poskusi. Obenem smo z asimptotsko enačbo (Neu in Krassowska 1999; Neu in Neu 2009) izračunali gostoto por na membranah celic spodnjih plasti kože, pri čemer smo predpostavljali, da padec napetosti na koži lahko določimo, če kožo razumemo kot napetostni delilnik. Ekvivalentno vezje Franzeve difuzijske celice in kože v njej je prikazano na sliki 15.
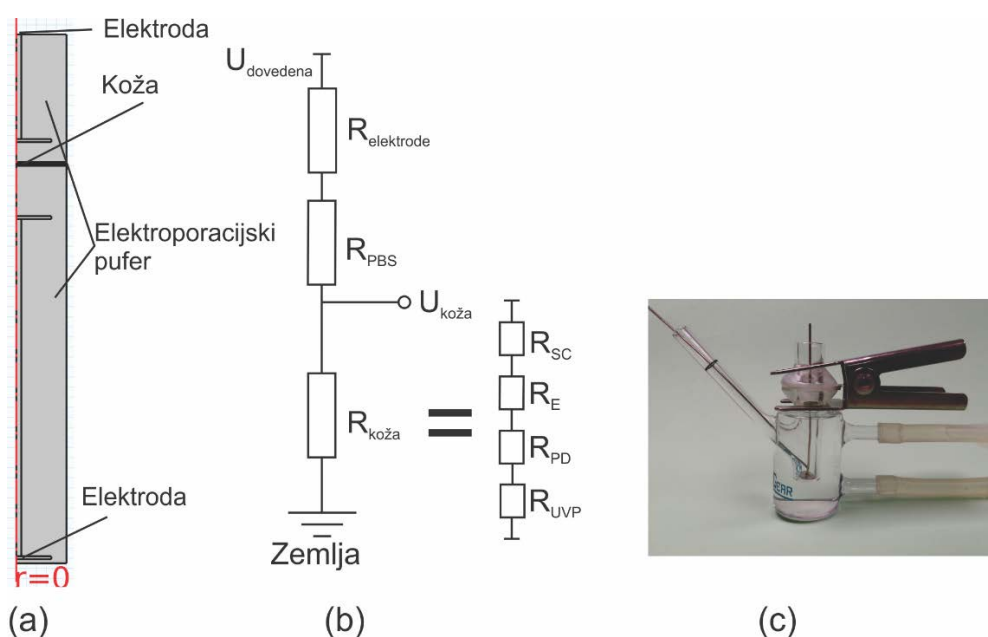
Slika 15: *Shema, ekvivalentno vezje in fotografija Franzeve difuzijske celice. Na sliki (a) lahko vidimo, da je bila koža na obeh straneh obdana z elektroporacijskim pufrom, v katerega so bile vstavljene platinaste elektrode. V (b) ekvivalentnem vezju so z upori so predstavljeni upornost stika kovina-elektrolit ($R_{elektrode}$), elektroporacijski pufer (R_{PBS}) in posamezne plasti kože (R_{SC} – rožena plast, R_E – epidermis, R_{PD} – papilarni dermis, R_{UVP} – žilna plast). Na sliki (c) lahko vidimo fotografijo Franzeve celice.*

Spremenjene električne lastnosti posameznih tkiv smo nato vstavili v numerični model Franzeve difuzijske celice ter modelirali tok skozi kožo in napetost na njej, če na elektrode dovedemo napetost, izmerjeno med poskusom na izhodu pulznega generatorja. Spreminjali smo gostoto transportnih območij, električno prevodnost transportnih območij in električno prevodnost spodnjih plasti kože, dokler nismo dosegli dobrega ujemanja s poskusi. Določili smo (lokalni) optimum parametrov. Zaradi visokega števila parametrov, ki jih v modelu lahko spreminjamo, in pomanjkanja meritev pri elektroporaciji kože, globalnega optimuma nismo mogli določiti. Za točno določitev vrednosti parametrov bi potrebovali več meritev, npr. električne lastnosti posameznih slojev pred elektroporacijo in po njej ter električno prevodnost lokalnih transportnih območij.

Ugotovili smo, da lahko dobro opišemo elektroporacijo z dolgimi nizkonapetostnimi pulzi, če upoštevamo širitev lokalnih transportnih območij, spremembo električne prevodnosti spodnjih plasti in polarizacijo elektrod. Izmerjeni in modelirani tok in napetost lahko vidimo na slikah 16a in 16b. Ujemanje modela in meritev pri elektroporaciji s kratkimi visokonapetostnimi pulzi je bilo slabše – napetost se je sicer dobro ujemala, a je model tok podcenjeval za približno 50%, kar lahko vidimo na slikah 16c in 16d. Razlog bi lahko bil v elektrokemijskih reakcijah, ki se dogajajo med elektroporacijo. Kemija pri visokonapetostnih pulzih je relativno neraziskano področje, obstaja le nekaj študij, ki se ukvarjajo z izpustom kovin iz elektrod (Kotnik et al. 2001; Roodenburg et al. 2005; Pataro et al. 2014) in z možnimi kemijskimi reakcijami, ki se dogajajo na elektrodah ali ob njih (Pataro et al. 2015a; Pataro et al. 2015b). Le redki modeli elektroporacije vključujejo elektrokemijo, npr. polarizacijo elektrod (Šel et al. 2003), čeprav je, kot se je izkazalo pri našem modelu, polarizacija elektrod bistveno zmanjšala napetost, dovedeno na kožo.
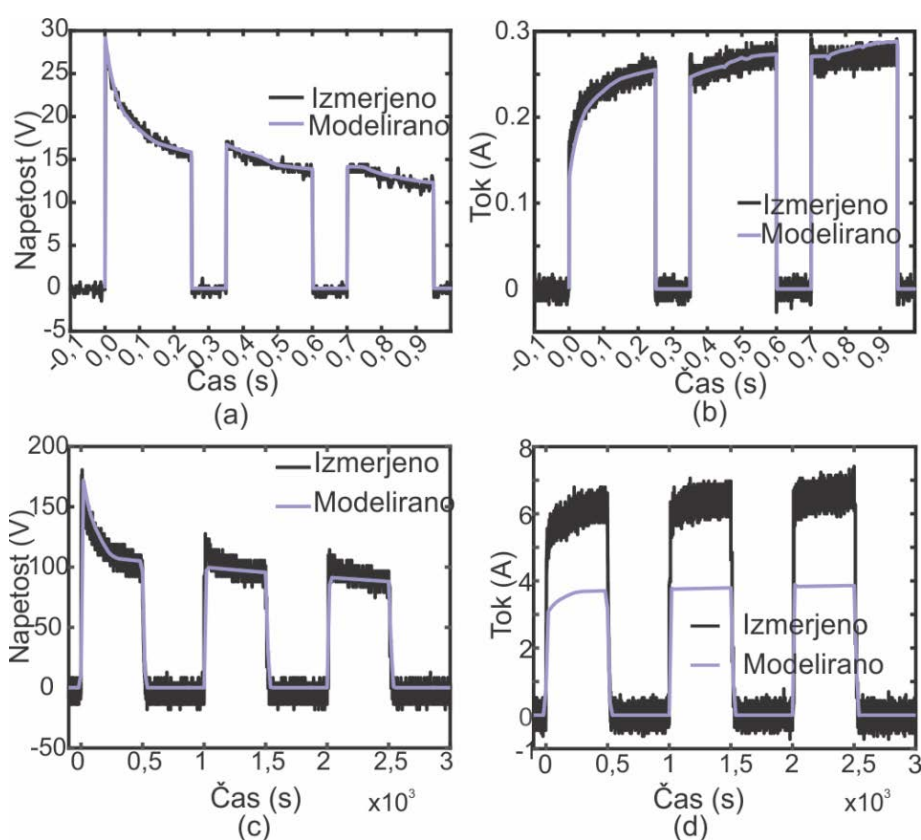
Slika 16: Z modelom električnih lastnosti elektroporirane kože smo opisali tokovnonapetostne meritve pri dovajanju dolgih nizkonapetostnih pulzov in kratkih visokonapetostnih pulzov. Pri nizkonapetostnih pulzih smo dobro opisali meritve, pri visokonapetostnih pa je model podcenjeval izmerjeni električni tok. Pri visokonapetostnih pulzih so bili prisotni še drugi mehanizmi, kot so npr. elektrokemijske reakcije, ki jih v model nismo vključili. Povzeto po (Dermol-Černe in Miklavčič 2018).

Naš model povezuje procese, ki se med elektroporacijo dogajajo na posamezni celici (nastanek por v celični membrani) in na plasti kože (nastanek lokalnih transportnih območij v roženi plasti), s tkivi (plasti kože) in celo z organi (koža). Z modelom lahko opišemo spremembe električnih lastnosti tkiv, pri čemer izhajamo iz mikrostrukture tkiva, obenem pa ostajajo numerični izračuni relativno hitri in preprosti. V prihodnosti bi v

model lahko vključili še termične pojave ali elektrokemijo. S tem lahko opišemo katero koli tkivo, če poznamo električne in geometrijske lastnosti osnovnih gradnikov tkiva.

Modeliranje transporta molekul skozi celično membrano

Pri zdravljenju tumorjev z elektrokemoterapijo je pomembno, da je v celotnem tumorju vzpostavljeno dovolj visoko električno polje (Miklavčič et al. 2006a), obenem pa mora biti v celicah dovolj molekul kemoterapevtika, da zagotovimo celično smrt (Tounekti et al. 1993; Tounekti et al. 2001; Miklavčič et al. 2014). Pri načrtovanju posegov bi bilo torej smiselno modelirati tudi transport kemoterapevtika v tumorske celice. Modelirali smo transport cisplatina v tumorske celice pri elektrokemoterapiji tumorjev. Za to smo uporabili model dvojne poroznosti. Za postavitev modela smo izvedli poskuse in vitro, v sodelovanju z Onkološkim inštitutom pa tudi poskuse in vivo. Meritve mase platine so potekale v sodelovanju z Inštitutom Jožef Štefan.

V študiji transporta majhnih molekul smo rezultate vnosa cisplatina v celice in vitro uporabili za opis transporta cisplatina v tumorjih in vivo. Celično suspenzijo mišjih melanomskih celic B16-F1 smo v rastnem mediju s serumom izpostavili 100 µs dolgim električnim pulzom s ponavljalno frekvenco 1 Hz. Z induktivno sklopljeno plazmo z masnim spektrometrom smo izmerili znotrajcelično maso platine. Najprej smo izvedli poskuse, pri katerih smo optimizirali protokol elektroporacije in vitro. Celice smo elektroporirali pri različnih zunajceličnih koncentracijah cisplatina in ugotovili, da je znotrajcelična masa platine linearno odvisna od zunajcelične koncentracije cisplatina (slika 17a). Zato smo nadaljnje poskuse izvedli pri 100 µM zunajcelični koncentraciji cisplatina, kar je dovolj visoka koncentracija, da smo lahko pri meritvah mase platine razlikovali med pulzi podobnih parametrov. Izmerili smo tudi dinamiko vnosa cisplatina v celice pri 100 µM zunajceličnem cisplatinu in ugotovili, da že 5 minut po pulzih dosežemo plato, zato smo vse nadaljnje poskuse izvajali z 10 minutno inkubacijo (slika 17b). Cisplatin se lahko veže na proteine v serumu in s tem postane biološko neaktiven (Takahashi et al. 1985). Celice smo elektroporirali s serumom ali brez njega in ugotovili, da v naših poskusih serum ni vplival na vnos cisplatina (slika 17c). Izmerili smo tudi celjenje membrane, tako da smo cisplatin dodali do 20 minut po pulzih. Celjenje por smo opisali z dinamiko prvega reda in izračunali, da je bila časovna konstanta celjenja por 2,29 minute. Po optimizaciji osnovnega protokola smo spreminjali število pulzov od 1 do 64 in električno polje od 0,4 kV/cm do 1,2 kV/cm. Maso znotrajcelične platine pri teh parametrih lahko vidimo na sliki 18.
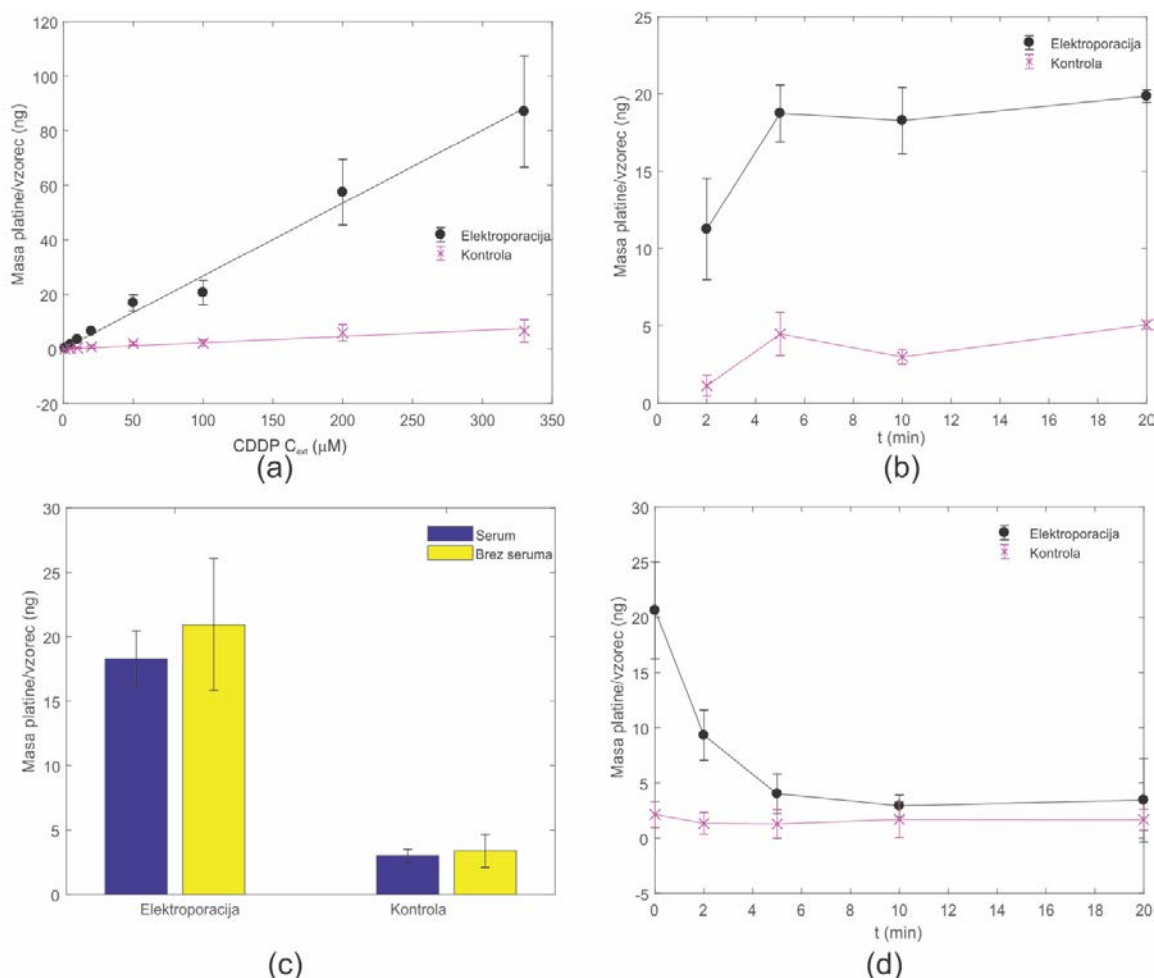
Slika 17: *Rezultati poskusov in vitro elektroporacije celic s cisplatinom. a) Znotrajcelična masa platine je bila linearno odvisna od zunajcelične koncentracije cisplatina. b) Vpliv časa inkubacije na znotrajcelično maso platine. Plato smo dosegli že 5 minut po dovedenih pulzih. c) Vpliv seruma na znotrajcelično maso platine. Ugotovili smo, da v 10 minutah po pulzih serum ne vpliva na vnos cisplatina. d) Po dovedenih električnih pulzih se je celična membrana celila z dinamiko prvega reda.*

Z modelom dvojne poroznosti (Mahnič-Kalamiza et al. 2014a; Mahnič-Kalamiza in Vorobiev 2014; Mahnič-Kalamiza et al. 2015; Mahnič-Kalamiza et al. 2017) smo izračunali koeficient prepustnosti celične membrane v odvisnosti od parametrov električnega polja. Obenem smo naredili poskuse in vivo, kjer smo v podkožni tumor B16-F10 intratumorsko vbrizgali cisplatin ter izmerili maso platine v serumu, celicah in intersticijski frakciji tik pred dovajanjem pulzov ter eno uro po končani terapiji. Zgradili smo numerični model tumorja ter z in vitro izračunanim koeficientom prepustnosti in difuzijsko konstanto cisplatina v intersticijski frakciji tumorja opisali maso platine v tumorjih in vivo. Opis je bil mogoč, če smo transport cisplatina po intersticijski frakciji zmanjšali s pomočjo transformacijskega koeficienta, s katerim smo upoštevali razlike v transportu in vitro ter in vivo. Pri transportu in vivo je zaradi bližine celic, visokega prostorninskega deleža celic ter prisotnosti celičnega matriksa na voljo manjša površina membrane, skozi katero lahko v celice pride cisplatin, otežena pa je tudi difuzija molekul po intersticijski frakciji. Obenem je zaradi visokega prostorninskega deleža in bližine celic zmanjšana tudi vsiljena transmembranska napetost na celicah. Prostorsko porazdelitev cisplatina eno uro po dovedenih pulzih, kar ustreza časovni točki, ko je bil tumor in vivo izrezan, lahko vidimo na sliki 19. Očitno je, da je prostorska porazdelitev koncentracije

cisplatina v tumorju nehomogena in se niža, ko se bližamo zunanjemu robu tumorja. V prihodnosti je potrebno še preveriti vpliv tipa tumorja in gostote celic v njem ter preveriti delovanje modela pri drugačnih parametrih električnega polja. Naš model ponuja korak naprej pri modeliranju transporta pri elektroporaciji na ravni tkiv, upoštevajoč transport na ravni ene celice. Z našim modelom bi lahko zmanjšali število poskusov in vivo ter bolj točno napovedali učinkovitost zdravljenja pri načrtih medicinskih posegov z elektroporacijo.
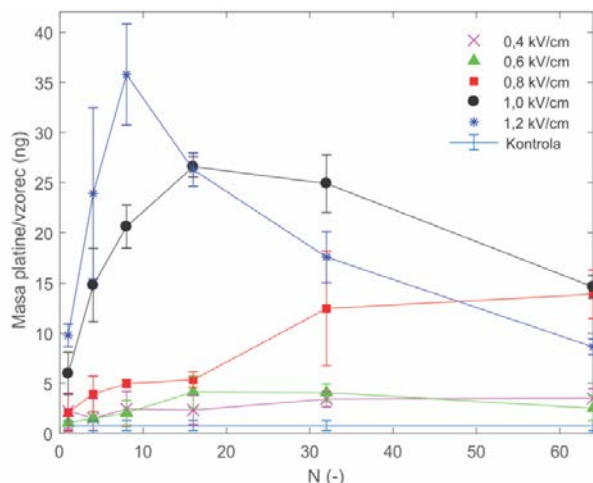
Slika 18: *Izmerjene znotrajcelične mase platine pri elektroporaciji celične suspenzije celic mišjega melanoma B16-F1. Vidimo lahko, da najvišji vnos dosežemo pri 8x100 µs pulzih pri 1,2 kV/cm.*
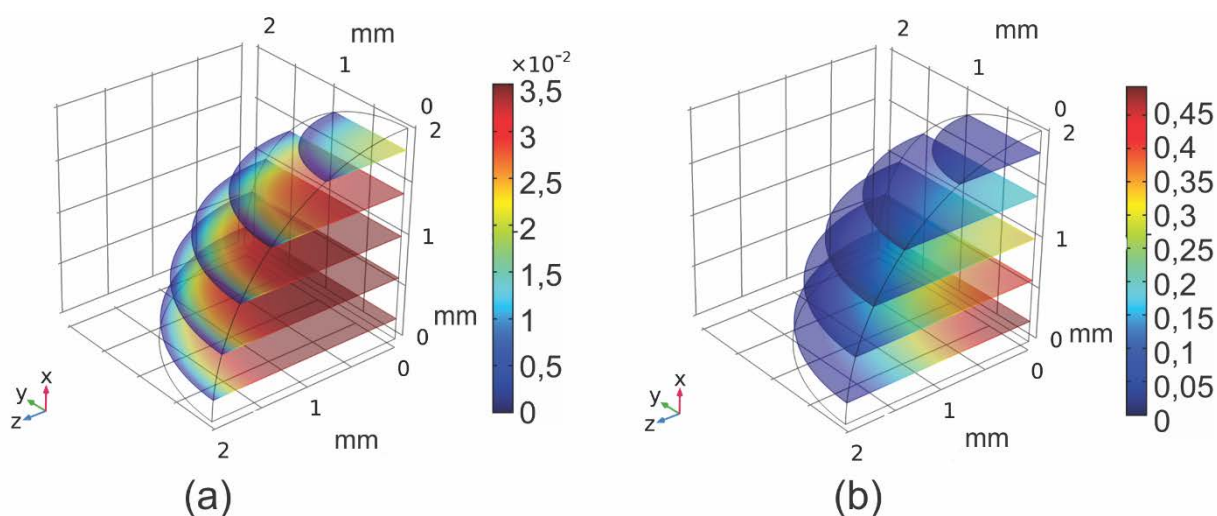
Slika 19: *Modelirana porazdelitev a) znotrajcelične in b) zunajcelične koncentracije cisplatina v tumorju v mol/m³. Koncentracija obeh je najvišja v sredini tumorja, nato pa postopoma upada do roba tumorja, kjer je koncentracija 0 mol/m³.*

Zaključek

V doktorski disertaciji sem se ukvarjala z modeliranjem procesov pri elektroporaciji na ravni celic ter na ravni tkiv. Na ravni celičnih suspenzij ali posameznih celic in vitro je poskuse relativno lahko izvajati, preizkusimo lahko več parametrov brez etičnih pomislekov, ki se pojavijo pri izvajanju poskusov in vivo (Workman et al. 2010). Naš cilj je bil, da z rezultati poskusov in vitro modeliramo dogajanje med elektroporacijo in vivo in po njej . Modele, ki smo jih zgradili, bi lahko v prihodnosti vključili v načrtovanje medicinskih posegov z elektroporacijo.

V prvem delu doktorske disertacije so opisani matematični modeli prepustnosti celične membrane in celične smrti. Ugotovili smo, da lahko s temi modeli dobro opišemo rezultate poskusov in vitro. Naše optimizirane modele celične smrti in vitro so že uporabili pri opisu ireverzibilne elektroporacije tkiv (Kranjc et al. 2017) in dosegli dobro ujemanje. V modelih celične smrti se z napovedjo približujemo preživetju 0, a ga nikoli ne dosežemo. Vprašanje je, kako nizko preživetje je potrebno zagotoviti, da uničimo tumor v celoti. Pri elektrokemoterapiji in pri netermičnem odstranjevanju tkiva z elektroporacijo preostale celice uniči imunski sistem (Neal et al. 2013; Serša et al. 2015).

Analizirali smo časovni potek vnosa barvila v celice pri elektroporaciji, kar lahko modeliramo z modelom prvega reda, ki tudi ustreza dinamiki celjenja por v celični membrani. V več študijah so določali hitrost celjenja celične membrane po elektroporaciji in izmerili, da je v območju minut tako in vitro kot tudi in vivo (Kinosita in Tsong 1977; Saulis et al. 1991; Čemažar et al. 1998; Shirakashi et al. 2004; Kandušer et al. 2006; Demiryurek et al. 2015), kar se sklada z našimi rezultati.

Pri elektroporaciji vzdražnih tkiv lahko pride do proženja akcijskega potenciala in krčenja mišic ter bolečine. S poskusi smo določili intenzivnostno-časovno krivuljo vzdražnih in nevzdražnih celičnih linij ter jo modelirali. V prihodnosti je potrebno ugotoviti, do kolikšne mere lahko iz in vitro depolarizacije in akcijskega potenciala napovemo krčenje mišic in bolečino in vivo. Pri uporabi intenzivnostno-časovnih krivulj za napovedovanje akcijskega potenciala v tkivih je potrebno upoštevati tudi, da nekaj časa po dovedenih pulzih tkivo ne zmore prožiti akcijskega potenciala. Izkazalo se je, da lahko elektroporacijski pulzi povzročijo škodo na membranskih proteinih, kot so napetostno odvisni kanali v celični membrani (Chen et al. 2006b; Azan et al. 2017). Čas odziva napetostno odvisnih kanalov je v okvirju milisekund (Gadsby 2009), kar je bistveno daljše kot nanosekundni pulzi. Vprašanje je torej, kako je sploh možno, da z nanosekundnimi pulzi prožimo akcijski potencial vzdražnih celic (Pakhomov et al. 2017).

V okviru študije o vzdražnih tkivih smo opazili, da pri pulzih dolžine 1 µs depolarizacijska intenzivnostno-časovna krivulja in krivulja prepustnosti po y-osi prideta zelo blizu skupaj. To opažanje je pomembno pri razlagi, zakaj s kratkimi bipolarnimi pulzi povzročimo prepustnost tkiv, obenem pa ne pride do vzdraženja. Pri 1 µs dosežemo namreč plato pri obeh intenzivnostno-časovnih krivuljah. Do podobnega zaključka so prišli v literaturi (Mercadal et al. 2017). Naši rezultati nakazujejo, da bi namesto s kratkimi bipolarnimi pulzi enak učinek dosegli s kratkimi monopolarnimi pulzi.

V drugem delu doktorske disertacije smo modelirali spremembe električnih lastnosti kože med elektroporacijo z nastankom por v celičnih membranah ter z nastankom lokalnih transportnih območij v

roženi plasti. V prihodnosti je potrebno podoben model zgraditi še za druga tkiva (npr. jetra ali mišice) in ga primerjati s tokovnonapetostnimi meritvami med elektroporacijo. Nadgradnja modela bi lahko bila, da namesto asimptotske oblike enačbe por uporabimo enačbe, ki predvidevajo spremembe v premeru por (Smith et al. 2004), s čimer bi prevodnost posamezne plasti kože določili z mehanizmi elektroporacije in ne le z najboljšim ujemanjem z meritvami. Z modelom smo sicer dosegli dobro ujemanje z meritvami pri dolgih nizkonapetostnih pulzih, pri kratkih visokonapetostnih pulzih pa ne. Pri kratkih visokonapetostnih pulzih se je pojavila dodatna komponenta električnega toka, ki je nismo mogli pojasniti z nastankom lokalnih transportnih območij. Tudi če smo predpostavili, da je cela rožena plast eno samo veliko transportno območje, je bil tok skozi kožo prenizek, obenem pa je bil v tem primeru padec napetosti na koži zelo majhen zaradi nizke upornosti kože. Pri meritvah napetosti na koži so uporabljali tanke bakrene žice. Na vsako stran kože je bila dana ena žica, pri tem se je ustvarila visoko prevodna pot za električni tok, saj je baker bolj prevoden kot koža ali pufer, v katerem je bila koža. S tem bi se lahko električni tok lokalno povišal, obenem pa ne bi vplival na padec napetosti na celotni koži. Vsekakor je v prihodnosti potrebno ovrednotiti elektrokemijske reakcije, ki se odvijajo med dovajanjem visokonapetostnih pulzov. Vemo namreč, da pride do izhajanja kovin iz elektrod, spremeni se pH tekočine, opazen je nastanek mehurčkov, ki so lahko ali posledica lokalnega izparevanja vode ali kemijskih reakcij, kjer nastajajo plini.

V model kože bi lahko vključili tudi termične vplive električnih pulzov. Zaradi Joulovega gretja se namreč poviša temperatura, z njo pa tudi električna prevodnost. Gretje je bilo v našem modelu vključeno posredno, z večanjem premera lokalnih transportnih območij, kar temelji na taljenju lipidov v roženi plasti. Morda bi v prihodnosti lahko v naš model vključili še model taljenja lipidov in nastanka lokalnih transportnih območij (Becker in Kuznetsov 2007; Becker 2012; Becker et al. 2014) – v našem modelu smo namreč velikosti lokalnih transportnih območij privzeli iz literature (Zorec et al. 2013a).

V modelu smo vsiljeno transmembransko napetost na celicah v spodnjih plasteh kože ocenili tako, da smo kožo obravnavali kot napetostni delilnik. Upoštevali smo debelino posamezne plasti in geometrijo celice. Pri tem smo zanemarili vpliv bližine celic, ki zmanjšuje vsiljeno transmembransko napetost. Možno je, da smo precenili spremembo v električni prevodnosti spodnjih plasti kože, obenem pa podcenili prevodnost lokalnih transportnih območij, njihovo gostoto in velikost. Električna prevodnost posameznih plasti kože vpliva na porazdelitev električnega polja in obratno – s pomočjo te odvisnosti bi v model lahko vključili tudi napake.

V tretjem delu doktorske disertacije smo se ukvarjali s transportom snovi po tkivih pri elektroporaciji. Naš model je veljaven za majhne molekule, podobne velikosti kot cisplatin (300 g/mol), kot so propidijev jodid, bleomicin, lucifer rumeno. Pokazalo se je, da večje molekule težje vstopajo preko celične membrane kot majhne molekule pri enakih parametrih električnih pulzov (Maček Lebar et al. 1998) že zaradi bistveno manjše difuzijske konstante večjih molekul po intersticijski frakciji tumorja. Pokazalo se je tudi, da večje molekule v celice vstopajo s pomočjo elektroforeze, manjše pa s pomočjo difuzije. Večje molekule (DNK) celično membrano prečkajo v več korakih, ki so opisani v literaturi (Rosazza et al. 2016). Predpostavili smo, da je ves transport difuzijski, kar pa ni nujno pravilno. Zaradi povišanega intersticijskega tlaka v tumorju (Baxter in Jain 1989; Boucher et al. 1990; Pušenjak in Miklavčič 2000) je povišan konvekcijski transport molekul iz njega, kar pomeni, da kemoterapevtik v tumor težko vstopi, ko je dovenden sistemsko,

oziroma da ga iz tumorja hitro odnaša, ko je doveden intratumorsko. Obstoječe meritve konvekcijske hitrosti v tumorju se niso skladale z našimi meritvami mase platine v celicah pred pulzi in eno uro po njih – izračunali smo namreč, da bi iz tumorja ves cisplatin izginil v nekaj minutah. V prihodnosti bi bilo smiselno ovrednotiti konvekcijski transport v tumorjih, ki jih uporabljamo v okviru naše študije. Model smo trenutno preizkusili le na eni vrsti tumorja. Znano je, da se tumorji bistveno razlikujejo v prostorninskem deležu celic in matriksa (Mesojednik et al. 2007), kar seveda vpliva na difuzijsko konstanto molekul po tumorju ter na površino celičnih membran, skozi katere lahko poteka transport. V prihodnosti bi lahko ovrednotili naš model še na drugih tipih tumorjev in ugotovili, ali obstaja določena preslikava med morfologijo tumorja, koeficientom transformacije in transportom po tumorju. Možno je, da takšna transformacija obstaja – višji kot je prostorninski delež celic v tumorju, nižji je transport kemoterapevtika v celice in nižji je transformacijski koeficient. Obenem se zastavlja vprašanje, če je transformacijski koeficient odvisen tudi od parametrov električnega polja. Trenutno smo model preizkusili le pri osmih pulzih in eni dovedeni napetosti. Smiselno bi bilo poskuse in vivo narediti še pri drugačnih parametrih električnih pulzov.

Pri intratumorskem dovajanju kemoterapevtika se izognemo običajni poti do celic v tumorju, ki jo mora kemoterapevtik preiti, če ga dovedemo sistemsko. Po sistemski administraciji mora namreč iz krvnih žil skozi žilne stene priti v okoliška tkiva (ali neposredno v tumorsko tkivo) in nato skozi intersticijsko frakcijo tumorja, kjer transport ovira višji intersticijski tlak v tumorju kot v okoliškem tkivu (Jain 1999; Jang et al. 2003), prečkati celično membrano in priti v celice. Če bi naš model želeli uporabljati tudi pri sistemski administraciji kemoterapevtika, bi morali dodati še izračun začetne koncentracije kemoterapevtika v tumorju. Pri intratumorski injekciji smo namreč lahko utemeljeno predpostavili, da je v tumorju začetna koncentracija kemoterapevtika enaka vbrizgani koncentraciji in je homogeno porazdeljena po celem tumorju.

V poskusih in vitro je bil cisplatin ali v celicah ali v zunajcelični tekočini. V poskusih in vivo smo vbrizgali 80 µl cisplatina oz. 26 µg platine v 35 mm^3 velike tumorje. Volumen injekcije je bil dvakrat večji kot volumen tumorja, ker smo uporabili že obstoječe rezultate iz literature (Uršič et al. 2018). V poskusih in vivo smo ugotovili, da je bilo 2 minuti po vbrizganju v tumorju in serumu le še 27% vbrizgane mase platine. Del cisplatina smo izgubili zaradi manjšega volumna tumorja od injiciranega volumna in zaradi izpiranja cisplatina iz tumorja. Če smo tumor izrezali eno uro po terapiji, je bilo vbrizgane mase platine v tumorju in v serumu 2% v kontrolnih vzorcih in 7% v elektroporiranih vzorcih. Del cisplatina smo izgubili pri mehanskem uničenju tumorja ter pri zbiranju krvi. Del cisplatina pa se je verjetno nabral v različnih organih, kar bi kasneje lahko povzročilo stranske učinke (Sancho-Martínez et al. 2012). V prihodnosti bi lahko ovrednotili, ali bi z vbrizganjem manjšega volumna cisplatina lahko ohranili enak učinek elektroporacije, obenem pa bi zmanjšali stranske učinke. Opaženo je bilo, da volumen vbrizganega kalcija ali virusov ni vplival na učinkovitost zdravljenja (Wang 2006; Frandsen et al. 2017). To lahko pojasnimo z našimi poskusi, pri katerih smo določali začetno koncentracijo cisplatina v tumorju. Čeprav se je pri vbrizganju izgubilo 70% vbrizganega cisplatina, je v tumorju ostal koncentrirani cisplatin, posledično pa je bil visok tudi koncentracijski gradient.

V literaturi lahko najdemo podatke, koliko molekul bleomicina potrebujemo, da pride do celične smrti (Tounekti et al. 1993; Tounekti et al. 2001). Podobno analizo bi bilo potrebno narediti tudi s cisplatinom,

kar bi nam omogočilo optimizacijo parametrov zdravljenja za čim višjo znotrajcelično koncentracijo cisplatina. Z induktivno sklopljeno plazmo z masno spektrometrijo lahko zelo natančno izmerimo maso in posledično število molekul v celicah. Če obenem pod enakimi pogoji s testom klonogenosti določimo še preživetje celic, lahko sklepamo na število molekul cisplatina, potrebnih za celično smrt.

Pri elektroporaciji lahko povišanje prevodnosti celične membrane in povišanje njene prepustnosti razumemo kot dva različna pojava (Miklavčič in Towhidi 2010; Leguèbe et al. 2014). Začetna ideja je bila, da bi ta pojava poskušali povezati in s spremembo električne prevodnosti celice napovedati prepustnost membrane, kar pa se je izkazalo za težko dosegljivo. Že pri začetnih poskusih smo namreč ugotovili, da pri isti prevodnosti zunajcelične tekočine, ki torej povzroči enako vsiljeno transmembransko napetost in enako gostoto por, dobimo bistveno drugačen vnos barvila v celico (Dermol et al. 2016). To torej nakazuje, da je elektroporacija bolj kompleksna in da samo nastanek por ne določa transporta v celice. Vseeno bi bilo v prihodnosti zanimivo ugotoviti, ali je povezava električne prevodnosti ter prepustnosti celične membrane možna in ali je prepustnost v večji meri določena z biološkimi procesi na celični membrani. Električna prevodnost celične membrane se namreč relativno hitro zmanjša, medtem ko transport poteka še več minut po dovedenih pulzih. Pri nanosekundnih pulzih so sicer ugotovili, da še nekaj časa po pulzih električna prevodnost celične membrane ostaja rahlo povišana (Pakhomov et al. 2007) in da trajanje povišane prevodnosti korelira s trajanjem transporta preko celične membrane. Druga razlaga podaljšanega transporta je, da električni pulzi povzročijo oksidacijo membrane, kar poruši urejenost lipidnega dvosloja in poveča prepustnost celične membrane (Benov et al. 1994; Gabriel in Teissié 1995; Maccarrone et al. 1995; Pakhomova et al. 2012).

Eden izmed problemov obstoječih modelov elektroporacije je pomanjkanje meritev, npr. nastanka in širjenja lokalnih transportnih območij v koži, električnih lastnosti posameznih tkiv med elektroporacijo v odvisnosti od parametrov električnih pulzov, prevodnosti lokalnih transportnih območij, konvekcijskega transporta v tumorjih, prostorske porazdelitve cisplatina v tumorjih pred elektroporacijo in po njej, vezavo cisplatina in vivo. Obstoječi modeli so namreč zelo kompleksni in vsebujejo veliko število parametrov, katerih vrednosti so v večini primerov le ocenjene na velikostni razred. Z optimizacijo parametrov modelov lahko torej najdemo več lokalnih minimumov, ne pa nujno globalnega, kot smo ugotovili v naši študiji (Dermol-Černe in Miklavčič 2018). Že pri sami geometriji lokalnih transportnih območij, ki nastanejo pri elektroporaciji, se vrednosti iz literature razlikujejo. Velikosti lokalnih transportnih območij se razlikujejo za več velikostnih razredov – od 10 μm do več sto mikrometrov (Pliquett et al. 1996; Pliquett et al. 1998; Gowrishankar et al. 1999a; Vanbever et al. 1999; Pavšelj in Miklavčič 2008a), primanjkuje pa meritev časovne dinamike širjenja por.

V prihodnosti bi modele, ki smo jih predstavili v tej disertaciji, lahko vpeljali v načrtovanje medicinskih posegov elektroporacije. Trenutno parametre zdravljenja optimiziramo tako, da zagotovimo, da je celoten tumor pokrit z dovolj visokim električnim poljem, okoliško tkivo pa je nepoškodovano. V začetku bi lahko najprej vpeljali matematične modele prepustnosti celične membrane in celične smrti, nato bi vključili modele transporta, s katerimi bi izračunali doseženo znotrajcelično koncentracijo kemoterapevtika oziroma točno število molekul znotraj posameznih celic. Lahko bi tudi zmanjšali krčenje mišic in bolečino, kar bi

skrajšalo in poenostavilo zdravljenje. Z vključitvijo meritev električnega polja v tkivu (Kranjc et al. 2014; Kranjc et al. 2015) pa bi se dalo odziv zdravljenja napovedati še bolj točno.

Matematično modeliranje procesov med elektroporacijo ima vsekakor prihodnost. Menim, da opis procesa z modelom olajša naše razumevanje. Uporaba modelov nam omogoča, da rezultate interpoliramo, saj izvajanje nešteto poskusov vseh možnih kombinacij ni smiselno tako s časovnega kot tudi s finančnega vidika. V okviru doktorske disertacije sem odgovorila na večino vprašanj, ki sem si jih postavila na začetku dela. Med delom pa so se porodila številna nova vprašanja, na katera je v prihodnosti vredno poiskati odgovor.

Izvirni prispevki k znanosti

V doktorski disertaciji so naslovljeni trije izvirni prispevki k znanosti.

Matematično modeliranje prepustnosti celične membrane in celične smrti

Z matematičnim modeliranjem lahko opišemo verjetnost za prepustnost ali celično smrti na ravni tkiv. Naredili smo pregled modelov prepustnosti celične membrane s področja elektroporacije evkariontskih celic in modelov celične smrti s področja elektroporacije evkariontskih in prokariontskih celic. Obstoječi modeli so večinoma izbrani na podlagi najboljšega ujemanja z rezultati poskusov in ne izhajajo iz mehanizmov elektroporacije. Parametre naših izbranih modelov smo določili s pomočjo rezultatov poskusov in vitro. Enostaven prenos optimiziranih modelov z ravni celic na tkiva ni mogoč. Ker moramo za vsako vrsto tkiva in vsako skupino električnih parametrov posebej optimizirati matematične modele, je njihova napovedna moč omejena.

Prehod modeliranja z nivoja ene same celice na nivo tkiv, pri čemer je predstavljen realističen tridimenzionalen model kože nadgrajen z modelom elektroporacije vseh bistvenih delov in sestavnih plasti

Elektroporacija celic in tkiv spremeni njihove električne lastnosti. V okviru doktorske disertacije smo modelirali časovno odvisno spremembo električne prevodnosti posameznih celic v koži – korneocitov, keratinocitov, papilarnega dermisa. Modelirali smo nastanek lokalnih transportnih območij v roženi plasti in nastanek por na celicah v spodnjih plasteh kože. Iz električnih lastnosti celic smo izračunali enakovredne električne lastnosti plasti kože – rožene plasti, epidermisa, papilarnega dermisa in žilne plasti. Naše izračune smo primerjali s tokovnonapetostnimi meritvami med elektroporacijo kože. Z našo metodo lahko modeliramo električne lastnosti med elektroporacijo katerih koli celic in tkiv. Edini pogoj je, da poznamo geometrijo celice ter električne lastnosti znotrajcelične tekočine, celične membrane in zunajceličnega prostora.

Matematično modeliranje transporta molekul (kemoterapevtika) skozi celično membrano na osnovi modela dvojne poroznosti

Za učinkovito elektrokemoterapijo je nujen vnos zadostne količine kemoterapevtika v celice. V načrtovanju posegov ob uporabi kritičnega električnega polja izračunamo, ali bo določeno območje uničeno ali ne, pri tem pa ne upoštevamo transporta kemoterapevtika v tumorske celice. V okviru tretjega izvirnega prispevka smo modelirali transport pri elektroporaciji tumorjev. Z modelom dvojne poroznosti smo izračunali in vitro koeficiente prepustnosti celične membrane v odvisnosti od parametrov električnega polja. Model dvojne poroznosti z diferencialnimi enačbami opiše difuzijo majhnih molekul topljenca skozi celično membrano in v tkivu. V numeričnem modelu tumorja smo s koeficientom prepustnosti izračunali transport po tumorju pri elektrokemoterapiji in model primerjali z rezultati vnosa cisplatina v podkožne tumorje na miših. Model je dobro opisal rezultate poskusov, če smo vanj vključili še koeficient transformacije, s katerim smo upoštevali razlike v mobilnosti majhnih molekul in vitro ter in vivo. V prihodnosti bi model lahko uporabili v načrtovanju posegov elektroporacije, kjer bi tako povišali natančnost napovedi celične smrti.

Introduction

Electroporation – mechanisms, and use

When short high voltage pulses are applied to cells and tissues, plasma membrane becomes transiently permeable to molecules which otherwise cannot freely pass in or out of the cell (Tsong 1991; Weaver 1993; Kotnik et al. 2012; Rems and Miklavčič 2016; Rems and Miklavčič 2016). The phenomenon is called electroporation as pores are presumably formed in the cell membrane (Abidor et al. 1979). After electroporation, pores can reseal, and cells recover – we consider this reversible electroporation. If the damage to the cell membrane is too extensive or if the homeostasis is severely altered, cells die - we consider this irreversible electroporation (Jiang et al. 2015a). Electroporation or pulsed electric field treatment is used in biotechnology (Haberl et al. 2013a; Haberl et al. 2013b; Mahnič-Kalamiza et al. 2014b; Kotnik et al. 2015), food-processing (Toepfl et al. 2014; Mahnič-Kalamiza et al. 2014b; Blahovec et al. 2017) and medicine (Yarmush et al. 2014). In medicine, it is used in gene electrotransfer (Daud et al. 2008; Heller and Heller 2015), DNA vaccination (Vasan et al. 2011; Gothelf and Gehl 2012; Calvet et al. 2014; Trimble et al. 2015), transdermal drug delivery (Denet et al. 2004; Zorec et al. 2013b), irreversible electroporation as a soft tissue ablation technique (Davalos et al. 2005; Garcia et al. 2010; Deodhar et al. 2011b; José et al. 2012; Cannon et al. 2013; Scheffer et al. 2014a; Jiang et al. 2015a; Ting et al. 2016; Lyu et al. 2017) and electrochemotherapy (Mali et al. 2013; Miklavčič et al. 2014; Edhemović et al. 2014; Campana et al. 2014; Mali et al. 2015; Gasbarrini et al. 2015; Bianchi et al. 2016).

Treatment planning of electrochemotherapy and ablation with irreversible electroporation

When treating tissues with electroporation-based medical treatments, we can use predefined electrode geometries and pulse parameters (Marty et al. 2006; Mir et al. 2006). When tumors are outside the target parameters, variable electrode geometry can be used. In this case, electrode geometry and pulse parameters have to be defined for each treatment separately (Kos et al. 2010; Miklavčič et al. 2010; Pavliha et al. 2012; Linnert et al. 2012; Edhemović et al. 2014). This is done in the process called treatment planning, when tumour geometry is extracted from medical images (Pavliha et al. 2013), and position and number of electrodes and electric pulse parameters are optimized to cover a tumour with a sufficiently high electric field for reversible or irreversible electroporation (Miklavčič et al. 2006a), depending on the chosen treatment. Simplifications done in the process and addressed in this thesis are the following.

1)   For each tissue type, the critical electric field for permeabilization or cell death used in the treatment planning was experimentally determined (Šel et al. 2005; Čorović et al. 2012). However, in reality, the transition from non-permeable to permeable cells and from alive to dead is continuous and should be described with appropriate continuous function.

2)   A possible upgrade of treatment plans is also taking into account excitability of tissues. In electroporation-based medical treatments, also excitable tissues are treated, either intentionally for example in irreversible electroporation of brain cancer (Salford et al. 1993; Agerholm-Larsen et al. 2011; Linnert et al. 2012; Garcia et al. 2012), gene electrotransfer (Hargrave et al. 2013; Hargrave et al. 2014; Bulysheva et

al. 2016) or ablation of the heart muscle (Lavee et al. 2007; Neven et al. 2014b; Neven et al. 2014a), and gene electrotransfer of skeletal muscles (Aihara and Miyazaki 1998; Heller and Heller 2015), or unintentionally when excitable tissues are in the vicinity of the target treated area. Unintentionally, we can affect the neurovascular bundle (Neal et al. 2014; Ting et al. 2016) when treating prostate cancer, neurons when treating bone metastases (Tschon et al. 2015; Gasbarrini et al. 2015) or spinal cord when treating tumors in the spine (Tschon et al. 2015). One of the main drawbacks to the treatment of tissues with pulsed electric fields is the discomfort and pain associated with repeated electrical stimulation (Miklavčič et al. 2005; Županič et al. 2007; Arena and Davalos 2012; Golberg and Rubinsky 2012), the need to administer muscle relaxants and anaesthesia (Ball et al. 2010) and synchronization with the electrocardiogram (Mali et al. 2008; Deodhar et al. 2011a; Mali et al. 2015). The neurons responsible for pain sensation (nociceptors) can be stimulated by electric pulses (Nene et al. 2006; Jiang and Cooper 2011). An important advance of the treatment would be to determine a point at which maximum permeability of the membrane could be achieved while minimizing excitation of the exposed excitable tissues.

3)   During the delivery of electric pulses, the electric conductivity of tissues increases, which is in treatment planning described by a phenomenological sigmoid function (Šel et al. 2005; Ivorra et al. 2009; Essone Mezeme et al. 2012a; Neal et al. 2012). Another possibility to model change in electric conductivity is to model change in tissues' dielectric properties by including the electroporation mechanisms, for example, pore formation. When electric pulses are delivered to the skin, also local transport region formation could be included in the model. In this way, instead of an experimentally determined change in conductivity of tissues, we could model and predict it based on the parameters of the delivered pulses.

4)   In the treatment planning of electrochemotherapy, we assume that in tumors electric field above 0.4 kV/cm has to be achieved to permeabilize cells. The treatment plan does not take into account transport of chemotherapeutics. However, the above-critical electric field does not guarantee transport. In electrochemotherapy with bleomycin, cell death occurs due to the influx of bleomycin in the cell and consequent DNA breakage (Tounekti et al. 1993; Tounekti et al. 2001).

Dielectric properties of electroporated cells

Electroporation changes dielectric properties of cell membranes of single cells. We can assess this change with dielectric impedance spectroscopy (Abidor et al. 1993; Schmeer et al. 2004), current-voltage measurements (Pliquett and Wunderlich 1983; Pavlin et al. 2005; Pavlin and Miklavčič 2008; Suzuki et al. 2011), optical methods (Hibino et al. 1991; Griese et al. 2002) or patch clamp (Pakhomov et al. 2007; Wegner 2015; Yoon et al. 2016; Napotnik and Miklavčič 2017). Electroporation also increases electric conductivity of cell monolayers (Ghosh et al. 1993; Müller et al. 2003; Stolwijk et al. 2011; García-Sánchez et al. 2015). Similar measurements were employed in electroporation of tissues. Dielectric properties of human, animal and plant tissues can be measured by dielectric spectroscopy (Barnes and Greenebaum 2006; Ivorra and Rubinsky 2007; Grimnes and Martinsen 2008; Dean et al. 2008; Zhuang et al. 2012; Dymek et al. 2014; Dymek et al. 2014; Trainito et al. 2015; Zhuang and Kolb 2015), current-voltage measurements during electroporation (Pavlin et al. 2005; Cukjati et al. 2007; Ivorra and Rubinsky 2007; Pavlin and Miklavčič 2008; Ivorra et al. 2009; Chalermchat et al. 2010; Neal et al. 2012; Becker et al. 2014; Dymek et al. 2015; Dymek et al. 2015), electric impedance tomography (Davalos et al. 2002; Davalos et al.

2004; Granot and Rubinsky 2007; Meir and Rubinsky 2014), and magnetic resonance electric impedance tomography (Kranjc et al. 2014; Kranjc et al. 2015; Kranjc et al. 2017). The efficiency of electroporation can be predicted by the change in electric conductivity of tissues (Cukjati et al. 2007; Ivorra et al. 2009; Neal et al. 2012). When measuring dielectric properties of tissues, secondary effects can affect measurements – such as change of cell radii (Serša et al. 2008; Sano et al. 2010; Deodhar et al. 2011b; Calmels et al. 2012), forming of edema (Ivorra et al. 2009), loss of ions from the cells (Pavlin et al. 2005), vascular lock (Ivorra and Rubinsky 2007; Serša et al. 2008). Electroporation changes specific conductivity of tissues mostly in the range of the β dispersion (Pliquett et al. 1995; Ivorra and Rubinsky 2007; Garner et al. 2007; Oblak et al. 2007; Ivorra et al. 2009; Neal et al. 2012; Zhuang et al. 2012; Salimi et al. 2013) because pore formation in the cell membrane affects cell membrane polarization due to increase in its electric conductivity.

Transport during and after electroporation

Transport during and after electroporation can occur via three different mechanisms: diffusion, electrophoresis, and endocytosis. During pulses the transport is electrodiffusive (Li and Lin 2011; Sadik et al. 2013), and after the pulses, it is diffusive (Pucihar et al. 2008). Endocytosis was observed after application of longer low-voltage pulses (Rols et al. 1995; Antov et al. 2005).

In vitro, transport due to electroporation is relatively easy to determine using fluorescent dyes and techniques like fluorescent microscopy, flow cytometry, spectrofluorometric measurements (Napotnik and Miklavčič 2017). In vivo, the transport due to electroporation is challenging to assess. [57]Co-bleomycin (Belehradek et al. 1994), ^{111}In-bleomycin (Engström et al. 1998), ^{99m}Tc-DTPA (Grafström et al. 2006), ^{51}Cr-EDTA (Batiuškaitė et al. 2003), gadolinium (Garcia et al. 2012), lucifer yellow (Kranjc et al. 2015) and cisplatin (Melvik et al. 1986; Čemažar et al. 1998; Čemažar et al. 1999; Ogihara and Yamaguchi 2000; Čemažar et al. 2001; Serša et al. 2010; Hudej et al. 2014; Čemažar et al. 2015) were already described in the literature.

When modeling transport, we have to keep in mind that the conditions in vitro and in vivo are different. In vitro, at a single cell level, the solute surrounds the cells. Solute can pass cell membrane anywhere as long as the membrane is permeable. The transport in the extracellular space is not limited. If there is enough of solute in the extracellular space, the transport stops when the cell membrane reseals. The transport through the membrane can be directly linked to the cell membrane permeability (Mahnič-Kalamiza et al. 2015). In vivo, the initial solute concentration varies spatially. All the solute available can enter cells before the membrane reseals, i.e., the extracellular compartment can be locally depleted. The transport of solute occurs via diffusion and convection (Canatella et al. 2004). Cells are close together which decreases the possible area for the uptake and decreases the induced transmembrane voltage due to electric field shielding. Already in spheroids, it was shown that transport of small molecules was spatially heterogeneous (Canatella et al. 2004; Gibot et al. 2013). Electric pulses cause vasoconstriction (Serša et al. 2008) which limits the transport of solute in or out of a tumor. Increased interstitial pressure, heterogeneous perfusion, defective lymphatic system, binding of drugs to non-target molecules and metabolism additionally affect transport in a tumor (Baxter and Jain 1989; Baxter and Jain 1990; Baxter and Jain 1991; Jain 1999).

It should be kept in mind that an increase in cell membrane conductivity is not the same as the increase in its permeability (Wegner et al. 2015). An increase in cell membrane conductivity starts immediately after pulse application (Pavlin and Miklavčič 2008) while the transport due to increased cell membrane permeability lasts for minutes or even hours after the application of electric pulses (Saulis et al. 1991; Golzio et al. 2002). Sufficiently high increase in conductivity indicates that the transport will occur (Cukjati et al. 2007; Ivorra and Rubinsky 2007; Pavlin and Miklavčič 2008; Ivorra et al. 2009; Neal et al. 2012)

Models of electroporation

Mathematical modeling offers a concise description of biological phenomena using mathematical and physical laws; it improves our understanding, our predictions, and decreases the number of needed experiments. In the clinical setting, modeling can help predict the treatment outcome and optimize the treatment to achieve the best results. In the field of electroporation, different spatial scales of biological systems are modeled separately: level of molecules (phospholipids), lipid bilayers, cells, and tissues. If in the process of modeling we do not achieve good agreement with experimental data, this indicates that we have not modeled all the relevant processes.

Models at the level of molecules

With molecular dynamics simulations, we can model how different molecules and ions behave when exposed to an electric field (Tieleman 2006; Böckmann et al. 2008; Delemotte and Tarek 2012; Casciola and Tarek 2016), but we are restrained to the time scale of 100 to 1000 nanoseconds. Molecular dynamics studies propose that during electroporation water fingers are formed in the cell membrane. Water fingers then evolve to hydrophilic pores. Molecular dynamics simulations were compared with experimental data – in simulations it was predicted that siRNA could cross the cell membrane in a few nanoseconds, which was also shown experimentally (Breton et al. 2012).

Models at the level of lipid bilayers

In polar solvent like water lipids spontaneously form a lipid bilayer. Models of electroporation of lipids bilayers are of three main groups (Chen et al. 2006a; Pavlin et al. 2008; Rems and Miklavčič 2014). In the first group are deterministic electromechanical models - hydrodynamic, elastic, hydroelastic, viscoelastic, where membranes are treated as elastic bodies, and their behavior is described with laws of electrostatic. This first group of models does not describe electroporation well. In the second group are models of pore formation which are stochastic and are derived from energy equations (Abidor et al. 1979). Pore formation and development during pulse application can be described by the Smoluchowski equation. The Smoluchowski equation is computationally demanding and was simplified by Neu and Krassowska to its asymptotic form (Neu and Krassowska 1999; Neu and Neu 2009). In the asymptotic form, we assume that all pores in the cell membrane are of fixed radii. The asymptotic model can be upgraded to include also increase in pore radii, but it is computationally demanding (Neu et al. 2003; Smith et al. 2004). In the third group is a kinetic scheme (Neumann et al. 1998; Miklavčič and Towhidi 2010), where lipid bilayer changes between permeable and non-permeable state (Böckmann et al. 2008). Transport of small molecules through a single pore can be modeled with the electrodiffusion equation (Granot and Rubinsky 2008; Li and Lin 2011; Smith and Weaver 2011; Movahed and Li 2012; Movahed and Li 2013). It was determined that

continuum models of electroporation of lipid bilayers correspond well to molecular dynamics simulations (Casciola et al. 2016; Rems et al. 2016).

Models at the level of single cells

Lipid bilayer together with proteins forms cell membrane. Cell membrane can be approximated by a dielectric surrounded by a conductor. At the cell level, there are several models existing – models of induced transmembrane voltage, pore formation, transport, permeability, cell death, and change in electric conductivity of cell. Time and spatial change of induced transmembrane voltage can be analytically calculated for isolated cells of simple shapes (Kotnik and Miklavčič 2000a; Kotnik and Miklavčič 2000b; Valič et al. 2003) but requires a numerical calculation for other more complicated shapes (Pucihar et al. 2006). When the induced transmembrane voltage is known, pore formation can be described either with asymptotic equation (Neu and Krassowska 1999; Neu and Neu 2009) or by also including the change in pore radii (Smith et al. 2004; Smith et al. 2014). Transport of molecules into a single cell can be described with the Neumann's kinetic scheme (Neumann et al. 1998; Miklavčič and Towhidi 2010), the pharmacokinetic model (Puc et al. 2003) or with the electrodiffusion equation (Pucihar et al. 2008; Li and Lin 2011; Li et al. 2013; Sadik et al. 2013; Sadik et al. 2014; Blumrosen et al. 2016). Electrical properties of cells can be calculated with an equivalent circuit (Pethig 1984; Gowrishankar and Weaver 2003). Cell permeability and cell survival can be modeled with mathematical models (Schoenbach et al. 2009; Dermol 2014; Dermol and Miklavčič 2014; Dermol and Miklavčič 2015; Dermol and Miklavčič 2016) which accurately describe the shape of the permeability and survival curves but are phenomenological and are not based on any mechanisms of electroporation. Cell permeability and conductivity can be modeled separately as two phenomena (Miklavčič and Towhidi 2010; Leguèbe et al. 2014).

Models at the level of cell clusters and tissues

Several cells together form either a monolayer or a tissue. Current tissue models are of two types – they either model the tissue as a bulk (Šel et al. 2005; Čorović et al. 2007; Pavšelj et al. 2007; Pavšelj and Miklavčič 2008b; Golberg and Rubinsky 2010; Neal et al. 2012; Čorović et al. 2012; Garcia et al. 2014) or also model the tissues' microscopic structure (Gowrishankar and Weaver 2003; Stewart Jr. et al. 2005; Gowrishankar and Weaver 2006; Esser et al. 2007; Joshi et al. 2008; Esser et al. 2009; Essone Mezeme et al. 2012b; Dymek et al. 2015).

The bulk tissue models describe the electric field distribution as a function of tissue properties, applied voltage and the geometry of the electrodes. Transport to cell clusters or tissues was modelled by statistical models which describe the data well but do not include specific transport mechanisms (Canatella and Prausnitz 2001), the kinetic scheme of electroporation (Neumann et al. 1998; Miklavčič and Towhidi 2010), the pharmacokinetic model (Puc et al. 2003; Agarwal et al. 2009), the electrodiffusion equation or the dual-porosity model (Mahnič-Kalamiza et al. 2014a; Mahnič-Kalamiza et al. 2015). The dual porosity model (Mahnič-Kalamiza et al. 2014a; Mahnič-Kalamiza et al. 2015) is based on the diffusion equation, connects pore formation with membrane permeability, and includes transport between several compartments - in our case between tumor cells, interstitial fraction and peritumoral environment and has the possibility to include also thermal relations (Mahnič-Kalamiza et al. 2017). Boyd and Becker also used the dual porosity model

by combining it with equations for the degree of electroporation, change of electrical conductivity, and membrane resealing (Boyd and Becker 2015; Argus et al. 2017).

The models in the second group include properties of single cells and thus local inhomogeneities. If tissues are made of spheroidal cells in low-volume fractions, their effective dielectric properties can be calculated using the Maxwell-Wagner, the Hanai-Bruggeman, and other approximations (Asami 2002). Tissue was sampled using Cartesian transport lattices and current, voltage, and electric charge through the lattice were calculated using the Kirchhoff's laws (Gowrishankar and Weaver 2003; Stewart Jr. et al. 2005; Gowrishankar and Weaver 2006; Esser et al. 2007; Esser et al. 2009). The equivalent circuit was used to analyze the effects of electroporation on cells and then averaged to obtain results for tissues (Ramos et al. 2003; Ramos 2005). Tissue was modeled with the two-dimensional Voronoi network, and the induced transmembrane voltage was calculated in each region (i.e., cell) (Joshi et al. 2008) The weakness of these models is, however, that they are in two-dimensions. Besides, in tissues, cells are packed close together, the local electric field decreases due to electric field shielding, and consequently, the induced transmembrane voltage is lower than in isolated cells (Susil et al. 1998), there are the blood flow (Serša et al. 2008), and the immune system (Serša et al. 1997; Neal et al. 2013; Serša et al. 2015) present. In 3-dimensions, tissue was numerically modeled as an infinite lattice of spherical cells (Pavlin et al. 2002; Ramos 2010). The cells were all of the same size, electrically unconnected and in an iterative arrangement which is not in agreement with the circumstances in tissues. Besides, maximal volume fraction was lower than the ones we encounter in most tissues. The model was upgraded using randomly distributed spheres of different sizes to model change in electric conductivity of the cell membrane and the fraction of permeabilized cells (Essone Mezeme et al. 2012b). A similar model was built for the description of electroporation of spinach leaves. The authors adapted the shapes and sizes of cells to the morphology of a spinach leaf; however, they modeled only a small part of a leaf (Dymek et al. 2015). The model by Huclova et al. (Huclova et al. 2010; Huclova et al. 2011; Huclova et al. 2012) offers a more realistic description since cells can be of different shapes, sizes, and distances between them can be adapted. The dielectric properties of cells are then averaged to obtain properties on the tissue level. The model by Huclova et al. describes the behavior of cells in the linear range, but we have added electroporation to it (Dermol-Černe and Miklavčič 2018). Instead of numerical calculations, the properties of tissues can be calculated analytically. The frequency dependent dielectric properties of tissues can be described using phenomenological models – the Debye, the Cole-Cole, and other models (Gabriel et al. 1996a; Gabriel et al. 1996b; Gabriel et al. 1996c; Asami 2002).

Aim

The aim of this thesis can be summarized in two points:

1) Use mathematical models to model cell membrane permeability and depolarization and cell death;
2) Include mechanisms of electroporation in models of change in dielectric properties of tissues and transport due to electroporation.

In the scope of the first aim, we fitted several mathematical models to experimental data of cell membrane permeability and cell death. We predicted the percentage of permeable cells, exposed to the inhomogeneous electric field, from the experiments on cells, exposed to the homogeneous electric field. We used optimized mathematical models of cell membrane permeability. We compared permeability and depolarization of cell membranes of excitable and non-excitable cells and modeled both phenomena. We made a review of the existing cell death models, usually employed in prediction of liquid food pasteurization and sterilization, and fitted the existing models to our experimental data of cell death caused by irreversible electroporation. We focused on time dynamics of dye uptake due to increased cell membrane permeability and the correlation between the membrane resealing and the transport of dye to cells.

In the scope of the second aim, we focused on two important phenomena present during electroporation – change in dielectric properties of cells and tissues and increased transport of molecules in and out of the cells. We studied the change in dielectric properties of skin when either long low-voltage or short high-voltage pulses were applied. We determined the contribution of local transport regions in the stratum corneum and the pore formation in the lower layers to the overall increase in electric conductivity. We modeled the pore formation with the asymptotic pore model and correlated the pore formation and local transport region formation to the shape of the current-voltage measurements in the Franz diffusion cell.

We also studied the transport of small molecules (e.g., cisplatin) in the tumor tissue after electroporation. We modeled cisplatin uptake by tumor cells in mouse melanoma tumors. Animal experiments take a long time, a limited number of parameters can be tested due to ethical issues, and they are expensive. Thus, we aimed to determine if experiments on cell level can be used to predict the treatment outcome in animal experiments with a possibility of later translation to medical treatments. We investigated the contribution of close cell contacts, high cell volume fraction and smaller available area of cell membrane for transport in vivo. We determined that cisplatin uptake in vivo can be determined from the cisplatin uptake in vitro, provided we take into account reduced mobility of the molecules.

Results and Discussion

In the present thesis, the aim was to link experiments on cell level (in vitro) to experiments on tissue level (in vivo) by using models describing electroporation-related processes at a single cell level and processes at the tissue level. Three original scientific contributions were made:

1. Mathematical modeling of cell membrane permeability and cell death;
2. The transition between single-cell models and the tissue models, where the realistic three-dimensional skin model is presented with the model of electroporation of all components and essential layers of the skin.
3. Mathematical modeling of transport of small molecules (chemotherapeutic) across the cell membrane using the dual porosity model.

The work presented in this thesis consists of two parts – experimental in a cell culture laboratory and modeling. I believe that only by using modeling we can understand experimental results and vice versa – models are only relevant when they are based on experimental measurements. Models based on a good experimental data facilitate our understanding of the modeled phenomena, enable us to make predictions about the behavior of biological systems and decrease number of needed experiments.

The work done in the scope of this thesis was presented in six papers and a book chapter. There, the results are presented and thoroughly discussed. Thus, the Results and Discussion section consist of the published papers, and the thesis will continue with a Conclusion and Future Work section. A summary of the work is the following.

The first contribution was addressed in four papers and one book chapter.

Paper 1 (Dermol and Miklavčič 2014) entitled **Predicting electroporation of cells in an inhomogeneous electric field based on mathematical modeling and experimental CHO-cell permeabilization to propidium iodide determination** described mathematical models of cell membrane permeability. We focused on four models – the symmetric and asymmetric sigmoid, the hyperbolic tangent and the Gompertz curve. From experimental data of the cell membrane permeability obtained on attached cell monolayers exposed to the homogeneous electric field, we predicted cell membrane permeability in the inhomogeneous electric field. Prediction of permeability was possible if the density of the cells in the homogeneous field was comparable to the density of cells in the inhomogeneous field. We conclude that models describing cell electroporation probability could be useful for development and presentation of treatment planning for electrochemotherapy and non-thermal irreversible electroporation.

Paper 2 (Dermol and Miklavčič 2015) entitled **Mathematical Models Describing Chinese Hamster Ovary Cell Death Due to Electroporation In Vitro** focused on mathematical models of cell survival. We exposed cell suspension to pulses of parameters similar to irreversible electroporation parameters - several tens of 100 μs long pulses of up to 4 kV/cm, delivered at the repetition frequency 1 Hz. Cell survival was evaluated with the clonogenic assay. Several models of survival previously used in the literature were fitted to our experimental results. The models were: the first-order kinetics, the Hülsheger, the Peleg-Fermi, the

Weibull, the Logistic, the adapted Gompertz, and the Geeraerd model. The most appropriate models of cell survival as a function of the treatment time were the adapted Gompertz and the Geeraerd models and, as a function of the electric field, the logistic, the adapted Gompertz, and the Peleg-Fermi models. The next steps to be performed are a validation of the most appropriate models on tissues and determination of the models' predictive power. A review of cell death models of the eukaryotic and prokaryotic cells is written in the book chapter (Dermol and Miklavčič 2016) entitled **Mathematical Models Describing Cell Death Due to Electroporation**.

Paper 3 (Dermol-Černe et al. 2018) entitled **Plasma membrane depolarization and permeabilization due to electric pulses in cell lines of different excitability** consists of the experimental part and modeling part regarding the cell depolarization and cell membrane permeability. The aspect of excitability is important when treating excitable tissues with electroporation or when excitable tissues are in the vicinity of the treated area. The experimental strength-duration curve to one pulse of length 10 ns – 10 ms was determined for excitable and non-excitable cells and then modeled with the Lapicque curve and the Hodgkin-Huxley model. The Hodgkin-Huxley model gave insight into the ability of the short bipolar to permeabilize but not excite the tissue. The permeability curve to one pulse of length 100 ns – 100 ms was obtained from the literature along with the Saulis model, and was additionally modeled with the Schwann equation. The depolarization threshold was higher for the excitable cells than for the non-excitable cells. All four cell lines responded similarly to pulses of standard electrochemotherapy parameters, and their permeability curves were modeled with the symmetric sigmoid. Thus, electroporation is a feasible means of treating excitable and non-excitable cells with pulses of similar parameters. Our results show the potential of achieving cell membrane permeability and minimizing or avoiding excitation/pain sensation which needs to be explored in more detail. In future studies, it should be established, to what extent the in vitro depolarization and excitability correlate to the actual excitation and pain sensation in vivo.

Paper 4 (Dermol et al. 2016) entitled **Cell Electrosensitization Exists Only in Certain Electroporation Buffers** consists of experimental work on the effect of pulse delivery in one or several trains on the uptake. Electroporation-induced cell sensitization was described as the occurrence of delayed hypersensitivity to electric pulses caused by pretreating cells with electric pulses. It was achieved by increasing the duration of the electroporation treatment at the same cumulative energy input. It could be exploited in electroporation-based treatments such as electrochemotherapy and tissue ablation with irreversible electroporation. The mechanisms responsible for cell sensitization, however, have not yet been identified. We investigated cell sensitization dynamics in five different electroporation buffers. We split a pulse train into two trains varying the delay between them and measured the time dynamics of propidium uptake by fluorescence microscopy. By fitting the first-order model to the experimental results, we determined the uptake due to each train (i.e., the first and the second) and the corresponding resealing constant. Cell sensitization was observed in the growth medium but not in other tested buffers. The effect of pulse repetition frequency, cell size change, cytoskeleton disruption and calcium influx do not adequately explain cell sensitization. Based on our results, we can conclude that cell sensitization is a sum of several processes and is buffer dependent. Further research is needed to determine its generality and to identify underlying mechanisms.

The second contribution was addressed in one paper.

Paper 5 (Dermol-Černe and Miklavčič 2018) entitled **From cell to tissue properties – modeling skin electroporation with pore and local transport region formation** modeled skin electroporation by pore formation and local transport region formation at the level of single cells and skin layers. We showed that it is possible to model electroporation at the level of single cell and then generalize the results to the bulk tissue where calculations are considerably faster. Current models of tissue electroporation either describe tissue with its bulk properties or include cell level properties, but model only a few cells of simple shapes in low-volume fractions or are in two dimensions. We constructed a 3-dimensional model of realistically shaped cells in realistic volume fractions. By using a 'unit cell' model, the equivalent dielectric properties of whole tissue could be calculated. We calculated the dielectric properties of electroporated skin. We modeled electroporation of single cells by pore formation on keratinocytes and on the papillary dermis which gave dielectric properties of the electroporated epidermis and papillary dermis. During skin electroporation, local transport regions were formed in the stratum corneum. We modeled local transport regions and increase in their radii or density which affected the dielectric properties of the stratum corneum. The final model of skin electroporation accurately described measured electric current and voltage drop on the skin during electroporation with long low-voltage pulses. The model also accurately described voltage drop on the skin during electroporation with short high-voltage pulses. However, our results indicated that during application of short high-voltage pulses additional processes might occur which increased the electric current. Our model connects the processes occurring at the level of cell membranes (pore formation), at the level of a skin layer (formation of local transport region in the stratum corneum) with the tissue (skin layers) and even level of organs (skin). Using a similar approach, electroporation of any tissue can be modeled, if the morphology of the tissue is known.

The third contribution was addressed in one paper.

Paper 6 (Dermol-Černe et al. 2018, submitted) entitled **Connecting the in vitro and in vivo experiments in electrochemotherapy: Modeling cisplatin transport in mouse melanoma by the dual-porosity model** was a modeling study where transport of chemotherapeutic in the tumor cells was modeled by the dual-porosity model based on experimental results obtained on cell suspension. In electrochemotherapy two conditions have to be met to be successful – the electric field of sufficient amplitude and sufficient uptake of chemotherapeutics. Current treatment plans only take into account the critical electric field to achieve cell membrane permeability. However, increased permeability of cell membrane alone does not guarantee uptake of chemotherapeutics and consequently successful treatment. In our study, we described the transport of cisplatin in vivo based on experiments performed in vitro. In vitro, a spectrum of parameters can be explored without ethical issues. In the experimental part of our study, we performed in vitro and in vivo experiments. Mouse melanoma B16-F1 cell suspension and inoculated B16-F10 tumors were exposed to electric pulses in the presence of the chemotherapeutic cisplatin. The uptake of cisplatin was measured by the inductively coupled plasma mass spectrometry. In modeling part of our study, we modeled the transport with the dual-porosity model which is based on the diffusion equation, connects pore formation with membrane permeability, and includes transport between several compartments. In our case, there were three compartments - tumor cells, interstitial fraction and peritumoral region. Our hypothesis was that in vitro permeability coefficient can be introduced in vivo, as long as tumor physiology is taken into account.

A transformation from in vitro to in vivo was possible by introducing a coefficient of transformation which takes into account in vivo characteristics, i.e., the smaller available area of the plasma membrane for transport due to high cell density, and presence of cell-matrix in vivo, thus reducing drug mobility. Our model offers a step forward to linking transport models at the cell level (in vitro) to the tissue level (in vivo).

Paper 1

Title: **Predicting electroporation of cells in an inhomogeneous electric field based on mathematical modelling and experimental CHO-cell permeabilization to propidium iodide determination**

Authors: Janja Dermol and Damijan Miklavčič

Publication: *Bioelectrochemistry,* vol. 100, pp. 52–61, Dec. 2014.

DOI: 10.1016/j.bioelechem.2014.03.011

Impact factor: 4.172 (2014), 3.854 (5-year)

Quartile: Q1 (Biology, Biophysics, Electrochemistry)

Rank: 13/85 (Biology), 15/73 (Biophysics), 5/28 (Electrochemistry)

Predicting electroporation of cells in an inhomogeneous electric field based on mathematical modeling and experimental CHO-cell permeabilization to propidium iodide determination

Janja Dermol, Damijan Miklavčič *

University of Ljubljana, Faculty of Electrical Engineering, Tržaška 25, SI-1000, Ljubljana, Slovenia

ARTICLE INFO

ABSTRACT

High voltage electric pulses cause electroporation of the cell membrane. Consequently, flow of the molecules across the membrane increases. In our study we investigated possibility to predict the percentage of the electroporated cells in an inhomogeneous electric field on the basis of the experimental results obtained when cells were exposed to a homogeneous electric field. We compared and evaluated different mathematical models previously suggested by other authors for interpolation of the results (symmetric sigmoid, asymmetric sigmoid, hyperbolic tangent and Gompertz curve). We investigated the density of the cells and observed that it has the most significant effect on the electroporation of the cells while all four of the mathematical models yielded similar results. We were able to predict electroporation of cells exposed to an inhomogeneous electric field based on mathematical modeling and using mathematical formulations of electroporation probability obtained experimentally using exposure to the homogeneous field of the same density of cells. Models describing cell electroporation probability can be useful for development and presentation of treatment planning for electrochemotherapy and non-thermal irreversible electroporation.

© 2014 Elsevier B.V. All rights reserved.

1. Introduction

High voltage electric pulses affect membrane's selective permeability. According to the theory electroporation of the membrane occurs as pores are formed in the membrane. Cell membrane thus becomes permeable for different molecules which otherwise cannot pass through the membrane in or out of the cell [1–3]. Increased membrane permeability occurs in the regions of the membrane where the transmembrane voltage exceeds a certain threshold, which is characteristic of each cell line, but also depends on pulse parameters [4,5]. If the cell is able to recover after the exposure to electric pulses we call this reversible electroporation. If the cell cannot recover and it does not survive electroporation we call it irreversible [6]. Electroporation is widely used in different areas—gene transfer [7–9], cancer treatment [10–12], biotechnology [13,14] and food processing [15–17].

When predicting the electroporation of cells, for example in a tissue, it is usually (implicitly) assumed that cells are electroporated if the induced transmembrane voltage exceeds the characteristic threshold [18,19]. If the induced transmembrane voltage is below the characteristic threshold the cells are not electroporated. In reality the transition from non-electroporated to reversibly and irreversibly electroporated

state is continuous. So far different mathematical models of electroporation have been proposed in the literature [20–22]. With the appropriately chosen mathematical model we could predict percentage of cells affected if a certain voltage is applied using specific electrode geometry.

In recent years electroporation based treatments have paved their way to clinical use. Electrochemotherapy for solid cutaneous, subcutaneous tumors and metastasis [11,23], as well as for deep seated tumors [24,25] is being used in clinics. Minimally invasive non-thermal irreversible electroporation as soft tissue ablation has also been proposed [6] and used in animal [26] and human clinics [27]. In all these cases treating deep seated tumors or soft tissue using minimally invasive procedures a need for pretreatment planning was clearly established [28–30]. Until now visualization of electric field distribution is used as being the most important predictor of tissue permeabilization and ablation [25,29,31,32].

There is a considerable number of studies of electroporation in dense cell suspensions available [33–36], but there are much less studies available on tissues [37–39]. In these latter studies besides the density of the cells, applied electric field, cell line, and cells' mutual electric shielding, the connections between the cells and their irregular shape could play an important role as well [4]. In our present study the experiments were performed on monolayers of cells of different densities.

When defining the duration and the voltage of the applied pulses we model the geometry of the electrodes and of the cells as a bulk 2D "tissue" layer. Electric field (E field) distribution is numerically calculated and

* Corresponding author. Tel.: +386 1 4768 456.
E-mail address: damijan.miklavcic@fe.uni-lj.si (D. Miklavčič).

adequate voltage is determined [40]. Because of the complexity of the tissues and electrodes analytical calculations are usually in most cases not possible. There is no conventional or easy way to measure E field in vivo. We have recently proposed a method based on current density imaging (CDI) and magnetic resonance electrical impedance tomography (MREIT) to measure E field in biological tissues [41,42]. However, the most reliable or even easy way is numerical modeling which we employed.

Until now, the calculated electric field is thresholded with two different thresholds to obtain three areas—the area where irreversible electroporation occurs, the area where reversible electroporation occurs and the area where electroporation does not occur. The cell response can be approximated with a step function. Electroporation is 100% if the applied electric field is above the characteristic electroporation threshold and 0% if it is below. In the same way area where irreversible electroporation occurs can be modeled. Irreversible electroporation is 100% if the applied electric field is above the characteristic threshold for irreversible electroporation and 0% if it is below.

The aim of our study was to predict a percentage of electroporated cells grown as a dense monolayer exposed to an inhomogeneous field. We performed experiments in a homogeneous electric field and determined the percentage of cell electroporation for a certain applied E. We used these results in four different mathematical models, which interpolated and extrapolated the percentage of electroporated cells to other values of E. We used homogeneous E for calculating parameters of the mathematical models because it is possible to determine the percentage of electroporated cells at a certain E. We validated the mathematical models by exposing cells to the inhomogeneous field and comparing predicted and experimentally determined values of percentage of electroporation. We used the inhomogeneous electric field for validation because in tumors and tissues the electric field around the electrodes is in almost all cases inhomogeneous. The predicted values were obtained by using the numerically calculated inhomogeneous E in mathematical models. We obtained the percentage of electroporation in the dependence on E for the area around the electrodes.

The advantage of this approach is that simple electrode geometry configurations can be used to calculate the parameters of the mathematical models. Mathematical models predicting cell electroporation can then be applied to arbitrary electrode geometry. This kind of mathematical relationship could allow us to present treatment plans in a clearer and more understandable way. At the moment, the treatment plans present the E field applied to a certain area of a tissue/tumor. Using this method the percentage of the electroporated area of a tissue/tumor could be shown. Eventually also the number and duration of pulses could be taken into account [43].

The block scheme on Fig. 1 shows the procedure used in our study. First, we exposed cells to the homogeneous field (block 1). Based on these results we determined the parameters of a mathematical model of cell electroporation (block 2). We used this mathematical model and inhomogeneous E field distribution to predict the percentage of electroporation (block 3). We then validated the model by exposing cells to the inhomogeneous field (block 4) by comparing predicted

and experimental values. If the results were not in good agreement, we adjusted the mathematical model (block 2) and repeated the prediction of electroporation and the validation of the mathematical model.

2. Methods

2.1. Cell line and cell culture

A series of experiments were performed on Chinese hamster ovary cells (CHO). Cells were grown in monolayers of different densities in Petri dishes 40 mm in diameter (TPP, Switzerland) in 2 mL of culture medium (Ham's Nutrient Mixtures HAM-F12, Sigma-Aldrich, Steinheim, Germany) supplemented with 10% FBS, antibiotics and L-glutamine for 2 days at 37 °C and 5% CO_2 (Kambič, Slovenia).

2.2. Pulse generator and pulse exposure

For the experiments electric pulse generator Cliniporator (IGEA, Italy) was used. For each experiment one rectangular pulse in the duration of 1 ms was applied. The voltages were chosen so that the maximal electric field in the homogeneous field was 1.6 kV/cm and in the inhomogeneous field it was 2.3 kV/cm. Therefore, for the homogeneous field the applied voltages were between 200 V and 800 V with a step of 200 V while for the inhomogeneous field the applied voltages were between 80 V and 140 V with a step of 20 V. Two different electrode configurations were used. For the homogeneous field two parallel Pt/Ir wire electrodes with 0.75 mm diameter and distance between the inner edges of the electrodes set at 5 mm [44] were positioned at the bottom of the Petri dish (Fig. 2a). For the inhomogeneous field we used one needle electrode pair with diameter 0.5 mm and distance between the inner edges of the electrodes set at 1.0 mm (Fig. 2b) [45].

Cells were exposed to the electric pulses in a medium of 1 mL HAM-F12 and 100 μL of 1.5 mM propidium iodide (PI). PI is a non-permeant fluorescent dye, which emits strong fluorescence after entering the cell and thus allows easy determination of cell electroporation and discrimination between electroporated and non-electroporated cells by thresholding fluorescent images (see 2.3 Fluorescence microscopy). After the exposure to an electric pulse the cells were incubated for 5 min at room temperature and then washed with HAM-F12.

2.3. Fluorescence microscopy

The cells were observed by an inverted microscope AxioVert 200 (Zeiss, Germany) under $10\times$ magnification. In each experiment in the homogeneous field up to five phase contrast and five corresponding fluorescent images were acquired from randomly selected fields of view between the electrodes. In the experiments in the inhomogeneous field four images were acquired when 80 V was applied and nine images when more than 80 V was applied to obtain the area around the electrodes. The number of experiments and images acquired in each experiment for each E for homogeneous field is shown in Table 1. The number
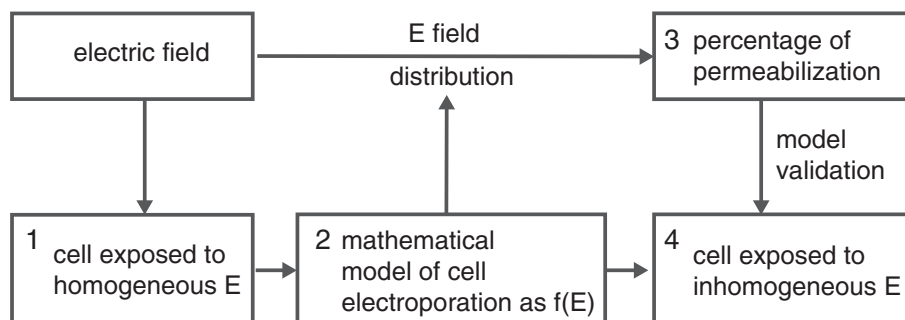

Fig. 1. A block scheme showing the layout of the article. Numbers in the blocks show the temporal sequence of our study.
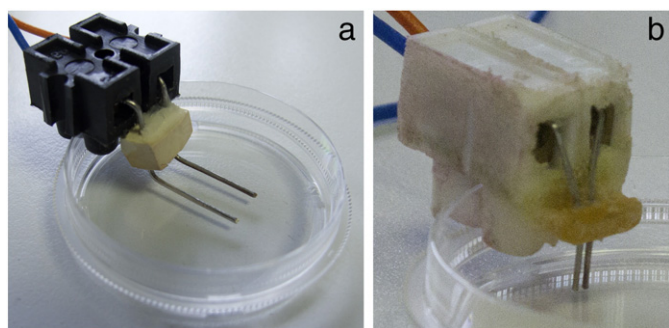
Fig. 2. Photos of electrodes, used in the experiments. a—Two parallel Pt/Ir wire electrodes with 0.75 mm diameter and distance between their inner edges set at 5 mm. b—One needle Pt/Ir electrode pair with diameter 0.5 mm and distance between the inner edges of the electrodes set at 1.0 mm.

of images used at different cell densities is also reported in Table 1. For the inhomogeneous field the number of experiments is reported in Table 2. In each experiment one pair of composed images was acquired (one fluorescent and one phase-contrast image). Fluorescent and phase-contrast images were then stacked together in Adobe Photoshop CS5 (Adobe Systems Inc., San Jose, CA, USA) to get one image of the whole area around the electrodes (Fig. 3a,b). For acquisition we used the VisiCam 1280 camera (Visitron, Germany) and MetaMorph PC software (Molecular Devices, USA).

2.4. Fitting of the mathematical models

First, the acquired fluorescent images from experiments in the homogeneous electric field were thresholded and electroporated cells were manually counted. Cells in the phase contrast images were manually counted as well. The percentage of the electroporated cells and standard deviation were calculated. The results were classified into three groups on the basis of the density of the cells i.e. on the number of the cells on the phase contrast images. The first group was the images with less than 300 cells, second was the images with density in the range from 300 to 600 cells and the third was the images with more than 600 cells per image. In Fig. 4 we can see how different groups of cell densities look like under the microscope. Fig. 4a shows a typical example of a least dense monolayer (less than 300 cells per image), Fig. 4b shows the typical example of a medium dense cell monolayer (from 300 to 600 cells per image) and Fig. 4c shows the densest monolayer (more than 600 cells per image).

Different mathematical models (symmetric sigmoid (Eq. (1)), asymmetric sigmoid (Eq. (2)), Gompertz curve (Eq. (3)) and hyperbolic tangent (Eq. (4))) suggested previously by other authors [20,46,47] were fitted in Matlab (R2010a, Mathworks, USA) to the experimental data of the percentage of electroporated cells in the homogeneous field using the method of non-linear least squares. We obtained an analytical

Table 2
Number of experiments (one petri dish and one composed image for one experiment) in the inhomogeneous field.

Voltage applied (V)	Number of experiments
80	9
100	12
120	6
140	8

expression with optimized parameters for each of the equations (Eqs. (1)–(4)).

$$p(E) = 1/(1 + \exp(-(E-E_{50\%})/b))^*100\% \tag{1}$$

$$p(E) = (1 + v^* \exp(-(E-E_{50\%})/b))^{\wedge}(-1/v)^*100\% \tag{2}$$

$$p(E) = \exp(-\exp(-(E-E_{50\%})/b))^*100\% \tag{3}$$

$$p(E) = (1 + \tanh(B^*(E-E_{50\%})))/2^*100\% \tag{4}$$

$E_{50\%}$ represents the electric field at which 50% of the cells are electroporated and p denotes the percentage of electroporated cells in the dependence of the applied electric field. Parameters b and B define the width of the curve, e.g. how quickly the cells go from the non-electroporated state to the electroporated state when the electric field is increasing. Parameter v defines the slope of the Eq. (2). E in all four equations means the applied electric field.

2.5. Modeling of the inhomogeneous electric field

Numerical calculations of the distribution of the inhomogeneous electric field were performed in COMSOL Multiphysics (version 3.5, COMSOL, Sweden). The model was made in the AC/DC module. The medium around the electrodes had its electrical conductivity set at 1.0 S/m which is the conductivity of the pulsing buffer. Since the pulse duration (1 ms) was much longer than a typical constant for polarization of the cell membrane (around 1 μs) [48] steady-state analysis was made. The calculated distribution of the electric field around the electrodes is shown in Fig. 5a.

The area around the electrodes in the inhomogeneous electric field was divided using contours into subareas where the electric field was within a certain range. An example of these contours is presented in Fig. 5b. When 80 V was applied the area was divided into 4 subareas, when 100 V was applied the area was divided into 5 subareas and when 120 V or 140 V was applied the area was divided into 6 subareas. The minimal electric field still analyzed was 0.30–0.39 kV/cm. The limits of the analyzed ranges of electric field for all of the applied voltages are presented in Table 3. Table 3 shows also the percentage of

Table 1
Number of experiments for each voltage in the applied homogeneous field. In each experiment at least three images were acquired from randomly chosen points of view. Number of image pairs (phase-contrast and fluorescent) for each density of the cells is reported in the 3rd, 4th and 5th columns.

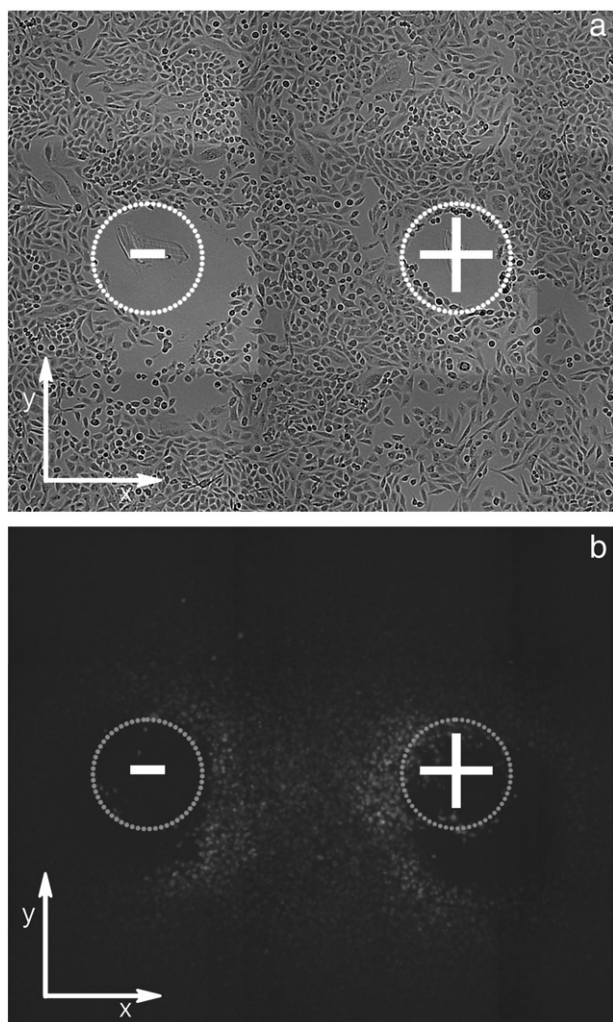| Applied voltage (V)	Number of experiments	Number of images (>600 cells/image)	Number of images (300–600 cells/image)	Number of images (<600 cells/image)
200	6	14	10	5
300	4	4	6	3
400	8	11	8	16
500	9	6	25	20
600	6	10	8	10
700	6	9	7	6
800	8	7	22	7

Fig. 3. a—Phase contrast composed image from under the microscope, 10× magnification, approximate position of the electrodes is marked with black circles, polarity of the electrodes is marked with + and − signs. b—Composed fluorescent image from under the microscope, 10× magnification, averaged 6 images, applied one pulse of 120 V, approximate position of the electrodes is marked with white circles, polarity of the electrodes is marked with + and − signs.

size of the area between two contours. The upper and lower limits of the area were set so that the areas between two contours were approximately the same in size. Therefore, the limits of the areas are not the same for different voltages applied (Table 3). For each of the applied voltages the corresponding contours (limits of the ranges of electric field) were superimposed to the microscopic images. An example of contours superimposed to the fluorescent image can be seen in Fig. 5c. The maximal values from Table 3 are based on a numerical calculation where this was the highest electric field value achieved when corresponding voltage was applied.

For each subarea from Table 3 cells on phase contrast images and on thresholded fluorescent images (Fig. 6a) were manually counted. The percentage of the electroporation and standard deviation in each area were determined.

In Comsol we transformed the calculated inhomogeneous electric field into the predicted percentage of the electroporated cells in the dependence on the geometry (Fig. 6b). We achieved transformation by using the numerically calculated inhomogeneous electric field values (Fig. 5a) in mathematical models (Eqs. (1)–(4)) with optimized coefficients to determine the predicted percentage of electroporated cells.

From the continuous distribution of the expected percentage of the electroporated cells (Fig. 6b) we determined areas with ranges of predicted percentage of electroporated cells. These areas had the same size and shape as the subareas of electric field around the electrodes (Fig. 5b). The values of the borders of these subareas were determined empirically. We put the image of areas with ranges of predicted percentage of electroporation on top of the image with areas with ranges of the electric field. We determined at which values of the borders the overlapping was complete. This allowed us to compare the predicted percentage of electroporation and the experimentally determined percentage of electroporation in the same subarea. The comparison was made for each of the mathematical models (Eqs. (1)–(4)) with optimized coefficients.

3. Results

We first determined the percentage of the electroporated cells exposed to a homogeneous electric field, and determined the influence of the cell density by fitting different mathematical models to the experimental data. Then we used the model with the best fit (highest R^2) to predict cell electroporation in the inhomogeneous field. Predicted values were compared to experimentally determined cell permeabilization in the inhomogeneous field.

3.1. Cell electroporation in a homogeneous electric field

Each of the four proposed mathematical models of electroporation (Eqs. (1)–(4)) was fitted to the experimental data from all three cell density groups, i.e. less than 300 cells per image, 300 to 600 cells per

the whole analyzed area without the electrodes taken by each of the ranges of electric field when different voltages are applied. Up to 0.8 kV/cm the limits are the same for all the applied voltages. The closer we get to the electrodes, the faster the electric field is increasing. Limits of electric field values in the inhomogeneous field were based on the
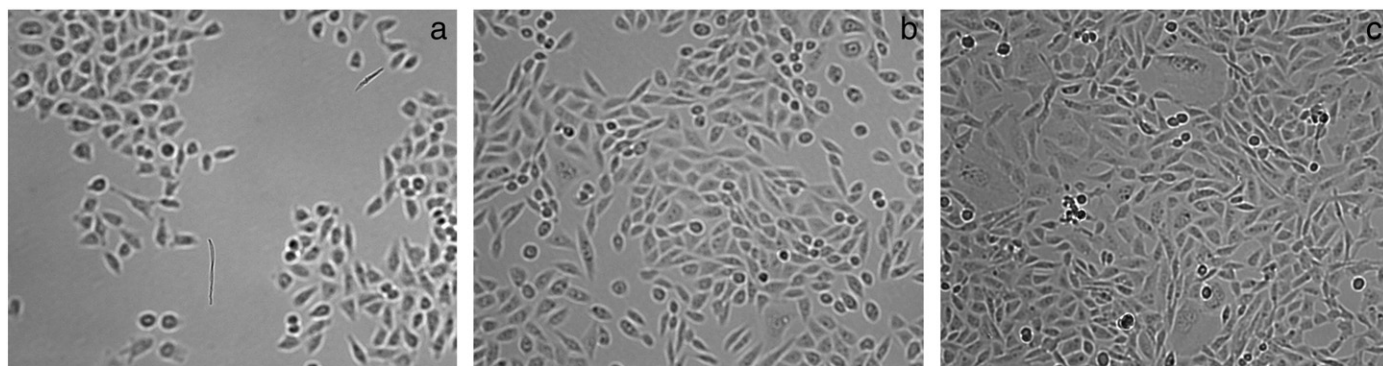

Fig. 4. Phase contrast microscopic images with different numbers of cells. a—Image belongs to the density group of under 300 cells per image. b—Image belongs to the density group of 300 to 600 cells per image. c—Image belongs to the density group of more than 600 cells per image.
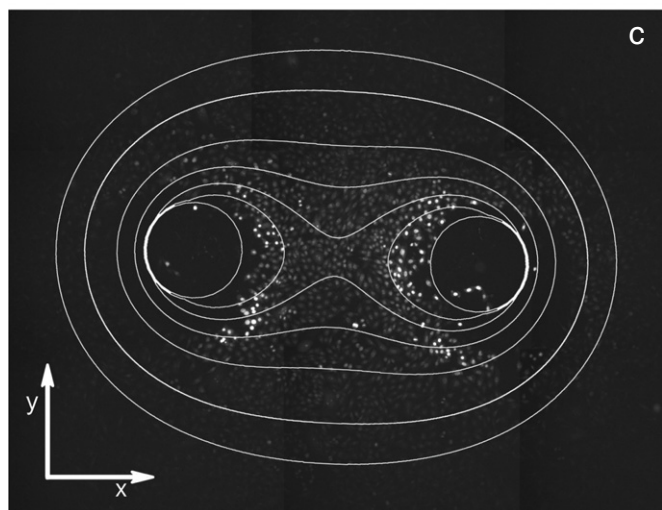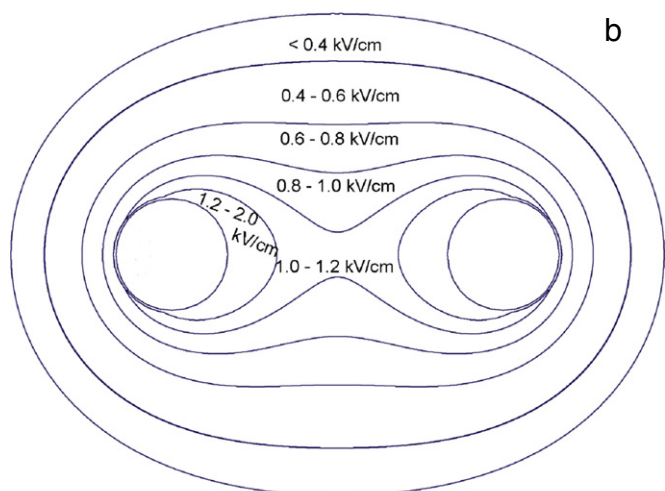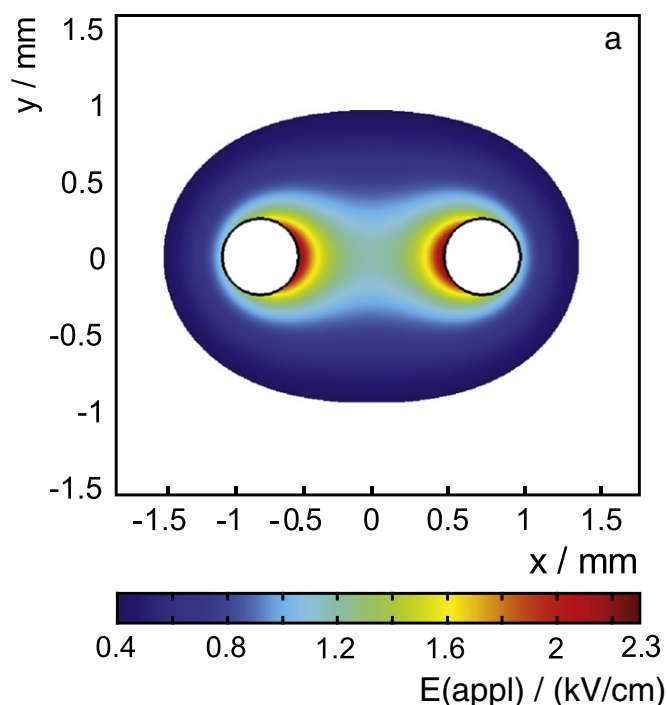
image and more than 600 cells per image. R^2 value and optimized parameters for all four mathematical models (Eqs. (1)–(2)) and all three density groups can be seen in Table 4. R^2 measures how successful the fit is in explaining the variation of the data i.e. R^2 is the correlation between predicted and observed values. The parameter R^2 was 0.990 or higher in all fits. Based on the experimental data which can be seen in Fig. 7 (triangles) we can see that the percentage of electroporated cells depends significantly on the cell density. In Fig. 7 data is presented only with Gompertz curve—the reason is explained later in this section. Somewhat surprising, the mathematical models of electroporation are not shifting to the higher values of E but are changing their slopes with different densities of the monolayer. All of the curves start to increase at approximately the same point (0.4 kV/cm) but reach their plateaus at different values of the electric field (1.2 kV/cm or more). At lower values of the electric field (less than 0.4 kV/cm) there was no electroporation detected. At the middle values of the electric field (0.4 kV/cm–1.2 kV/cm) where the curves are approximately linear, the slopes of the fitted models are different for each of the ranges of densities. When the density of the cells was lower the curve was steeper. We can see the change in the slope in Fig. 7 where the Gompertz curve (Eq. (3)) was fitted to all three density groups.

For further analysis images with the density of the cells in the range from 300 to 600 cells per image were chosen. In the experiments in the inhomogeneous electric field the actual density of the cells was higher in some areas of the composed image (more than 600 cells per image) but lower in the others. Therefore, 300 to 600 cells per image were selected as an approximation for an average cell density and further analysis was based only on density from 300 to 600 cells per image.

Fig. 8 presents the influence of the chosen mathematical model on the predicted percentage of electroporated cells. It seems as if there were only two different models shown instead of four. Namely, hyperbolic tangent and symmetric sigmoid are completely overlapping and therefore there is no visible difference on the graph. The same is true for the Gompertz curve and asymmetric sigmoid. All the mathematical models were used with parameters fitted to data from experiments in the homogeneous field. From the R^2 coefficients in Table 4 we can observe that the Gompertz curve and asymmetric sigmoid when the density of the cells is 300–600 cells per image offer the best fit to the experimental data of the four curves used. Although Gompertz curve and asymmetric sigmoid are overlapping and both offer almost equally good fit to the experimental data we have chosen the Gompertz curve (Eq. (3)) for further analysis.

In Fig. 7 we can observe the influence of the density of the monolayer, whereas in Fig. 8 we can see the influence of the chosen mathematical model on the percentage of electroporation. Fig. 9 is based on Figs. 7 and 8, as it combines the appropriate density of the monolayer (Fig. 7) and the best fit based on the R^2 value (Fig. 8). The appropriate density is the density of the monolayer exposed to an inhomogeneous field, i.e. 300–600 cells per image.

3.2. Cell electroporation in an inhomogeneous electric field

On the basis of the results acquired in experiments in the homogeneous electric field and the model of geometry of the two needle electrodes different mathematical models of cell electroporation as a function of electric field (Eqs. (1)–(4)) were applied to the numerically calculated inhomogeneous electric field.

We transformed a numerically calculated electric field (Fig. 5a) into the predicted percentage of the electroporated cells (Fig. 6b). In Fig. 9

Fig. 5. Distribution of the electric field strength in the plane of cell monolayer. a—Continuous distribution of the electric field strength when 120 V is applied. b—Contours which mark the borders between different ranges of the electric field when 120 V is applied. Range of electric field in a certain area is written in the corresponding area. c—Fluorescent microscopic composed image with superimposed contours of ranges of electric field, one 1 ms pulse of 120 V applied.

Table 3

Ranges of E-field vector when different voltages are applied and the size of the area in percents of the whole analyzed area without the electrodes. If a certain range is not analyzed when that voltage is applied there is a sign – in the corresponding cell. When the sum of percentages is not 100% it is so because of rounding of the numbers.

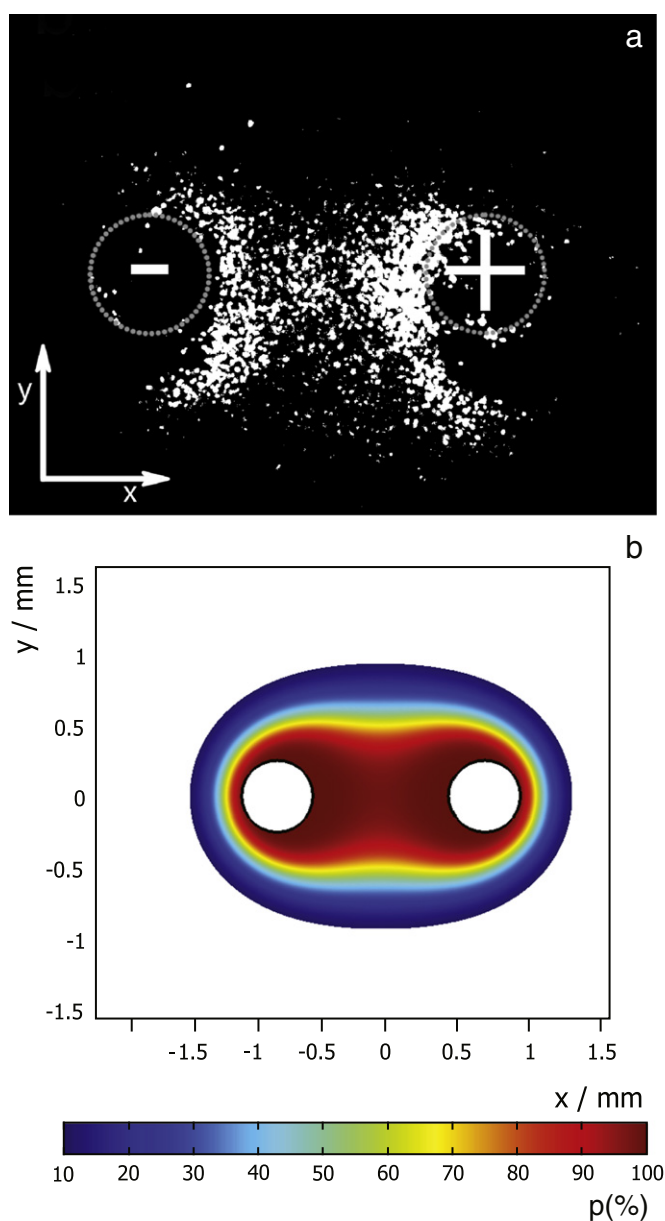| E-field strength range (kV/cm)	80 V area (%)	100 V area (%)	120 V area (%)	140 V area (%)
0.3–0.4	33	30	29	28
0.4–0.6	47	33	29	28
0.6–0.8	12	19	16	15
0.8–1.0	–	12	13	10
0.8–1.5	8	–	–	–
1.0–1.2	–	–	7	10
1.0–1.6	–	6	–	–
1.2–2.0	–	–	5	–
1.2–2.3	–	–	–	9

Fig. 6. a—Thresholded fluorescent microscopic image, averaged 6 images, approximate position of the electrodes is marked with gray circles; signs + and − in the circles mark the polarity of the electrodes. b—Predicted percentage of the electroporated cells (*p*) in the plane of cell monolayer when 120 V is applied; transformation from the electric field strength to the predicted percentage is made by the Gompertz curve for densities from 300 to 600 cells per image.

we can see both the theoretically predicted and experimentally determined values. With the variation of the different models used for modeling the phenomena the difference in predicted ranges was minimal. This can be seen from comparing black vertical bars (Gompertz curve (Eq. (3)), 300 to 600 cells per image) and dark gray vertical bars (symmetric sigmoid (Eq. (1)), 300 to 600 cells per image) in Fig. 9. The predicted ranges of the percentage of the electroporated cells are almost the same. The difference in ranges was maximally 4% at lower electric field strengths. If we compare ranges predicted by these two curves (Eqs. (1) and (3)) based on the same density (300 to 600 cells per image) with the light gray bars, which represent a denser monolayer (more than 600 cells per image), we can observe that the predicted ranges are quite different at lower as well as at higher electric field strengths. Other combinations of the interpolation curve and the density of the cells were made as well (Table 4) but for the sake of stressing the influence of the density and of the mathematical model only the Gompertz curve for 300–600 and more than 600 cells per image and symmetric sigmoid for 300–600 cells per image are shown. Aside from the symmetric sigmoid (Eq. (1)) also the hyperbolic tangent (Eq. (4)) could be shown.

4. Discussion

The aim of our study was to compare different mathematical models that would allow transformation of the numerically calculated values of the electric field into the predicted percentage of electroporated cells. This kind of transformation and prediction would simplify presentation of treatment plans for electrochemotherapy and non-thermal irreversible electroporation. We upgraded the usual assumption that the percentage of the electroporated cells is 100% if the electric field is above the characteristic threshold and 0% if it is below [49]. Here the prediction was continuous and all the values between 0% and 100% were predicted. We investigated and compared the effects of the cell density and of the used mathematical model (Eqs. (1)–(4)). We started our study with the model of continuous electric field distribution presented in Fig. 5a, transforming it into the predicted percentage of electroporated cells as shown in Fig. 6b. In Fig. 6a we can see that the pattern of the electroporated and non-electroporated cells is in good agreement with the predicted shape in Fig. 6b.

If we look at Fig. 6a it appears as if there were more cells electroporated around the positive electrode. However, the analysis of the percentages of electroporated cells around each of the electrode (data not shown) showed that there was no significant difference between the percentages around the positive and around the negative electrode.

In the course of the transformation from the electric field strength in the homogeneous field to the percentage of electroporated cells in the inhomogeneous electric field we reached two main conclusions. The first one was about the changing of the slope of the mathematical model of electroporation in the homogeneous field and the second one was about the choice of the mathematical model, fitted to the

Table 4
Results for the goodness of the fit (R^2) and the curves' parameters for all of the four proposed curves for all three density groups. The fit is based on the percentage of electroporated cells in the homogenous field. The parameters are explained in 2.4 Fitting of the mathematical models.

Type of the curve	R-square [a]			Parameters		
	<300 cells/image	300–600 cells/image	>600 cells/image	<300 cells/image	300–600 cells/image	>600 cells/image
Symmetric sigmoid	0.992	0.990	0.964	$E_{50\%} = 0.659$ $b = 0.1090$	$E_{50\%} = 0.6879$ $b = 0.1242$	$E_{50\%} = 0.9231$ $b = 0.2353$
Asymmetric sigmoid	0.997	0.998	0.965	$E_{50\%} = 0.5869$ $v = 5e-8$ (fixed at bound) $b = 0.1529$	$E_{50\%} = 0.6061$ $v = 2e-8$ (fixed at bound) $b = 0.1772$	$E_{50\%} = 1.057$ $v = 2.557$ $b = 0.1494$
Gompertz curve	0.997	0.998	0.958	$E_{50\%} = 0.5869$ $b = 0.1529$	$E_{50\%} = 0.6061$ $b = 0.1772$	$E_{50\%} = 0.7567$ $b = 0.343$
Hyperbolic tangent	0.992	0.990	0.964	$E_{50\%} = 0.659$ $B = 4.587$	$E_{50\%} = 0.6879$ $B = 4.027$	$E_{50\%} = 0.9231$ $B = 0.9231$

[a] Goodness-of-fit.

experimental data. In general results obtained are in good agreement with the results found in the literature, describing experiments with suspensions. Nevertheless, the change of the models' slopes with respect to cell density seems rather surprising and contradictory to theoretical considerations [47].

First, we will discuss the change of models' slope. Experimental observation where the slope of the model changes can be observed in [35]. There we can see that the curve of detected fluorescence shifted with a change of pulse parameters (when longer pulses were used the slope was steeper). No curve which would show the dependence on the cell density is shown; we can only see that with the same pulse protocol and higher density of the suspension fewer cells are electroporated.

As it can be observed from Fig. 7, the model of electroporation did not shift but changed its slope when monolayers of cells with different densities were used for experiments. In previous studies it has been observed that with increasing densities of cell suspensions the base point of the curves and the point where the curves reach their plateaus shifted to the higher electric field with the slope of the curve being the same [47]. In our study one part of the observation was similar—the points where the curves reach their plateau values shifted to the higher electric field values when we increased the density of the cell monolayer. On the other hand, the base point where a minimal fluorescence of the cells

was detected was the same for all of the densities. Therefore, the slope of the curves changed.

It is known that with denser suspensions we get lower induced transmembrane voltage due to the mutual electrical shielding [33–36]. In the monolayers the situation is the same—with denser monolayers we get lower induced transmembrane voltage and lower percentage of the electroporated cells. However, we should not neglect the effect of the cells' geometry [50,51] which is deviatory from spheres and the electrical connections between the cells, e.g. gap junctions [52]. It seems that the cell's geometry and connections between the cells are related to the curves' slopes, which might be an area of further research.

The standard deviation in Figs. 7 and 8 is relatively high; the reason is counting of the cells. All means of cell counting are subjected to errors because of noise and artifacts, various cell shapes, and cells in close contact without clear boundaries between them. Considering that we had monolayers of very high density the calculated standard deviation is within the expected values as reported in the literature [53]. The error would be lower if using cells in suspension; however the cells in suspension and in tissues behave very differently. In a suspension there are no connections between the cells and they are all approximately spherical.
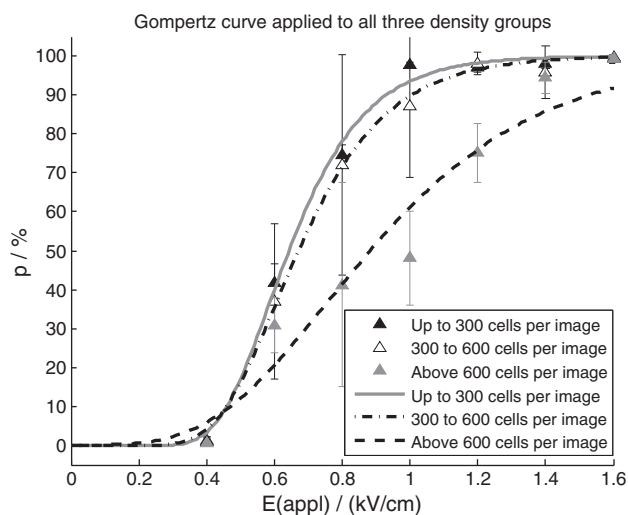

Fig. 7. Percentage (p) of electroporated cells determined by propidium iodide staining in the dependence on the applied electric field. The Gompertz curve is fitted to all three groups of different densities of the cells. Mean experimental values from experiments, made in the homogeneous field are marked with triangles; vertical bar denotes one standard deviation. Black triangle and gray solid line represent density up to 300 cells per image, hollow triangle and dotted black line represent density from 300 to 600 cells per image, and gray triangle and dashed black line represent density above 600 cells per image.
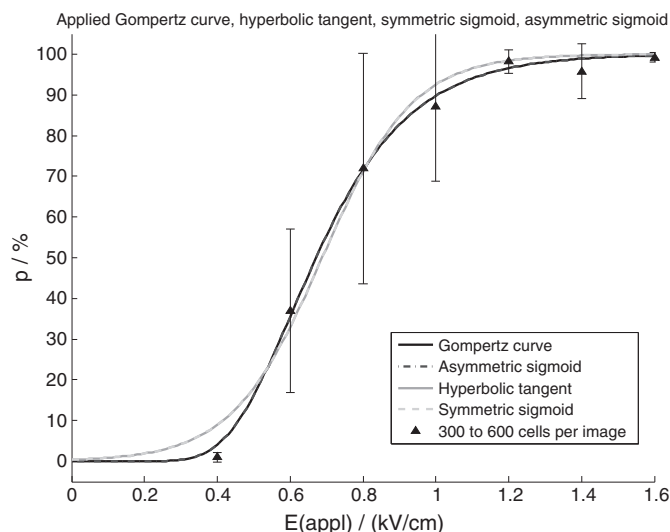
Fig. 8. Percentage (p) of electroporated cells determined by propidium iodide staining in dependence on the applied electric field. Four different models of electroporation were fitted to the experimental data of the percentage of electroporated cells in the homogeneous field. Triangles represent the mean experimental values for the percentage of electroporated cells in the homogeneous electric field; vertical bar denotes one standard deviation. Black solid line represents Gompertz line, black dashed line represents asymmetric sigmoid, gray solid line represents hyperbolic tangent and gray dashed line represents symmetric sigmoid.

Fig. 9. Predicted (vertical bars) and experimentally determined percentage (triangles) of the electroporation; model for a cell response made by the Gompertz curve (Eq. (3)) and symmetric sigmoid (Eq. (1)) for different densities. Three bars in one set from left to right are the Gompertz curve for densities from 300 to 600 cells per image (black bar), the symmetric sigmoid for densities from 300 to 600 cells per image (dark gray bar) and the last bar t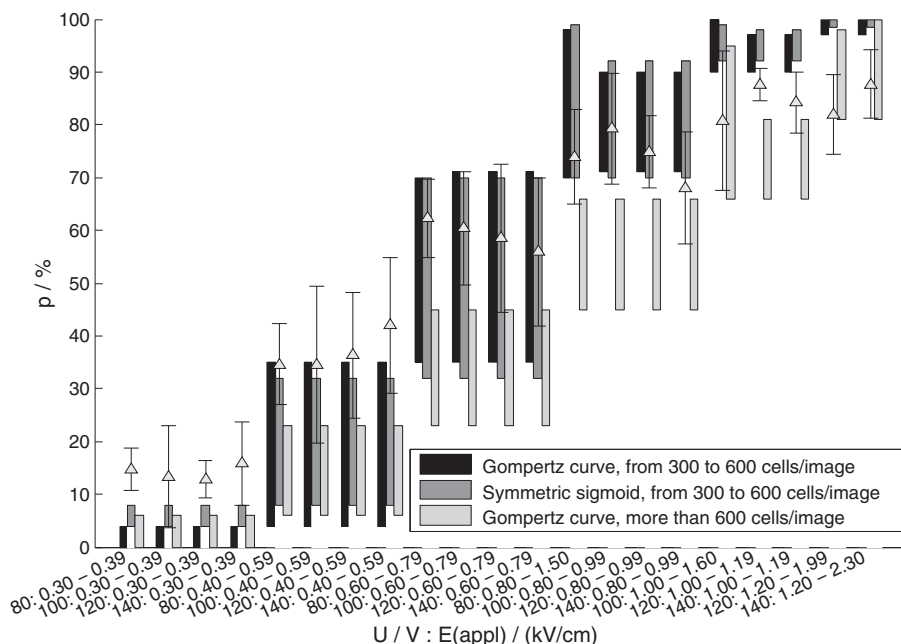he Gompertz curve for densities of more than 600 cells per image (light gray bar). The vertical bar at experimentally determined values represents one standard deviation. Labels on the x-axis mean the applied voltage and the area with the corresponding electric field range for that applied voltage.

In the past, different mathematical models have been proposed for describing the dependence between the percentage of the electroporated cells and the electric field. For example, a hyperbolic tangent law for permeabilization as a function of the electric field has been proposed [47]. In statistical physics the hyperbolic tangent is commonly used for describing two-state systems, for example the polarized light. Similarly, electroporated and non-electroporated cells can also be viewed as two states in a system and hyperbolic tangent law describes the crossover from the non-electroporated to the electroporated state.

In [20] two different ways of describing the cell electroporation fraction have been used. The first one was sigmoid function which is often fitted to the experimental data. The second one was a curve which derived from a hypothetical normal distribution of cell radii. In this case the curve was obtained from a step function (electroporation is 0% when the applied electric field is under the threshold for electroporation and 100% when the applied electric field is above the threshold). Cell radius was varied according to the normal distribution with empirically determined values for mean cell radius and its standard deviation. Goodness-of-fit between the normal distribution curve on one side and the experiments on the other showed that experimental results were in good agreement with the theoretically predicted values. Nevertheless, the authors could not decide which of the two curves was more appropriate.

The Gompertz curve is used for describing the systems which saturate in a long period of time, for example the growth of the tumors [46]. The growth is slower at the beginning. Then the size starts to increase faster. The growth is limited after a certain time period when the size of the tumor reaches a plateau value. The growth can be compared to the percentage of cell electroporation as a function of the electric field where we obtain high percentage of cells being electroporated, but with an increasing electric field the increase e.g. from 97% to 100% of electroporated cells is difficult to obtain.

Up to a certain electric field reached there are almost no cells electroporated. From 0.4 kV/cm to 1.0 kV/cm the percentage of the electroporated cells quickly increases and then it reaches the plateau value. The described logic is the reason that we proposed the Gompertz curve for describing the electroporation of the cells. It is not necessary

that the Gompertz curve is symmetric. The asymmetry in the model is appropriate because in reality the percentage of the electroporated cells depends also on the cell radius, and according to the literature the cell radii are not symmetrically distributed [20] which was also the case in our study (data not shown).

Therefore, we can expect that the mathematical model of electroporation is asymmetric as well. This asymmetry was also the reason why we chose the asymmetric sigmoid curve for analysis.

So far not many studies of a statistical evaluation of electroporation are available. For evaluating the area of irreversible electroporation a statistical model based on the Peleg–Fermi model combined with a numerical solution of the multidimensional electric field equation cast in a dimensionless form was used [21]. This model directly incorporates the dependence of cell death on pulse number (n) and on electric field (E). It is expressed by Eqs. (5)–(7), where S means the survival ratio and E_c marks the intersection of the curve with the y-axis. Coefficients k_1 and k_2 are cell type and pulse type specific.

$$S = 1/(1 + \exp(E - E_c(n))/A(n)) \tag{5}$$

$$E_c(n) = E_{c0}{}^* \exp(-k_1{}^*n) \tag{6}$$

$$A(n) = A_0{}^* \exp(-k_2{}^*n) \tag{7}$$

The problem with this model is that it was not validated since it was tested only on extrapolated data reported in the literature for prostate cancer cell death caused by irreversible electroporation [54]. Authors stated that real curves and parameters should be developed for each specific tissue. Also the Fermi–Peleg model should be validated first in vitro and then in vivo.

Several microbial inactivation curves have been effectively described by Weibull distribution. In this model parameters were dependent on the media type and treatment parameters (electric field and treatment time) [22,55] but not on pulse number and pulse length like the Peleg–Fermi statistical model. Therefore, this model is not as interesting

for our study as the Peleg–Fermi model. Also, in the area of microbial inactivation by pulsed electric fields many mathematical models exist [22, 56], but they all describe survival of the cells in dependence on applied electric field and treatment time, with treatment time most often reported as the sum of duration of all of the applied pulses. All these models (Weibull, Peleg–Fermi, log-linear etc.) describe the survival of the cells. In our study on the other hand, survival of the cells has not been determined. Therefore, these models were not used in our study.

In our study four mathematical models (Eqs. (1)–(4)) were chosen, used and evaluated. We achieved good agreement with all of them since R^2 was 0.990 or higher in all four cases (see Table 4); therefore, for the analysis of the effect of the cell density on electroporation any of them might be used. For further analysis of the effect of cell density we considered the two curves with the highest R^2—Gompertz curve and asymmetric sigmoid. If parameter v in the asymmetric sigmoid model (Eq. (2)) was negative, no fit could be achieved because complex values were computed by model function. Therefore, we set a lower limit for this parameter at 0. Although we managed to complete the fitting, the parameter v was fixed at bound, which meant that the best fit was not achieved. The asymmetric sigmoid model was thus not used in the next step of the analysis.

For the analysis of the effect of the interpolation curve on the prediction of the percentage of electroporation we used only the Gompertz curve (Eq. (3)) and symmetric sigmoid (Eq. (1)). There was no need to do the analysis both with hyperbolic tangent (Eq. (4)) and symmetric sigmoid (Eq. (1)) since they can be seen as equivalent (see their overlapping in Fig. 8).

If we look at Fig. 9 we can see that under our experimental conditions the percentage of the affected cells depends more on the density of the cells than on a type of the curve. When different curve was used for the same density (compare dark gray bars for the symmetric sigmoid (Eq. (1)) and black bars for the Gompertz curve (Eq. (3)) in Fig. 9) the difference between predicted ranges was 4% at lower electric field strengths (0.30–0.39 kV/cm) and even less for the higher ones. The reason for the 4% difference can be observed from Fig. 8. There we can see that at lower electric field values Eqs. (1) and (3) deviate the most one from another.

At lower electric field values the symmetric sigmoid overestimates the experimental results while the Gompertz curve offers better fit. This means that the percentage predicted by the symmetric sigmoid (Eq. (1)) is higher than the one predicted by the Gompertz curve (Eq. (3)) which is not in very good agreement with experimental results. But since the predicted ranges of electroporation are still quite similar (0–4% for Eq. (3) and 4–8% for Eq. (1)) and they both underestimate experimental results we can conclude that the choice of the curve is not of highest importance.

The reason for discrepancy at the higher electric field could be the fact that mathematical models for electroporation allow 100% electroporation although in reality there are always some cells which do not respond to electric pulses and stay unaffected at least to very high values of electric field. This is particularly true with single pulse applied at very high electric fields (data not shown) as was the case in our experiments. This could be the reason why the predicted ranges in Fig. 9 are above the experimentally measured values.

In vitro a small fraction of dead cells is always detected, which explains the deviation of experimental data at the lowest electric field strength from theoretical prediction by mathematical models for electroporation.

If we look at the light gray bars at Fig. 9 (Gompertz curve (Eq. (3)) for densities above 600 cells) per image, we can see that they do not reproduce the experimental results (triangles) properly. The mathematical model of electroporation is underestimating the experimental results at all of the applied electric field strengths for at least 10%. The reason is in the density of the cells. Prediction was made on monolayers of more than 600 cells per image. The experiments were performed

on monolayers of less than 600 cells per image. This means that the density of the cells is a very important factor. It must be the same in experiments used for prediction and in experiments where we predict the percentage of electroporated cells. The prediction offered better agreement only at the higher values of the electric field because the electric field was already strong enough for all of the curves to reach their plateau values. Therefore, we can say that the density of the cell monolayer is very important for predicting the percentage of electroporation.

In previously published works a strong dependence between the cells' electroporation and the density of the cells was already shown [33,34]. In our study we went one step further and showed that the cell density not only has a strong influence on the cells' electroporation but is under our experimental conditions the most important factor influencing the prediction of electroporation. We eliminated the effect of the size of the cells since the experiments in homogeneous and inhomogeneous field were made on monolayers of similar density. Our experiments have been performed in vitro on CHO cells. Our results were obtained using single pulse of 1 ms duration; however we need to establish how the parameters of curves depend on duration and number of pulses, and different cells. In addition, there might be other parameters besides the density of the cells which have an important influence on the prediction of electroporation. How this translates into tissue remains to be determined; tissue level determination and validation are still needed [38,39].

References

[1] E. Neumann, K. Rosenheck, Permeability changes induced by electric impulses in vesicular membranes, J. Membr. Biol. 10 (1972) 279–290.
[2] T. Kotnik, P. Kramar, G. Pucihar, D. Miklavčič, M. Tarek, Cell membrane electroporation—Part 1: the phenomenon, Electr. Insul. Mag. 28 (2012) 14–23.
[3] T.Y. Tsong, Electroporation of cell membranes, Biophys. J. 60 (1991) 297–306.
[4] T. Kotnik, G. Pucihar, D. Miklavčič, Induced transmembrane voltage and its correlation with electroporation-mediated molecular transport, J. Membr. Biol. 236 (2010) 3–13.
[5] M. Čemažar, T. Jarm, D. Miklavčič, A. Maček Lebar, A. Ihan, N.A. Kopitar, et al., Effect of electric-field intensity on electropermeabilization and electrosensitivity of various tumor-cell lines in vitro, Electro- Magnetobiol. 17 (1998) 263–272.
[6] B. Rubinsky, G. Onik, P. Mikus, Irreversible electroporation: a new ablation modality—clinical implications, Technol. Cancer Res. Treat. 6 (2007).
[7] E. Neumann, M. Schaefer-Ridder, Y. Wang, P.H. Hofschneider, Gene transfer into mouse lyoma cells by electroporation in high electric fields, EMBO J. 1 (1982) 841–845.
[8] L.C. Heller, R. Heller, Electroporation gene therapy preclinical and clinical trials for melanoma, Curr. Gene Ther. 10 (2010) 312–317.
[9] A.I. Daud, R.C. DeConti, S. Andrews, P. Urbas, A.I. Riker, V.K. Sondak, et al., Phase I trial of interleukin-12 plasmid electroporation in patients with metastatic melanoma, J. Clin. Oncol. 26 (2008) 5896–5903.
[10] L.M. Mir, Therapeutic perspectives of in vivo cell electropermeabilization, Bioelectrochemistry 53 (2001) 1–10.
[11] B. Mali, T. Jarm, M. Snoj, G. Serša, D. Miklavčič, Antitumor effectiveness of electrochemo-therapy: a systematic review and meta-analysis, Eur. J. Surg. Oncol. 39 (2013) 4–16.
[12] D. Miklavčič, G. Serša, E. Brecelj, J. Gehl, D. Soden, G. Bianchi, et al., Electrochemotherapy: technological advancements for efficient electroporation-based treatment of internal tumors, Med. Biol. Eng. Comput. 50 (2012) 1213–1225.
[13] J. Teissié, N. Eynard, M.-C. Vernhes, A. Bénichou, V. Ganeva, B. Galutzov, et al., Recent biotechnological developments of electropulsation. A prospective review, Bioelectrochemistry 55 (2002) 107–112.
[14] S. Haberl, M. Jarc, A. Štrancar, M. Peterka, D. Hodžić, D. Miklavčič, Comparison of alkaline lysis with electroextraction and optimization of electric pulses to extract plasmid DNA from Escherichia coli, J. Membr. Biol. 246 (11) (2013) 861–867.

[15] H.L.M. Lelieved, S. Notermans, S.W.H. de Haan, Food Preservation by Pulsed Electric Fields: From Research to Application, World Publishing Limited, Cambridge, England, 2007.

[16] S. Schilling, S. Schmid, H. Jaeger, M. Ludwig, H. Dietrich, S. Toepfl, et al., Comparative study of pulsed electric field and thermal processing of apple juice with particular consideration of juice quality and enzyme deactivation, J. Agric. Food Chem. 56 (2008) 4545–4554.

[17] S. Haberl, D. Miklavčič, G. Serša, W. Frey, B. Rubinsky, Cell membrane electroporation—Part 2: the applications, IEEE Electr. Insul. Mag. 29 (2013) 29–37.

[18] E. Tekle, R.D. Astumian, P.B. Chock, Electro-permeabilization of cell membranes: effect of the resting membrane potential, Biochem. Biophys. Res. Commun. 172 (1990) 282–287.

[19] J. Teissié, M.-P. Rols, An experimental evaluation of the critical potential difference inducing cell membrane electropermeabilization, Biophys. J. 65 (1993) 409–413.

[20] M. Puc, T. Kotnik, L.M. Mir, D. Miklavčič, Quantitative model of small molecules uptake after in vitro cell electropermeabilization, Bioelectrochemistry 60 (2003) 1–10.

[21] A. Goldberg, B. Rubinsky, A statistical model for multidimensional irreversible electroporation cell death in tissue, Biomed. Eng. OnLine 9 (2010).

[22] M.F. San Martín, D.R. Sepúlveda, B. Altunakar, M.M. Góngora-Nieto, B.G. Swanson, G. V. Barbosa-Cánovas, Evaluation of selected mathematical models to predict the inactivation of *Listeria innocua* by pulsed electric fields, LWT 40 (2007) 1271–1279.

[23] B. Mali, D. Miklavčič, L.G. Campana, M. Čemažar, G. Serša, M. Snoj, et al., Tumor size and effectiveness of electrochemotherapy, Radiol. Oncol. 47 (2013) 32–41.

[24] I. Edhemovic, E.M. Gadzijev, E. Brecelj, D. Miklavčič, B. Kos, A. Županič, et al., Electrochemotherapy: a new technological approach in treatment of metastases in the liver, Technol. Cancer Res. Treat. 10 (2011) 475–485.

[25] F. Mahmood, J. Gehl, Optimizing clinical performance and geometrical robustness of a new electrode device for intracranial tumor electroporation, Bioelectrochemistry 81 (2011) 10–16.

[26] R.E. Neal, J.H. Rossmeisl, P.A. Garcia, O.I. Lanz, N. Henao-Guerrero, R.V. Davalos, Successful treatment of a large soft tissue sarcoma with irreversible electroporation, J. Clin. Oncol. 29 (2011) e372–e377.

[27] G. Onik, B. Rubinsky, Irreversible electroporation: first patient experience focal therapy of prostate cancer, in: B. Rubinsky (Ed.), Irreversible Electroporation, Springer Berlin Heidelberg, Berlin, Heidelberg, 2010, pp. 235–247.

[28] D. Miklavcic, M. Snoj, A. Zupanic, B. Kos, M. Cemazar, M. Kropivnik, et al., Towards treatment planning and treatment of deep-seated solid tumors by electrochemotherapy, Biomed. Eng. OnLine 9 (2010) 10.

[29] D. Pavliha, B. Kos, A. Županič, M. Marčan, G. Serša, D. Miklavčič, Patient-specific treatment planning of electrochemotherapy: procedure design and possible pitfalls, Bioelectrochemistry 87 (2012) 265–273.

[30] P.A. Garcia, J.H. Rossmeisl, R.E. Neal, T.L. Ellis, R.V. Davalos, A parametric study delineating irreversible electroporation from thermal damage based on a minimally invasive intracranial procedure, Biomed. Eng. OnLine 10 (2011) 34.

[31] A. Županič, B. Kos, D. Miklavčič, Treatment planning of electroporation-based medical interventions: electrochemotherapy, gene electrotransfer and irreversible electroporation, Phys. Med. Biol. 57 (2012) 5425–5440.

[32] A. Županič, D. Miklavčič, Tissue heating during tumor ablation with irreversible electroporation, Elektroteh. Vestn. 78 (2011) 42–47.

[33] M. Pavlin, N. Pavšelj, D. Miklavčič, Dependence of induced transmembrane potential on cell density, arrangement, and cell position inside a cell system, IEEE Trans. Biomed. Eng. 49 (2002) 605–612.

[34] R. Susil, D. Šemrov, D. Miklavčič, Electric field induced transmembrane potential depends on cell density and organization, Electro- Magnetobiol. 17 (1998) 391–399.

[35] G. Pucihar, T. Kotnik, J. Teissié, D. Miklavčič, Electropermeabilization of dense cell suspensions, Eur. Biophys. J. 36 (2007) 172–185.

[36] M. Pavlin, D. Miklavčič, The effective conductivity and the induced transmembrane potential in dense cell systems exposed to DC and AC electric fields, IEEE Trans. Plasma Sci. 37 (2009).

[37] D. Miklavčič, D. Šemrov, H. Mekid, L.M. Mir, A validated model of in vivo electric field distribution in tissues for electrochemotherapy and for DNA electrotransfer for gene therapy, Biochim. Biophys. Acta 1523 (2000) 73–83.

[38] Z. Qin, J. Jiang, G. Long, B. Lindgren, J.C. Bischof, Irreversible electroporation: an in vivo study with dorsal skin fold chamber, Ann. Biomed. Eng. 41 (2013) 619–629.

[39] R.E. Neal, J.L. Millar, H. Kavnoudias, P. Royce, F. Rosenfeldt, A. Pham, et al., In vivo characterization and numerical simulation of prostate properties for non-thermal irreversible electroporation ablation: characterized and simulated prostate IRE, Prostate 74 (5) (2014) 458–468.

[40] N. Pavšelj, D. Miklavčič, Numerical modeling in electroporation-based biomedical applications, Radiol. Oncol. 42 (2008) 159–168.

[41] M. Kranjc, F. Bajd, I. Sersa, D. Miklavcic, Magnetic resonance electrical impedance tomography for monitoring electric field distribution during tissue electroporation, IEEE Trans. Med. Imaging 30 (2011) 1771–1778.

[42] M. Kranjc, F. Bajd, I. Sersa, E.J. Woo, D. Miklavcic, Ex vivo and in silico feasibility study of monitoring electric field distribution in tissue during electroporation based treatments, PLoS One 7 (2012) e45737.

[43] G. Pucihar, J. Krmelj, M. Reberšek, T. Napotnik, D. Miklavčič, Equivalent pulse parameters for electroporation, IEEE Trans. Biomed. Eng. 58 (2011) 3279–3288.

[44] S. Mazères, D. Šel, M. Golzio, G. Pucihar, Y. Tamzali, D. Miklavčič, et al., Non invasive contact electrodes for in vivo localized cutaneous electropulsation and associated drug and nucleic acid delivery, J. Controlled Release (2009) 125–131.

[45] M. Golzio, J. Teissié, Direct assay of electropermeabilization in a 2D pseudo tissue, Phys. Chem. Chem. Phys. 12 (2010) 14670.

[46] A.K. Laird, Dynamics of tumour growth, Br. J. Cancer 18 (1964) 490–502.

[47] M. Essone Mezeme, G. Pucihar, M. Pavlin, C. Brosseau, D. Miklavčič, A numerical analysis of multicellular environment for modeling tissue electroporation, Appl. Phys. Lett. 100 (2012) 143701.

[48] C. Polk, E. Postow, Handbook of Biological Effects of Electromagnetic Fields, 2nd ed. CRC Press, Florida, 2000.

[49] B. Kos, A. Županič, T. Kotnik, M. Snoj, G. Serša, D. Miklavčič, Robustness of treatment planning for electrochemotherapy of deep-seated tumors, J. Membr. Biol. 236 (2010) 147–153.

[50] L. Towhidi, T. Kotnik, G. Pucihar, S.M.P. Firoozabadi, H. Mozdarani, D. Miklavčič, Variability of the minimal transmembrane voltage resulting in detectable membrane electroporation, Electromagn. Biol. Med. 27 (2008) 372–385.

[51] B. Valič, M. Golzio, M. Pavlin, A. Schatz, C. Faurie, B. Gabriel, et al., Effect of electric field induced transmembrane potential on spheroidal cells: theory and experiment, Eur. Biophys. J. (2003) 519–528.

[52] G. Pucihar, D. Miklavčič, The influence of intracellular connections on the electric field induced membrane voltage and electroporation of cells in clusters, in: O. Dössel, W.C. Schlegel (Eds.), World Congr. Med. Phys. Biomed. Eng. Sept. 7–12 2009 Munich Ger, Springer Berlin Heidelberg, Berlin, Heidelberg, 2009, pp. 74–77.

[53] M. Usaj, D. Torkar, M. Kanduser, D. Miklavcic, Cell counting tool parameters optimization approach for electroporation efficiency determination of attached cells in phase contrast images: cell counting tool parameters optimization approach, J. Microsc. 241 (2011) 303–314.

[54] P.J. Canatella, J.F. Karr, J.A. Petros, M.R. Prausnitz, Quantitative study of electroporation-mediated molecular uptake and cell viability, Biophys. J. 80 (2001) 755–764.

[55] I. Álvarez, J. Raso, F.J. Sala, S. Condón, Inactivation of *Yersinia enterocolitica* by pulsed electric fields, Food Microbiol. 20 (2003) 691–700.

[56] I. Álvarez, R. Virto, J. Raso, S. Condón, Comparing predicting models for the *Escherichia coli* inactivation by pulsed electric fields, Innov. Food Sci. Emerg. Technol. 4 (2003) 195–202.

Paper 2

Title: **Mathematical Models Describing Chinese Hamster Ovary Cell Death Due to Electroporation In Vitro**

Authors: Janja Dermol and Damijan Miklavčič

CrossMark

Mathematical Models Describing Chinese Hamster Ovary Cell Death Due to Electroporation In Vitro

Janja Dermol[1] · Damijan Miklavčič[1]

Abstract Electroporation is a phenomenon used in the treatment of tumors by electrochemotherapy, non-thermal ablation with irreversible electroporation, and gene therapy. When treating patients, either predefined or variable electrode geometry is used. Optimal pulse parameters are predetermined for predefined electrode geometry, while they must be calculated for each specific case for variable electrode geometry. The position and number of electrodes are also determined for each patient. It is currently assumed that above a certain experimentally determined value of electric field, all cells are permeabilized/destroyed and under it they are unaffected. In this paper, mathematical models of survival in which the probability of cell death is continuously distributed from 0 to 100 % are proposed and evaluated. Experiments were performed on cell suspensions using electrical parameters similar to standard electrochemotherapy and irreversible electroporation parameters. The proportion of surviving cells was determined using clonogenic assay for assessing the ability of a cell to grow into a colony. Various mathematical models (first-order kinetics, Hülsheger, Peleg-Fermi, Weibull, logistic, adapted Gompertz, Geeraerd) were fitted to experimental data using a non-linear least-squares method. The fit was evaluated by calculating goodness of fit and by observing the trend of values of models' parameters. The most appropriate models of cell survival as a function of treatment time were the adapted Gompertz and the Geeraerd models and, as a function of the electric field, the logistic, adapted Gompertz and Peleg-Fermi models. The next steps to be performed are validation of the most appropriate models on tissues and determination of the models' predictive power.

Keywords Clonogenic assay · Cell death probability · Treatment planning · Electrochemotherapy · Predictive models · Non-thermal irreversible electroporation

Introduction

Electroporation is a phenomenon that occurs when short high voltage pulses are applied to cells and tissues. This exposure of cells to electric pulses results in pores being formed in the cell membrane. Membranes become permeable to molecules that cannot otherwise pass in or out of the cell (Kotnik et al. 2012; Weaver 1993). If the cell is able to recover, it is considered reversible electroporation. If the damage to the cell is too extensive and the cell dies, it is considered irreversible electroporation. The existence of the pores has been shown by molecular dynamics (Delemotte and Tarek 2012) and calculated by various theoretical models (Neu and Neu 2009; Weaver and Chizmadzhev 1996). Electroporation is already being used in medicine, e.g., electrochemotherapy (Edhemović et al. 2014), non-thermal irreversible electroporation as a method of tissue ablation (Cannon et al. 2013; Davalos et al. 2005; Garcia et al. 2014; Long et al. 2014; Neal et al. 2013), gene therapy (Daud et al. 2008; Heller and Heller 2010), DNA vaccination (Calvet et al. 2014), and transdermal drug delivery (Denet et al. 2004; Yarmush et al. 2014), as well as in biotechnology (Kotnik et al. 2015) and food processing (Mahnič-Kalamiza et al. 2014; Sack et al. 2010). It has been shown that a sufficient electric field (E-field) is the most important factor—all the cells in the tumor have to be permeabilized (in electrochemotherapy) (Miklavčič

✉ Damijan Miklavčič
damijan.miklavcic@fe.uni-lj.si

[1] Faculty of Electrical Engineering, University of Ljubljana, Tržaška 25, 1000 Ljubljana, Slovenia

Springer

et al. 1998) or irreversibly electroporated (in irreversible electroporation) to eradicate the tumor. *E*-field distribution also corresponds to tissue necrosis (Long et al. 2014; Miklavčič et al. 2000).

When performing electrochemotherapy, irreversible electroporation or gene therapy, fixed electrode configurations with predefined pulse parameters can be used (Heller et al. 2010; Mir et al. 2006). Alternatively, variable electrode configurations can be used when the target tumor is outside the standard parameters (Linnert et al. 2012; Miklavčič et al. 2012). When using variable electrode configurations, a plan is needed of the electrodes' position and the parameters of electric pulses that offer sufficient *E*-field in the tissue (Campana et al. 2013; Miklavčič et al. 2010; Neal et al. 2015; Šel et al. 2007; Županič et al. 2012). Treatment planning of electroporation-based medical applications has already been successfully used on colorectal liver metastases in humans (Edhemović et al. 2014), and on spontaneous malignant intracranial glioma in dogs (Garcia et al. 2011a, b). It is currently assumed in treatment plans that above an experimentally determined threshold value of *E*-field, all cells are permeabilized or destroyed and below this threshold cells are not affected or do not die—i.e., we assume a step-like response. In reality, though, the transition from non-electroporated to electroporated state and from reversibly to irreversibly electroporated state is continuous. Mathematical models of cell permeabilization and survival can be implemented in order to present treatment plan in a clearer way and to obtain a better prediction of the tissue damaged (Dermol and Miklavčič 2014; Garcia et al. 2014). In addition, mathematical models allow us to interpolate the predicted survival of the cells and predict survival for other parameters than those used for curve fitting. The mathematical models of survival have to be adaptable and describe the experimental data well (high goodness of fit). Goodness of fit is not only an important criterion but trends of the optimized values of the parameters and the predictive power of the model are also important. In an ideal case, the models would include all the parameters important for cell death due to electroporation, but would have the lowest possible number of parameters.

There are only a few reports describing the probability of cell permeabilization (Dermol and Miklavčič 2014) and cell survival after irreversible electroporation (Garcia et al. 2014; Golberg and Rubinsky 2010) using mathematical models. The first attempt using mathematical model of survival to describe cell death after irreversible electroporation was made by (Golberg and Rubinsky 2010). They successfully fitted the Peleg-Fermi model to experimental data of prostate cancer cells' death described in (Canatella et al. 2001). Later, (Garcia et al. 2014) simulated irreversible electroporation on liver tissue and characterized

cell death using the Arrhenius rate equation for thermal injury and the Peleg-Fermi model for electrical injury. The authors determined that using commercially available bipolar electrodes (AngioDynamics, Queensbury, USA) and standard irreversible electroporation parameters (90 pulses, 100 μs duration, 1 Hz, 3000 V) most cell death is a consequence of electrical damage. In that study, the volume of the thermally destroyed tissue did not surpass 6 % of the whole destroyed volume and was concentrated in the immediate vicinity of the electrodes.

Until now, the Peleg-Fermi model has been the only mathematical model used for describing cell death as a consequence of irreversible electroporation in medicine. However, mathematical modeling of cell death has a long history in the field of microbiology, e.g., food sterilization (Peleg 2006). Most models from the field of microbiology describe thermal microbial inactivation; an independent variable is treatment time (*t*). We used these models (first-order kinetics, Weibull, logistic, adapted Gompertz, Geeraerd) in original and in transformed forms. In the original forms, the models remained unchanged, treatment time was an independent variable, and *E*-field was a parameter. In the transformed forms, *E*-field became the independent variable. There was no need to transform the Hülsheger model and the Peleg-Fermi model, since the independent variables were *E*-field and treatment time (Hülsheger et al. 1981) or *E*-field and the number of pulses (Peleg 1995). In existing studies, mathematical models have not yet been used as a function of the *E*-field. Since *E*-field is a dominant parameter for predicting the effect of the electroporation, we were interested in obtaining models as a function of *E*-field. We also provide an explanation of the reasoning for the transformation for each of the transformed models.

In (Canatella et al. 2001), the authors exposed prostate cancer cells to 1–10 exponentially decaying pulses in the range of 0.1–3.3 kV/cm, with time constants in the range of 50 μs–20 ms. In our experiments, up to 90 square pulses, 0–4.0 kV/cm, 50–200 μs were applied, which are typically used in electrochemotherapy and irreversible electroporation treatments. Clonogenic assay was used as a measure of the ability of the cells to reproduce (Franken et al. 2006).

Our study is the first attempt to compare different mathematical models describing the survival of animal cells due to electroporation. We present the results obtained with electrical parameters similar to those typically used in electrochemotherapy and in irreversible electroporation clinical treatments. We evaluate the trends/meaning of the parameters of the mathematical models, determine whether and which models could be used for describing cell death, and which models should be validated in the treatment planning and treatment response prognostics of electrochemotherapy and irreversible electroporation.

Materials and Methods

Cell Preparation and Electroporation

Chinese hamster ovary cells (CHO-K1; European Collection of Cell Cultures, Great Britain) were grown in 25-mm^2 culture flasks (TPP, Switzerland) for 2–3 days in an incubator (Kambič, Slovenia) at 37 °C and humidified 5 % CO_2 in HAM-F12 growth media (PAA, Austria) supplemented with 10 % fetal bovine serum (Sigma Aldrich, Germany), L-glutamine (Stem-Cell, Canada) and antibiotics penicillin/streptomycin (PAA, Austria), and gentamycin (Sigma Aldrich, Germany). The cell suspension was prepared on the day of experiments. Cells were centrifuged and resuspended in potassium phosphate electroporation buffer (10 mM K_2HPO_4/KH_2PO_4 in a ratio 40.5:9.5, 1 mM $MgCl_2$, 250 mM sucrose, pH 7.4, 1.62 mS/cm, 260 mOsm) at a concentration 10^6 cells/ml.

A drop of cell suspension (100 μl) was pipetted between two parallel stainless steel electrodes (Fig. 1) with the distance between them set at 2 mm. The surface of the electrodes was much larger than the contact surface between the cell suspension and the electrodes. All the cells were thus exposed to approximately the same electric field, which was estimated as the voltage applied divided by the distance between the electrodes. Pulses were delivered using a Betatech electroporator (Electro cell B10 HVLV, Betatech, France) and monitored with an oscilloscope LeCroy Wave-Surfer 422, 200 MHz and a current probe AP015 (both LeCroy, USA). The parameters of the applied electric pulses are summarized in Table 1. The electrodes were washed with
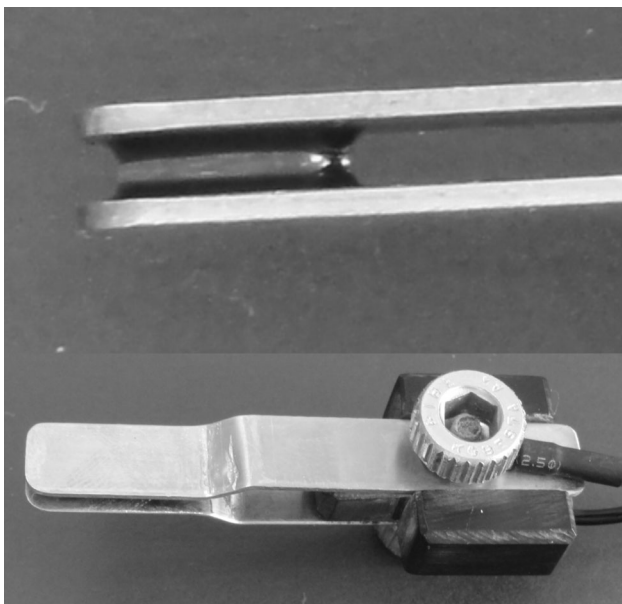

Fig. 1 Stainless steel parallel plate electrodes with a droplet of cell suspension between the electrodes (*upper image*). Inter-electrode distance is 2 mm

sterile 0.9 % NaCl and dried with sterile gauze between samples. After pulse application, 80 μl of cell suspension was transferred into a microcentrifuge tube in which there was already 920 μl of HAM-F12. In the control, sample cells were put between the electrodes and no pulses were delivered. Control was performed at the beginning and at the end of each experiment to monitor whether the survival or number of cells in the suspension during an experiment had decreased. After all the samples had been exposed to electric pulses (10–20 min), cells were diluted in 0.9 % NaCl and plated in triplicates in 6-well plates (TPP, Switzerland) in 3 ml of HAM-F12. Different numbers of cells were plated, shown in Table 2 for parameters with different lengths of pulses and in Table 3 for parameters with different numbers of pulses (Franken et al. 2006). In preliminary experiments, we determined how many cells have to be seeded in order to obtain around 100 colonies per well. When more intense treatments (600 V, 50–90 pulses and 800 V, 30–90 pulses) were applied, often no cells survived but, because of experimental conditions, we could not seed more cells than the given number. Cells were grown for 6 days at 37 °C and 5 % CO_2.

After 6 days, HAM-F12 was removed and cells were fixed with 1 ml of 70 % ethanol (Lekarna Ljubljana, Slovenia) per well. Cells were left in ethanol for at least 10 min, which rendered all cells dead. Colonies were colored with 200 μl of crystal violet (0.5 % w/v in distilled water) per well. Excessive crystal violet was washed away with pipe water. Colonies that had more than 50 cells were counted. The proportion of surviving cells (S) was calculated as

$$S = \frac{\text{number of colonies after the treatment}}{\text{number of seeded cells } \times \text{ PE}}, \quad (1)$$

where plating efficiency (PE) is defined as

$$PE = \frac{\text{number of colonies formed in the control}}{\text{number of colonies seeded in the control}}. \quad (2)$$

The number of colonies formed in the control was calculated as an average of the triplicates of the colonies formed in the controls at the beginning and at the end of the experiment. The number of colonies seeded in control samples was 100. There was no difference between the two controls, so we could pool the results. At least four independent experiments were performed for each pulse parameter, and mean and standard deviation were then calculated.

In order to determine whether our pulses were indeed not causing significant heating, we measured the temperature of the cell suspension before any pulses were applied and within 5 s after the application of 90 pulses, 4.0 kV/cm, i.e., the most intense exposure. Because of the limitations of the temperature probe, the temperature could not be measured during the pulse application. We used the fiber optic sensor system ProSens (opSens, Canada) with a

Table 1 Experimental parameters of electric pulses, pulse repetition frequency 1 Hz

	Voltage/V	Electric field/kV/cm	Number of pulses/-	Pulse duration/μs
Varying pulse length	0–800, step 100	0–4, step 0.5	8	50, 100 or 200
Varying pulse number	0–800, step 200	0–4, step 1	30, 50, 70 or 90	100

Table 2 Number of plated cells in experiments with different lengths of the pulses, 8 pulses, 1 Hz pulse repetition frequency

Voltage/V	Electric field/kV/cm	Number of plated cells/-		
		For 50 μs	For 100 μs	For 200 μs
0	0	100	100	100
100	0.5	100	100	100
200	1.0	120	120	120
300	1.5	150	150	150
400	2.0	200	200	200
500	2.5	200	400	400
600	3.0	400	1000	1000
700	3.5	1000	2500	2500
800	4.0	2500	10,000	25,000

Table 3 Number of plated cells in experiments with different numbers of the pulses, 100 μs, 1 Hz pulse repetition frequency

Voltage/V	Electric field/kV/cm	Number of plated cells/-			
		For 30 pulses	For 50 pulses	For 70 pulses	For 90 pulses
0	0	100	100	100	100
200	1.0	120	150	200	200
400	2.0	1000	2500	25,000	25,000
600	3.0	25,000	25,000	25,000	25,000
800	4.0	25,000	25,000	25,000	25,000

fiber optic temperature sensor, which was inserted in the cell suspension between the electrodes. In addition, a numerical model of the cell suspension droplet between the electrodes was made and temperature distribution after 90 pulses of 4.0 kV/cm was calculated (Appendix).

Fitting of the Mathematical Models of Survival to the Experimental Results

Different mathematical models of survival were fitted to the experimental data: (i) the first-order kinetics model (Bigelow 1921), (ii) the Hülsheger model (Hülsheger et al. 1981), (iii) the Peleg-Fermi model (Peleg 1995), (iv) the Weibull model (van Boekel 2002), (v) the logistic model (Cole et al. 1993), (vi) the adapted Gompertz model (Linton, 1994), and (vii) the Geeraerd model (Geeraerd et al. 2000). The method of non-linear least squares was applied using Matlab R2011b (Mathworks, USA) and Curve fitting toolbox. Optimal values of the parameters of the mathematical models and R^2 values were determined. R^2 or the coefficient of determination is a statistical measure for the goodness of fit, i.e., it is a correlation between the predicted and experimentally determined values. Its values can be between 0 and 1 and the closer its value is to 1, the better the

fit is. Natural logarithms of mathematical models were fitted to natural logarithms of the experimental data. This prevented the residuals at higher proportions of surviving cells from influencing the R^2 value the most. Treatment time t was understood as the time of exposure of cells to the electric field (E-field). It was calculated as

$$t = NT, \tag{3}$$

where N means number of the applied pulses and T the duration of one pulse.

The first-order kinetics model has a long history (Bigelow 1921):

$$S(t) = \exp(-kt). \tag{4}$$

Here, t denotes the time of exposure of bacteria to high temperature and k is the first-order parameter, i.e., the speed of decrease of the number of bacteria as a function of the duration of their exposure to heat.

Hülsheger studied the effect of E-field on $E.$ $coli$ and derived an exponential empirical model (Hülsheger et al. 1981):

$$S(t, E) = \left(\frac{t}{t_c}\right)^{\frac{-(E-E_c)}{k}}, \tag{5}$$

where k is a constant, which depends on the type of microorganism, E_c is the critical value of E-field below which there will be no inactivation (100 % survival), and t_c is the extrapolated critical value of t below which there will also be no inactivation.

The Peleg-Fermi model (Peleg 1995) has already been used for modeling irreversible electroporation (Garcia et al. 2014; Golberg and Rubinsky 2010) and is defined as

$$S(E, N) = \frac{1}{1 + \exp\left(\frac{E - E_c(N)}{k(N)}\right)}, \tag{6}$$

$$E_c(N) = E_{c0} \exp(-k_1 N), \tag{7}$$

$$k(N) = k_0 \exp(-k_2 N), \tag{8}$$

where E_c means critical E-field, N is the number of applied pulses, k is the kinetic constant that defines the slope of the curve, E_{c0} is the intersection of $E_c(N)$ with the y axis, k_0 is a constant in kV/cm, k_1 and k_2 are non-dimensional constants that depend on the parameters of the pulses and on the cells.

The Weibull model describes the time to failure of electronic devices after they have suffered some stress. The Weibull model is based on the observation that cells die at different times, which are statistically distributed. Cell death due to electroporation can also be described using the Weibull model (van Boekel 2002). We made a parallel: cell death as a function of E-field is also statistically distributed. In addition, no-one has so far observed any correlation between biological parameters and the parameters of the Weibull model. We thus transformed the Weibull model as a function of treatment time to a function of E-field. In previous studies, the independent variable was treatment time (time of exposure to high temperature or E-field). The Weibull model as a function of t is

$$S(t) = \exp\left(-\left(\frac{t}{b}\right)^n\right), \tag{9}$$

where t denotes time of exposure, b is a scale parameter, and n is a shape parameter. We can transform the Weibull model and obtain a model as a function of E:

$$S(E) = \exp\left(-\left(\frac{E}{b}\right)^n\right), \tag{10}$$

where all the parameters have the same meaning as in (9).

The logistic model can be used for describing distributions with a sharp peak and long tails (Cole et al. 1993). The logistic model is defined as

$$S(t) = 10^{\left(\frac{\omega - \alpha}{1 + \exp\left(\frac{4\sigma(\tau - \log_{10}(t))}{\omega - \alpha}\right)}\right)}, \tag{11}$$

where parameter α denotes the common logarithm of the upper asymptote (survival around $t = 0$), ω the common

logarithm of the lower asymptote (survival when $t \to \infty$), σ the maximum slope, and τ the position of the maximum slope. We measured the proportion of surviving cells. After a short treatment time, most of the cells are still alive, survival is 1. Therefore,

$$\alpha = \log(\text{upper asymptote}) = \log 1 = 0. \tag{12}$$

This allows us to simplify the Eq. (11) by assuming $\alpha = 0$:

$$S(t) = 10^{\left(\frac{\omega}{1 + \exp\left(\frac{4\sigma(\tau - \log_{10}(t))}{\omega}\right)}\right)}, \tag{13}$$

where all the parameters have the same meaning as in (11).

A cumulative distribution of cell death was obtained in the experimental results. This means that the experimental data point of proportion of destroyed cells includes also cells that would already die at shorter treatment times or lower E-field values. A derivative of the cumulative cell death distribution shows how cell death is spread over different treatment times or E-field values; it shows cell death distribution. Because our experimental data was discontinuous, we obtained the derivative by calculating the difference in survival between two consecutive data points. We thus obtained the proportion of cells that die in a certain range of treatment time or E-field values, for example from 3000 to 5000 μs or from 1 to 2 kV/cm. Shorter treatment times or lower E-field values do not kill cells in that range. In dependence on the logarithm of the treatment time, the derivative of the cumulative cell death distribution (the derivative of experimental results) has a sharp peak and two long tails. A similar shape of cell death distribution is obtained as a function of E-field (without the logarithm). As already mentioned, the logistic model is suitable for distributions with a sharp peak and long tails. This was our basis for the transformation from treatment time as the independent variable to E-field as the independent variable. The model is

$$S(E) = 10^{\left(\frac{\omega}{1 + \exp\left(\frac{4\sigma(\tau - E)}{\omega}\right)}\right)}, \tag{14}$$

where σ and τ have the same meaning as in (11) and ω denotes survival when $E \to \infty$.

The Gompertz model is usually used for describing growth of a tumor but in an adapted form it has also been used for cell survival (Linton 1994):

$$S(t) = \exp\left(Ae^{-e^{(B_0 + B_1 t)}} - Ae^{-e^{B_0}}\right). \tag{15}$$

A denotes the natural logarithm of the lower asymptote, B_0 is the length of the upper asymptote, and B_1 is connected to the speed of cell death. B_1's absolute value determines the speed, the minus sign means a decrease in the number of

cells and plus means an increase. The adapted Gompertz model is purely empirical and was chosen because it offers an excellent goodness of fit. High R^2 is also obtained if the independent variable is E-field instead of treatment time. This was the reason for the transformation from treatment time as the independent variable to E-field as the independent variable. We transformed the adapted Gompertz model to a model as a function of E:

$$S(E) = \exp(Ae^{-e^{(B_0 + B_1 E)}} - Ae^{-e^{B_0}}), \tag{16}$$

where all the parameters mean the same as in (15).

Geeraerd defined a model that describes exponential decay of the number of surviving cells and a lower asymptote that models the remaining resistant cells (Geeraerd et al. 2000; Santillana Farakos et al. 2013):

$$S(t) = (Y_0 - N_{res})\exp(-kt) + N_{res}. \tag{17}$$

Y_0 means the number of cells at the beginning of experiments, N_{res} is the lower asymptote, and k is the specific inactivation rate (the slope of the exponentially decaying part of the curve). In our study, the number of cells was substituted by the proportion of cells in order to scale the model to our experimental data. At the beginning of our experiments, the proportion of survival was always 1. We simplified the Geeraerd model into

$$S(t) = (1 - N_{res})\exp(-kt) + N_{res}, \tag{18}$$

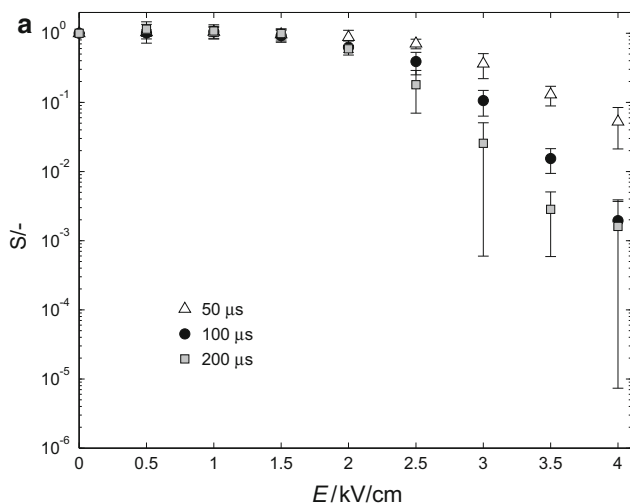where all the parameters have the same meaning as in (17).

Results

Experimental Results

Figure 2 shows the experimental results—Fig. 2a for different pulse lengths and Fig. 2b for different numbers of pulses. Experimental results are shown in a semi-logarithmic scale, which enables low proportions of surviving cells to be visualized. It can be observed in Fig. 2a that longer pulses of the same electric field (E-field) cause lower survival. However, with 8, 200 µs pulses of 4.0 kV/cm, survival is still higher than with 50 or more 100 µs pulses of 4.0 kV/cm (Fig. 2b). When the E-field increases from 1.0 to 2.0 kV/cm, the survival after 50 pulses applied drops by two decades, while after 70 and 90 pulses it drops by three decades. In Fig. 2b, it can be seen that the experimental values of survival are very similar for 50, 70, and 90 pulses of 3.0 kV/cm and 4.0 kV/cm.

Results of the Mathematical Modeling

The results of the mathematical modeling are presented in two ways. First, Tables 4, 5, 6, and 7 summarize the optimal values of the parameters and R^2 values for all the mathematical models described in the Materials and Methods section. Figures 3, 4, 5, and 6 show plotted optimized mathematical models. When the results of the fitting are presented in linear scale, the curves go straight and exactly

Fig. 2 Experimental results of the clonogenic assay for different pulse lengths (**a**) and for different numbers of pulses (**b**) as a function of the applied electric field (E). Mean ± one standard deviation is shown, pulse repetition frequency 1 Hz. If mean minus standard deviation is lower than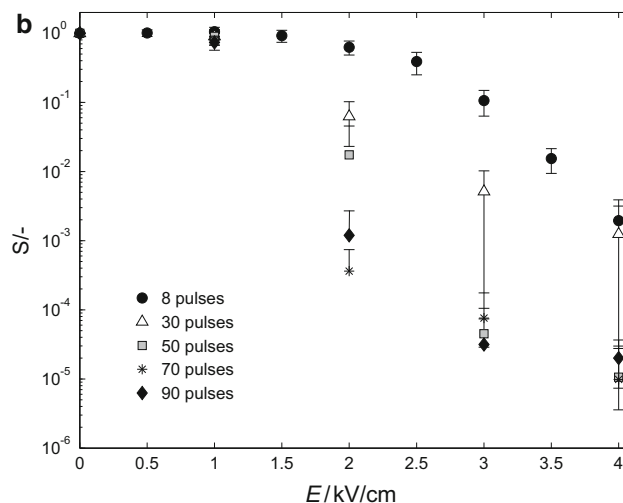 0, it cannot be presented in a semi-logarithmic scale and there is no error bar. The survival is lower when longer pulses are applied and the electric field is held fixed. However, higher number of pulses decreases the survival considerably. With 8, 200 µs pulses of 4 kV/cm, the survival is still higher than with 50 or more 100 µs pulses, 4 kV/cm

Table 4 Calculated optimal values of parameters of mathematical models as a function of treatment time and R^2 value for different electric field values

Mathematical models	Parameters	Optimized values of parameters and R^2 value		
		For 2.0 kV/cm (400 V)	For 3.0 kV/cm (600 V)	For 4.0 kV/cm (800 V)
First-order kinetics model (4)	k	0.0008805	0.001382	0.001582
	R^2	0.9096	0.8237	0.4747
Weibull model (9)	b	908	112	3.178
	n	0.8915	0.5490	0.3105
	R^2	0.9135	0.9442	0.9225
Logistic model (13)	ω	–3.925	–6.026	–20.760
	σ	–5.059	–4.240	–2.815
	τ	3.659	3.532	4.078
	R^2	0.9346	0.9607	0.9260
Adapted Gompertz model (15)	A	–8.18	–14.15	–16.05
	B_0	1.419	0.3732	1.8e-6
	B_1	–0.0004339	–0.0004419	–0.001291
	R^2	0.9389	0.9661	0.8539
Geeraerd model (18)	N_{res}	0.0005619	4.157e−5	4.014e−5
	k	0.001004	0.002011	0.007824
	R^2	0.9390	0.9788	0.8411

In all the experiments, pulses of 100 µs duration with pulse repetition frequency 1 Hz were applied

through the experimental results. In semi-logarithmic scale, deviations are more easily noticed. When fitting survival models to experimental results, it is advisable also to look at the data in semi-logarithmic scale. All our results are therefore presented in semi-logarithmic scale. When comparing the values of our optimized parameters with the values in other studies, it must be borne in mind that on the x axis there are t in µs or E-field in kV/cm.

Mathematical Models Describing Cell Survival as a Function of Treatment Time

A good fit could not be achieved using the Hülsheger model (5) because there were problems with the initial value of the parameters and local minima. The results are thus not shown and we do not discuss them.

In Fig. 3, (3.0 kV/cm, 100 µs, 1 Hz) it can be observed that the Weibull model (9), the logistic (13), the adapted Gompertz (15), and the Geeraerd models (18) are all similarly shaped and go very close to the experimental points. From the point of goodness of fit, they can be seen as equally good. The first-order kinetics model (4) is only able to describe a straight line in semi-logarithmic scale (Fig. 3, gray dashed line). It is unadaptable and offers low R^2 (0.47–0.90). Because of very low goodness of fit, the meaning of its parameters is not relevant.

Table 4 gives the optimized values of the parameters of the mathematical models as a function of treatment time. In

the Weibull model (9), the values of n and b decrease with a higher applied E-field. In the logistic model (13), the value of the parameter ω decreases with higher E. The values of parameter τ are very similar. The values of σ increase with longer pulses, as expected (higher value, steeper slope). In the adapted Gompertz model (15), the values of parameter A decrease, which means a lower asymptote is reached. The values of parameters B_0 and B_1 also decrease, which means faster cell death with longer pulses applied. In the Geeraerd model (18), N_{res} corresponds to the remaining surviving cells and decreases with higher E (similar to parameter A in the Gompertz model). Parameter k corresponds to the speed of decrease and also increases, both as expected.

Mathematical Models Describing Cell Survival as a Function of Electric Field

In Fig. 4 (8, 100 µs pulses, 1 Hz), it can be observed that all models look very similar. The difference is in their behavior at high E-fields, i.e., in extrapolation of the data. In terms of goodness of fit, all four models on Fig. 4 (Peleg-Fermi (6), Weibull (10), logistic (14) and Gompertz (16)) can be considered equal.

In Fig. 5 (90, 100 µs pulses, 1 Hz), however, the differences among the models are more pronounced. They no longer overlap as shown in Fig. 4. The Peleg-Fermi (6) and Weibull models (10) go close but not exactly through the

Table 5 Calculated optimal values of parameters of mathematical models as a function of electric field and R^2 for different lengths of the pulses

Mathematical models	Parameters	Optimal values of parameters and R^2 value		
		For 50 μs	For 100 μs	For 200 μs
Peleg-Fermi model (6)	E_c/kV/cm	2.766	2.344	2.001
	k/kV/cm	0.4160	0.2677	0.2871
	R^2	0.9968	0.9975	0.9836
Weibull model (10)	b	2.992	2.408	1.936
	n	2.831	3.645	2.695
	R^2	0.9900	0.9964	0.9615
Logistic model (14)	ω	−1.555	−3.780	−2.961
	σ	−0.963	−1.888	−2.082
	τ	3.383	3.537	2.916
	R^2	0.9966	0.9951	0.9809
Adapted Gompertz model (16)	A	−5.348	−19.080	−7.692
	B_0	3.528	2.683	4.149
	B_1	−1.013	−0.6438	−1.505
	R^2	0.9987	0.9991	0.9961

In all the experiments, 8 pulses with pulse repetition frequency 1 Hz were applied

Table 6 Optimized values of parameters of mathematical models as a function of E and R^2 for different numbers of the pulses; the column 8 pulses is the same as the column 100 μs in Table 5

Mathematical models	Parameters and R^2	Optimal values of parameters and R^2 value				
		For 8 pulses	For 30 pulses	For 50 pulses	For 70 pulses	For 90 pulses
Peleg-Fermi model (6)	E_c (kV/cm)	2.3440	0.9720	0.9517	0.4298	0.4853
	k (kV/cm)	0.2677	0.4260	0.2446	0.2833	0.2852
	R^2	0.9975	0.8959	0.9637	0.9085	0.9148
Weibull model (10)	b	2.336	1.030	0.731	0.388	0.416
	n	3.410	1.439	1.480	1.076	1.098
	R^2	0.9989	0.9652	0.9408	0.9004	0.9039
Logistic model (14)	ω	−3.78	−2.93	−4.99	−4.58	−4.63
	σ	−1.888	−1.474	−3.308	−5.029	−4.483
	τ	3.537	2.260	2.243	1.754	1.863
	R^2	0.9951	0.9918	0.9989	0.9825	0.9995
Adapted Gompertz model (16)	A	−19.08	−7.23	−11.74	−10.82	−10.96
	B_0	2.683	2.439	3.849	3.372	3.348
	B_1	−0.643	−1.221	−1.894	−2.221	−2.037
	R^2	0.9991	0.9987	0.9999	0.9865	0.9999

In all the experiments, pulses of 100 μs duration with pulse repetition frequency 1 Hz were applied

experimental points (R^2 between 0.90 and 0.91), since they cannot model the lower asymptote but only a shoulder and then a constant decrease of cell survival (on a semi-logarithmic scale). The logistic and the adapted Gompertz models, on the other hand, go exactly through the experimental points ($R^2 > 0.99$) and also look very similar. From the point of view of the adaptability of the models, the logistic and Gompertz models are better than the Weibull (10) and Peleg-Fermi models (6).

Table 5 shows the results of fitting mathematical models as a function of E-field for different pulse lengths. The results of fitting the Peleg-Fermi model (6), the Weibull model (10), the logistic model (14), and the adapted Gompertz model (16) as a function of E-field are presented. For each model, the optimal values of the parameters and R^2 value for three different pulse durations (50, 100 and 200 μs) are shown.

Table 6 presents the results of fitting mathematical models as a function of E-field for different numbers of pulses. Optimal values of parameters and R^2 values for each fit are shown. The pulse length was held fixed at 100 μs. It can be seen that R^2 values are relatively high for

Table 7 Calculated optimal values of parameters of additional Peleg-Fermi mathematical models (7), (8) for E_c and k as functions of N

Mathematical models	Parameters	Optimal values of parameters and R^2 value
Peleg-Fermi mathematical model for $E_c(N)$ (7)	E_{co} (kV/cm)	2.734
	k_1	0.02506
	R^2	0.9237
Peleg-Fermi mathematical model for $k(N)$ (8)	k_0 (kV/cm)	0.3259
	k_2	0.001598
	R^2	0.04916

all the fits in Tables 5 and 6. The trends of the models are therefore analyzed more carefully for each of the models separately in the following paragraphs.

The plotted optimized Peleg-Fermi model (6) is presented in Fig. 6a. The Peleg-Fermi model (6) has an additional two models, which describe E_{c0} (7) and k (8) as functions of the number of pulses (N). Optimal parameters of these two models (7), (8) are plotted in Fig. 6b. In Fig. 6a, it can be seen that for higher numbers of pulses (50 or more), the model does not go exactly through the experimental points. For 8 and for 30 pulses, the Peleg-Fermi model describes the data very well, since there are no problems with modeling the lower asymptote. In Fig. 6b, it can be seen that Eq. (7) fits the experimental points well (black circles). However, Eq. (8) does not fit the data well (white squares on Fig. 6b), $R^2 = 0.049$. Equation (8) suggests an exponential dependence of k on
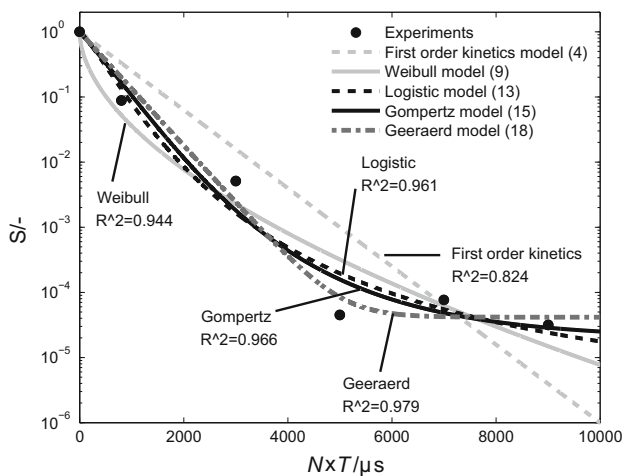

Fig. 4 Mathematical models (*lines*) and experimental results (*symbols*) showing cell survival as a function of electric field (8 pulses, 100 μs, 1 Hz). On *y* axis, there is the proportion of the surviving cells (S) in logarithmic scale. For each fit, R^2 value is shown. All the models as a function of electric field offer a similarly good fit ($R^2 > 0.99$). We found the adapted Gompertz (16), the Peleg-Fermi model (6)–(8), and maybe the logistic (14) model to be the most suitable

the number of pulses, while in our data the value of k is almost constant.

Table 7 presents additional results of fitting the Peleg-Fermi model, in which optimal values of the parameters and R^2 value for each fit of Eqs. (7) and (8) are shown. As already observed in Fig. 6b, Eq. (8) does not describe our data well. It can be observed that the goodness of fit is relatively high for the Peleg-Fermi model (>0.89) for different durations (Table 4), as well for different numbers of pulses (Table 5).

The Weibull model as a function of E-field (10) has a similar shape as the Peleg-Fermi model (6) (Fig. 5). The Weibull model cannot describe a sigmoid shape in semi-logarithmic scale, so a deviation at higher E-field of more than 8 pulses is noticeable (compare gray solid lines in Figs. 4 and 5). The meaning of the parameters of the Weibull model has not yet been established (10) and there is also no trend in the value of parameter n in our results. The value of parameter b decreases with longer pulses (Table 5) and with a higher number of pulses applied (Table 6).

The logistic (14) model is more adaptable and has a concave (Fig. 4) or sigmoid shape (Fig. 5) in semi-logarithmic scale. When fitting the logistic model (14) to the results of different pulse lengths (Table 5), σ decreases (faster death). Parameter τ denotes where on the x axis the decrease is fastest. It is similar for all pulse lengths (Table 5). When only 8 pulses of different lengths are applied (Table 5), the asymptote is not reached (Fig. 1a). Although the model predicts an asymptote, it is outside the

Fig. 3 Mathematical models (*lines*) and experimental results (*symbols*) showing cell survival as a function of the treatment time (3 kV/cm, 100 μs, 1 Hz). On *y* axis, there is the proportion of the surviving cells (S) in logarithmic scale. For each fit, R^2 value is shown. Except for the first-order kinetics model (4), all the models offer a good fit ($R^2 > 0.94$). We found the adapted Gompertz (15) and the Geeraerd model (18) to be the most suitable
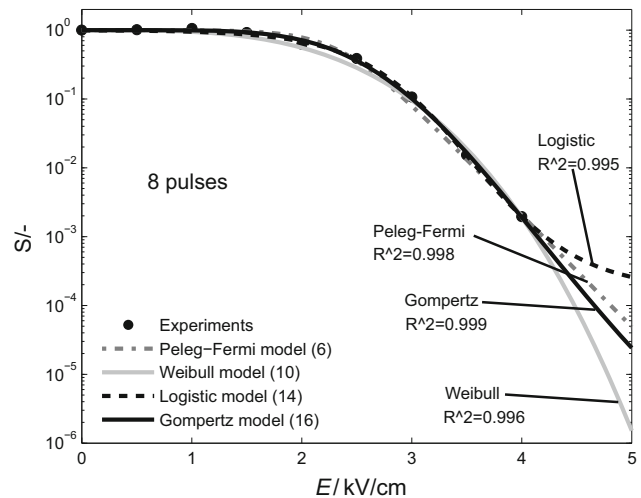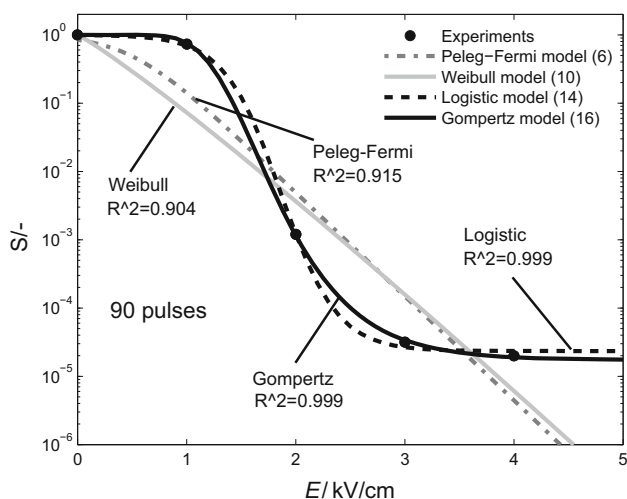
Fig. 5 Mathematical models (*lines*) and experimental results (*symbols*) showing cell survival as a function of electric field (90 pulses, 100 μs, 1 Hz). On *y* axis, there is the proportion of the surviving cells in logarithmic scale. For each fit, R^2 value is shown. Experimental values at 3 kV/cm and at 4 kV/cm (the lower asymptote) are on the limit of our detection. We found the adapted Gompertz (16), the Peleg-Fermi model (6)–(8), and maybe the logistic (14) model to be the most suitable

range in which our models are valid. In this case, the value of ω is not relevant since the models are not meant for extrapolation of the data. When fitting the logistic model to the results of different numbers of pulses, the parameters cannot be so easily explained. Parameter ω is similar with more pulses applied (Table 6) since we reach a similar lower asymptote (Fig. 1b). Parameter σ is similar for 70 and 90 pulses and on average higher than for 30 and 50 pulses. This means faster cell death when 70 or 90 pulses

are applied. Parameter τ mostly decreases with a higher number of pulses applied (Table 6), which means that cells die at lower *E*-fields when more pulses are applied.

When applying the adapted Gompertz model (16) to the results of different pulse lengths, the values of parameter *A* are quite different (Table 5) because the lower asymptote was not reached in the experiments (Fig. 2a). Parameter *A* also does not have a trend with different numbers of pulses applied (Table 6), but the reason could be that with 50, 70, or 90 pulses, there is a similar proportion of surviving cells at higher *E*-field (around 10^{-5}). Parameters B_0 and B_1 in Table 5 have similar values since the experimental values for different lengths of the applied pulses are similar. The value of B_0 is similar for different numbers of pulses (Table 6) since it denotes the length of the upper asymptote, which is similar for all lengths of pulses (Fig. 5). B_1 decreases with more pulses (Table 6), which means faster death with more pulses applied.

Discussion

Several mathematical models are able to describe experimental results. The most appropriate models as a function of treatment time are the adapted Gompertz (15) and the Geeraerd models (18). The logistic model (13) can be used but a clearer meaning of its parameters needs to be established. The most appropriate models as a function of electric field (*E*-field) were the Peleg-Fermi (6), the logistic (14), and the adapted Gompertz models (16). Mathematical models of cell survival could thus be integrated into treatment planning of electrochemotherapy and irreversible
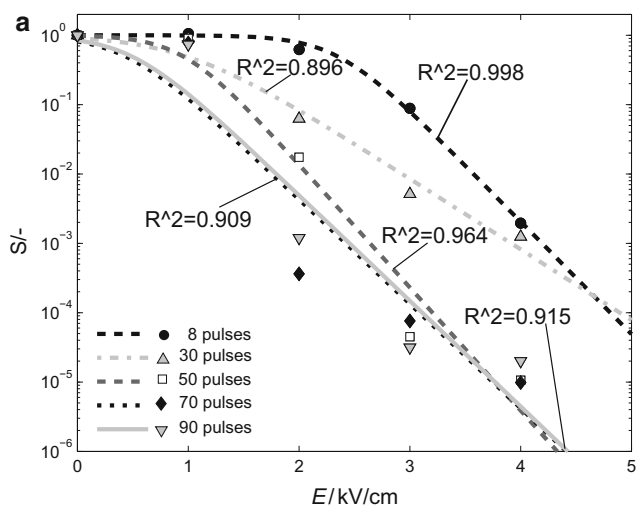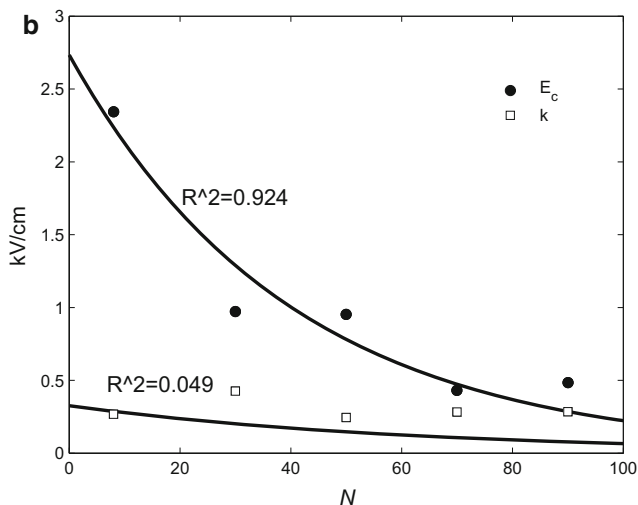

Fig. 6 The Peleg-Fermi model (6) for different numbers of pulses applied. For each fit, R^2 value is shown. **a** Symbols are the experimental values for 1 Hz, 100 μs, *lines* show the Peleg-Fermi model (6). **b** Symbols are the optimized values of E_c and *k*, *lines* show the optimized mathematical models (7) and (8). On *y* axis, there are

the values of E_c and *k* in kV/cm. Since the Peleg-Fermi model (6) incorporates dependence on *E* as well as on *N* (7), (8) it already connects two treatment parameters (electric field and number of the pulses) and can therefore be used more easily than other models investigated in this study

electroporation as a method of tissue ablation. It must be emphasized that the models should not be extrapolated, since they predict different behaviors at very high E-fields or very long treatment time. Some of them keep on decreasing and some of them reach a stable value on a semi-logarithmic scale.

Experimental Considerations

The electrical parameters chosen for the experiments were similar to electrochemotherapy and irreversible electroporation electrical parameters typically used in vivo. For electrochemotherapy parameters, we used a fixed number of pulses (8) and we varied the length of the pulses. In electrochemotherapy treatments, 100 μs pulses are usually used but to evaluate the trend of the parameters of the mathematical models we also applied 50 μs and 200 μs pulses (results on Fig. 2a). For irreversible electroporation parameters, we tried to cover the parameter space as equally as possible. In an orthogonal space, where on one axis there was number of the pulses (N) and on the other E-field, we equidistantly sampled it by increasing the voltage by 200 V and the number of pulses by 30 (results on Fig. 2b).

An important aspect of irreversible electroporation experiments is the effect of increased temperature. Because of high voltage, many pulses, and high current, the temperature in the tissue or (as in our case) in the cell suspension can be increased considerably by Joule heating (Županič and Miklavčič 2011). Heating can change the conductivity of the cells, as well as damage them (Neal et al. 2012). Cell death could therefore be a thermal and not electrical effect (Garcia et al. 2014). The temperature of the suspension was therefore measured before and within 5 s after the end of application of 90 pulses, 4.0 kV/cm (the most severe electrical parameters employed in our study). Even with the most severe electrical parameters, the temperature within 5 s after the end of pulse application did not surpass 40 °C. This proved that, under our experimental conditions, cell death can indeed be considered solely as a consequence of irreversible electroporation.

The percentage of surviving cells was first evaluated using tetrazolium based assay (MTS assay). The MTS assay, however, proved not suitable for distinguishing between low proportions of surviving cells and it cannot be used to quantify the number of living cells exactly. The MTS assay is based on measurements of absorbance, which is then correlated to the number of metabolically active cells. After reaching 2 % of the surviving/metabolically active cells, the number did not drop, no matter how much higher an E-field or how many more pulses we applied. Since irreversible electroporation can be used successfully to treat tumors, a lower percentage of surviving cells should be achievable. In addition, metabolic activity and the ability to divide do not necessarily correlate. We therefore decided to use clonogenic assay, which requires more time than the MTS assay but enables exact quantification of the number of clonogenic cells. With more severe treatments, we could detect as low as 1 surviving cell in 25,000 (4×10^{-5} survival). In some experiments, the survival was lower than 4×10^{-5} because the final proportion of surviving cells was calculated as a mean over at least four repetitions. Often no cells survived (0 survival) with severe treatments. In calculating the mean, the 0 survival caused the final proportion of the survival to be lower than 4×10^{-5}. The detection limit of our clonogenic assay was thus reached at approximately 4×10^{-5}. The lower asymptote that can be observed in Fig. 2b for 50, 70, and 90 pulses at 3.0 and 4.0 kV/cm could be a consequence of the detection limit. For more precise (and lower), proportions of surviving cells at high E-field values and many pulses, more cells should be seeded, which can be achieved using a denser cell suspension. However, more precise results with denser cell suspension are perhaps not even needed. *In vivo*, the last few clonogenic cells seem to be eradicated by the immune system when performing electrochemotherapy (Calvet et al. 2014; Mir et al. 1992; Serša et al. 1997), as well as irreversible electroporation (Neal et al. 2013). The proportion of cells needed to kill to cause a complete response and destroy the whole tumor should be determined in future studies.

In our experimental results, we determined that the transition area between maximum and minimum survival gets narrower, i.e., the death of cells is quicker with higher numbers of pulses applied (Fig. 1b). This is in agreement with the theoretical predictions made (Garcia et al. 2014) using the Peleg-Fermi model. The authors predicted that the transition zone between electroporated and non-electroporated tissue becomes sharper when more pulses are applied.

There are also other parameters of the electric pulses, and biological parameters, which could affect the survival of cells. For example, the pulse repetition frequency in our experiments was always 1 Hz and when calculating the treatment time as $t = NxT$, we ignored the effect of pulse repetition frequency. There are contradicting studies that report on its effect on cell survival (Pakhomova et al. 2013; Pucihar et al. 2002; Silve et al. 2014). The effect of pulse repetition frequency on the shape of survival curves needs also to be investigated in future studies. It must be emphasized that even if $t_1 = t_2 = N_1 T_1 = N_2 T_2$ his cannot be necessarily understood as equal if $T_1 \neq T_2$ and $N_1 \neq N_2$. Different repetition frequencies affect cell permeabilization, and cell survival and temperature increase differently. We therefore present and discuss the results of different numbers and different lengths of applied pulses separately.

The value of E-field applied in the tissue is needed for correct prediction of surviving cells. At the moment, the most reliable method of determining E-field in tissues is numerical modeling. However, in future, the E-field in tissue could be monitored using current density imaging and magnetic resonance electrical impedance tomography (Kranjc et al. 2012, 2015). Cell survival in tissue could be correlated even better by taking into account conductivity changes (Kranjc et al. 2014) measured during application of the pulses.

One possible problem with prediction of cell death in tissues is the use of mathematical models fitted in vitro in an in vivo environment. Tissues, unlike cell suspensions, are heterogeneous; there are connections between cells; cells are irregularly shaped; extracellular fluid is more conductive than the pulsing buffer used in our study; and there is an immune system present. Before starting clinical studies, the parameters of electric pulses are first tested on cell lines. In the past, good correlation was found between the behavior of cells in vitro and in vivo. We expect survival curves in tissues to have a similar shape as in our in vitro study. The question is whether there will be a lower asymptote present or survival as a function of treatment time or E-field will keep decreasing. Our models can describe both options. The optimal values of the parameters depend on the sensitivity of the cells to the electric pulses and will probably be different. If the threshold values of the E-field for reversible and irreversible electroporation for different tissues are compared, different values can be found. For example, in vivo the threshold values of the E-field for muscle (8×100 µs pulses) for reversible electroporation have been determined to be 0.08 kV/cm and 0.2 kV/cm (parallel and perpendicular directions, respectively) and for irreversible electroporation to be 0.4 kV/cm (the same for parallel and perpendicular directions of muscle fibers) (Čorović et al. 2010, 2012). In vivo the threshold for irreversible electroporation of healthy prostate tissue has been determined to be 1 kV/cm (90×70 µs pulses) (Neal et al. 2014), and for healthy brain tissue 0.5 kV/cm (90×50 µs pulses) (Garcia et al. 2010). For healthy liver tissue, the threshold for reversible electroporation has been reported to be 0.36 kV/cm and for irreversible electroporation 0.64 kV/cm (Miklavčič et al. 2000). The thresholds thus seem to be different for different tissues (Jiang et al. 2015). In vitro the thresholds are usually higher and different for different cell lines: for reversible electroporation around 0.4 kV/cm and for irreversible electroporation around 1.0 kV/cm for 8×100 µs pulses (Čemažar et al. 1998). The curves in vivo can therefore be expected to have a similar shape but they will be scaled according to the thresholds for different types of tissue.

Mathematical Modeling

It was mentioned in the Introduction section that predictive power is one of the three most important criteria for choosing the model (in addition to goodness of fit and trends of values of the optimized parameters of the models). In our current study, however, predictive power was not assessed. For assessing predictive power, our optimized models must be validated on the samples for which the survival will be predicted. In our case, the models will be used in predicting death of tissues in electrochemotherapy and irreversible electroporation. Validation of the models on tissues is beyond the scope of this paper but must be done before implementing the models in actual treatment planning of electroporation-based treatments. The reader should also note that all the models approach 0 survival asymptotically but can never actually reach 0 survival. As already discussed, it is still not known how many cells must be killed to achieve a complete response of the tumor. Based on the fact that the immune system seems to eradicate the last remaining tumor cells, it seems that our models adequately describe 0 to 100 % survival. It remains to be established, however, what percentage of cells actually needs to be killed by irreversible electroporation.

Mathematical Models Describing Cell Survival as a Function of Treatment Time

We fitted the first-order kinetics (4), the Weibull (9), the logistic (13), the adapted Gompertz (15), and the Geeraerd (18) models to the experimental data as a function of treatment time. At 1.0 kV/cm (200 V), the percentage of surviving cells decreased to 68 % for 90 pulses, 100 µs, 1 Hz. The results of fitting the models to 200 V are thus not presented, since the decrease in survival was too small to be relevant for describing cell death due to electroporation.

It can be seen in Fig. 3 that, except for the first-order kinetics model (4), all the models describe the experimental points well. From the point of goodness of fit, the Weibull (9), the logistic (13), the adapted Gompertz (15), and the Geeraerd model (18) are equal. The next criterion is the trend of parameters which is to be discussed for each model separately in the next paragraph.

The first-order kinetics model (4) has a very low R^2 (Table 4) and it is not suitable for describing cell death. It is still very often used for describing microbial inactivation. (Peleg 2006) stated that the first-order kinetics model is popular because any data can be described with it if the data are sampled too sparsely. The second reason for its popularity is its long history. In the Weibull model (9), the parameters have a trend. However, in many studies, it has been shown that parameter n is not connected to any

biological or other parameter (Álvarez et al. 2003; Mafart et al. 2002; Stone et al. 2009; van Boekel 2002). It only describes the shape of the curve (concave, convex, linear). The Weibull model is often used because it is highly adaptable and can describe different shapes. Because the Weibull model was used in many previous studies, but the meaning of the parameters was not established in any of them, the Weibull model is most likely not suitable for predicting cell death after electroporation. The logistic model (14) has a high R^2 and most of its parameters can be connected to some biological parameter. It may be suitable for predicting cell death due to electroporation but the meaning of its parameters must be more clearly defined. In the adapted Gompertz model (16), both parameters B_0 and B_1 behave as expected (shorter upper asymptote and steeper decline). The Geeraerd model was defined for the shapes of curves just like ours—first the number of the cells exponentially decreases and, after a certain treatment time, it reaches a lower asymptote. The R^2 value was high and there was a trend of the values of the parameters.

It can be concluded that, as a function of treatment time, adapted Gompertz and Geeraerd models are suitable, while the logistic model has potential but should be tested with more electrical parameters.

Mathematical Models Describing Cell Survival as a Function of Electric Field

It can be seen in Fig. 4 that if there is no lower asymptote present, all the models describe the data well and have a similar R^2 value. In Fig. 5, a lower asymptote is present and the goodness of fit is different for different models. Looking at Figs. 4 and 5, it can be said that the logistic (14) and the adapted Gompertz models (16) are most suitable. In the Weibull model (10) (Tables 5, 6), there is no trend in the values of the optimized parameters. The Weibull model is not suitable for the use in treatment planning. The adapted Gompertz model (16) has high R^2 and the values of its parameters can be explained. The adapted Gompertz model is thus suitable for describing cell death after electroporation.

The logistic model (14) is highly adaptable. Because of the detection limit, not all values of the parameters behave as expected. Until the detection limit is reached (Fig. 2a), all the parameters can be explained (Table 5). It can therefore be said that the logistic model is probably suitable but it should be tested on a larger dataset.

We mentioned before that the Peleg-Fermi model (6) does not well describe cell death for higher numbers of the pulses. The reason is that it is not suitable for describing lower asymptotes. However, it is very likely that the lower asymptote is a consequence of the detection limit of the clonogenic assay. In this case, it is not problematic that the lower asymptote cannot be described. If it is discovered

in vivo that there is a lower asymptote present, the usefulness of the Peleg-Fermi model will have to be evaluated separately for in vivo data. When the Peleg-Fermi model (6) was fitted to our in vitro experimental results, the E-field was the independent variable and the number of the pulses or their length was the parameters. Unfortunately, with different lengths of applied pulses, we could not model the change of $k(N)$ and $E_c(N)$, since there is no model to connect k and E_c with the length of the applied pulses. With different numbers of applied pulses (Table 6), we could also evaluate models for $E_c(N)$ (7) and $k(N)$ (8) (Table 7). The value of E_c decreases with a higher number of pulses (Table 6), is in agreement with our understanding of E_c as a critical E-field (Pucihar et al. 2011) and can be described using the proposed model (7). E_c changes less with a higher number of pulses. An even higher number of pulses applied would probably not lower the critical electric field but most likely only increase the heating. Values of k are approximately similar for all different numbers of applied pulses and they cannot be described using the proposed model (8). One reason may be the sensitivity of the clonogenic assay, as mentioned before. With more pulses, there could be even lower proportions of surviving cells, the model would be steeper and the value of parameter k would decrease. In (Golberg and Rubinsky 2010), the model was fitted to experimental data of up to 10 pulses applied, while in our study we fitted it to up to 90 pulses applied. Equation (8) may be exponential for up to 10 pulses applied but for more pulses it seems more like a constant. Equation (8) should be verified on tissues to see whether there is an exponential dependency. We assume that the Peleg-Fermi model (6), (7) will be suitable for use in treatment planning of electrochemotherapy and irreversible electroporation, while the dependency of parameter k on the number of pulses (8) remains questionable.

We next compared the values of our optimized parameters to the values reported in the literature. Our values of E_c and k are lower than in (Golberg and Rubinsky 2010) and optimized to describe the experimental results for 8–90 pulses. The authors in (Golberg and Rubinsky 2010) optimized their parameters to 1–10 pulses, whereby the decrease of the number of cells in dependency on the E-field is slower and smaller than for more pulses. This could explain the lower values of k and E_c as well as the non-exponential dependence of Eq. (8). The Peleg-Fermi model (6) seems the most promising of all the models analyzed in this study, since it also includes dependency on the number of pulses.

It can be concluded that the Peleg-Fermi (6), the adapted Gompertz (16), and probably also the logistic model (14) can all be used for describing cell death due to electroporation and could all be used in treatment planning of electrochemotherapy and irreversible electroporation.

Table 8 Parameters, used in our numerical model, with their symbols, values, and units

Name of the parameter	Symbol	Value	Units
Electrical conductivity	σ_s	0.162[S/m] $\times$ (1 + 0.02 $\times$ (T[degC]-20))	S/m
	σ_e	1.73913[MS/m] $\times$ (1 + 0.00094 $\times$ (T[degC]-20))	
Heat capacity at constant pressure	Cp_s	4200	J/(kg K)
	Cp_e	500	
Density	ρ_s	1000	kg/m^3
	ρ_e	8000	
Thermal conductivity	k_s	0.58	W/(m K)
	k_e	15	
Relative permittivity	ε_s	80	–
	ε_e	1	

Subscript s denotes cell suspension and subscript e denotes electrodes

Since the Peleg-Fermi model incorporates dependence on E-field as well as on the number of pulses it already connects two electrical parameters and can therefore be used more easily, while such connections still have to be determined for other models.

Conclusion

Mathematical models can describe cell death after electroporation. Hopefully, they can also be used in treatment planning of electrochemotherapy and irreversible electroporation as a method of tissue ablation. Mathematical models suitable for treatment planning have to describe the data well, have predictive power, and their parameters have to have a trend. Using the probability of cell death, the treatment plan can be made more reliable and also more comprehensive. Instead of displaying the electric field around the electrodes, the probability of tissue destruction around the electrodes can be shown. In this study, it was shown that not only the Peleg-Fermi but also other models are suitable for describing in vitro experimental results. However, it still needs to be determined whether the proposed mathematical models also have predictive and not just descriptive power. Our results are valid only for one cell line in suspension under our experimental conditions. The question is whether mathematical models could also be translated to tissues and more complex geometries. This validation should be done on tissues since the models will be used on tissues. Applying mathematical models of survival to tissues is thus the next step.

Appendix: Numerical Model of Temperature Distribution

We calculated temperature distribution to determine that 90, 100 μs pulses of 4 kV/cm and 1 Hz repetition frequency do not induce significant Joule heating. A numerical model of a drop of cell suspension between parallel plate electrodes was made in Comsol Multiphysics (v4.4, Comsol, Sweden) using Electric Currents, Heat Transfer, and Multiphysics modules in time-dependent analysis. Electrodes were modeled as two blocks of 20 $\times$ 10 $\times$ 1 mm and a drop of cell suspension was modeled as a block of 7 $\times$ 7 $\times$ 2 mm. Two boundaries, one on each electrode, were modeled as terminals, with +400 V and −400 V in the first 90 s of the simulation, while the other boundaries were electrically insulated. Similar as in (Garcia et al. 2011a, b), only one pulse was applied for 90 s, but we multiplied the Joule heating by the duty cycle (duration/period) to adjust the amount of delivered energy. We ran the simulation for an additional 5 s after the pulse application to validate the model with our temperature measurements, since measurements of temperature were made within 5 s after the pulse application.

The change of conductivity due to cell electroporation was disregarded in the model, since our cell suspension was dilute. The values of parameters used in the simulation are shown in Table 8. The properties of the cell suspension (except for electrical conductivity, which is characteristic of our electroporation buffer) are the same as for water.

The model was validated with current and temperature measurements at 90, 100 μs pulses, 4 kV/cm, 1 Hz repetition frequency. The predicted current (3.3 A) was in the same range as the measured current (from 2.9 to 3.5 A). Temperature measured within 5 s after the pulse application was 37.0 °C, while the predicted temperature 5 s after
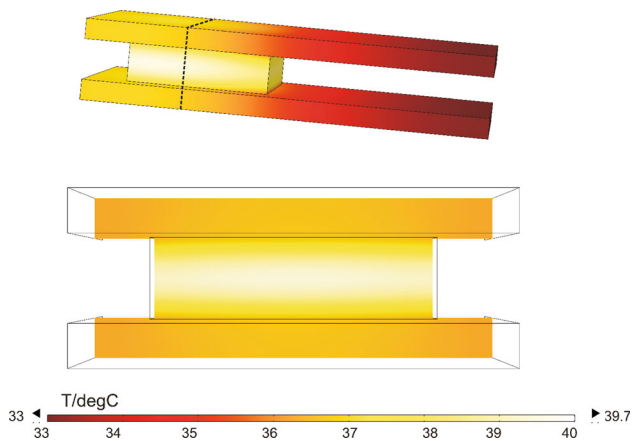
Fig. 7 Temperature distribution after 90, 100 μs pulses of 4 kV/cm. The *upper image* shows the temperature distribution on the surface of the electrodes and on the drop of the cell suspension. The *black dashed line* in the *upper image* shows where a cut plane for the lower image was made. The *lower image* shows a cut plane of the temperature distribution which goes through the middle of the electrodes. We can see that the temperature does not surpass 42 °C, therefore cell death can be ascribed solely to electroporation

the pulse application was 37.6 °C. The model thus adequately described our experiments.

The temperature distribution on the surface of the cell suspension and on the electrodes, and a slice through the drop of cell suspension after 90 pulses, is shown in Fig. 7. Since the temperature of the cell suspension does not exceed 42 °C, under our experimental conditions cell death can indeed be ascribed to electroporation.

References

Álvarez I, Virto R, Raso J, Condón S (2003) Comparing predicting models for the *Escherichia coli* inactivation by pulsed electric fields. Innov Food Sci Emerg Technol 4:195–202. doi:10.1016/S1466-8564(03)00004-3

Bigelow WD (1921) The logarithmic nature of thermal death time curves. J Infect Dis 29:528–536

Calvet CY, André FM, Mir LM (2014) Dual therapeutic benefit of electroporation-mediated DNA vaccination in vivo: enhanced gene transfer and adjuvant activity. OncoImmunology 3:e28540. doi:10.4161/onci.28540

Campana LG, Di Barba P, Dughiero F, Rossi CR, Sieni E (2013) Optimal needle positioning for electrochemotherapy: a constrained multiobjective strategy. IEEE Trans Magn 49:2141–2144. doi:10.1109/TMAG.2013.2241031

Canatella PJ, Karr JF, Petros JA, Prausnitz MR (2001) Quantitative study of electroporation-mediated molecular uptake and cell viability. Biophys J 80:755–764

Cannon R, Ellis S, Hayes D, Narayanan G, Martin RCG (2013) Safety and early efficacy of irreversible electroporation for hepatic tumors in proximity to vital structures. J Surg Oncol 107:544–549. doi:10.1002/jso.23280

Čemažar M, Jarm T, Miklavčič D, Maček Lebar A, Ihan A, Kopitar NA, Serša G (1998) Effect of electric-field intensity on

electropermeabilization and electrosensitivity of various tumor-cell lines in vitro. Electro-Magnetobiology 17:263–272

Cole MB, Davies KW, Munro G, Holyoak CD, Kilsby DC (1993) A vitalistic model to describe the thermal inactivation of Listeria monocytogenes. J Ind Microbiol 12:232–239. doi:10.1007/BF01584195

Čorović S, Županič A, Kranjc S, Al Sakere B, Leroy-Willig A, Mir LM, Miklavčič D (2010) The influence of skeletal muscle anisotropy on electroporation: in vivo study and numerical modeling. Med Biol Eng Comput 48:637–648. doi:10.1007/s11517-010-0614-1

Čorović S, Mir LM, Miklavčič D (2012) In vivo muscle electroporation threshold determination: realistic numerical models and in vivo experiments. J Membr Biol 245:509–520. doi:10.1007/s00232-012-9432-8

Daud AI, DeConti RC, Andrews S, Urbas P, Riker AI, Sondak VK, Munster PN, Sullivan DM, Ugen KE, Messina JL, Heller R (2008) Phase I trial of interleukin-12 plasmid electroporation in patients with metastatic melanoma. J Clin Oncol 26:5896–5903

Davalos RV, Mir LM, Rubinsky B (2005) Tissue ablation with irreversible electroporation. Ann Biomed Eng 33:223–231. doi:10.1007/s10439-005-8981-8

Delemotte L, Tarek M (2012) Molecular dynamics simulations of lipid membrane electroporation. J Membr Biol 245:531–543. doi:10.1007/s00232-012-9434-6

Denet A-R, Vanbever R, Préat V (2004) Skin electroporation for transdermal and topical delivery. Adv Drug Deliv Rev 56:659–674. doi:10.1016/j.addr.2003.10.027

Dermol J, Miklavčič D (2014) Predicting electroporation of cells in an inhomogeneous electric field based on mathematical modeling and experimental CHO-cell permeabilization to propidium iodide determination. Bioelectrochemistry 100:52–61

Edhemović I, Brecelj E, Gasljević G, Marolt Mušič M, Gorjup V, Mali B, Jarm T, Kos B, Pavliha D, Grčar Kuzmanov B, Čemažar M, Snoj M, Miklavčič D, Gadžijev EM, Serša G (2014) Intraoperative electrochemotherapy of colorectal liver metastases: electrochemotherapy of liver metastases. J Surg Oncol 110:320–327

Franken NAP, Rodermond HM, Stap J, Haveman J, van Bree C (2006) Clonogenic assay of cells in vitro. Nat Protoc 1:2315–2319

Garcia PA, Rossmeisl JH, Neal RE, Ellis TL, Olson JD, Henao-Guerrero N, Robertson J, Davalos RV (2010) Intracranial nonthermal irreversible electroporation. In vivo analysis. J Membr Biol 236:127–136. doi:10.1007/s00232-010-9284-z

Garcia PA, Pancotto T, Rossmeisl JH, Henao-Guerrero N, Gustafson NR, Daniel GB, Robertson JL, Ellis TL, Davalos RV (2011a) Non-thermal irreversible electroporation (N-TIRE) and adjuvant fractionated radiotherapeutic multimodal therapy for intracranial malignant glioma in a canine patient. Technol Cancer Res Treat 10:73–83

Garcia PA, Rossmeisl JH, Neal RE, Ellis TL, Davalos RV (2011b) A parametric study delineating irreversible electroporation from thermal damage based on a minimally invasive intracranial procedure. Biomed Eng OnLine 10:34

Garcia PA, Davalos RV, Miklavčič D (2014) A numerical investigation of the electric and thermal cell kill distributions in electroporation-based therapies in tissue. PLoS ONE 9:e103083

Geeraerd AH, Herremans CH, Van Impe JF (2000) Structural model requirements to describe microbial inactivation during a mild heat treatment. Int J Food Microbiol 59:185–209

Golberg A, Rubinsky B (2010) A statistical model for multidimensional irreversible electroporation cell death in tissue. Biomed Eng OnLine 9:13

Heller LC, Heller R (2010) Electroporation gene therapy preclinical and clinical trials for melanoma. Curr Gene Ther 10:312–317

Heller R, Cruz Y, Heller LC, Gilbert RA, Jaroszeski MJ (2010) Electrically mediated delivery of plasmid DNA to the skin, using

a multielectrode array. Hum Gene Ther 21:357–362. doi:10.1089/hum.2009.065

Hülsheger H, Potel J, Niemann EG (1981) Killing of bacteria with electric pulses of high field strength. Radiat Environ Biophys 20:53–65

Jiang C, Davalos RV, Bischof JC (2015) A review of basic to clinical studies of irreversible electroporation therap. IEEE Trans Biomed Eng 62:4–20. doi:10.1109/TBME.2014.2367543

Kotnik T, Kramar P, Pucihar G, Miklavčič D, Tarek M (2012) Cell membrane electroporation—Part 1: the phenomenon. IEEE Electr Insul Mag 28:14–23

Kotnik T, Frey W, Sack M, Haberl Meglič S, Peterka M, Miklavčič D (2015) Electroporation-based applications in biotechnology. Trends Biotechnol. doi:10.1016/j.tibtech.2015.06.002

Kranjc M, Bajd F, Serša I, Woo EJ, Miklavčič D (2012) Ex vivo and in silico feasibility study of monitoring electric field distribution in tissue during electroporation based treatments. PLoS ONE 7:e45737

Kranjc M, Bajd F, Serša I, Miklavčič D (2014) Magnetic resonance electrical impedance tomography for measuring electrical conductivity during electroporation. Physiol Meas 35:985–996

Kranjc M, Markelc B, Bajd F, Čemažar M, Serša I, Blagus T, Miklavčič D (2015) In situ monitoring of electric field distribution in mouse tumor during electroporation. Radiology 274:115–123. doi:10.1148/radiol.14140311

Linnert M, Iversen HK, Gehl J (2012) Multiple brain metastases—current management and perspectives for treatment with electrochemotherapy. Radiol Oncol. doi:10.2478/v10019-012-0042-y

Linton RH (1994) Use of the Gompertz Equation to Model Non-linear Survival Curves and Predict Temperature, pH, and Sodium Chloride Effects for Listeria monocytogenes Scott A. Faculty of the Virginia Polytechnic Institute and State University, Blacksburg

Long G, Bakos G, Shires PK, Gritter L, Crissman JW, Harris JL, Clymer JW (2014) Histological and finite element analysis of cell death due to irreversible electroporation. Technol Cancer Res Treat 13:561–569

Mafart P, Couvert O, Gaillard S, Leguerinel I (2002) On calculating sterility in thermal preservation methods: application of the Weibull frequency distribution mode. Int J Food Microbiol 72:107–113

Mahnič-Kalamiza S, Vorobiev E, Miklavčič D (2014) Electroporation in food processing and biorefinery. J Membr Biol 247:1279–1304

Miklavčič D, Beravs K, Šemrov D, Čemažar M, Demšar F, Serša G (1998) The importance of electric field distribution for effective in vivo electroporation of tissues. Biophys J 74:2152–2158

Miklavčič D, Šemrov D, Mekid H, Mir LM (2000) A validated model of in vivo electric field distribution in tissues for electrochemotherapy and for DNA electrotransfer for gene therapy. Biochim Biophys Acta BBA-Gen Subj 1523:73–83. doi:10.1016/S0304-4165(00)00101-X

Miklavčič D, Snoj M, Županič A, Kos B, Čemažar M, Kropivnik M, Bračko M, Pečnik T, Gadžijev EM, Serša G (2010) Towards treatment planning and treatment of deep-seated solid tumors by electrochemotherapy. Biomed Eng OnLine 9:10. doi:10.1186/1475-925X-9-10

Miklavčič D, Serša G, Brecelj E, Gehl J, Soden D, Bianchi G, Ruggieri P, Rossi CR, Campana LG, Jarm T (2012) Electrochemotherapy: technological advancements for efficient electroporation-based treatment of internal tumors. Med Biol Eng Comput 50:1213–1225. doi:10.1007/s11517-012-0991-8

Mir LM, Orlowski S, Poddevin B, Belehradek J (1992) Electrochemotherapy tumor treatment is improved by interleukin-2 stimulation of the host's defenses. Eur Cytokine Netw 3:331–334

Mir LM, Gehl J, Serša G, Collins CG, Garbay J-R, Billard V, Geertsen PF, Rudolf Z, O'Sullivan GC, Marty M (2006) Standard operating procedures of the electrochemotherapy: instructions for the use of bleomycin or cisplatin administered either systemically or locally and electric pulses delivered by the CliniporatorTM by means of invasive or non-invasive electrodes. Eur J Cancer Suppl 4:14–25

Neal RE 2nd, Garcia PA, Robertson JL, Davalos RV (2012) Experimental characterization and numerical modeling of tissue electrical conductivity during pulsed electric fields for irreversible electroporation treatment planning. IEEE Trans Biomed Eng 59:1076–1085

Neal RE 2nd, Rossmeisl JH, Robertson JL, Arena CB, Davis EM, Singh RN, Stallings J, Davalos RV (2013) Improved local and systemic anti-tumor efficacy for irreversible electroporation in immunocompetent versus immunodeficient mice. PLoS ONE 8:e64559. doi:10.1371/journal.pone.0064559

Neal RE 2nd, Millar JL, Kavnoudias H, Royce P, Rosenfeldt F, Pham A, Smith R, Davalos RV, Thomson KR (2014) In vivo characterization and numerical simulation of prostate properties for non-thermal irreversible electroporation ablation: characterized and Simulated Prostate IRE. Prostate. doi:10.1002/pros.22760

Neal RE 2nd, Garcia PA, Kavnoudias H, Rosenfeldt F, Mclean CA, Earl V, Bergman J, Davalos RV, Thomson KR (2015) In vivo irreversible electroporation kidney ablation: experimentally correlated numerical models. IEEE Trans Biomed Eng 62:561–569. doi:10.1109/TBME.2014.2360374

Neu WK, Neu JC (2009) Theory of Electroporation. In: Efimov IR, Kroll MW, Tchou PJ (eds) Cardiac Bioelectric Therapy. Springer, US, Boston, MA, pp 133–161

Pakhomova ON, Gregory BW, Pakhomov AG (2013) Facilitation of electroporative drug uptake and cell killing by electrosensitization. J Cell Mol Med 17:154–159

Peleg M (1995) A model of microbial survival after exposure to pulsed electric fields. J Sci Food Agric 67:93–99

Peleg M (2006) Advanced quantitative microbiology for foods and biosystems: models for predicting growth and inactivation. CRC series in contemporary food science. Taylor & Francis, Boca Raton

Pucihar G, Mir LM, Miklavčič D (2002) The effect of pulse repetition frequency on the uptake into electropermeabilized cells in vitro with possible applications in electrochemotherapy. Bioelectrochem Amst Neth 57:167–172

Pucihar G, Krmelj J, Reberšek M, Napotnik T, Miklavčič D (2011) Equivalent pulse parameters for electroporation. IEEE Trans Biomed Eng 58:3279–3288

Sack M, Sigler J, Frenzel S, Eing C, Arnold J, Michelberger T, Frey W, Attmann F, Stukenbrock L, Müller G (2010) Research on industrial-scale electroporation devices fostering the extraction of substances from biological tissue. Food Eng Rev 2:147–156. doi:10.1007/s12393-010-9017-1

Santillana Farakos SM, Frank JF, Schaffner DW (2013) Modeling the influence of temperature, water activity and water mobility on the persistence of Salmonella in low-moisture food. Int J Food Microbiol 166:280–293. doi:10.1016/j.ijfoodmicro.2013.07.007

Šel D, Lebar AM, Miklavčič D (2007) Feasibility of employing model-based optimization of pulse amplitude and electrode distance for effective tumor electropermeabilization. IEEE Trans Biomed Eng 54:773–781. doi:10.1109/TBME.2006.889196

Serša G, Miklavčič D, Čemažar M, Belehradek J, Jarm T, Mir LM (1997) Electrochemotherapy with CDDP on LPB sarcoma: comparison of the anti-tumor effectiveness in immunocompetent and immunodeficient mice. Bioelectrochem Bioenerg 43:270–283

Silve A, Guimerà Brunet A, Al-Sakere B, Ivorra A, Mir LM (2014) Comparison of the effects of the repetition rate between microsecond and nanosecond pulses: electropermeabilization-induced electro-desensitization? Biochim Biophys Acta BBA-Gen Subj 1840:2139–2151

Stone G, Chapman B, Lovell D (2009) Development of a log-quadratic model to describe microbial inactivation, illustrated by thermal inactivation of Clostridium botulinum. Appl Environ Microbiol 75:6998–7005. doi:10.1128/AEM.01067-09

Van Boekel M (2002) On the use of the Weibull model to describe thermal inactivation of microbial vegetative cells. Int J Food Microbiol 74:139–159. doi:10.1016/S0168-1605(01)00742-5

Weaver JC (1993) Electroporation: a general phenomenon for manipulating cells and tissues. J Cell Biochem 51:426–435

Weaver JC, Chizmadzhev YA (1996) Theory of electroporation: a review. Bioelectrochem Bioenerg 41:135–160. doi:10.1016/S0302-4598(96)05062-3

Yarmush ML, Golberg A, Serša G, Kotnik T, Miklavčič D (2014) Electroporation-based technologies for medicine: principles, applications, and challenges. Annu Rev Biomed Eng 16:295–320. doi:10.1146/annurev-bioeng-071813-104622

Županič A, Miklavčič D (2011) Tissue heating during tumor ablation with irreversible electroporation. Elektrotehniški Vestn Engl Ed 78:42–47

Županič A, Kos B, Miklavčič D (2012) Treatment planning of electroporation-based medical interventions: electrochemotherapy, gene electrotransfer and irreversible electroporation. Phys Med Biol 57:5425–5440. doi:10.1088/0031-9155/57/17/5425

Book chapter

Title: **Mathematical Models Describing Cell Death Due to Electroporation**

Authors: Janja Dermol and Damijan Miklavčič

Publication: Handbook of Electroporation

Publisher: Springer, Cham

Year: 2017

DOI: 10.1007/978-3-319-32886-7_13

Online ISBN: 978-3-319-32886-7

Print ISBN: 978-3-319-32885-0

Mathematical Models Describing Cell Death Due to Electroporation

Janja Dermol and Damijan Miklavčič

Contents

Abstract

Various models have been developed to describe microbial inactivation by pulsed electric field treatment, and they have just recently been used for describing eukaryotic cell death due to irreversible electroporation. In microbial inactivation, the mathematical models of cell death enable the adaptation of the pulse parameters to achieve sufficient microbial reduction at the lowest energy input while

J. Dermol (✉) • D. Miklavčič

Faculty of Electrical Engineering, University of Ljubljana, Ljubljana, Slovenia
e-mail: Janja.dermol@fe.uni-lj.si; damijan.miklavcic@fe.uni-lj.si

preserving flavor and sensitive compounds in the food. For precise prediction, the geometry of the treatment chamber, the fluid flow, the temperature, and the electric field distribution should also be taken into account. In electroporation-based medical treatments, currently, a deterministic critical value of electric field is used to delineate between the destroyed and the unaffected tissue. Consequently, tumor cells which have higher electroporation threshold than the experimentally determined may remain viable and cause incomplete tumor elimination. On the contrary, the more sensitive surrounding tissue could be damaged. Mathematical models of cell death help to achieve sufficient cell death while minimizing the damage to the surrounding vital structures. In this chapter, different models are described which were already used for describing microbial inactivation in liquid foods or eukaryotic cell death (the first order, the Hülsheger, the Peleg-Fermi, the Weibull, the logistic, the Adapted/Modified Gompertz, the Geeraerd, the quadratic, the Peleg-Penchina model). The cell death models have already been used for predicting survival in realistic setups like the treatment chamber in microbial inactivation and different electrode geometries and tissues in irreversible electroporation treatments. In conclusion, cell death models are useful in predicting the treatment outcome. Unfortunately, since the mechanisms of cell death due to electroporation are not yet fully elucidated, the models are empiric. There is no direct connection between the parameters of the models and the biological/electrical parameters. Thus, it is unclear which model is the most appropriate to use. The models have to be optimized for each specific cell type and electric pulses separately. The transferability from the in vitro to the in vivo level is questionable.

Introduction

Mathematical modeling is becoming indispensable in the field of life sciences. It enables description and prediction of a response of a biological system knowing the excitation and other parameters, and gives insights into the mechanisms of phenomena. The number of biological experiments can be decreased which decreases the time and costs needed to obtain results. In the field of electroporation, models exist on different levels – molecules, lipid bilayers, cells, and tissues. Cell death or inactivation models are used for the description of microbial inactivation and recently also eukaryotic cell death in irreversible electroporation as nonthermal soft tissue ablation. In this chapter, the statistical models of cell death are described on the level of cells and tissues.

Currently, there is no complete explanation of cell death due to electroporation ("▶ Cell Death Due to Electroporation"), neither for prokaryotic nor eukaryotic

cells. The cell death is believed to be caused by the following mechanisms. First, high electric pulses can cause membrane destruction and necrotic cell death. Second, there is the apoptotic cell death, reasons for which are not yet clear. Third, in vivo, last of the clonogenic cells are destroyed by the immune system ("▶ Immunological Response During Electroporation"). Thus, the currently used cell death models are empirical and were developed on the basis of the best fit to the experimental results.

Microbial Inactivation

In liquid food pasteurization by pulsed electric fields (PEF), short high-voltage electric pulses are applied to decrease the number of microbes and quality-degrading enzymes, and extending the shelf-life while retaining flavor and nutrients (Lelieveld et al. 2007; Sun 2014). In the literature on cell death models, the expressions bacterial and microbial cell death are both used. The microbe is a short expression for microorganisms not visible with a naked eye which includes besides bacteria also protozoa, fungi, and viruses. Thus, bacteria are a subgroup of microorganisms. Since cell death models have been used for describing cell death of various microorganisms (i.e., bacteria, yeast), expression microbial cell death models is used through this chapter. Mathematical modeling of microbial cell death ("▶ Modeling Microbial Inactivation by Pulsed Electric Field") is necessary to adapt the pulse parameters and achieve sufficient decrease of microorganisms at a minimum energy input while preserving the sensitive compounds in the food (Huang et al. 2012). In the food industry, at least five log reductions of bacteria are required for food pasteurization. Applying too gentle pulses may cause food spoilage and health-related problems while applying too severe pulses may cause Joule heating and decrease the quality of food. The cell death models have been used on a variety of liquid food (e.g., fruit juices, milk, water, liquid egg yolks) or models of such liquids. When predicting the microbial inactivation by the PEF treatment, the geometry of the treatment chamber is modeled, and the electric field, the temperature distribution, and fluid flow are (numerically) calculated (Gerlach et al. 2008). Microbial cell death prediction can be included using the cell death models as a function of the electric field, treatment time, the number of the applied pulses, and/or the pulse repetition frequency (Huang et al. 2013). The inactivation of the quality-degrading enzymes and the degradation of the health-related compounds can also be modeled with similar models as the inactivation of microorganisms due to their similar kinetics.

Electroporation-Based Medical Treatments

When treating eukaryotic cells with electroporation, currently, the three main applications are the electrochemotherapy, the irreversible electroporation ("▶ Tissue Ablation by Irreversible Electroporation"), and the gene electrotransfer for gene therapy and DNA vaccination (Yarmush et al. 2014). When treating tumors with electrochemotherapy, pulses of standard parameters and fixed electrode

configurations can be used. However, if the tumor is larger than 2 cm and/or has an irregular shape, a variable electrode configuration should be used. For the irreversible electroporation treatments (Jiang et al. 2015), protocols are already set up in the commercially available electroporators, but the ablated volumes do not always correlate to the predicted ones (Bhutiani et al. 2016). In the electrochemotherapy, irreversible electroporation, and also in gene electrotransfer treatments, the need for patient-specific treatment planning ("▶ Treatment Planning for Electrochemotherapy and Irreversible Electroporation of Deep-Seated Tumors") is on the rise. The number, the geometry of the electrodes, and the parameters of the electric pulses must be optimized considering the specifics of the cause and the treatment (Županič et al. 2012). In electrochemotherapy, all tumor cells must be reversibly permeabilized, while the surrounding tissue, especially critical structures, should be undamaged. In irreversible electroporation, the tumor must be irreversibly electroporated without significant thermal damage, while the surrounding tissue, especially critical structures like nerves and vessels, should remain largely undamaged. In gene electrotransfer, cells must be reversibly permeabilized, and their viability must remain high. Currently, an experimentally determined critical electric field is used to predict and delineate between the alive and the irreversibly electroporated tissue – the response is modeled by a step function (Fig. 1). The assumption of a step function is, however, too simplistic even for cell suspensions of the same cell line (Canatella et al. 2001; Dermol and Miklavčič 2015) since cells among other differ in size and position in a cell cycle. In tissues, especially in tumors, this inhomogeneity is amplified since cells additionally differ in shape and tissues are comprised of different cell types. In a tumor, in addition to the tumor cells, stromal cells are present in the microenvironment. Therefore, in reality, the transition from alive to irreversibly electroporated state is continuous and distributed over a range of electric field values. The width of this range, as well as the threshold voltage, also depend on the number and length of the applied pulses (Canatella et al. 2001; Garcia et al. 2014).

When predicting the survival with the fixed threshold, the cells which have higher critical threshold than the experimentally determined can survive and cause incomplete tumor elimination or its later recurrence. On the other hand, applying more severe electric pulses than necessary can cause tissue necrosis, excessive Joule heating, and thermal damage. By using cell death models to predict the treated volume, the efficiency of the electroporation-based medical treatments and therapies can be increased. Cell death models allow interpolation and predict survival at parameters which were not experimentally determined. The last few of the clonogenic cells are eradicated by the immune system ("▶ Immune Response After Electroporation and Electrochemotherapy") (Yarmush et al. 2014) which should be considered when determining the tolerated percentage of the survived cells in electroporation-based treatments. A complete eradication of all tumor cells may not be needed.

In electrochemotherapy and gene electrotransfer, using cell death models is not enough to correctly predict the treatment outcome. In the electrochemotherapy treatments, the application of electric pulses increases the permeability of the cell
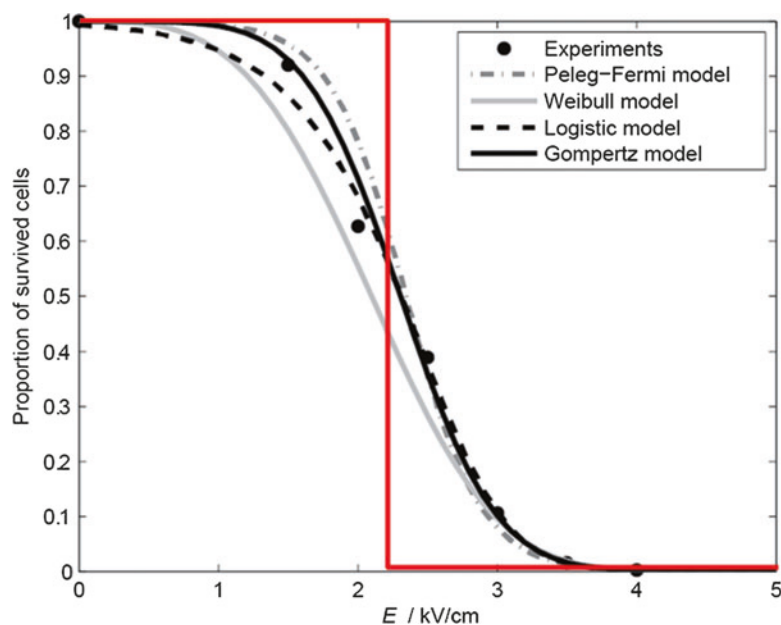
Fig. 1 The comparison of the currently used and the proposed way of modeling cell death. The *red line* shows the currently used step response where below a critical electric field all cells are regarded alive and above all dead. The *gray* and *dark* lines show the suggested cell death models which predict a gradual decrease in cell survival. *Black circles* are the experimentally determined values. It is clear that the experimental values are better described with different cell death models than with a step response

membrane to the chemotherapeutics. Two commonly used chemotherapeutics are cisplatin and bleomycin. Cell death is mostly caused by the cytotoxic effects of chemotherapeutics, although, in the vicinity of the electrodes, cells can be irreversibly electroporated. To correctly predict the affected regions, a model of permeability to cytotoxic drugs and their transport across the membrane as a function of electric pulses should be included in the treatment planning of electrochemotherapy (Dermol and Miklavčič 2014). Namely, when the number of the molecules of chemotherapeutic entering each cell can be calculated, it can be predicted whether the cell will die or not. In the gene electrotherapy, electric pulses increase the permeability of the cell membrane to the DNA. The exact mechanisms of gene electrotherapy are complex and also depend on genes. The presumed steps in the process are electropermeabilization of the cell membrane, electrophoretic migration of the DNA towards membrane, DNA/membrane interaction, DNA translocation across the membrane, intracellular migration of DNA through the cytoplasm, DNA passage through the nuclear envelope, and gene expression (Rosazza et al. 2016). To correctly predict where the transfection will occur, each step should be modeled.

Models Used to Describe Cell Death in Suspension

Ideally, cell death model would include all the parameters, important for cell death. A problem arises since the exact mechanisms of cell death due to electroporation are not completely known. Cell death depends on many parameters, among others on the electric field; the duration and the number of the applied pulses; the pulse repetition frequency; the properties of the cells; their size, shape, orientation in the electric field; their concentration in the treated medium; the properties of the treated medium or food; pH; temperature; configuration of the electrodes or the treatment chamber; and the concentration of the chemotherapeutics (in electrochemotherapy). The most important parameters for cell death should be identified and included in the model. It should also be determined which parameters can be excluded to simplify the models and the fitting. In summary, the cell death model due to electroporation should describe the experimental results well, include all the important electrical and biological parameters, have high predictive power, and a minimum number of parameters to be optimized.

Various models have been developed and used to describe microbial cell death due to pulsed electric field (PEF) treatment in liquid food pasteurization (Álvarez et al. 2003; Peleg 2006; San Martín et al. 2007; Huang et al. 2012). Only recently, interest to develop and use such models has been expressed in tissue ablation due to irreversible electroporation, i.e., IRE treatment. Most of the models used, however, are empirical, and their parameters have no physical meaning and even have no parameters that could be explicitly linked to treatment parameters such as electric field, pulse duration, the number of pulses, and pulse shape. There is also no solid link demonstrated between cell membrane permeabilization and cell death.

In microbial cell death models, the independent variable is usually the treatment time which is easily determined in the case of thermal, irradiation, high pressure, ultrasound, or other continuous treatment. The treatment time of the PEF treatment is more difficult to determine since multiple short pulses are applied at different pulse repetition frequencies. Nevertheless, the treatment time (t) is usually calculated by multiplying the number of pulses with the duration of one pulse ($t = NT$), where N denotes the number of the pulses and T the duration of one pulse. This way of calculating the treatment time assumes that only the product of N and T affects the survival but not the duration or the number of the pulses by itself. The effect of the pulse repetition frequency is also neglected. In microbial cell death models, the electric field, the number of pulses, or their repetition frequency were used as independent variables. With the exception of the quadratic model, however, no model so far included more than two independent variables.

The electric field is the most important parameter in electroporation-based treatments (Miklavčič et al. 2006). The survival curves as a function of the electric field are usually composed of three parts: a shoulder (upper asymptote) which is then followed by a steep decline in cell number and eventually, a tail (lower asymptote) is reached. The tail can be a caused by either a resistant subpopulation of cells or the reached limit of the survival assay. Several different curves can describe the survival

data. When presenting the survival curves and the cell death models, they should be plotted on a semilogarithmic scale. There, deviations and small percentages of survival are more easily noticed. The quality of the fit should be evaluated using various statistical measures: the goodness-of-fit (R^2), the root-mean-square error (RMSE), and/or accuracy parameter (A_f). R^2 is a statistical measure of how close the regression line is to the experimental data; RMSE is a measure of the average deviation between the observed and predicted data; and A_f measures the accuracy of the estimates obtained by the models. Other criteria for evaluating the suitability of a model are the number of the models' parameters (which should be low), the inclusion of more independent variables, and a high predictive power. In continuation, models which were already used for describing microbial or eukaryotic cell death are described.

The First-Order Kinetics Model

The first-order kinetics model was developed almost a century ago (Huang et al. 2012). It derives from the assumption that all cells in a population are equally sensitive to the treatment. When used in PEF treatments, it describes cell death as a function of the treatment time:

$$S(t) = \exp(-kt),\tag{1}$$

where S denotes the survival, t the treatment time, and k is a first-order parameter, i.e., the speed of the decrease. The model predicts that the viability decreases immediately – there is no shoulder at short treatment time. The first-order kinetic model did not provide a good fit to electroporation treatment of eukaryotic cells (Dermol and Miklavčič 2015). It has also been observed that it does not describe all microbial inactivation data well. It was stated that the model describes the data sufficiently well only when the data is sampled too scarcely (Peleg 2006). The deviations from the first-order kinetics model could among others be explained by the statistical distribution of cell radii (Lebovka and Vorobiev 2004).

The first-order parameter k was found to be temperature dependent which could be modeled in thermal treatments as well as in PEF treatments. In PEF treatments, the temperature of the sample increases due to the Joule heating and consequently the electrical conductivity of the sample is also increased. The parameter k could be modeled by Arrhenius equation as:

$$k = k_t \exp\left(-\frac{E_A}{RT}\right)\tag{2}$$

Where k_t is the rate constant at the reference temperature, E_A the activation energy, R is the gas constant, and T is the sample temperature in Kelvins.

Traditionally, the sensitivity of microorganisms to static treatments is described using the decimal reduction time (D_t). It denotes the treatment time needed to obtain

one decimal reduction of the cell population, i.e., 10 % of the initial population survives. It is defined as $D_t = \frac{2.303}{k}$ since the first-order kinetics model is based on natural and the decimal reduction time on the decimal logarithm.

If the treated cell population consists of two populations of which each has its first-order dynamics, the biphasic model can be used:

$$S(t) = fe^{-k_1t} + (1-f)e^{-k_2t}, \tag{3}$$

where f denotes the proportion of the first subpopulation in the whole population, and k_1 and k_2 are the first order parameters of the first and the second subpopulation, respectively. In case there are more subpopulations, the decrease of each subpopulation can be modeled with its own exponential factor which is then added to the (Eq. 3).

The Hülsheger Model

Hülsheger studied the effect of electric field on the inactivation of *E. coli* (Huang et al. 2012). He derived an empirical formula which has two independent variables – the treatment time (t) and the electric field (E). As a function of the electric field, the survival showed a linear decline when the electric field exceeded a certain critical electric field (E_c) which was modeled as:

$$S(E) = \exp(-b_E(E - E_c)), \tag{4}$$

where S is the survival, b_E is the regression coefficient, and E_c is the critical value of electric field below which there will be no inactivation (i.e., the lowest electric field that causes inactivation). When $E < E_c$, the model predicts the survival above one which is incorrect and the survival must be fixed at one.

As a function of the treatment time, the results were modeled as:

$$S(t) = \exp\left(-b_t \ln\left(\frac{t}{t_c}\right)\right), \tag{5}$$

where S is the survival, b_t is the regression coefficient, and t_c is the extrapolated critical value of treatment time below which there will be no inactivation (i.e., the shortest treatment time which causes inactivation). For treatment times shorter than the critical treatment time, the model predicts the survival to be more than 1. Thus, also here, for $t < t_c$ the survival should be fixed at one.

Both models Eqs. 4 and 5 were joined in:

$$S(t, E) = \left(\frac{t}{t_c}\right)^{-\frac{E-E_c}{k}} \tag{6}$$

where k is the independent inactivation constant, and other parameters have the same meaning as in Eqs. 4 and 5. The parameters t_c, E_c, and k were proposed to be microorganism dependent within a certain range of experimental parameters.

Although the Hülsheger model includes two independent variables, it cannot universally describe the experimentally determined cell death. With the Hülsheger model, some microbial cell death results were possible to model, and some were not (Huang et al. 2012), while only one study unsuccessfully fit it to the eukaryotic cell death data (Dermol and Miklavčič 2015).

The Peleg-Fermi Model

The Peleg-Fermi model has been successfully fit to various microbial inactivation data (Huang et al. 2012) and was also the first to be used for describing eukaryotic cell death due to electroporation (Golberg and Rubinsky 2010). It derives from the Fermi's equation which is used to describe the behavior of materials at their glass transition temperature. The Peleg-Fermi model is one of the most promising since it describes the data well and includes two independent variables – electric field (E) and the number of the applied pulses (N):

$$S(E,N) = \frac{1}{1 + \exp\left(\dfrac{E - E_c(N)}{k(N)}\right)} \tag{7}$$

$$E_c(N) = E_{c0}\exp(-k_1 N) \tag{8}$$

$$k(N) = k_0\exp(-k_2 N) \tag{9}$$

where $E_c(N)$ is the critical electric field where the survival drops to 50 %, $k(N)$ is the kinetic constant describing the slope of the curve, E_{c0} is the intersection of $E_c(N)$ with the y-axis, k_0 (in the same units as the electric field), k_1 and k_2 are constants which change depending on the parameters of the pulses and the properties of the cells. The critical electric field depends on the number and length of the applied pulses (Pucihar et al. 2011). For values below the critical electric field, the Peleg-Fermi model predicts survival to be 100 %. The Peleg-Fermi model described various experimental data well, although the $k(N)$ and $E_c(N)$ did not always change exponentially as a function of the pulse number (Dermol and Miklavčič 2015; Sharabi et al. 2016). Unfortunately, the pulse length and the pulse repetition frequency are not included in the model, and the dependency on them is included indirectly via the parameters of the model. An example of fitting the Peleg-Fermi model to the eukaryotic cell death due to irreversible electroporation in vitro is shown in Fig. 2.
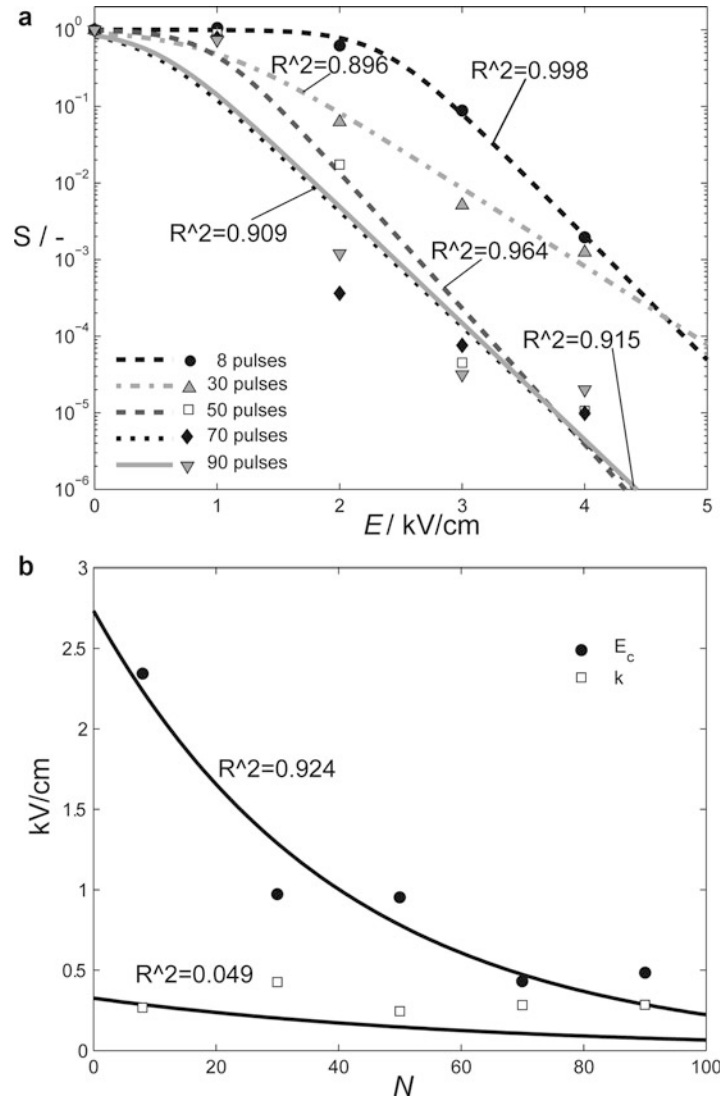
Fig. 2 The Peleg-Fermi model, fit to eukaryotic cell death data in a wide range of pulse number and electric field values. (**a**) symbols show the experimental values for 100 μs, 1 Hz repetition frequency at different pulse numbers (8, 30, 50, 70, and 90), lines show the fitted Peleg-Fermi model (Eq. 7). (**b**) symbols are the optimized values of E_c and k for different pulse numbers, lines show the fitted models for $E_c(N)$ and $k(N)$ (Eqs. 8 and 9) (Reprinted from Journal of Membrane Biology, Vol 248/Issue 5, Dermol J, Miklavčič D, Mathematical Models Describing Chinese Hamster Ovary Cell Death Due to Electroporation In Vitro, Pages 865–881, Copyright 2015 Springer Science + Business Media New York)

The Weibull Model

The Weibull model was originally used to describe the time to failure of electronic devices after stress was imposed on them. A parallel can be made when stress, for example, thermal, high pressure, or PEF treatment, is applied to biological cells. Time to cell death after the stress can be described using the Weibull model (San Martín et al. 2007). The Weibull model was successfully used to describe microbial (Huang et al. 2012) and eukaryotic cell death (Dermol and Miklavčič 2015) using various pulse parameters. Although the Weibull model is very adaptable, no clear connection between the electrical/biological parameters and the optimized parameters of the model was made. In some cases, the scale parameter b was exponentially dependent on the electric field. The model is:

$$S(x) = \exp\left(-\left(\frac{x}{b}\right)^n\right), \tag{10}$$

where x denotes the treatment time or the electric field, b is the scale (in the same units as x), and n is the shape parameter. The scale parameter determines the characteristic time or the characteristic electric field at which 63 % of the cells die. With different values of the shape parameter, the shape of the survival curve varies between the convex ($n < 1$), linear ($n = 1$), and concave curve ($n > 1$) in semi-logarithmic scale.

The Logistic Model

The logistic model can be used for describing distributions with a sharp peak and long tails (Cole et al. 1993). When taking into account that survival of cells before the treatment is 100 %, the logistic model can be written as either Eq. 11 or 12, depending on what is chosen as the independent variable. The equations are:

$$S(E) = 10^\wedge\left(\frac{\omega}{1 + \exp(4\sigma(\tau - E)\omega^{-1})}\right) \tag{11}$$

$$S(t) = 10^\wedge\left(\frac{\omega}{1 + \exp(4\sigma(\tau - \log_{10}t)\omega^{-1})}\right) \tag{12}$$

where E denotes the electric field, t the treatment time, ω the common logarithm of the lower asymptote, σ the maximum slope, and τ the position of the maximum slope. Survival curves show the cumulative cell death as a function of the independent variable, i.e., applied electric field or treatment time. Thus, each data point includes cells which died due to the corresponding or less severe parameter. The cell death distribution is obtained as a derivative of the cumulative distribution. Only cell death due to the corresponding parameter is plotted. In electroporation treatments, the distribution of cell death with a sharp peak and long tails is obtained when the

independent variable is either the electric field or the common logarithm of the treatment time. The logistic model was successfully fit to inactivation of microorganisms by PEF treatment (Huang et al. 2012) and to eukaryotic cell death (Dermol and Miklavčič 2015).

The Adapted/Modified Gompertz Model

The Gompertz model is usually used for describing the growth of a tumor, but in modified form, it can also describe cell death. Originally, it was used for describing bacterial (Linton et al. 1995) cell death due to thermal treatment, but later it was extended to describing bacterial cell death due to pulsed electric field treatment and eukaryotic (Dermol and Miklavčič 2015) cell death due to electroporation. The model is written as:

$$S(x) = \exp\left(A \exp\left(-e^{(B_0 + B_1 x)}\right) - A \exp\left(-e^{B_0}\right)\right) \tag{13}$$

where x denotes either the treatment time or the electric field, A is the natural logarithm of the survival in the stationary phase (the natural logarithm of the tail), B_0 is the length of the shoulder, and B_1 the speed of the increase (when it is positive) or decrease (when it is negative) in cell number.

The Geeraerd Model

The Geeraerd model (Geeraerd et al. 2000) describes the exponential decrease of cells including a tail which models the resistant cell subpopulation. Assuming the initial survival is 100 %, the Geeraerd model can be written as:

$$S(t) = (1 - N_{res})\exp(-kt) + N_{res} \tag{14}$$

Where N_{res} represents the tail and k is the inactivation rate. Since the model does not also include a shoulder, it cannot be used universally for all cell death results. The Geeraerd model was so far successfully fit to experimental data of microbial inactivation after mild heat treatment and eukaryotic cell death due to electroporation.

The Quadratic Model

The quadratic model is currently the only model which can model dependency on two or more independent variables. As the independent variable x, various parameters have been used – the electric field, the treatment time, the pulse repetition

frequency, the pH, and the concentration of some compound. The model is written as:

$$S(x) = k_1 + k_2 x + k_3 x^2 \tag{15}$$

where the parameter k_1 is the central point of the system, k_2 is the coefficient of the linear effect, and k_3 of the quadratic effect of the independent variable. It is also possible to fit more parameters at once by joining several quadratic models into one:

$$S(x_1, x_2) = k_1 + k_2 x_1 + k_3 x_1{}^2 + k_4 x_2 + k_5 x_2{}^2 + k_6 x_1 x_2 \tag{16}$$

where x_1 and x_2 denote two independent variables which were marked as the x in the (Eq. 15), k_1 is the central point of the system, k_2 and k_4 represent the linear, k_3 and k_5 the quadratic, and k_6 the interactive effects of the independent variables. If some of the terms are nonsignificant under certain experimental conditions, they can be omitted from the model. By quadratic model fitting, the interaction between different experimental parameters can be determined. The quadratic model was successfully fit to microbial inactivation results as well as to the inactivation of the enzymes and health-related compounds like vitamins (Huang et al. 2012).

The Peleg-Penchina Model

The Peleg-Penchina model is also an empirical model but can describe only the convex curves (Peleg and Penchina 2000; Álvarez et al. 2003) in the semilogarithmic scale. It is written as:

$$S(t) = 10 \hat{\ } (-m \ln(1 + kt)) \tag{17}$$

where t is the treatment time of the PEF treatment; m and k are the parameters of the model, which have to be optimized; and ln denotes the natural logarithm. Together with the Eq. 17, the authors introduced a way of describing bacterial survival when the intensity of the lethal agent (e.g., temperature, chemical agent, PEF treatment) varies either between treatments or during one treatment.

As long as the mechanisms of cell death due to electroporation (PEF treatment) are not known, it is difficult to decide which model is superior to others, and they can all be regarded as equivalent. An example of fitting several cell death models to eukaryotic and bacterial cell death results is shown in Fig. 3.
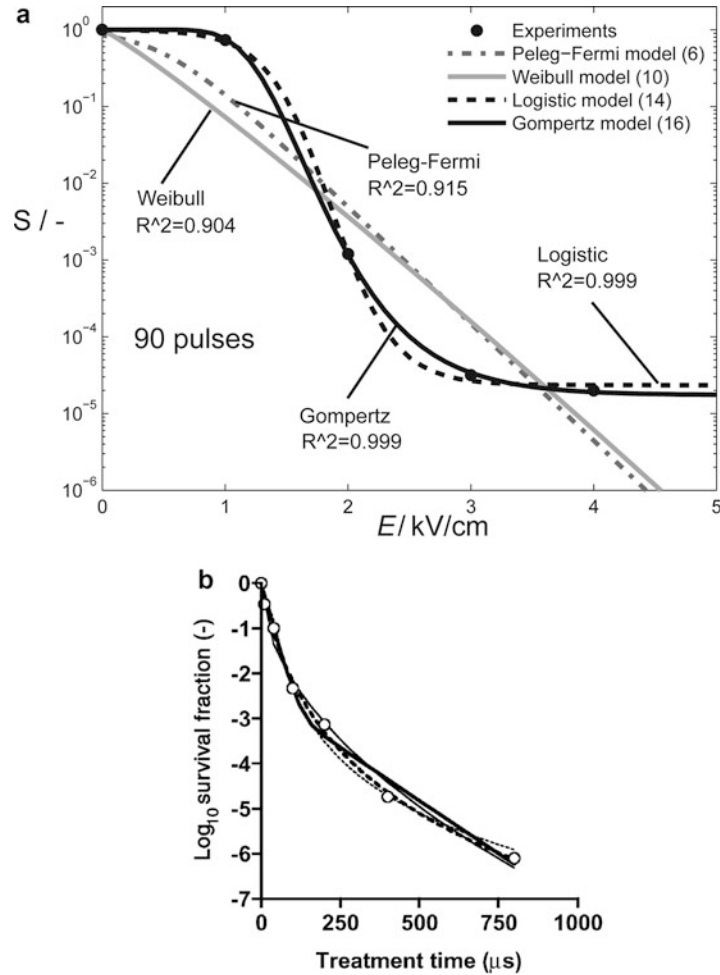
Fig. 3 (**a**) Different cell death models as a function of the electric field (the Peleg-Fermi, the Weibull, the Logistic, the Adapted Gompertz model) were fitted to the experimental data of eukaryotic cell death when 90, 100 μs pulses were applied to the cell suspension. Symbols show the experimental values and lines the models. It can be seen that several models describe the experimental data well Observed values are marked by circles, model 1 by a bold line, model 2 by a dotted line, model 3 by a thin line, and model 4 by a dashed line. (Reprinted from Journal of Membrane Biology, Vol 248/Issue 5, Dermol J, Miklavčič D, Mathematical Models Describing Chinese Hamster Ovary Cell Death Due to Electroporation In Vitro, Pages 865–881, Copyright 2015 Springer Science + Business Media New York 2015). (**b**) Different cell death models as a function of the treatment time were fitted to the survival of *E. coli* after pulsed electric field treatment. Model 1 is the biphasic model, model 2 is the sigmoidal equation, model 3 is the Weibull model, and model 4 is the Peleg-Penchina model. A good fit was obtained with all tested models (Reprinted from Innovative Food Science & Emerging Technologies, Vol 4/edition number 4, Alvarez I, Virto R, Raso J, Condon S, Comparing predicting models for the *Escherichia coli* inactivation by pulsed electric fields, Pages No 195–202, Copyright (2003), with permission from Elsevier)

Models Used to Describe Cell Death In Vitro on Attached Cells and Cells in 3D Tissue-Like Structure

In liquid food pasteurization, the microorganisms are suspended in the food. However, they can also grow in layers, for example, on surgical meshes. Surgical mesh is thin mesh which supports or reinforces damaged tissue. The cell death models were applied to PEF treatments of medical mesh implants, on which 2D layers of bacteria can form as a biofilm ("▶ Electroporation of Biofilms") (Khan et al. 2016). The authors successfully described the data using the Weibull model.

The cell death models have not yet been applied to the attached or 3D eukaryotic cell models. The optimization of the models in vitro would need to be done anew since the critical electric fields are different for the attached than for the suspended cells due to a different shape, density, and connections between cells (Pucihar et al. 2006; Towhidi et al. 2008).

Models of Cell Death Used in the Treatment Chamber and In Vivo

Microorganisms grow in suspensions and 2D layers. Thus, there are no reports on using the mathematical models to describe PEF inactivation of microorganisms in vivo. There is, however, an example of modeling the treatment chamber ("▶ Optimization of Pulsed Electric Field Treatment Chamber") with included suspension of bacteria. Huang et al. predicted the inactivation of bacteria in watermelon juice by first building a 2D numerical model of the treatment chamber and using the Hülsheger model to describe the inactivation (Huang et al. 2013). Authors obtained very good predictions. Cells respond to the electric field to which they are exposed. In treatment chambers (as well as in tissue when performing the IRE treatment), the electric field can be highly inhomogeneous. In future, to obtain the optimal conditions for microbial inactivation, first optimization of the treatment chambers' geometry and the parameters of electric pulses should be done.

There are just a few reports of using cell death models to describe and predict the extent of eukaryotic cell death due to electroporation in vivo. Golberg and Rubinsky were first to suggest using statistical cell death models in vivo (Golberg and Rubinsky 2010). They fit the Peleg-Fermi model to the results of an in vitro study of electroporation of prostate cell line. Then, the fitted Peleg-Fermi model was theoretically applied to the 2D case of tissue electroporation using needle electrodes. The spatial distribution of probability of cell death the authors obtained is shown in Fig. 4. It was shown that there exists an area where the cell death probability ranges from 0 % to 100 % and the deterministic critical electric field is not an optimal choice for predicting the electroporation-based medical treatment outcome.

A theoretical study of commercially available bipolar electrodes used in irreversible electroporation treatments was done by Garcia et al. (2014). The authors determined the extent of the cell death caused by the heating and by the electroporation when standard IRE pulses were applied. The thermal damage was evaluated using the Arrhenius integral and the electrical damage using the Peleg-Fermi model.
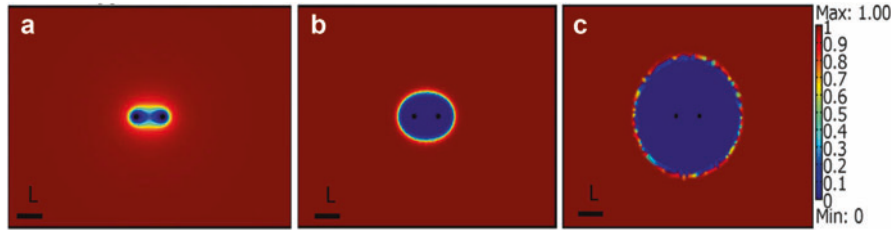
Fig. 4 The Peleg-Fermi model was fit to the 2D model of prostate tissue treated by irreversible electroporation using needle electrodes. The legend on the right shows the probability of cell death. Around the electrodes exists an area where the probability of cell death is between 0 % and 100 %, thus the deterministic critical electric field is not sufficient for predicting cell death in vivo. (**a**–**c**) show the predicted cell death when a different number of 100 μs pulses of the same voltage (1.5 arbitrary unit) are applied: (**a**) 10 pulses, (**b**) 50 pulses, (**c**) 100 pulses (Reprinted from BioMedical Engineering OnLine, Vol 9, Golberg A, Rubinsky B, A statistical model for multidimensional irreversible electroporation cell death in tissue, Page No 13, Copyright 2010 Golberg and Rubinsky; licensee BioMed Central Ltd.)

The electrical damage due to electroporation around the bipolar electrodes is shown in Fig. 5. Different combinations of pulse number and electric field lead to different probabilities of cell death as shown in Fig. 6.

A study in vivo was performed by Sharabi et al., who analyzed the brain electroporation using the Peleg-Fermi model to describe cell death as well as the disruption of the blood–brain barrier (Sharabi et al. 2016). The authors concluded that the Peleg-Fermi model could be successfully used to describe the electroporation of rat brain, although they found that the $E_c(N)$ was better described using power than an exponential function, especially in the range of a high number of pulses (more than 90). As shown in (Eq. 8), $E_c(N)$ in the Peleg-Fermi model can be expressed as $E_c(N) = E_{c0}\exp(-k_1 N)$. Sharabi et al. obtained better fit using the equation:

$$E_c(N) = E_{c0}N^{-k_1}, \tag{18}$$

where E_{c0} denotes the critical electric field, N the number of the applied pulses, and k_1 is a constant.

In electroporation-based medical treatments, the desired use of the models is in tissues in vivo. It is questionable to what extent the in vitro optimized models can be used in vivo. The thresholds for cell death due to electroporation in vivo (Jiang et al. 2015) seem to be different than in vitro (Dermol and Miklavčič 2015). In vivo, the
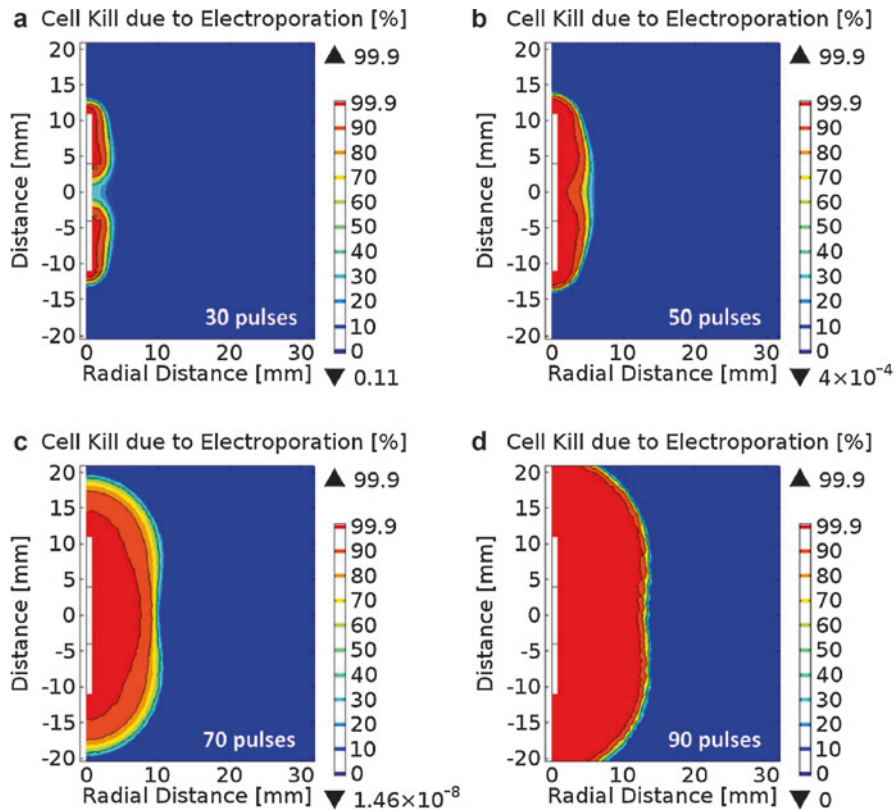
Fig. 5 The probability of cell death due to electroporation around the commercially available bipolar electrodes at different pulse numbers (**a** – 30, **b** – 50, **c** – 70, and **d** – 90) when applying 100 µs pulses of 3000 V at 1 Hz. The transition zone where the cell death decreases from 100 % to 0 % becomes sharper with increasing pulse number (Reprinted from PLoS ONE, Vol 9/Issue 8, Garcia PA, Davalos RV, Miklavčič D, A Numerical Investigation of the Electric and Thermal Cell Kill Distributions in Electroporation-Based Therapies in Tissue, Pages No e103083, Copyright 2014 Garcia et al.)

cells are connected, they are of different size and shape, their density varies, there are different types of cells in each tissue, and the immune system is present. It seems that the cell death models optimized in vitro may not be directly transferable in vivo but would need to be optimized separately.
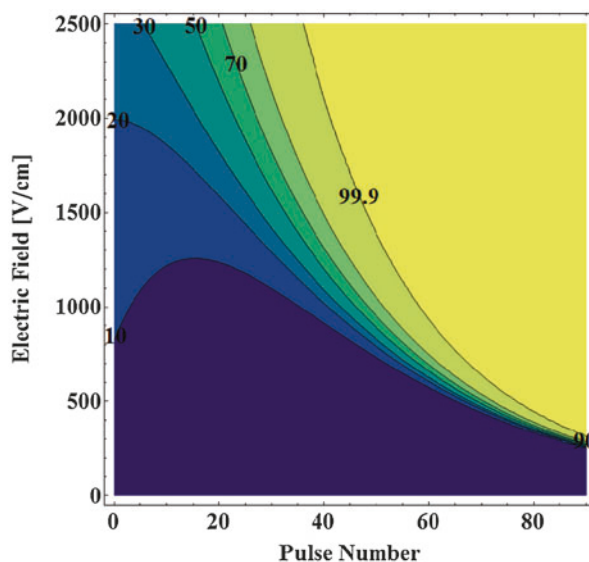
Fig. 6 The probability of cell death due to electroporation as a function of pulse number and electric field. The cell death is predicted by the Peleg-Fermi model optimized for the prostate cancer cell death. The contours show the predicted cell death (denoted with numbers in *bold*) using various combinations of electric field and pulse number. To achieve 99.9 % cell death a certain minimal electric field and a number of pulses should be applied (Reprinted from PLoS ONE, Vol 9/Issue 8, Garcia PA, Davalos RV, Miklavčič D, A Numerical Investigation of the Electric and Thermal Cell Kill Distributions in Electroporation-Based Therapies in Tissue, Pages No e103083, Copyright 2014 Garcia et al.)

Conclusions

Using cell death models in treatment planning could increase the efficiency of PEF microbial inactivation and electroporation-based medical treatments. However, currently, it is unclear which model is the most appropriate since they are all empirical, and mostly, there is no clear relation between the electrical/biological parameters and parameters of the cell death models. Although the cell death models describe data well, they must be optimized for each cell type/tissue and different electric pulses separately. A direct translation of in vitro optimized models to an in vivo environment is questionable. In future, cell death models should be based on mechanisms of cell death due to electroporation, include all and only the relevant treatment parameters, and describe and predict the cell death accurately.

Cross-References

References

Álvarez I, Virto R, Raso J, Condón S (2003) Comparing predicting models for the *Escherichia coli* inactivation by pulsed electric fields. Innovat Food Sci Emerg Technol 4:195–202. doi:10.1016/S1466-8564(03)00004-3

Bhutiani N, Doughtie CA, Martin RCG (2016) Ultrasound validation of mathematically modeled irreversible electroporation ablation areas. Surgery 159:1032–1040. doi:10.1016/j.surg.2015.10.030

Canatella PJ, Karr JF, Petros JA, Prausnitz MR (2001) Quantitative study of electroporation-mediated molecular uptake and cell viability. Biophys J 80:755–764. doi:10.1016/S0006-3495(01)76055-9

Cole MB, Davies KW, Munro G, Holyoak CD, Kilsby DC (1993) A vitalistic model to describe the thermal inactivation of *Listeria monocytogenes*. J Ind Microbiol 12:232–239. doi:10.1007/BF01584195

Dermol J, Miklavčič D (2014) Predicting electroporation of cells in an inhomogeneous electric field based on mathematical modeling and experimental CHO-cell permeabilization to propidium iodide determination. Bioelectrochemistry 100:52–61. doi:10.1016/j.bioelechem.2014.03.011

Dermol J, Miklavčič D (2015) Mathematical models describing Chinese hamster ovary cell death due to electroporation in vitro. J Membr Biol 248:865–881. doi:10.1007/s00232-015-9825-6

Garcia PA, Davalos RV, Miklavčič D (2014) A numerical investigation of the electric and thermal cell kill distributions in electroporation-based therapies in tissue. PLoS One 9, e103083. doi:10.1371/journal.pone.0103083

Geeraerd AH, Herremans CH, Van Impe JF (2000) Structural model requirements to describe microbial inactivation during a mild heat treatment. Int J Food Microbiol 59:185–209. doi:10.1016/S0168-1605(00)00362-7

Gerlach D, Alleborn N, Baars A, Delgado A, Moritz J, Knorr D (2008) Numerical simulations of pulsed electric fields for food preservation: a review. Innovat Food Sci Emerg Technol 9:408–417. doi:10.1016/j.ifset.2008.02.001

Golberg A, Rubinsky B (2010) A statistical model for multidimensional irreversible electroporation cell death in tissue. Biomed Eng OnLine 9:13. doi:10.1186/1475-925X-9-13

Huang K, Tian H, Gai L, Wang J (2012) A review of kinetic models for inactivating microorganisms and enzymes by pulsed electric field processing. J Food Eng 111:191–207. doi:10.1016/j.jfoodeng.2012.02.007

Huang K, Yu L, Ling G, Wang J (2013) Coupled simulations in colinear and coaxial continuous pulsed electric field treatment chambers. Trans ASABE 56:1473–1484. doi:10.13031/trans.56.9167

Jiang C, Davalos RV, Bischof JC (2015) A review of basic to clinical studies of irreversible electroporation therapy. IEEE Trans Biomed Eng 62:4–20. doi:10.1109/TBME.2014.2367543

Khan SI, Blumrosen G, Vecchio D, Golberg A, McCormack MC, Yarmush ML, Hamblin MR, Austen WG (2016) Eradication of multidrug-resistant pseudomonas biofilm with pulsed electric fields: eradication of multidrug-resistant pseudomonas. Biotechnol Bioeng 113:643–650. doi:10.1002/bit.25818

Lebovka NI, Vorobiev E (2004) On the origin of the deviation from the first-order kinetics in inactivation of microbial cells by pulsed electric fields. Int J Food Microbiol 91:83–89. doi:10.1016/S0168-1605(03)00321-0

Lelieveld H, Notermans S, Haan SWHD (2007) Food preservation by pulsed electric fields: from research to application, 1st edn. Woodhead Publishing, Cambridge

Linton RH, Carter WH, Pierson MD, Hackney CR (1995) Use of a modified Gompertz equation to model nonlinear survival curves for *Listeria monocytogenes* Scott A. J Food Prot 58:946–954

Miklavčič D, Čorović S, Pucihar G, Pavšelj N (2006) Importance of tumour coverage by sufficiently high local electric field for effective electrochemotherapy. Eur J Cancer Suppl 4:45–51. doi:10.1016/j.ejcsup.2006.08.006

Peleg M (2006) Advanced quantitative microbiology for foods and biosystems: models for predicting growth and inactivation. Taylor & Francis, Boca Raton

Peleg M, Penchina CM (2000) Modeling microbial survival during exposure to a lethal agent with varying intensity. Crit Rev Food Sci Nutr 40:159–172. doi:10.1080/10408690091189301

Pucihar G, Kotnik T, Valič B, Miklavčič D (2006) Numerical determination of transmembrane voltage induced on irregularly shaped cells. Ann Biomed Eng 34:642–652. doi:10.1007/s10439-005-9076-2

Pucihar G, Krmelj J, Reberšek M, Napotnik T, Miklavčič D (2011) Equivalent pulse parameters for electroporation. IEEE Trans Biomed Eng 58:3279–3288. doi:10.1109/TBME.2011.2167232

Rosazza C, Haberl Meglič S, Zumbusch A, Rols M-P, Miklavčič D (2016) Gene electrotransfer: a mechanistic perspective. Curr Gene Ther 16:98–129. doi:10.2174/1566523216666160331130040

San Martín MF, Sepúlveda DR, Altunakar B, Góngora-Nieto MM, Swanson BG, Barbosa-Cánovas GV (2007) Evaluation of selected mathematical models to predict the inactivation of *Listeria innocua* by pulsed electric fields. LWT- Food Sci Technol 40:1271–1279

Sharabi S, Kos B, Last D, Guez D, Daniels D, Harnof S, Mardor Y, Miklavčič D (2016) A statistical model describing combined irreversible electroporation and electroporation-induced blood–brain barrier disruption. Radiol Oncol 50:28–38

Sun D-W (ed) (2014) Emerging technologies for food processing, 2nd edn. Academic/Elsevier, Amsterdam

Towhidi L, Kotnik T, Pucihar G, Firoozabadi SMP, Mozdarani H, Miklavčič D (2008) Variability of the minimal transmembrane voltage resulting in detectable membrane electroporation. Electromagn Biol Med 27:372–385. doi:10.1080/15368370802394644

Yarmush ML, Golberg A, Serša G, Kotnik T, Miklavčič D (2014) Electroporation-based technologies for medicine: principles, applications, and challenges. Annu Rev Biomed Eng 16:295–320. doi:10.1146/annurev-bioeng-071813-104622

Županič A, Kos B, Miklavčič D (2012) Treatment planning of electroporation-based medical interventions: electrochemotherapy, gene electrotransfer and irreversible electroporation. Phys Med Biol 57:5425–5440. doi:10.1088/0031-9155/57/17/5425

Paper 3

Title: **Plasma membrane depolarization and permeabilization due to electric pulses in cell lines of different excitability**

Authors: Janja Dermol-Černe, Damijan Miklavčič, Matej Reberšek, Primož Mekuč, Sylvia. M. Bardet, Ryan Burke, Delia Arnaud-Cormos, Philippe Leveque and Rodney O'Connor

Paper 3

Plasma membrane depolarization and permeabilization due to electric pulses in cell lines of different excitability

Janja Dermol-Černe [a], Damijan Miklavčič [a], Matej Reberšek [a], Primož Mekuč [a], Sylvia M. Bardet [b], Ryan Burke [b], Delia Arnaud-Cormos [b], Philippe Leveque [b], Rodney O'Connor [c,*]

[a] University of Ljubljana, Faculty of Electrical Engineering, Tržaška cesta 25, SI-1000 Ljubljana, Slovenia
[b] University of Limoges, CNRS, XLIM, UMR 7252, F-87000 Limoges, France
[c] École des Mines de Saint-Étienne, Department of Bioelectronics, Georges Charpak Campus, Centre Microélectronique de Provence, 880 Route de Mimet, 13120 Gardanne, France

ARTICLE INFO

ABSTRACT

In electroporation-based medical treatments, excitable tissues are treated, either intentionally (irreversible electroporation of brain cancer, gene electrotransfer or ablation of the heart muscle, gene electrotransfer of skeletal muscles), or unintentionally (excitable tissues near the target area). We investigated how excitable and non-excitable cells respond to electric pulses, and if electroporation could be an effective treatment of the tumours of the central nervous system. For three non-excitable and one excitable cell line, we determined a strength-duration curve for a single pulse of 10 ns–10 ms. The threshold for depolarization decreased with longer pulses and was higher for excitable cells. We modelled the response with the Lapicque curve and the Hodgkin-Huxley model. At 1 μs a plateau of excitability was reached which could explain why high-frequency irreversible electroporation (H-FIRE) electroporates but does not excite cells. We exposed cells to standard electrochemotherapy parameters (8×100 μs pulses, 1 Hz, different voltages). Cells behaved similarly which indicates that electroporation most probably occurs at the level of lipid bilayer, independently of the voltage-gated channels. These results could be used for optimization of electric pulses to achieve maximal permeabilization and minimal excitation/pain sensation. In the future, it should be established whether the in vitro depolarization correlates to nerve/muscle stimulation and pain sensation in vivo.

© 2018 Elsevier B.V. All rights reserved.

1. Introduction

Short, high-voltage pulses increase the permeability of cell membranes to different molecules (reversible electroporation) or cause cell death (irreversible electroporation) [1–3]. Electroporation is used in biotechnology, food-processing [4–6] and medicine [7], e.g. gene electrotransfer [8–10], DNA vaccination [11–14], transdermal drug delivery [15,16], IRE as a soft tissue ablation technique [17–20] and electrochemotherapy [21–24].

In medical applications of electroporation, different types of tissues and tumours are treated, among them, also excitable tissues, e.g. critical structures like nerves and spine. Non-excitable as well as excitable cells can be depolarized, i.e. their transmembrane potential increases. However, only excitable cells can produce action potentials due to their expression of a high density of voltage-gated channels which enables electrical communication between cells [25]. Types of excitable cells include neurones, muscle, endocrine and egg cells.

In the literature, there are several examples of electrochemotherapy, irreversible electroporation and gene electrotransfer of excitable tissues by electric pulses. Brain cancer is treated with irreversible electroporation, and electric pulses can transiently disturb the blood-brain-barrier and allow chemotherapeutics to enter the brain [26–31]. Treating prostate cancer can affect the neurovascular bundle [32,33], treating bone metastases can affect nerves [21,34], treating tumours in the spine can affect the spinal cord [34]. When treating tumours in other parts of the body, electrodes will invariably be in the vicinity of the nerves or muscles where the electric field is high enough for excitation or even permeabilization. Electric pulses are also used for ablation of myocardial tissue to treat atrial fibrillation [35–37]. Muscles are a popular target for gene electrotransfer as they are easily accessible and transfected [38,39]. Among them, the heart can be electroporated to treat ischemia [40,41]. Other examples of the application of electric pulses to excitable cells include electroporation of neurons as a labelling technique which

enables subsequent analyses [42–46]. Studies exist on the influence of nsPEF on intracellular calcium and release of catecholamine in endocrine cells [47–49].

Several studies showed that the effect of electric pulses on the functionality of excitable tissues was only short-term. After irreversible electroporation the nerves of different animal models recovered electrophysiologically, histologically and functionally [34,50–52] or at least showed a potential for regeneration [53]. After electroporation of individual rat neocortex neurons, in vitro and in vivo, the membrane potential, the action potential waveform and passive membrane properties remained unchanged [54]. After pulmonary vein ablation with electroporation, the histology and functionality of phrenic nerve remained unchanged [55]. There was no histological damage on nerves in the neurovascular bundle when treating prostate with irreversible electroporation [51].

One of the main drawbacks to the treatment of tissues with pulsed electric fields is the discomfort and pain associated with repeated electrical stimulation [56–59], the need to administer muscle relaxants and anaesthesia [60] and synchronization with the electrocardiogram [61–63]. The neurons responsible for pain sensation (nociceptors) can be stimulated by electric pulses [64,65]. An important advance of the treatment would be to determine a point at which maximum permeability of the membrane could be achieved while minimizing excitation of the exposed excitable cells. In electrochemotherapy, for example, this would translate to maximum drug delivery to tumour cells with minimum tissue damage to surrounding regions, reduced pain experienced by the patient, and minimal use of muscle relaxants. One suggested option is applying short bipolar pulses which do not cause muscle contraction but come at the expense of delivering higher energy than with longer monopolar pulses [66].

Questions that need to be answered include, (i) whether excitable and non-excitable tissues respond similarly to electroporation pulses, (ii) can electroporation be an effective treatment of cancers of the central nervous system, (iii) are the properties of surrounding excitable tissues significantly altered or damaged due to the treatment. In our paper, we evaluated the depolarization and membrane permeability of four cell lines, one excitable and three non-excitable. For each cell line, we determined the strength-duration curve to one pulse of durations between 10 ns and 10 ms. Additionally, response of excitable cell line was modelled with the Lapicque curve and the Hodgkin-Huxley model. Lapicque curve is an empirical description of the strength-duration curve and the Hodgkin-Huxley model is a set of differential equations, describing the dynamics of voltage-gated channels when they are exposed to electric stimulus. Our study shows that higher electric fields are needed for depolarization of excitable cell line than for depolarization of non-excitable cell lines. We compared the depolarization results with previously experimentally determined electroporation results modelled with the Saulis model [67]. We explain the lack of excitation after electroporation with short 1 μs pulses as well as high frequency short bipolar pulses (H-FIRE). This lack of excitability with short bipolar pulses can be explained by reaching a plateau of excitation and electroporation around 1 μs. We also determined the permeability curve to pulses of standard electrochemotherapy parameters (8 × 100 μs, 1 Hz at different electric field amplitudes). All four cell lines were permeabilized at approximately the same electric field, and the permeabilization curves were similarly shaped which indicates that electroporation is independent of voltage-gated channels.

2. Materials and methods

2.1. Cell culture/preparation

Four cell lines of different excitability were used (Fig. 1). CHO Chinese hamster ovary cells (European Collection of Authenticated Cell Cultures ECACC, CHO-K1, cat. no. 85051005, obtained directly from the repository), U-87 MG human glioblastoma cells (ECACC, Public Health England, cat. no. 89081402), and HT22 immortalized mouse hippocampal neurons (The Salk Institute, La Jolla, CA) were grown in an humidified environment at 37 °C at 5% CO_2. CHO cells were grown in the Ham-F12 (Sigma-Aldrich, Germany), U-87 MG in MEM (Sigma-Aldrich, Germany) and HT22 cells in DMEM (Sigma-Aldrich, Germany) growth medium. All growth media were supplemented with 10% fetal bovine serum, L-glutamine and antibiotics. Cells were grown either on Poly-Lysine (Sigma-Aldrich, Germany) coated 22 mm glass coverslips which were put inside a plastic ring or on 40 mm Petri dishes (TPP, Austria). The HT22 cell line was differentiated by 48 h incubation in the Neurobasal medium (Gibco, USA) supplemented with 0.5 mM L-glutamine and B-27 serum-free supplement as advised by the manufacturer. In this time, the cells stopped dividing and changed their morphology (Fig. 1c vs d). We tested the excitability by chemically exciting the cells by varying the concentration of extracellular potassium ions and comparing the response to a 1 ms pulse at 0.6 kV/cm.

2.2. Cell labelling – depolarization and membrane permeability

In the depolarization experiments, we labelled the cells with the plasma membrane potential indicator fluorescent dye (PMPI) of the FLIPR Membrane Potential Assays Kit (Molecular Devices, USA). For 30 min before the experiments, cells were incubated at 37 °C and 5% CO_2 in Live Cell Imaging Solution (Fischer Scientific, France) supplemented with 1 mg/ml 20% D-glucose (Gibco, France) and 0.5 μl/ml PMPI. PMPI consists of a two-part system which includes a fluorescent anionic voltage-sensor and a quencher. When the interior of the cell has a relatively negative charge (in the state of resting potential or repolarization), the anion dye remains bound to the external surface of the plasma membrane. In this state, the quencher in the extracellular fluid prevents fluorescence excitation. During depolarization the voltage sensor translocates to the interior of the plasma membrane. This translocation is reversible as we observe cells return to their base-level fluorescence approximately 30 min after exposure to pulse. An increase in fluorescence is observed because the quenching agent is restricted to the extracellular environment. The time-constant of sensor translocation is in the range of seconds [68].

To determine whether cells were excitable, cells were exposed to different extracellular concentrations of potassium ions (2.5 mM, 25 mM, 50 mM, 75 mM, 100 mM, 140 mM), while the NaCl (140 mM in the original Live Cell Imaging Solution) was substituted for KCl in an equimolar manner. The buffer was changed every 5 min, and the cells were continuously imaged. Increased concentration of extracellular K^+ ions increases the equilibrium potential of K^+ and causes depolarization. Chemical depolarization is slow and does not cause action potential but accommodation. In electrical depolarization experiments, images were acquired every 30 s for 15–30 min, and pulse was delivered 5 min after the beginning of imaging.

In permeability experiments, we labelled the cells with the YO-PRO-1® (YP) (Molecular Probes, USA). Right before the experiments, the growth medium was changed with the Live Cell Imaging Solution supplemented with 1 mg/ml 20% D-glucose (Gibco, France) and 1 μM YP. Images were acquired every 3 s for 6 min, and 8 × 100 μs pulses were delivered 30 s after the beginning of the imaging.

2.3. Exposure of cells to electric pulses

Three different pulse generators were used, each for a different pulse duration range. For 10 ns pulses, we used a commercially available nsPEF (nanosecond pulsed electric fields) generator (FPG 10-1NM-T, FID Technology, Germany) where the electric field was numerically determined [69] (Fig. 3a). For pulse exposures of 550 ns–1 μs, we used a laboratory prototype pulse generator (University of Ljubljana) based on H-bridge digital amplifier with 1 kV MOSFETs (DE275-102N06A, IXYS, USA) [70] (Fig. 3b). For pulse exposures of 10 μs–10 ms we used a commercially available BetaTech electroporator (Electro cell B10,
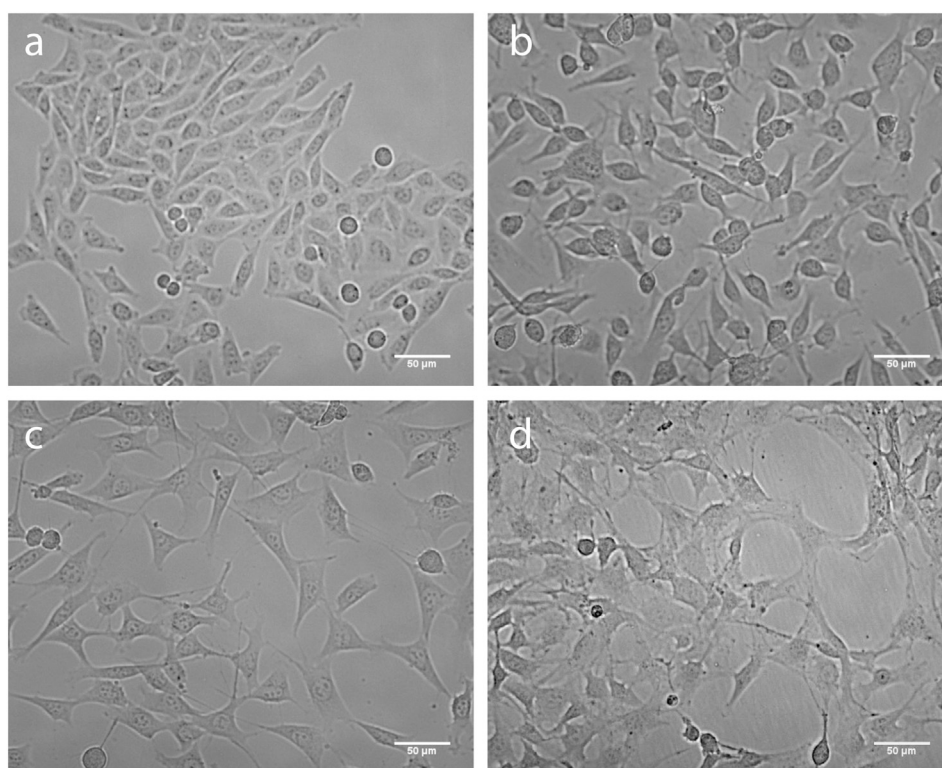
Fig. 1. Phase-contrast images of all four cell lines used in experiments. a - CHO, b - U-87 MG, c - undifferentiated HT22 and d - differentiated HT22.

BetaTech, France). In all experiments, we measured the delivered voltage and current by oscilloscope (DPO 4104, Tektronix, USA or Wavesurfer 422, 200 MHz, LeCroy, USA), voltage probe (tap-off 245 NMFFP-100, Barth Electronics Technology, USA for 10 ns pulses or differential probe ADP305, LeCroy, USA for longer pulses) and a current probe (CP030, LeCroy, USA or Pearson current monitor model 2877, Pearson Electronics, Inc., USA). We used different systems as not all pulse generators were available in both laboratories.

For 10 ns pulses, we used two stainless-steel needle electrodes with a 1.2 mm gap (Fig. 2a) [69]. For pulses longer than 10 ns we used either stainless-steel wire electrodes with a 4 mm inter-electrode distance or Pt/Ir wire electrodes with 1 mm, 2.2 mm or 5 mm inter-electrode distance (Fig. 2b) [70], depending on the electric field needed and the power limitations of the generators. The electric field in the middle between the electrodes was nearly homogeneous and could be approximated as the applied voltage divided by the distance between the electrodes [70].

In depolarization experiments, we delivered one pulse, and we varied the pulse duration (10 ns, 550 ns, 1 μs, 10 μs, 100 μs, 1 ms, 10 ms), and voltage to determine the minimum electric field intensity required to cause a change in membrane potential (depolarization) that was statistically different from control conditions. This minimum electric field intensity was considered to be the depolarization threshold. In membrane permeability experiments, we delivered 8×100 μs pulses at 1 Hz repetition frequency.

2.4. Fluorescence microscopy and measurement

Imaging was performed on two different fluorescent microscopy systems due to different availability of pulse generators in the two
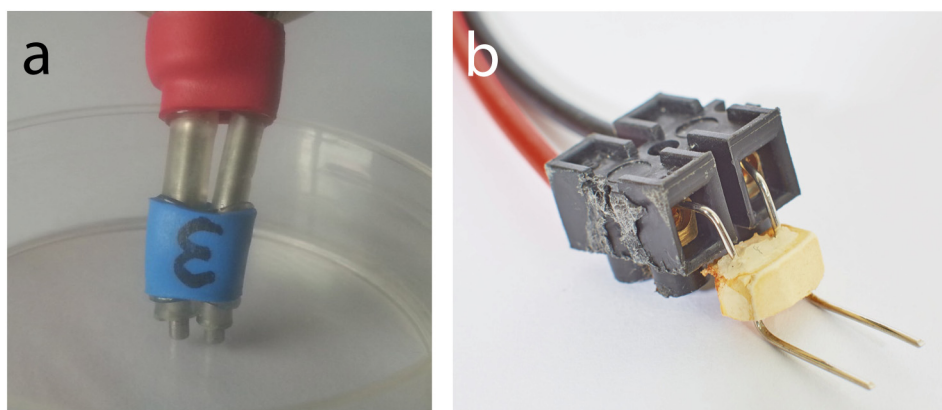

Fig. 2. Photos of the electrodes, used in our experiments. a - electrodes used for delivering 10 ns with 1.2 mm gap, b - electrodes used for delivering pulses longer than 10 ns with 5 mm inter-electrode distance.
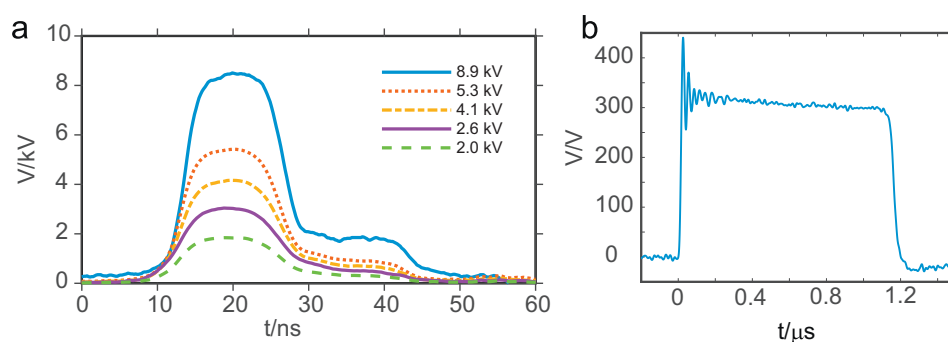
Fig. 3. Traces of pulses applied in the experiments. a - traces of 10 ns pulses generated by a commercial 10 ns nsPEF generator [69], b - a trace of 1 μs pulse generated by a prototype generator from University of Ljubljana [70]. Voltage V/kV or V/V is presented as a function of time t/ns or t/μs, a and b, respectively.

laboratories where the work was done. However, by repeating several samples on both systems, we determined that the difference in systems did not influence the results. Either a DMI6000 inverted microscope (Leica Microsystems, Germany) with EMCCD camera (EMCCD Evolve 512, Roper, USA) or an AxioVert 200 inverted microscope (Zeiss, Germany) with VisiCam 1280 CCD camera (Visitron, Germany) and either a 100× oil immersion or 40× dry objective for PMPI and 20× dry objective for YP were used for experiments. Samples were excited with appropriate wavelengths using the Spectra 7 light engine (Lumencor USA) or a monochromator (High-Speed Polychromator, Visitron Systems GmbH, Germany) and the emission light was selected through appropriate filters. Images were acquired using MetaFluor and MetaMorph PC software (both Molecular Devices, USA).

2.5. Image analysis

First, the background was subtracted, each cell was selected by using freehand tool, and its mean fluorescence was determined. In depolarization experiments, we determined the maximal fluorescence in the first 2.5 min and normalized it to the base line (the value of fluorescence prior exposure to pulses). In permeability experiments, the cells do not take up any YP without the electric pulses applied. Thus, we reported the values either raw or normalized to the fluorescence at maximal pulse parameters (8 × 100 μs, 1.2 kV/cm, 1 Hz repetition frequency).

2.6. Statistical analysis

The threshold of depolarization was determined using ANOVA tests. The threshold was determined as the lowest field intensity required to produce a statistically significant membrane depolarization. The statistical parameters are given in the Appendix, Table A1. The threshold of electroporation (the fluorescence that was significantly different from the control) and the comparisons of the change in maximal fluorescence between all four cell lines were determined using t-test ($p < 0.05$) in SigmaPlot v.11 (Systat Software, San Jose, CA).

3. Calculation/models

3.1. Cell excitability

Cell excitability models described the depolarization/action potential thresholds of the excitable differentiated HT22 cell line as the models we used are valid for excitable cells. We modelled the strength-duration curve with two models – the Lapicque curve [71] which is one of the most often used experimentally tested theoretical model and the Hodgkin-Huxley model [72] which is a phenomenological description of the activity of voltage-gated channels.

The Lapicque curve is in the form:

$$I = b\left(1 + \frac{c}{T}\right),\tag{1}$$

where b denotes the rheobase, c the chronaxie and T the duration of the stimulus. Since we were controlling the electric field to which cells were exposed, we substituted the current (I) with the electric field (E). For the rheobase value we took the depolarization threshold at applied 10 ms, i.e. 0.28 kV/cm. The chronaxie should thus be the pulse duration at twice the rheobase, i.e. around 6 μs. However, with these parameters, the curve fits the data poorly, and thus we determined the parameter c to be 1.88 μs. A non-physiological value of parameter indicates that the Lapicque curve is not an optimal choice for description of our data.

One of the classical models describing neuronal excitation is the Hodgkin-Huxley (HH) model. We numerically calculated the strength-duration curve via the HH model as described in [71]. For several pulse durations, we calculated the corresponding critical transcellular voltage which triggers the action potential (Fig. 4). The K, Na, and leakage current were modelled separately for the anodic and cathodic pole of the cell and coupled via the equivalent circuit (Fig. 1A in [71]). Cells were modelled as idealized planar cells with two uniformly polarized flat surfaces. The corresponding external electric field was calculated by dividing the transcellular voltage with the diameter of the cell. We modelled monopolar as well as bipolar pulses. The bipolar pulse consisted of a positive pulse immediately followed by a negative pulse. The duration of the bipolar pulse is the duration of a separate positive or negative pulse– the whole duration was thus twice this value. The cell excitability calculations were performed in Matlab, R2017a (Mathworks, USA). Shape of the strength-duration curve depends on the time constant of the membrane (Fig. 3 in [71]).
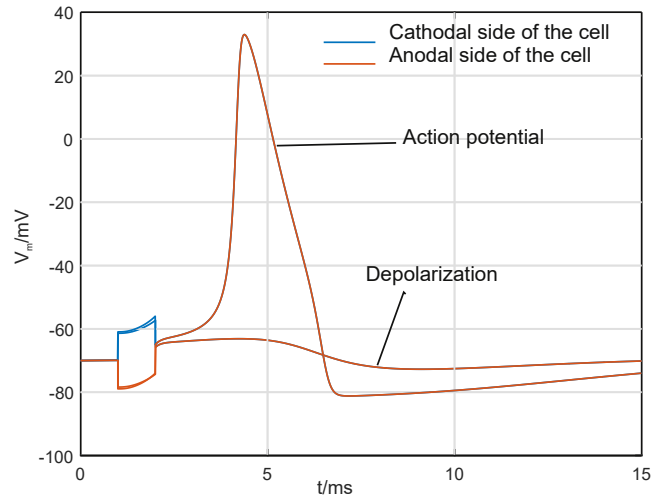
Fig. 4. Example of depolarization without and with initiated action potential. Blue and orange lines denote the voltage at the cathodal and anodal pole of the cell, respectively. After the stimulus, only the orange line is visible as the blue and orange lines are one on top of another and overlap. In this example, one 1 ms pulse was applied just below and at the threshold. Induced transmembrane voltage V_m/mV is presented as a function of time t/ms. (For interpretation of the references to colour in this figure legend, the reader is referred to the web version of this article.)

3.2. Plasma membrane permeabilization

Permeabilization consisted of two sets of experiments – those with the application of one pulse (results previously published in [67]) and the application of 8 pulses (data acquired in this study).

When one pulse was applied, two models were used – a time-dependent Schwann equation or theory of kinetics of pore formation. First, we used the time-dependent Schwann equation for prolate ellipsoidal cells [73,74]:

$$\Delta V_{crit} = E \frac{R_1{}^2 - R_2{}^2}{R_1 - \frac{R_2{}^2}{\sqrt{R_1{}^2 - R_2{}^2}} \log\left(\frac{R_1 + \sqrt{R_1{}^2 - R_2{}^2}}{R_2}\right)} \frac{R_2 \cos(\varphi)}{\sqrt{R_1{}^2 \sin^2\varphi + R_2{}^2 \cos^2\varphi}} \left(1 - \exp\left(-\frac{t}{\tau}\right)\right), \tag{2}$$

where the time constant of the membrane was 0.87 μs (τ) as determined in [67] and $R_1 = 27$ μm $\pm$ 7 μm and $R_2 = 10$ μm $\pm$ 5 μm which we determined from 131 differentiated HT22 cells on phase-contrast images. The critical threshold of electroporation (V_{crit}) 1.776 V was obtained by the least-square method, but the fit was poor ($R^2 = 0.53$) Parameter t denotes time and φ the angle between the electric field and position on the plasma membrane. Because we were interested in the maximal transmembrane voltage, we assumed $\varphi = 0$ (prolate ellipsoid oriented in the direction of the electric field. Electric field (E) was expressed and we calculated the critical applied electric field for electroporation.

Second, we used the expression for a fraction of electroporated cells as derived by [75]. We used the optimized parameters for attached cells in a monolayer from (Eq. (5) and Fig. 5 in this [67]):

$$F_p(E, t_p) = 1 - \exp(-k_f(E)t_p) \tag{3a}$$
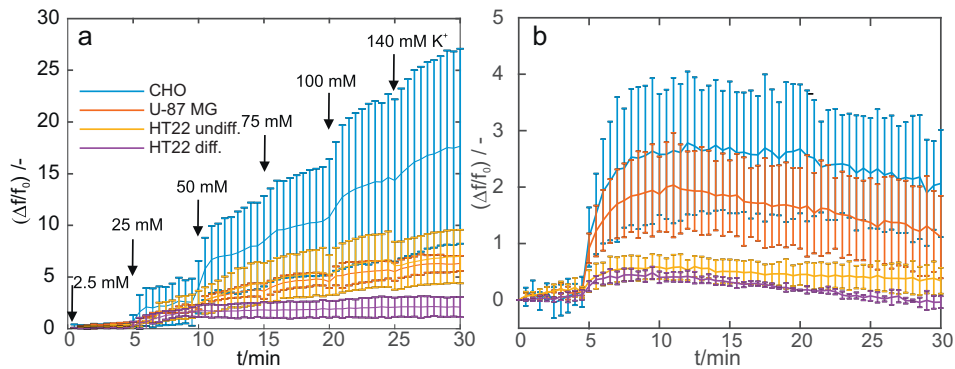
Fig. 5. Time-dynamics of electrical and chemical depolarization of all four cell lines. a) Chemical depolarization for all four cell lines. The K$^+$ concentration was increased every 5 min. The arrows mark which K$^+$ concentration cells were exposed to from that time point further. b) Electrical depolarization when 1 pulse of 1 ms and 0.6 kV/cm was applied. In a and b the increase over base level ($\Delta f/f_0$)/arbitrary units is presented as a function of time t/min with shown 1 standard deviation.

$$k_f(E) = \frac{2\pi\nu R^2}{a} \exp\left(-\frac{\Delta W_0}{k_b T}\right) \int_{-\pi}^{\pi} \exp\left[\pi C_m r^2 \frac{\left(\frac{\varepsilon_w}{\varepsilon_m}-1\right)}{2k_b T}\left(K_1 ER \ \cos(\theta)\left(1-\exp\left(\frac{-t_p}{K_2\tau}\right)\right) + \Delta\varphi\right)^2\right] d\theta, \tag{3b}$$

where F_p denotes the fraction of electroporated cells (0.7), t_p the duration of the pulse, ν the frequency of lateral fluctuations of the lipids (10^{11} s^{-1}), R is by fitting determined cell radius (15.9 μm) [67], a the area per lipid molecule (0.6 nm^2), ΔW_0 the energy barrier for pore formation (46.4 $k_b T$), k_b the Boltzmann constant, T the temperature in kelvins, r the radius of the pore (0.32 nm), C_m the capacity of the membrane (1 μF/cm^2), ε_w (78) and ε_m (4) the relative permittivity of the water in the pore and membrane, respectively, K_1 (1.24) and K_2 (2.56) two numerical parameters, τ the membrane time constant (0.87 μs), $\Delta\varphi$ resting membrane voltage (−25 mV). The values were used as optimized by experimental data on attached CHO cells and electroporation was determined by Fura-2AM [67].

When 8 pulses were applied, the normalized fluorescence curve was obtained by:

$$f_n(E) = \frac{f(E) - f(E = 0 \text{ kV/cm})}{f\left(E = 1.2\frac{\text{kV}}{\text{cm}}\right) - f(E = 0 \text{ kV/cm})} \tag{4}$$

where $f_n(E)$ denotes the normalized fluorescence, $f(E)$ the raw fluorescence and E the applied electric field. The normalized fluorescence curve was then fitted using a symmetric sigmoid to obtain permeabilization curve [76]:

$$p(E) = \frac{1}{1 + \exp\left(-\frac{E - E_{50\%}}{b}\right)} \tag{5}$$

where p denotes the normalized permeabilization, E the applied electric field, $E_{50\%}$ the electric field where 50% of the final fluorescence was reached and b the width of the curve. Permeabilization curve is based on normalized fluorescence of the population and not the exact percentage of permeabilized cells.

The raw values of YO-PRO-1-® fluorescence were described using a first-order uptake model, which gave information on the resealing speed [77]. The model was:

$$f(t) = S\left(1 - \exp\left(-\frac{t}{\tau}\right)\right) \tag{6}$$

where S is the reached plateau, t is the time, f is the raw fluorescence and τ is the time constant of the resealing when 63% of the permeable structures in the membrane are resealed. A higher value of τ means slower resealing than lower value of τ. For curve fitting, we used Matlab R2015 (Mathworks, USA) and the Curve Fitting Toolbox. The goodness of the fit was evaluated using R-squared value, whose value closer to 1 indicates better fit.

4. Results

Results are divided into two sections – cell depolarization and plasma membrane permeabilization after one pulse and plasma membrane permeabilization after pulses of standard electrochemotherapy parameters. Results in the cell depolarization section were obtained with the PMPI dye. Results in the plasma membrane permeabilization section were obtained with the YO-PRO-1® dye.

4.1. Cell depolarization and plasma membrane permeabilization after one pulse

Fig. 5 shows the response of excitable and non-excitable cells to electrochemical and electrical depolarization. In Fig. 5a, the differential behavior of cells to depolarization by increasing extracellular K$^+$ concentrations is shown. In Fig. 5b, the results to electrical depolarization after 1 pulse of 1 ms (the most relevant point for neurostimulation) at 0.6 kV/cm is shown. We compared the intensity of the response and thus exposed all four cell lines to electric pulses of the same parameters. The increase in fluorescence was observed when the pulse was applied at threshold or above-threshold electric fields. We also tested several different pulse durations and electric fields. Depolarization curves for other pulse durations were similar in shape and values as the curves after excitation with 1 ms pulse.

Fig. 6 shows the strength-duration depolarization curve (right y-axis) and strength-duration permeabilization curve (left y-axis). Both aspects (depolarization and membrane permeabilization) were experimentally determined as well as modelled. The experimental depolarization threshold was determined from the membrane depolarization curves, for each pulse duration and cell line separately. It is shown in

grey symbols – x denotes the CHO cells, Δ the U-87 MG cells, □ the undifferentiated HT22 cells and ○ the differentiated HT22 cells. The exact values are stated in Table 1. We can see that with increasing pulse
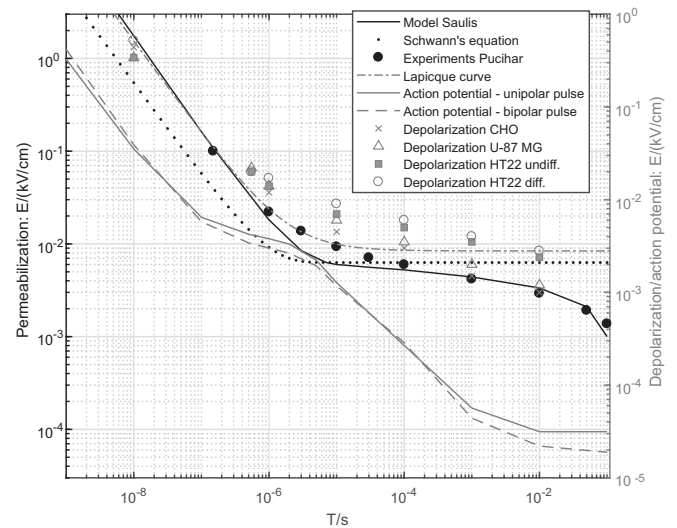
Fig. 6. The depolarization strength-duration curve for CHO, U-87 MG, undifferentiated and differentiated HT22 cells and permeabilization curve from [67] for CHO cells. Black lines and left y-axis show permeabilization to a single pulse of duration T/s. Grey lines and right y-axis show depolarization and action potential due to the application of a single pulse of duration T/s. Depolarization was determined using the PMPI dye and the electroporation by the Fura-2AM dye. Lines correspond to models and symbols to experimental values. External electric field $E/(\text{kV/cm})$ is presented as a function of pulse duration T/s.

Table 1
The depolarization thresholds for all tested pulse durations and cell lines. The results are the same as in the Fig. 6. The asterisk (*) denotes that the threshold is only estimated due to the variability of the data.

Electric field (kV/cm)	10 ns	550 ns	1 µs	10 µs	100 µs	1 ms	10 ms
CHO	44	2.0	1.2	0.45	0.30	0.15	0.10
U-87 MG	34	2.2	1.4	0.60	0.35	0.20	0.12
Undifferentiated HT22	34	2.0	1.4	0.70	0.50	0.35	0.24
Differentiated HT22	52	2.0	1.7*	0.90	0.60	0.40	0.28

Table 2
Parameters of the fitted symmetric sigmoid to the normalized data of YO-PRO-1® uptake. 8×100 µs pulses were delivered at repetition frequency 1 Hz. The numbers denote the optimal value and the corresponding 95% confidence intervals.

Cell line	$E_{50\%}$ (kV/cm)	b (kV/cm)	R-squared
CHO	0.80 ± 0.06	0.15 ± 0.11	0.98
U-87 MG	0.81 ± 0.10	0.13 ± 0.09	0.99
HT22 undifferentiated	0.94 ± 0.07	0.12 ± 0.06	0.99
HT22 differentiated	0.91 ± 0.07	0.12 ± 0.06	0.99

duration the depolarization threshold decreased. At most of the pulse durations, the threshold for depolarization was the highest for the differentiated HT22 cell line. The statistical parameters of the analysis of the experimental depolarization threshold are shown in the Appendix in Table A1. The depolarization strength-duration curve was modelled using the Lapicque curve and the Hodgkin-Huxley model. The models are only valid for excitable cell lines which have voltage-gated channels. In excitable cells we obtained excitability strength-duration curve and in non-excitable cell lines we obtained depolarization strength-duration curve. The modelled curves are presented with grey lines – in dash-dot line is the Lapicque curve, in solid line is the Hodgkin-Huxley model for the unipolar pulses and in dashed line is the Hodgkin-Huxley model for bipolar pulses. The Hodgkin-Huxley model predicts a plateau at around 1 µs and is also slightly better at describing the data than the Lapicque curve.

Experimental electroporation thresholds are shown in filled black circles [67]. By the Saulis model modelled electroporation threshold is presented in black lines. The dashed line is the Schwann's equation. Both models follow a similar dynamics up to 1 ms, but for longer pulses, the Saulis model predicts lower electroporation thresholds and matches the experimental data better. In the Schwann model, the threshold of electroporation was assumed to be constant for all pulse lengths, although it is possible that it changed. The Saulis model was obtained by fitting the model to the experimental results [67] and thus followed the experimental data better than the Schwann equation. Depolarization and electroporation thresholds follow a similar dependency, although the electroporation thresholds are slightly higher than the depolarization thresholds. The same dependency indicates that electroporation and depolarization behave similarly as a function of the applied electric field.

4.2. Plasma membrane permeability after pulses of standard electrochemotherapy parameters

In plasma membrane permeability experiments, we delivered 8×100 µs pulses of different voltage at 1 Hz repetition frequency. These parameters are the standard electrochemotherapy parameters and were used to evaluate the possibility of using electrochemotherapy

as treatment of excitable tissues or in the vicinity of excitable tissues. The normalized plasma membrane permeabilization curve (Eq. 4) to YO-PRO-1® is for all four cell lines shown in Fig. 7. The threshold of electroporation of the U-87 MG and CHO cells was 0.4 kV/cm while of the undifferentiated and differentiated HT22 cells it was 0.6 kV/cm. The threshold was determined as electric field intensity where the fluorescence 6.5 min after pulse application was significantly higher than the fluorescence of the control. With the increase of the electric field, the permeabilization also increased in a similar way for all four cell lines. The permeabilization curve could be described using a symmetric sigmoid (Eq. 5), which is shown in Fig. 7b. The symmetric sigmoid parameters (Table 2) show that all four cell lines reached 50% permeabilization between 0.8 and 0.9 kV/cm ($E_{50\%}$).

An example of the time dynamics of the uptake at applied 8×100 µs at 1.2 kV/cm is shown in Fig. 8a. From the time-lapse of the YO-PRO-1® uptake, we obtained the maximal fluorescence. The maximal fluorescence (Fig. 8b) was the highest for the U-87 MG cells and the lowest for the CHO cells (CHO vs U-87 MG is just significant at p = 0.0468, CHO vs. undifferentiated HT22 p = 0.0002, CHO vs. differentiated HT22 p = 0.0008.). There were no significant differences in the maximal fluorescence between the differentiated and undifferentiated HT22s while for all other pairwise comparisons the difference was significant (t-test, p < 0.05). We obtained the resealing constant (τ) (Fig. 8c) by fitting a first-order uptake model (Eq. 6). The value of time constant τ (Fig. 8c) corresponds to the time when 63% of the pores in the membrane resealed. The resealing was the fastest for the U-87 MG cells, similar for the undifferentiated HT22s and CHO and slower for the differentiated HT22 cells. Statistical significance of the fit is obtained by comparing the error bars which represent a statistical error of 5%.

5. Discussion

Our study we aimed at comparing the depolarization thresholds between excitable and non-excitable cells, to determine if excitable and non-excitable cells respond similarly to electroporation pulses, and to determine if electroporation can be an effective treatment of cancers of the central nervous system. For each cell line, we determined the strength-duration curve to one pulse of lengths between 10 ns and
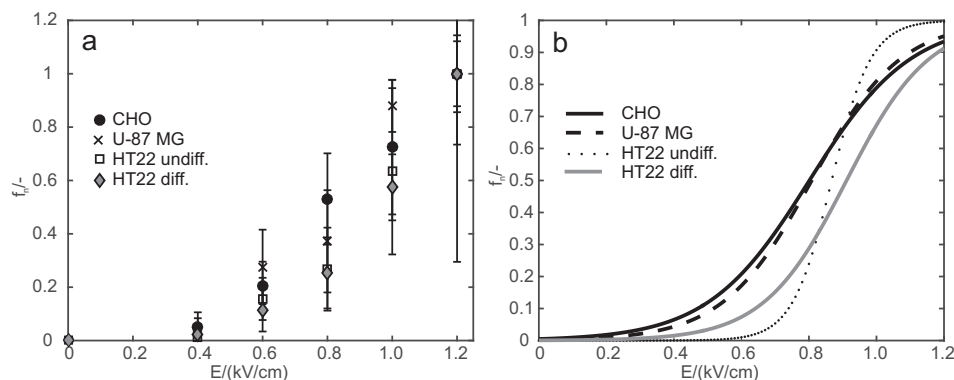

Fig. 7. Normalized fluorescence (a) and permeabilization curve (b) of all four cell lines to YO-PRO-1®, 5 min after the pulse application. The threshold for electroporation was reached at 0.4 kV/cm (U-87 MG and CHO) or 0.6 kV/cm (undifferentiated dernd dfierentiated HT22 cells). a) Normalized values, the bars are one standard deviation and b) the fitted symmetric sigmoid. Normalized fluorescence $f_n/-$ is presented as a function of applied electric field $E/(kV/cm)$.
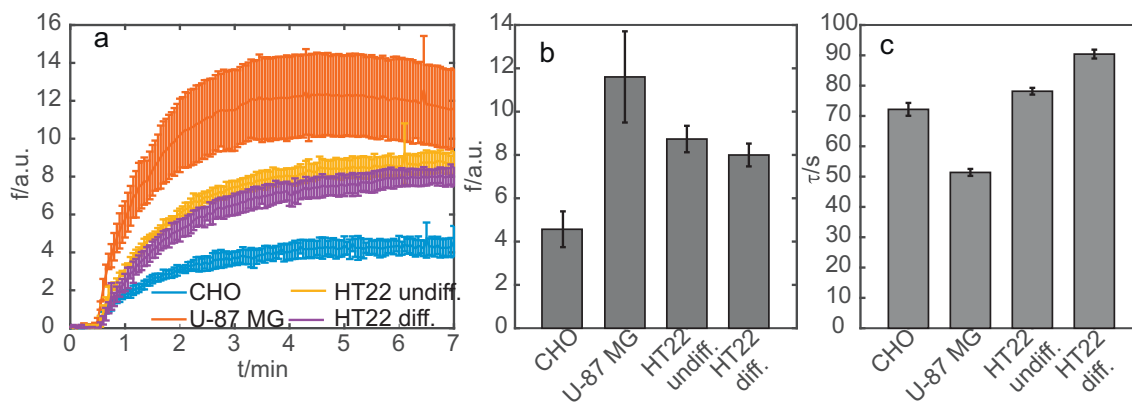
Fig. 8. Time dynamics of the YO-PRO-1® (YP) uptake and its analysis. a - Time dynamics of the YP uptake of all four cell lines at 1.2 kV/cm, 8×100 µs, 1 Hz repetition frequency. One bar means one standard deviation. Fluorescence f/arbitrary units is presented as a function of time t/min. b - The maximal value of YP fluorescence for all four cell lines at applied 8×100 µs pulses of 1.2 kV/cm, 1 Hz repetition frequency. Value of maximal fluorescence f/arbitrary units is shown for each cell line. c - The resealing constant when 8×100 µs pulses at 1.2 kV/cm are applied to all four cell lines. Value of time constant of resealing τ/s is presented for each cell line. Each error bar represents 95% confidence interval of the fitted optimal value of the resealing constant. The R-squared value was in all fits above 0.98.

10 ms. We modelled the strength-duration curve of excitable cells by the Lapicque curve and the Hodgkin-Huxley model. We compared the excitability results with permeabilization to 1 pulse of durations between 150 ns and 100 ms, previously experimentally determined and modelled using the Saulis model [67]. We also determined the permeability curve to 8×100 µs pulses, delivered at 1 Hz and different electric field intensities. For the assessment of cell depolarization we used the PMPI dye. For the assessment of the plasma membrane permeabilization we used the YO-PRO-1® (YP) dye. Thus, we assume all results obtained with the dye PMPI to be depolarization due to voltage-gated channels opening or formation of the pores in the membrane. We assume all results obtained with the YP to be due to influx of YP through the voltage-gated channels or through permeable plasma membrane. Our methodology does not allow us to make distinction between molecules entering through voltage-gated channels or through pores/defects in the cell membrane.

The dye PMPI of the FLIPRR Membrane Potential Assay Kit is a valuable tool for the measurement of membrane potential [78] and ion channel pharmacology [79,80]. Although electrophysiology is considered the gold standard for measurement of membrane potential, PMPI has several advantages, namely the ease of use, the ability to monitor long-term changes in multiple cells simultaneously. Furthermore, PMPI has been compared directly to electrophysiology data with a good agreement [68]. The quencher in the PMPI usually remains in the extracellular fluid due to its large size and continues to quench the fluorescence in the extracellular environment. However, when the plasma membrane is permeabilized, the quencher could potentially enter the cell through pores formed in the membrane and decrease the fluorescence in the cell. When we delivered pulses well above the depolarization threshold, we observed a decrease in a fluorescent signal which could be indicative of cell electroporation. In the future, it should be established to what extent the PMPI dye could also serve as cell membrane permeabilization indicator.

The results of electrochemical depolarization show that with increasing K^+ concentration, the fluorescence and thus the transmembrane voltage are increasing which is in agreement with theory. However, it was unexpected that the highest fluorescence was achieved with CHO cells and not with the differentiated HT22 cells. Excitable cells typically have a higher density of voltage-gated channels, and thus more ions should enter the cell when these channels are open. Results for electrical depolarization to 1 ms and 0.6 kV/cm show similar trends – the highest change in fluorescence was measured with the CHO cells, and the response of the differentiated and non-differentiated HT22 cells was similar (Fig. 5) which was surprising. CHO cells are non-excitable cells and would be expected to have a low background of voltage-

gated ion channels; however, some reports indicate that these cells express voltage-gated Na^+ channels [81] and a lack delayed rectifier K^+ currents [82]. This would explain why CHO cells exhibited more significant and prolonged depolarization in our experiments compared to other cells evaluated. Future investigations should examine the influence of voltage-gated Na^+ channel inhibitors on CHO depolarization. This finding highlights the importance of considering the endogenous complement of voltage-gated ion channels expressed in a given cell line It is also commensurate with our recent results using PMPI voltage imaging to demonstrate the numerous ion channels present and implicated in the depolarization of U-87 MG cells by short electric pulses [83]. Another difference between the CHO cells and other three cell lines is their pattern of growth. CHO cells tend to form colonies and are in close contact to one another which causes electric field shielding and lower induced transmembrane voltage [84]. Cells of U-87 MG and HT22 cell lines were grown to be more isolated (Fig. 1).

Our strength-duration curve was determined for pulse lengths between 10 ns and 10 ms. As expected, the electric field needed to depolarize cells decreased with increasing pulse duration [71,85,86]. In [86], the strength-duration curve was measured for frog muscles between 1 ns and 100 ms. The authors determined that the thresholds for pulses of 100 µs or shorter followed a linear curve (in log-log scale) which confirmed that the signal was due to the opening of the ionic channels and not due to electroporation. Our results had roughly the same dependency but the linear curve followed a linear dynamics for pulses shorter than 1 µs. The differentiated HT22 cells are excitable [87] and because of similar shape of the strength-duration curve to the curve by Rogers et al. [86] we can assume that for short pulses we also measured predominantly opening of the voltage-gated channels and not membrane electroporation. The other three cell lines are not excitable, and the depolarization threshold only shows when the transmembrane voltage was significantly increased above the resting voltage. The reasons for the discrepancy between the data by Rogers et al. and our study could be that they used exponential pulses instead of square pulses used in our study, and determined the threshold by observing the twitching of the muscle while we used a fluorescent dye.

For the depolarization of the differentiated HT22 cells, higher electric field intensity was needed at most pulse lengths. These results are expected due to the more negative resting membrane voltage of differentiated non-dividing cells [88] for which a higher change in membrane potential is needed to reach the threshold of depolarization. However, at pulse lengths of 10 ns the difference in the critical membrane voltage between the differentiated HT22 cells and non-excitable cells was up to 0.6 V (approximating cells as prolate spheroids with $R_1 = 27$ µm and $R_2 = 10$ µm), which

cannot be explained solely by a lower resting transmembrane voltage (around 50 mV difference between the excitable and non-excitable cells). The endogenous voltage-gated channels present in the plasma membrane of the CHO cells could explain this observation.

First, we tried modelling the depolarization data with Lapicque's curve which is similar to the Bleiss curve used in [86] but is valid for square pulses. We could not describe the shape of the strength-duration curve well, and the optimized value of the chronaxie was higher than predicted from the value of the rheobase. Thus, we decided to fit the Hodgkin-Huxley model, a more complex model, which takes into account the dynamics of the voltage-gated channels. The Hodgkin-Huxley model in [71] couples the voltage on the anodal and cathodal pole of the cell via the equivalent circuit. We modelled the cell as an idealized planar structure which does not accurately describe cell shape but it does give a general idea of the shape of strength-duration curve. Even when calculating the strength-duration curve for a spherical cell, the shape of the strength-duration curve remained the same, it only slightly moved along the y-axis (Fig. 7 in [71]).The shape of the strength-duration curve is not linear. The Hodgkin-Huxley model qualitatively followed the data well for pulses shorter than 10 μs, but for longer pulses, the predicted depolarization threshold decreased more than the experimentally determined one. The reasons for deviation at long pulses could be the following. First, we were also electroporating cells enough for the dye to enter the cell but not the quencher. Second, our system was not sufficiently sensitive to determine very low depolarization thresholds. Third, for exact determination of the depolarization thresholds or action potential (for the differentiated HT22 cells) electrophysiological measurements are necessary. Fourth, also other channels contributed to the dependency of depolarization observed in our experiments but were not included in the model.

In [52] the authors achieved excitation of a peripheral nerve with a nanosecond pulse without electroporation. The presence of action potential without electroporation is in agreement with our modelling since the thresholds for depolarization were lower than electroporation thresholds. Additionally, the nerves' refractory properties were not affected.

We found the plateau of depolarization thresholds at 1 μs intriguing and decided to try the same model on bipolar pulses. The results of this model offered an interesting perspective on the potential mechanism of the H-FIRE protocol [66]. In Fig. 6, we can see that around 1 μs there is an overlap of the depolarization thresholds determined by the Hodgkin-Huxley model and of the Saulis permeabilization model. This overlap could explain why with 1 μs bipolar pulses, electroporation was observed while muscle contractions were not [66]. In our model, with currently chosen parameters the threshold for electroporation was still higher than for an action potential, but the parameters of the Hodgkin-Huxley model were not optimized to describe our data, and we used the same values as in [71]. Optimizing the values of the Hodgkin-Huxley model could bring curves closer together. The Hodgkin-Huxley model and permeabilization model also indicate that short monopolar pulses could be better at not exciting the tissues since the threshold for action potential was calculated to be higher than that of the bipolar pulses. A similar explanation why the H-FIRE pulses do not excite the cells was offered in [89] by numerical modelling of the response of nerves to bipolar pulses. These authors showed that by using short bipolar pulses, it was possible to ablate a tissue region without triggering action potentials in the nearby nerve. The reason proposed being that the stimulation threshold rises faster than the irreversible electroporation threshold. Further experiments are now needed to test these hypotheses, comparing the thresholds for action potentials and electroporation in excitable tissues with monopolar versus bipolar pulses in the 1 μs range.

The repolarization time of all four cell lines was in the range of minutes. The values for CHO, U-87 MG and non-differentiated HT22s are in agreement with the current knowledge existing as these cell lines do not have I_K voltage-gated potassium channels, responsible for fast

repolarization. The values of repolarization of differentiated HT22 cells are much longer than traditionally observed during neural depolarization, which is in the range of milliseconds. There are several possible explanations for this discrepancy. First, as the assessment method, we used PMPI dye entering the cell and then being pumped out. PMPI dye has a time constant of several seconds [90] and can be understood as a low-pass filter. Second, our experiments were performed at room temperature which slows down the speed of the Na/K pump. Third, it is possible that delivery of a single pulse led to a burst of action potentials and thus a prolonged depolarization. Fourth, that cells were depolarized as well as electroporated. Fifth, electroporation causes leakage of ATP [91] which is necessary for driving the pumps, and lack of ATP could slow them down. Sixth, due to high induced transmembrane voltage ion channels could be damaged [92,93].

The time required for reaching the peak fluorescence in depolarization experiments coincided with the resealing time observed in the permeabilization experiments. It is possible that during depolarization and permeabilization experiments, PMPI and YP were entering through the voltage-gated channels [94] as well as through pores formed in the plasma membrane. Even when using channel inhibitors, a total inhibition of depolarization could not be achieved which indicates that during depolarization ions also enter through pores [83].

An interesting study where also a fluorescent dye was used to assess depolarization/action potential and plasma membrane electroporation of hippocampal neurons was recently performed by Pakhomov et al. [95]. They determined that the activation of voltage-gated sodium channels enhanced the depolarizing effect of electroporation. The authors used the Fluo-Volt dye which enables imaging of fast changes in the range of ms. On the other hand, the PMPI dye enables imaging in the range of seconds to minutes, and it enables to capture slow, persistent changes in the transmembrane potential in the non-excitable cells.

In the next part of our study, we exposed cells to 8×100 μs pulses, which are typically used in electrochemotherapy treatments. All four cell lines reached the threshold of electroporation at approximately the same value - between 0.4 and 0.6 kV/cm. The permeabilization curve of all four lines could be described using a symmetric sigmoid. Although the differentiation causes a drop in the resting membrane potential [88], the lower, i.e. more negative resting membrane potential did not affect the threshold of electroporation as it was similar for excitable and non-excitable cells. The permeabilization curves then followed similar dependency (Fig. 7b) and reached 50% of the maximal fluorescence around 0.9 kV/cm. We can conclude that irrespective of the excitability, all four cell lines responded similarly to electroporation pulses. The results are in agreement with electroporation being a physical means of disturbing plasma membrane in the lipid domain of the membrane. If the voltage-gated ion channels contributed to the YP uptake, it was much lower than the uptake through the permeabilized membrane.

The fluorescence reached was the highest for the U-87 MG cell line and the lowest for the CHO cell line while the fluorescence of the differentiated and undifferentiated HT22 cells was between the levels of the CHO and U-87 MG cells. Since the cells were grown attached in a monolayer, the lowest fluorescence of the CHO cell line can be explained by the tendency of CHO cells to grow in colonies in proximity which decreases the area of the plasma membrane available for dye uptake. Another reason could be that the proximity of cells decreases the induced transmembrane potential due to shielding [76,84,96] although it is unexpected that the proximity did not affect the threshold of electroporation. YP starts to emit fluorescent light after binding to nucleic acids. Thus different concentration of intracellular nucleic acids could also affect the fluorescence.

From the time-lapse images of the YP uptake, the resealing speed could be determined. The values of resealing constants were in the same range as in [77] although the electroporation buffer we used in this study was not tested previously. The cancerous U-87 MG cell line resealed much faster than the other (normal) three cell lines which is

in agreement with [97] where it was observed that cancerous cells resealed 2–3 times faster than normal ones due to lower tension levels in their lipid membranes.

6. Conclusions

In summary, the depolarization threshold was higher for the excitable cells than for the non-excitable cells. The strength-duration curve of excitable cells was described with the Lapicque curve and the Hodgkin-Huxley model. However, neither of the models described the behaviour at all pulse durations. The Hodgkin-Huxley model gave insight into the ability of the H-FIRE to permeabilize but not excite the tissue. All four cell lines responded similarly to pulses of standard electrochemotherapy parameters. The shape of the permeability curve was similar to curves already published in the literature [98]. Thus, electroporation is a feasible means of treating excitable and non-excitable cells with pulses of similar parameters. Furthermore, our results show the potential of achieving permeabilization and minimizing or avoiding excitation/pain sensation which needs to be explored in more detail. In future studies, it should be established, however, to what extent in vitro depolarization and excitability correlate to the actual excitation and pain sensation in vivo.

Acknowledgement

Conflict of interests

The authors have declared that no competing interests exist.

Authorship

JDČ: acquisition of the data, analysis and interpretation of the data, drafting the paper, final approval of the paper.

DM: conception and design of the study, analysis and interpretation of the data, drafting the paper, final approval of the paper.

MR: design of the ns-μs pulse generator, used in the study, final approval of the paper.

PM: design of the ns-μs pulse generator, used in the study, final approval of the paper.

SMB: acquisition of the data, analysis and interpretation of the data, final approval of the paper.

RB: acquisition of the data, analysis and interpretation of the data, final approval of the paper.

DAC: design of the ns pulse exposure setup, final approval of the paper.

PL: analysis and interpretation of the data, design of the ns pulse exposure setup, final approval of the paper.

ROC: conception and design of the study, acquisition of the data, analysis and interpretation of the data, drafting the paper, final approval of the paper.

Appendix A

Table A1

Statistical parameters of the strength-duration curve statistical analysis by ANOVA for the CHO cell line (Table A1a), the U-87 MG cell line (Table A1b) the undifferentiated HT22 (Table A1c) and the differentiated HT22 cell line (Table A1d). F(x,y) means the F-test value, where x, y are the degrees of freedom of the between-group comparison and the within-group comparison. Where F_w is indicated, the assumption of homogeneity of variance was not met; therefore, a Welch's adjustment for the ANOVA was calculated and reported. The statistical significance provides the p-values which are compared to our alpha criterion of $\alpha = 0.05$. The effect size column provides an indication of the variability in response that can be attributed to the PEF. As an example, $\Omega^2 = 0.47$ means that 47% of the change in membrane potential can be attributed to the PEF.

Table A1a

CHO	F	p	Ω^2
10 ns	$F(2, 17) = 9.00$	$p < 0.01$	0.47
550 ns	$F(3, 15) = 4.56$	$p = 0.02$	0.36
1 μs	$F(3, 16) = 91.52$	$p < 0.01$	0.93
10 μs	$F_W(3, 6.08) = 14.12$	$p < 0.01$	0.67
100 μs	$F(4, 19) = 10.35$	$p < 0.01$	0.61
1 ms	$F_W(3, 5.55) = 53.76$	$p < 0.01$	0.89
10 ms	$F(3, 13) = 10.80$	$p < 0.01$	0.63

Table A1b

U-87 MG	F	p	Ω^2
10 ns	$F(4, 19) = 2.90$	$p < 0.01$	0.80
550 ns	$F(3, 15) = 3.60$	$p = 0.04$	0.29
1 μs	$F(3, 16) = 4.32$	$p = 0.02$	0.33
10 μs	$F_W(4, 9.27) = 43.54$	$p < 0.01$	0.63
100 μs	$F(3, 21) = 47.64$	$p < 0.01$	0.85
1 ms	$F_W(4, 6.62) = 13.96$	$p < 0.01$	0.71
10 ms	$F(3, 19) = 10.66$	$p < 0.01$	0.56

Table A1c

Undifferentiated HT22	F	p	Ω^2
10 ns	$F_W(3, 3.06) = 21.88$	$p = 0.01$	0.81
550 ns	$F(2, 9) = 12.96$	$p < 0.01$	0.67
1 μs	$F(3, 9) = 11.14$	$p < 0.01$	0.70
10 μs	$F(4, 10) = 5.24$	$p = 0.02$	0.53
100 μs	$F(2, 12) = 3.79$	$p = 0.05$	0.27
1 ms	$F(3, 10) = 9.06$	$p < 0.01$	0.63
10 ms	$F(4, 13) = 4.15$	$p = 0.02$	0.41

Table A1d

Differentiated HT22	F	p	Ω^2
10 ns	$F_W(3, 11.76) = 13.41$	$p < 0.01$	0.60
550 ns	$F(2, 10) = 5.20$	$p = 0.03$	0.39
1 μs	$F(2, 16) = 4.56$	$p = 0.03$	0.29
10 μs	$F(6, 21) = 3.97$	$p < 0.01$	0.39
100 μs	$F(4, 16) = 6.13$	$p < 0.01$	0.49
1 ms	$F(3, 19) = 8.80$	$p < 0.01$	0.50
10 ms	$F(4, 20) = 6.02$	$p < 0.01$	0.45

References

[1] T. Kotnik, P. Kramar, G. Pucihar, D. Miklavčič, M. Tarek, Cell membrane electroporation- part 1: the phenomenon, IEEE Electr. Insul. Mag. 28 (2012) 14–23, https://doi.org/10.1109/MEI.2012.6268438.
[2] T.Y. Tsong, Electroporation of cell membranes, Biophys. J. 60 (1991) 297–306, https://doi.org/10.1016/S0006-3495(91)82054-9.
[3] J.C. Weaver, Electroporation: a general phenomenon for manipulating cells and tissues, J. Cell. Biochem. 51 (1993) 426–435.
[4] T. Kotnik, W. Frey, M. Sack, S. Haberl Meglič, M. Peterka, D. Miklavčič, Electroporation-based applications in biotechnology, Trends Biotechnol. (2015) https://doi.org/10.1016/j.tibtech.2015.06.002.
[5] S. Mahnič-Kalamiza, E. Vorobiev, D. Miklavčič, Electroporation in food processing and biorefinery, J. Membr. Biol. 247 (2014) 1279–1304.
[6] S. Toepfl, C. Siemer, G. Saldaña-Navarro, V. Heinz, Overview of pulsed electric fields processing for food, Emerg. Technol. Food Process. Elsevier 2014, pp. 93–114 http://linkinghub.elsevier.com/retrieve/pii/B9780124114791000061, Accessed date: 29 June 2016.
[7] M.L. Yarmush, A. Golberg, G. Serša, T. Kotnik, D. Miklavčič, Electroporation-based technologies for medicine: principles, applications, and challenges, Annu. Rev.

Biomed. Eng. 16 (2014) 295–320, https://doi.org/10.1146/annurev-bioeng-071813-104622.

[8] A.I. Daud, R.C. DeConti, S. Andrews, P. Urbas, A.I. Riker, V.K. Sondak, P.N. Munster, D.M. Sullivan, K.E. Ugen, J.L. Messina, R. Heller, Phase I trial of interleukin-12 plasmid electroporation in patients with metastatic melanoma, J. Clin. Oncol. 26 (2008) 5896–5903.

[9] R. Heller, Y. Cruz, L.C. Heller, R.A. Gilbert, M.J. Jaroszeski, Electrically mediated delivery of plasmid DNA to the skin, using a multielectrode array, Hum. Gene Ther. 21 (2010) 357–362, https://doi.org/10.1089/hum.2009.065.

[10] R. Heller, L.C. Heller, Gene ELECTROTRANSFER CLINICAL TRIALS, Adv. Genet. Elsevier 2015, pp. 235–262http://linkinghub.elsevier.com/retrieve/pii/S0065266014000078, Accessed date: 26 January 2016.

[11] C.Y. Calvet, F.M. André, L.M. Mir, Dual therapeutic benefit of electroporation-mediated DNA vaccination in vivo: enhanced gene transfer and adjuvant activity, OncoImmunology 3 (2014), e28540. https://doi.org/10.4161/onci.28540.

[12] C.L. Trimble, M.P. Morrow, K.A. Kraynyak, X. Shen, M. Dallas, J. Yan, L. Edwards, R.L. Parker, L. Denny, M. Giffear, A.S. Brown, K. Marcozzi-Pierce, D. Shah, A.M. Slager, A.J. Sylvester, A. Khan, K.E. Broderick, R.J. Juba, T.A. Herring, J. Boyer, J. Lee, N.Y. Sardesai, D.B. Weiner, M.L. Bagarazzi, Safety, efficacy, and immunogenicity of VGX-3100, a therapeutic synthetic DNA vaccine targeting human papillomavirus 16 and 18 E6 and E7 proteins for cervical intraepithelial neoplasia 2/3: a randomised, double-blind, placebo-controlled phase 2b trial, Lancet 386 (2015) 2078–2088, https://doi.org/10.1016/S0140-6736(15)00239-1.

[13] S. Vasan, A. Hurley, S.J. Schlesinger, D. Hannaman, D.F. Gardiner, D.P. Dugin, M. Boente-Carrera, R. Vittorino, M. Caskey, J. Andersen, Y. Huang, J.H. Cox, T. Tarragona-Fiol, D.K. Gill, H. Cheeseman, L. Clark, L. Dally, C. Smith, C. Schmidt, H.H. Park, J.T. Kopycinski, J. Gilmour, P. Fast, R. Bernard, D.D. Ho, In vivo electroporation enhances the immunogenicity of an HIV-1 DNA vaccine candidate in healthy volunteers, PLoS One 6 (2011), e19252. https://doi.org/10.1371/journal.pone.0019252.

[14] G. Serša, J. Teissié, M. Čemažar, E. Signori, U. Kamenšek, G. Marshall, D. Miklavčič, Electrochemotherapy of tumors as in situ vaccination boosted by immunogene electrotransfer, Cancer Immunol. Immunother. 64 (2015) 1315–1327, https://doi.org/10.1007/s00262-015-1724-2.

[15] A.-R. Denet, R. Vanbever, V. Préat, Skin electroporation for transdermal and topical delivery, Adv. Drug Deliv. Rev. 56 (2004) 659–674, https://doi.org/10.1016/j.addr.2003.10.027.

[16] B. Zorec, V. Préat, D. Miklavčič, N. Pavšelj, Active enhancement methods for intra- and transdermal drug delivery: a review, Zdrav. Vestn. 82 (2013) 339–356.

[17] B. Al-Sakere, F. André, C. Bernat, E. Connault, P. Opolon, R.V. Davalos, B. Rubinsky, L. M. Mir, Tumor ablation with irreversible electroporation, PLoS One 2 (2007), e1135. https://doi.org/10.1371/journal.pone.0001135.

[18] R.V. Davalos, L.M. Mir, B. Rubinsky, Tissue ablation with irreversible electroporation, Ann. Biomed. Eng. 33 (2005) 223–231, https://doi.org/10.1007/s10439-005-8981-8.

[19] C. Jiang, R.V. Davalos, J.C. Bischof, A review of basic to clinical studies of irreversible electroporation therapy, IEEE Trans. Biomed. Eng. 62 (2015) 4–20, https://doi.org/10.1109/TBME.2014.2367543.

[20] H.J. Scheffer, K. Nielsen, M.C. de Jong, A.A. van Tilborg, J.M. Vieveen, A.R. Bouwman, S. Meijer, C. van Kuijk, P.M. van den Tol, M.R. Meijerink, Irreversible electroporation for nonthermal tumor ablation in the clinical setting: a systematic review of safety and efficacy, J. Vasc. Interv. Radiol. 25 (2014) 997–1011, https://doi.org/10.1016/j.jvir.2014.01.028.

[21] A. Gasbarrini, W.K. Campos, L. Campanacci, S. Boriani, Electrochemotherapy to metastatic spinal melanoma: a novel treatment of spinal metastasis? Spine 40 (2015) E1340–E1346, https://doi.org/10.1097/BRS.0000000000001125.

[22] B. Mali, T. Jarm, M. Snoj, G. Serša, D. Miklavčič, Antitumor effectiveness of electrochemo-therapy: a systematic review and meta-analysis, Eur. J. Surg. Oncol. 39 (2013) 4–16.

[23] D. Miklavčič, B. Mali, B. Kos, R. Heller, G. Serša, Electrochemotherapy: from the drawing board into medical practice, Biomed. Eng. Online 13 (2014) 29, https://doi.org/10.1186/1475-925X-13-29.

[24] G. Bianchi, L. Campanacci, M. Ronchetti, D. Donati, Electrochemotherapy in the treatment of bone metastases: a phase II trial, World J. Surg. 40 (2016) 3088–3094, https://doi.org/10.1007/s00268-016-3627-6.

[25] B. Hille, Ionic Channels of Excitable Membranes, 2nd ed. Sinauer Associates, Sunderland, Mass, 1992.

[26] P.A. Garcia, J.H. Rossmeisl, J.L. Robertson, J.D. Olson, A.J. Johnson, T.L. Ellis, R.V. Davalos, 7.0-T magnetic resonance imaging characterization of acute blood-brain-barrier disruption achieved with intracranial irreversible electroporation, PLoS ONE 7 (2012), e50482. https://doi.org/10.1371/journal.pone.0050482.

[27] P.A. Garcia, T. Pancotto, J.H. Rossmeisl, N. Henao-Guerrero, N.R. Gustafson, G.B. Daniel, J.L. Robertson, T.L. Ellis, R.V. Davalos, Non-thermal irreversible electroporation (N-TIRE) and adjuvant fractionated radiotherapeutic multimodal therapy for intracranial malignant glioma in a canine patient, Technol. Cancer Res. Treat. 10 (2011) 73–83.

[28] M. Hjouj, D. Last, D. Guez, D. Daniels, S. Sharabi, J. Lavee, B. Rubinsky, Y. Mardor, MRI study on reversible and irreversible electroporation induced blood brain barrier disruption, PLoS One 7 (2012), e42817. https://doi.org/10.1371/journal.pone.0042817.

[29] M. Linnert, H.K. Iversen, J. Gehl, Multiple brain metastases - current management and perspectives for treatment with electrochemotherapy, Radiol. Oncol. 46 (2012)https://doi.org/10.2478/v10019-012-0042-y.

[30] J.H. Rossmeisl, P.A. Garcia, T.E. Pancotto, J.L. Robertson, N. Henao-Guerrero, R.E. Neal, T.L. Ellis, R.V. Davalos, Safety and feasibility of the NanoKnife system for irreversible electroporation ablative treatment of canine spontaneous intracranial gliomas, J. Neurosurg. 123 (2015) 1008–1025, https://doi.org/10.3171/2014.12.JNS141768.

[31] S. Sharabi, B. Kos, D. Last, D. Guez, D. Daniels, S. Harnof, Y. Mardor, D. Miklavčič, A statistical model describing combined irreversible electroporation and electroporation-induced blood-brain barrier disruption, Radiol. Oncol. 50 (2016) 28–38.

[32] R.E. Neal, J.L. Millar, H. Kavnoudias, P. Royce, F. Rosenfeldt, A. Pham, R. Smith, R.V. Davalos, K.R. Thomson, In vivo characterization and numerical simulation of prostate properties for non-thermal irreversible electroporation ablation: characterized and simulated prostate IRE, Prostate 74 (2014) 458–468, https://doi.org/10.1002/pros.22760.

[33] F. Ting, M. Tran, M. Böhm, A. Siriwardana, P.J. Van Leeuwen, A.-M. Haynes, W. Delprado, R. Shnier, P.D. Stricker, Focal irreversible electroporation for prostate cancer: functional outcomes and short-term oncological control, Prostate Cancer Prostatic Dis. 19 (2016) 46–52, https://doi.org/10.1038/pcan.2015.47.

[34] M. Tschon, F. Salamanna, M. Ronchetti, F. Cavani, A. Gasbarrini, S. Boriani, M. Fini, Feasibility of electroporation in bone and in the surrounding clinically relevant structures: a preclinical investigation, Technol. Cancer Res. Treat. (2015)https://doi.org/10.1177/1533034615604454.

[35] J. Lavee, G. Onik, P. Mikus, B. Rubinsky, A novel Nonthermal energy source for surgical epicardial atrial ablation: irreversible electroporation, Heart Surg. Forum 10 (2007) E162–E167, https://doi.org/10.1532/HSF98.20061202.

[36] K. Neven, V. van Driel, H. van Wessel, R. van Es, P.A. Doevendans, F. Wittkampf, Myocardial lesion size after epicardial electroporation catheter ablation after subxiphoid puncture, Circ. Arrhythm. Electrophysiol. 7 (2014) 728–733, https://doi.org/10.1161/CIRCEP.114.001659.

[37] F. Xie, F. Varghese, A.G. Pakhomov, I. Semenov, S. Xiao, J. Philpott, C. Zemlin, Ablation of myocardial tissue with nanosecond pulsed electric fields, PLoS One 10 (2015), e0144833. https://doi.org/10.1371/journal.pone.0144833.

[38] J. Gehl, T.H. Sørensen, K. Nielsen, P. Raskmark, S.L. Nielsen, T. Skovsgaard, L.M. Mir, In vivo electroporation of skeletal muscle: threshold, efficacy and relation to electric field distribution, Biochim. Biophys. Acta Gen. Subj. 1428 (1999) 233–240, https://doi.org/10.1016/S0304-4165(99)00094-X.

[39] S. Satkauskas, M.F. Bureau, M. Puc, A. Mahfoudi, D. Scherman, D. Miklavcic, L.M. Mir, Mechanisms of in vivo DNA electrotransfer: respective contributions of cell electropermeabilization and DNA electrophoresis, Mol. Ther. 5 (2002) 133–140, https://doi.org/10.1006/mthe.2002.0526.

[40] E.L. Ayuni, A. Gazdhar, M.N. Giraud, A. Kadner, M. Gugger, M. Cecchini, T. Caus, T.P. Carrel, R.A. Schmid, H.T. Tevaearai, In vivo electroporation mediated gene delivery to the beating heart, PLoS One 5 (2010), e14467. https://doi.org/10.1371/journal.pone.0014467.

[41] A.A. Bulysheva, B. Hargrave, N. Burcus, C.G. Lundberg, L. Murray, R. Heller, Vascular endothelial growth factor-A gene electrotransfer promotes angiogenesis in a porcine model of cardiac ischemia, Gene Ther. 23 (2016) 649–656, https://doi.org/10.1038/gt.2016.35.

[42] J. De Vry, P. Martínez-Martínez, M. Losen, Y. Temel, T. Steckler, H.W.M. Steinbusch, M.H. De Baets, J. Prickaerts, In vivo electroporation of the central nervous system: a non-viral approach for targeted gene delivery, Prog. Neurobiol. 92 (2010) 227–244, https://doi.org/10.1016/j.pneurobio.2010.10.001.

[43] P. Lovell, S.H. Jezzini, L.L. Moroz, Electroporation of neurons and growth cones in Aplysia californica, J. Neurosci. Methods 151 (2006) 114–120, https://doi.org/10.1016/j.jneumeth.2005.06.030.

[44] R. Kanjhan, D.I. Vaney, Semi-loose seal Neurobiotin electroporation for combined structural and functional analysis of neurons, Pflugers Arch. - Eur. J. Physiol. 457 (2008) 561–568, https://doi.org/10.1007/s00424-008-0539-9.

[45] M. Barker, B. Billups, M. Hamann, Focal macromolecule delivery in neuronal tissue using simultaneous pressure ejection and local electroporation, J. Neurosci. Methods 177 (2009) 273–284, https://doi.org/10.1016/j.jneumeth.2008.10.021.

[46] T. Heida, J.B.M. Wagenaar, W.L.C. Rutten, E. Marani, Investigating membrane breakdown of neuronal cells exposed to nonuniform electric fields by finite-element modeling and experiments, IEEE Trans. Biomed. Eng. 49 (2002) 1195–1203, https://doi.org/10.1109/TBME.2002.803503.

[47] G. Craviso, P. Chatterjee, G. Maalouf, A. Cerjanic, J. Yoon, I. Chatterjee, P. Vernier, Nanosecond electric pulse-induced increase in intracellular calcium in adrenal chromaffin cells triggers calcium-dependent catecholamine release, IEEE Trans. Dielectr. Electr. Insul. 16 (2009) 1294–1301, https://doi.org/10.1109/TDEI.2009.5293941.

[48] G.L. Craviso, S. Choe, I. Chatterjee, P.T. Vernier, Modulation of intracellular Ca^{2+} levels in chromaffin cells by nanoelectropulses, Bioelectrochemistry 87 (2012) 244–252, https://doi.org/10.1016/j.bioelechem.2011.11.016.

[49] G.L. Craviso, S. Choe, P. Chatterjee, I. Chatterjee, P.T. Vernier, Nanosecond electric pulses: a novel stimulus for triggering Ca^{2+} influx into chromaffin cells via voltage-gated Ca^{2+} channels, Cell. Mol. Neurobiol. 30 (2010) 1259–1265, https://doi.org/10.1007/s10571-010-9573-1.

[50] W. Li, Q. Fan, Z. Ji, X. Qiu, Z. Li, The effects of irreversible electroporation (IRE) on nerves, PLoS One 6 (2011), e18831. https://doi.org/10.1371/journal.pone.0018831.

[51] G. Onik, P. Mikus, B. Rubinsky, Irreversible electroporation: implications for prostate ablation, Technol. Cancer Res. Treat. 6 (2007) 295–300.

[52] M. Casciola, S. Xiao, A.G. Pakhomov, Damage-free peripheral nerve stimulation by 12-ns pulsed electric field, Sci. Rep. 7 (2017) 10453, https://doi.org/10.1038/s41598-017-10282-5.

[53] H. Schoellnast, S. Monette, P.C. Ezell, A. Deodhar, M. Maybody, J.P. Erinjeri, M.D. Stubblefield, G.W. Single, W.C. Hamilton, S.B. Solomon, Acute and subacute effects of irreversible electroporation on nerves: experimental study in a pig model, Radiology 260 (2011) 421–427, https://doi.org/10.1148/radiol.11103505.

[54] T. Nevian, F. Helmchen, Calcium indicator loading of neurons using single-cell electroporation, Pflugers Arch. - Eur. J. Physiol. 454 (2007) 675–688, https://doi.org/10.1007/s00424-007-0234-2.

[55] V.J.H.M. van Driel, K. Neven, H. van Wessel, A. Vink, P.A.F.M. Doevendans, F.H.M. Wittkampf, Low vulnerability of the right phrenic nerve to electroporation ablation, Heart Rhythm. 12 (2015) 1838–1844, https://doi.org/10.1016/j.hrthm.2015.05.012.

[56] C.B. Arena, R.V. Davalos, Advances in therapeutic electroporation to mitigate muscle contractions, J. Membr. Sci. Technol. 02 (2012) https://doi.org/10.4172/2155-9589. 1000e102.

[57] A. Golberg, B. Rubinsky, Towards electroporation based treatment planning considering electric field induced muscle contractions, Technol. Cancer Res. Treat. 11 (2012) 189–201, https://doi.org/10.7785/tcrt.2012.500249.

[58] D. Miklavčič, G. Pucihar, M. Pavlovec, S. Ribarič, M. Mali, A. Maček-Lebar, M. Petkovšek, J. Nastran, S. Kranjc, M. Čemažar, G. Serša, The effect of high frequency electric pulses on muscle contractions and antitumor efficiency in vivo for a potential use in clinical electrochemotherapy, Bioelectrochemistry 65 (2005) 121–128, https://doi.org/10.1016/j.bioelechem.2004.07.004.

[59] A. Županič, S. Ribarič, D. Miklavčič, Increasing the repetition frequency of electric pulse delivery reduces unpleasant sensations that occur in electrochemotherapy, Neoplasma 54 (2007) 246–250.

[60] C. Ball, K.R. Thomson, H. Kavnoudias, Irreversible electroporation: a new challenge in "out of operating theater" anesthesia, Anesth. Analg. 110 (2010) 1305–1309, https://doi.org/10.1213/ANE.0b013e3181d27b30.

[61] A. Deodhar, T. Dickfeld, G.W. Single, W.C. Hamilton, R.H. Thornton, C.T. Sofocleous, M. Maybody, M. Gónen, B. Rubinsky, S.B. Solomon, Irreversible electroporation near the heart: ventricular arrhythmias can be prevented with ECG synchronization, AJR Am. J. Roentgenol. 196 (2011) W330–335, https://doi.org/10.2214/AJR.10.4490.

[62] B. Mali, V. Gorjup, I. Edhemovic, E. Brecelj, M. Cemazar, G. Sersa, B. Strazisar, D. Miklavcic, T. Jarm, Electrochemotherapy of colorectal liver metastases - an observational study of its effects on the electrocardiogram, Biomed. Eng. Online 14 (2015) S5, https://doi.org/10.1186/1475-925X-14-S3-S5.

[63] B. Mali, T. Jarm, S. Corovic, M.S. Paulin-Kosir, M. Cemazar, G. Sersa, D. Miklavcic, The effect of electroporation pulses on functioning of the heart, Med. Biol. Eng. Comput. 46 (2008) 745–757, https://doi.org/10.1007/s11517-008-0346-7.

[64] N. Jiang, B.Y. Cooper, Frequency-dependent interaction of ultrashort E-fields with nociceptor membranes and proteins, Bioelectromagnetics 32 (2011) 148–163, https://doi.org/10.1002/bem.20620.

[65] D. Nene, N. Jiang, K.K. Rau, M. Richardson, B.Y. Cooper, in: G.T. Shwaery, J.G. Blitch, C. Land (Eds.),Nociceptor activation and damage by pulsed E-fields 2006 p. 621904, https://doi.org/10.1117/12.665181.

[66] C.B. Arena, M.B. Sano, J.H. Rossmeisl, J.L. Caldwell, P.A. Garcia, M. Rylander, R.V. Davalos, High-frequency irreversible electroporation (H-FIRE) for non-thermal ablation without muscle contraction, Biomed. Eng. Online 10 (2011) 102, https://doi.org/10.1186/1475-925X-10-102.

[67] G. Pucihar, J. Krmelj, M. Reberšek, T. Napotnik, D. Miklavčič, Equivalent pulse parameters for electroporation, IEEE Trans. Biomed. Eng. 58 (2011) 3279–3288, https://doi.org/10.1109/TBME.2011.2167232.

[68] D.F. Baxter, M. Kirk, A.F. Garcia, A. Raimondi, M.H. Holmqvist, K.K. Flint, D. Bojanic, P. S. Distefano, R. Curtis, Y. Xie, A novel membrane potential-sensitive fluorescent dye improves cell-based assays for ion channels, J. Biomol. Screen. 7 (2002) 79–85, https://doi.org/10.1177/108705710200700110.

[69] L. Carr, S.M. Bardet, R.C. Burke, D. Arnaud-Cormos, P. Leveque, R.P. O'Connor, Calcium-independent disruption of microtubule dynamics by nanosecond pulsed electric fields in U87 human glioblastoma cells, Sci. Rep. 7 (2017) 41267, https://doi.org/10.1038/srep41267.

[70] D.C. Sweeney, M. Reberšek, J. Dermol, L. Rems, D. Miklavčič, R.V. Davalos, Quantification of cell membrane permeability induced by monopolar and high-frequency bipolar bursts of electrical pulses, Biochim. Biophys. Acta Biomembr. 1858 (2016) 2689–2698, https://doi.org/10.1016/j.bbamem.2016.06.024.

[71] D. Boinagrov, J. Loudin, D. Palanker, Strength-duration relationship for extracellular neural stimulation: numerical and analytical models, J. Neurophysiol. 104 (2010) 2236–2248, https://doi.org/10.1152/jn.00343.2010.

[72] F. Santamaria, J.M. Bower, Hodgkin–Huxley MODELS, Encycl. Neurosci. Elsevier 2009, pp. 1173–1180, https://doi.org/10.1016/B978-008045046-9.01413-3.

[73] T. Kotnik, D. Miklavčič, T. Slivnik, Time course of transmembrane voltage induced by time-varying electric fields—a method for theoretical analysis and its application, Bioelectrochem. Bioenerg. 45 (1998) 3–16, https://doi.org/10.1016/S0302-4598 (97)00093-7.

[74] T. Kotnik, D. Miklavčič, Analytical description of transmembrane voltage induced by electric fields on spheroidal cells, Biophys. J. 79 (2000) 670–679, https://doi.org/10.1016/S0006-3495(00)76325-9.

[75] G. Saulis, M.S. Venslauskas, Cell electroporation, Bioelectrochem. Bioenerg. 32 (1993) 221–235, https://doi.org/10.1016/0302-4598(93)80047-X.

[76] J. Dermol, D. Miklavčič, Predicting electroporation of cells in an inhomogeneous electric field based on mathematical modeling and experimental CHO-cell permeabilization to propidium iodide determination, Bioelectrochemistry 100 (2014) 52–61, https://doi.org/10.1016/j.bioelechem.2014.03.011.

[77] J. Dermol, O.N. Pakhomova, A.G. Pakhomov, D. Miklavčič, Cell electrosensitization exists only in certain electroporation buffers, PLoS One 11 (2016), e0159434. https://doi.org/10.1371/journal.pone.0159434.

[78] I. Goehring, A.A. Gerencser, S. Schmidt, M.D. Brand, H. Mulder, D.G. Nicholls, Plasma membrane potential oscillations in insulin secreting Ins-1 832/13 cells do not require glycolysis and are not initiated by fluctuations in mitochondrial bioenergetics, J. Biol. Chem. 287 (2012) 15706–15717, https://doi.org/10.1074/jbc.m111.314567.

[79] M. Spitzner, J. Ousingsawat, K. Scheidt, K. Kunzelmann, R. Schreiber, Voltage-gated K^+ channels support proliferation of colonic carcinoma cells, FASEB J. 21 (2006) 35–44, https://doi.org/10.1096/fj.06-6200com.

[80] C. Wolff, B. Fuks, P. Chatelain, Comparative study of membrane potential-sensitive fluorescent probes and their use in ion channel screening assays, J. Biomol. Screen. 8 (2003) 533–543, https://doi.org/10.1177/1087057103257806.

[81] P.H. Lalik, D.S. Krafte, W.A. Volberg, R.B. Ciccarelli, Characterization of endogenous sodium channel gene expressed in Chinese hamster ovary cells, Am. J. Phys. 264 (1993) C803–809.

[82] S.P. Yu, G.A. Kerchner, Endogenous voltage-gated potassium channels in human embryonic kidney (HEK293) cells, J. Neurosci. Res. 52 (1998) 612–617, https://doi.org/10.1002/(SICI)1097-4547(19980601)52:5<612::AID-JNR13>3.0.CO;2-3.

[83] R.C. Burke, S.M. Bardet, L. Carr, S. Romanenko, D. Arnaud-Cormos, P. Leveque, R.P. O'Connor, Nanosecond pulsed electric fields depolarize transmembrane potential via voltage-gated K(+), Ca(2+) and TRPM8 channels in U87 glioblastoma cells, Biochim. Biophys. Acta 1859 (2017) 2040–2050, https://doi.org/10.1016/j.bbamem.2017.07.004.

[84] R. Susil, D. Šemrov, D. Miklavčič, Electric field induced transmembrane potential depends on cell density and organization, Electro- Magnetobiol. 17 (1998) 391–399.

[85] N. Brunel, M.C.W. van Rossum, Quantitative investigations of electrical nerve excitation treated as polarization. Louis Lapicque 1907, Biol. Cybern. 97 (2007) 341–349, https://doi.org/10.1007/s00422-007-0189-6.

[86] W.R. Rogers, J.H. Merritt, J.A. Comeaux, C.T. Kuhnel, D.F. Moreland, D.G. Teltschik, J.H. Lucas, M.R. Murphy, Strength-duration curve for an electrically excitable tissue extended down to near 1 nanosecond, IEEE Trans. Plasma Sci. 32 (2004) 1587–1599, https://doi.org/10.1109/TPS.2004.831758.

[87] D. Moreau, C. Lefort, J. Pas, S.M. Bardet, P. Leveque, R.P. O'Connor, Infrared neural stimulation induces intracellular Ca(2+) release mediated by phospholipase C, J. Biophotonics (2017) https://doi.org/10.1002/jbio.201700020.

[88] M. Levin, C.G. Stevenson, Regulation of cell behavior and tissue patterning by bioelectrical signals: challenges and opportunities for biomedical engineering, Annu. Rev. Biomed. Eng. 14 (2012) 295–323, https://doi.org/10.1146/annurev-bioeng-071811-150114.

[89] B. Mercadal, C.B. Arena, R.V. Davalos, A. Ivorra, Avoiding nerve stimulation in irreversible electroporation: a numerical modeling study, Phys. Med. Biol. (2017) https://doi.org/10.1088/1361-6560/aa8c53.

[90] R. Fairless, A. Beck, M. Kravchenko, S.K. Williams, U. Wissenbach, R. Diem, A. Cavalié, Membrane potential measurements of isolated neurons using a voltage-sensitive dye, PLoS One 8 (2013), e58260. https://doi.org/10.1371/journal.pone.0058260.

[91] M.P. Rols, C. Delteil, M. Golzio, J. Teissié, Control by ATP and ADP of voltage-induced mammalian-cell-membrane permeabilization, gene transfer and resulting expression, Eur. J. Biochem. 254 (1998) 382–388 FEBS.

[92] W. Chen, Z. Zhongsheng, R.C. Lee, Supramembrane potential-induced electroconformational changes in sodium channel proteins: a potential mechanism involved in electric injury, Burns J. Int. Soc. Burn Inj. 32 (2006) 52–59, https://doi.org/10.1016/j.burns.2005.08.008.

[93] A. Azan, V. Untereiner, L. Descamps, C. Merla, C. Gobinet, M. Breton, O. Piot, L.M. Mir, Comprehensive characterization of the interaction between pulsed electric fields and live cells by confocal Raman microspectroscopy, Anal. Chem. 89 (2017) 10790–10797, https://doi.org/10.1021/acs.analchem.7b02079.

[94] T.G. Banke, S.R. Chaplan, A.D. Wickenden, Dynamic changes in the TRPA1 selectivity filter lead to progressive but reversible pore dilation, AJP Cell Physiol. 298 (2010) C1457–C1468, https://doi.org/10.1152/ajpcell.00489.2009.

[95] A.G. Pakhomov, I. Semenov, M. Casciola, S. Xiao, Neuronal excitation and permeabilization by 200-ns pulsed electric field: an optical membrane potential study with FluoVolt dye, Biochim. Biophys. Acta Biomembr. 1859 (2017) 1273–1281, https://doi.org/10.1016/j.bbamem.2017.04.016.

[96] G. Pucihar, T. Kotnik, J. Teissié, D. Miklavčič, Electropermeabilization of dense cell suspensions, Eur. Biophys. J. 36 (2007) 172–185.

[97] T.H. Hui, Z.L. Zhou, H.W. Fong, R.K.C. Ngan, T.Y. Lee, J.S.K. Au, A.H.W. Ngan, T.T.C. Yip, Y. Lin, Characterizing the malignancy and drug resistance of cancer cells from their membrane resealing response, Sci. Rep. 6 (2016) 26692, https://doi.org/10.1038/srep26692.

[98] M. Čemažar, T. Jarm, D. Miklavčič, A. Maček Lebar, A. Ihan, N.A. Kopitar, G. Serša, Effect of electric-field intensity on electropermeabilization and electrosensitivity of various tumor-cell lines in vitro, Electro- Magnetobiol. 17 (1998) 263–272.

Paper 4

Title: **Cell Electrosensitization Exists Only in Certain Electroporation Buffers**

Authors: Janja Dermol, Olga N. Pakhomova, Andrei G. Pakhomov and Damijan Miklavčič

Publication: *PLoS One*, vol. 11, no. 7, p. e0159434, Jul. 2016.

DOI: 10.1371/journal.pone.0159434

Impact factor: 2.806 (2016), 3.394 (5-year)

Quartile: Q1 (Multidisciplinary Sciences)

Rank: 15/64 (Multidisciplinary Sciences)

PLOS | ONE

RESEARCH ARTICLE

Cell Electrosensitization Exists Only in Certain Electroporation Buffers

Janja Dermol[1], Olga N. Pakhomova[2], Andrei G. Pakhomov[2], Damijan Miklavčič[1] *

1 Faculty of Electrical Engineering, University of Ljubljana, Ljubljana, Slovenia, **2** Frank Reidy Research Center for Bioelectrics, Old Dominion University, Norfolk, Virginia, United States of America

* Damijan.miklavcic@fe.uni-lj.si

Abstract

Electroporation-induced cell sensitization was described as the occurrence of a delayed hypersensitivity to electric pulses caused by pretreating cells with electric pulses. It was achieved by increasing the duration of the electroporation treatment at the same cumulative energy input. It could be exploited in electroporation-based treatments such as electrochemotherapy and tissue ablation with irreversible electroporation. The mechanisms responsible for cell sensitization, however, have not yet been identified. We investigated cell sensitization dynamics in five different electroporation buffers. We split a pulse train into two trains varying the delay between them and measured the propidium uptake by fluorescence microscopy. By fitting the first-order model to the experimental results, we determined the uptake due to each train (i.e. the first and the second) and the corresponding resealing constant. Cell sensitization was observed in the growth medium but not in other tested buffers. The effect of pulse repetition frequency, cell size change, cytoskeleton disruption and calcium influx do not adequately explain cell sensitization. Based on our results, we can conclude that cell sensitization is a sum of several processes and is buffer dependent. Further research is needed to determine its generality and to identify underlying mechanisms.

Introduction

Electroporation is a phenomenon resulting in a transient increase in membrane permeability, which occurs when short high voltage pulses are applied to cells and tissues [1,2]. If cells can recover, we consider this reversible electroporation. If the damage is too extensive and they die, we consider this irreversible electroporation (IRE). Electroporation is used in medicine, e.g. electrochemotherapy (ECT) [3–6], non-thermal IRE as a method of tissue ablation [7–9], gene therapy [10,11], DNA vaccination [12,13] and transdermal drug delivery [14–16], as well as in biotechnology [17], and food processing [18–20].

For tumor eradication, ECT, IRE, and gene therapy are successfully used. However, it was shown that electroporation of tumors larger than 2 cm in diameter is not as successful as of smaller tumors [21]. When treating tumors with IRE, a high number of pulses is delivered, which can cause significant Joule heating and thermal damage and complicate the treatment [22,23]. Provided the effect of the electric pulses be enhanced, we can treat larger tumors with

116

fewer pulses of lower voltage. Pulse effect amplification can be achieved using molecules that enhance cell sensitivity to electric pulses, e.g. DMSO or surfactant $C_{12}E_8$ [8].

Lately, several reports on a so-called phenomenon of cell sensitization have been published [24–29]. By increasing the duration of an electroporation treatment (e.g. by decreasing the pulse repetition frequency or by splitting the delivered pulse train in more trains with delays between them), a decrease in cell viability and a much higher uptake of molecules were achieved. When applying conventional 100 µs pulses, 5 minute delay between the two trains was suggested [25], but also shorter delays led to cell sensitization [27,30]. Cell sensitization has been observed as decreased membrane integrity, increased mass transport across the membrane, and decreased cell viability. Similarly as with square pulses, it has been shown that exposing cells to AC electric fields increased their sensitivity to subsequent millisecond square pulses [31].

Cell sensitization could be beneficially used in the electroporation-based treatments. It is possible that it is already influencing the outcome of the IRE and the ECT. Namely, in the IRE, 90 pulses synchronized with a heartbeat are delivered between each pair of electrodes [8]. Usually, four electrodes are inserted, and IRE can last up to 9 minutes (four electrodes equals six pairs, 6x90 pulses at around 1 Hz take 9 minutes). In ECT, eight pulses at 1 Hz or 5 kHz are applied [32]. When using hexagonal electrodes, pulses are effectively delivered between 7 electrodes (12 pairs) [33]. Between each electrode pair, four pulses are delivered, and the procedure is repeated with four pulses of reverse polarity (twelve pairs, 8x12 pulses at around 1 Hz take 1.5 minute). If we consider the switching time [34], both treatments already fall within the time range for cell sensitization. The mechanisms of the delayed cell sensitization are not yet known. The proposed mechanisms are: 1) calcium uptake [24,25], 2) ATP leakage [24,25], 3) reactive oxygen species formation [24,25], 4) cell swelling [24,25], 5) cytoskeleton disruption [28], 6) reduced pore edge line tension which lowers the electroporation threshold [26,27], 7) extended pore opening times [26,27], and 8) the decrease of high conductance membrane state which allows for the creation of additional defects [35].

We would like to emphasize the difference in the definition of the cell sensitization in the already published studies and our paper. So far, cell sensitization has been defined as an increase in total molecular uptake or decrease in cell survival after applying a split dose as opposed to a single dose. The contribution of separate pulse trains to the final uptake and survival has not been investigated although, in our opinion, it is very important for the applicability of cell sensitization. When applying a single dose, we can reach saturation in mass transport [36,37]. Pulses at the end of the train contribute to the uptake less than pulses at the beginning [35,38]. With splitting the dose in half, we avoid saturation which is then mistakenly regarded as cell sensitization although cells respond to the first and the second pulse train in a similar way. In our experiments, we distinguished contributions of the first and the second pulse train. We considered the cells sensitized when the uptake due to the second pulse train was higher than the uptake due to the first train, irrespective of the final fluorescence level.

In preliminary experiments, we tested cell sensitization in a standard low-conductivity electroporation buffer. Surprisingly, splitting the dose in half lowered the final fluorescence. We were intrigued and decided to test propidium uptake in the growth medium, where cell sensitization has been previously observed [24,25,27]. There, splitting the dose in half increased the final fluorescence. We repeated experiments in three more electroporation buffers to investigate the effect of electrical conductivity, calcium influx, and sucrose concentration; splitting the dose in half again did not increase the final propidium uptake. Then, we analyzed the contributions of the separate pulse trains to the final fluorescence. The response of cells to pulse splitting in different electroporation buffers was complex and varied among others in the increased or decreased sensitivity to the second pulse train, in the resealing speed, and in the efficiency of

split versus single dose. Although cell sensitization has already been defined as a phenomenon and models have been constructed describing it [39], further research is needed to determine its generality and the involved mechanisms.

Materials and Methods

Cell preparation

Chinese hamster ovary cells (European Collection of Authenticated Cell Cultures ECACC, cells CHO-K1, cat. no. 85051005, obtained directly from the repository) were grown in 25 cm^2 culture flasks (TPP, Switzerland) for 2–3 days in an incubator (Kambič, Slovenia) at 37°C and humidified 5% CO_2 in HAM-F12 growth medium (PAA, Austria). The growth medium was supplemented with 10% fetal bovine serum (Sigma-Aldrich, Germany), L-glutamine (StemCell, Canada) and antibiotics penicillin/streptomycin (PAA, Austria) and gentamycin (Sigma-Aldrich, Germany). On the day of the experiments, the cell suspension was prepared. Cells were detached by 2.5 ml of 10x trypsin-EDTA (PAA, Austria), diluted 1:9 in Hank's basal salt solution (StemCell, Canada). After 1.5 minute the trypsin was inactivated by 2.5 ml of the growth medium. Cells were transferred to 50 ml centrifuge tube and centrifuged 5 minutes at 180g and 24°C. Then, cells were resuspended in the growth medium at 6x10^4 cells/ml. 500 μl of cell suspension was added per well in 24-well plate. The plates were moved to the incubator for 15–40 minutes until cells attached to the bottom of the well but maintained their spherical shape [40].

Before the experiments, cells were washed with a fresh electroporation buffer and 500 μl of the new electroporation buffer was added to each well. For fluorescence measurements, the electroporation buffer included 150 μM propidium iodide (Life Technologies, USA). The composition of the tested electroporation buffers is given in Table 1. The electrical conductivity was measured with conductometers MA 5959 (Metrel, Slovenia) or S230 SevenCompact (Mettler Toledo, Switzerland) at 37°C and the osmolality by freezing point depression with Knauer cryoscopic unit (model 7312400000, Knauer, Germany). $MgCl_2$, NaCl, K_2HPO_4, $CaCl_2$, HEPES, and sucrose were from Sigma-Aldrich, Germany, and KH_2PO_4 from Merck, Germany

Electroporation and image acquisition

We used Pt/Ir wire electrodes with 0.8 mm diameter and 4 mm inter-electrode distance positioned at the bottom of the plate as shown in Fig 1. The plate was put under the microscope with a heated stage (37°C). Square pulses (300V or 0.75 kV/cm, 100 μs, 10 Hz) were applied using the βtech electroporator (Electro cell B10, Betatech, France) and monitored with an oscilloscope WaveSurfer 422, 200 MHz and a current probe AP015 (Teledyne LeCroy, Chestnut

Table 1. Composition of electroporation buffers.

| Electroporation buffer	Composition	Electrical conductivity [mS/cm]	Osmolality [mOsm/kg]
The growth medium HAM-F12	Inorganic salts, amino acids, vitamins and other components (PAA Austria, cat. no. E15-016), 10% fetal bovine serum, L-glutamine, and antibiotics	17.14	260–320 (based on the producer's data sheet)
The low-conductivity buffer	10 mM KH_2PO_4/K_2HPO_4 in ratio 40.5:9.5, 1 mM $MgCl_2$, 250 mM sucrose	1.78	292
The hyperosmotic buffer	10 mM KH_2PO_4/K_2HPO_4, 1 mM $MgCl_2$, 400 mM sucrose	1.76	475
The high-conductivity buffer	10 mM KH_2PO_4/K_2HPO_4 in ratio 40.5:9.5, 1 mM $MgCl_2$, 150 mM NaCl	19.12	300
The buffer with calcium	10 mM HEPES, 250 mM sucrose, 0.7 mM $MgCl_2$, 0.3 mM $CaCl_2$	0.38	281

118
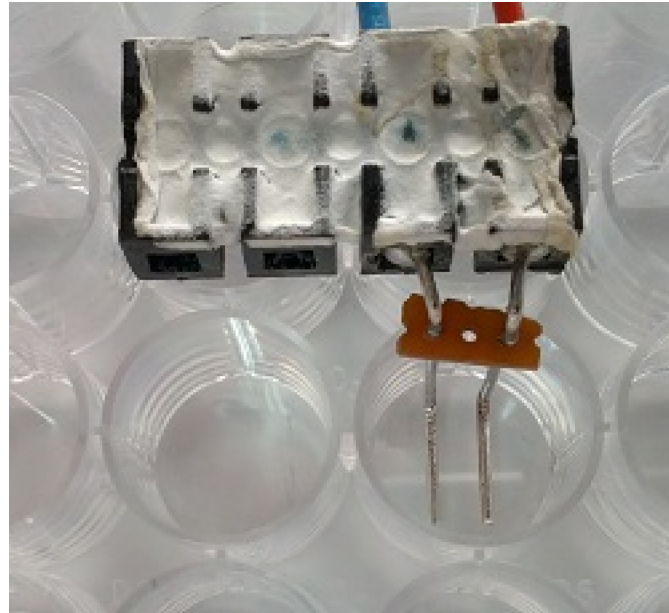
Fig 1. Photo of the electrodes attached to the bottom of the 24-well plate. The plate was put under a microscope. The images were acquired from between the electrodes where the electric field was approximately homogeneous and could be calculated as the ratio of the applied voltage and inter-electrode distance.

Ridge, NY). In fluorescence measurements, we exposed cells to either half dose (four 100 μs pulses), single dose (eight 100 μs pulses) or split dose (4+4, 100 μs pulses with 1, 2 or 3 minute delay) (Fig 2). In the cell size measurements, we exposed cells only to the half dose (four 100 μs pulses). 300 V was chosen based on the preliminary experiments, where most of the cells were permeabilized, but the survival was not affected. 3 minutes was chosen as the delay that produced cell sensitization in other studies [30] and where the measured final fluorescence value of the split dose was higher (the growth medium) or lower (the low-conductivity buffer) than of the single dose.

Cells were observed by the inverted microscope AxioVert 200 (Zeiss, Germany) under 20x objective for fluorescence (535 nm excitation, 617 nm emission) and 40x for cell size measurements. Images were acquired using the VisiCam 1280 camera (Visitron, Germany) and the MetaMorph PC software (Molecular Devices, USA) in a time lapse: one image every 8 or 10 s for 8 minutes (fluorescence measurements) or 2 s for 3 minutes (cell size measurements). We chose a field of view in the middle between the electrodes where the electric field distribution was approximately homogeneous, and electric field was calculated as a ratio of the applied voltage to inter-electrode distance [41]. The numbers of the experiments and the analyzed cells for each protocol are shown in Table 2. The exposure time in fluorescence measurements was different across tested buffers, and the absolute values of fluorescence should not be directly compared.

Images were analyzed using the ImageJ software (http://imagej.nih.gov/ij/). On fluorescent images, each cell was manually outlined, and its average fluorescence intensity through the whole stack was automatically measured. Fluorescence intensity before the pulse application was subtracted to compensate for the background fluorescence. In preliminary experiments, it was determined that in all tested buffers, there was no measurable spontaneous propidium uptake on the same time scale without applying electric pulses. For cell size measurements, the threshold was applied to the bright-field images, cells were automatically outlined, and their
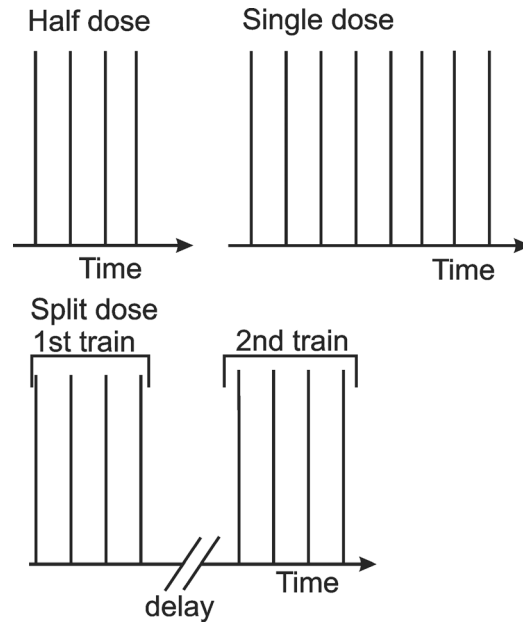
119

Fig 2. Scheme of the used protocols. In the half dose, four 100 μs pulses, and in the single dose, eight 100 μs pulses were applied. In the split dose, two trains of four 100 μs pulses were applied and the delay between the end of the first and the beginning of the second train was 1, 2 or 3 min. In all experiments, 300 V or 0.75 kV/cm were applied. The repetition frequency was 10 Hz.

doi:10.1371/journal.pone.0159434.g002

area in each image was measured. The measured area was normalized to the size of the area before pulse application to determine a relative change in the cross-section. In each time step, the average value and the standard error were determined.

Table 2. Number of experiments and analyzed cells in each experiment.

Type of experiment			No. of experiments	No. of analyzed cells
Fluorescence measurement	The growth medium	4 pulses	3	19
		8 pulses	5	34
		4+4 pulses, 1 min delay	6	31
		4+4 pulses, 2 min delay	6	37
		4+4 pulses, 3 min delay	7	40
	The low-conductivity buffer	4 pulses	5	34
		8 pulses	6	45
		4+4 pulses, 1 min delay	6	38
		4+4 pulses, 2 min delay	8	55
		4+4 pulses, 3 min delay	7	48
	The hyperosmotic buffer	4 pulses	4	21
		8 pulses	3	20
		4+4 pulses, 3 min delay	4	23
	The high-conductivity buffer	8 pulses	3	24
		4+4 pulses, 3 min delay	3	23
	The buffer with calcium	8 pulses	3	21
		4+4 pulses, 3 min delay	3	25
Cell size measurement	The growth medium		4	19
	The low-conductivity buffer		7	25

doi:10.1371/journal.pone.0159434.t002

120

The model fitting

The quantitative results of the uptake were acquired by fitting a first-order model [42]:

$$f(t) = C\left(1 - \exp\left(-\frac{t}{\tau}\right)\right) \qquad (1)$$

to the experimental results using the Curve fitting toolbox and Matlab R2011b (Mathworks, USA). S signifies the plateau of the fluorescence; τ is the relaxation time of propidium uptake when the cells reach 63% of the final fluorescence. The time course of propidium uptake reflects the resealing process of the membrane and τ can also be understood as a resealing constant [42]. The derivation is in the S1 Appendix.

The model:

$$f(t) = S_1\left(1 - \exp\left(-\frac{t}{\tau_1}\right)\right) + S_2\left(1 - \exp\left(-\frac{t - t_{delay}}{\tau_2}\right)\right) * \left(t > t_{delay}\right) + kt \qquad (2)$$

was fitted to the split dose results. Parameter t_{delay} is the inter-train delay, k is the slope of the linear part of the propidium uptake. An example of the fitted curve and the parameters is shown in Fig 3. The first order kinetics model described the majority of our data sufficiently well ($R^2 > 0.97$), but it predicted that after the exponential closing of the pores the transport will stop, and the fluorescence will not increase. In our experimental results, the shape of the propidium uptake curves indicated that there was an additional process present that caused the linear uptake. We modeled it with a linear uptake process ('kt') which we assumed present from the beginning of the treatment. Since we do not know what exactly caused the linear uptake, it seemed inappropriate to ascribe it only to one of the trains.

We fitted Eq 1 to the half and the single dose and Eq 2 to the split dose results. The optimal values of the parameters and the R^2 (the coefficient of determination) value are presented in Table 3. In the split dose protocols, we normalized the S_2 and τ_2 values to the average S_1 or τ_1 value in the same buffer (unless stated differently in Table 3). If $S_2/S_1 > 1$, cells were assumed sensitized, if $S_2/S_1 < 1$, they were assumed desensitized, and if $S_2/S_1 \approx 1$ the trains were assumed equally effective. Ratio τ_2/τ_1 gave information whether the resealing after the second train was faster ($\tau_2/\tau_1 < 1$) or slower ($\tau_2/\tau_1 > 1$) than after the first train or similar to the first train ($\tau_2/\tau_1 \approx 1$). The values of parameters S_1 and τ_1 should be the same for all first trains (half and split dose) in each buffer. The difference in their values was due to the biological variability and the

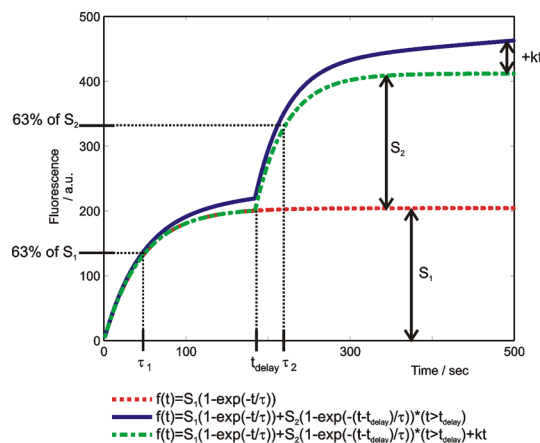**Fig 3. An example of fitted first-order models to the results of propidium uptake in the growth medium.** Meaning of S_1, S_2, τ_1 τ_2, t_{delay} and the increase due to 'kt' are shown.

doi:10.1371/journal.pone.0159434.g003

121

Table 3. The optimal values of parameters and the R^2 of fitted Eqs 1 and 2. A–The growth medium, B–the low-conductivity buffer, C–the hyperosmotic buffer, D–the high-conductivity buffer, E–the buffer with calcium. Values in bold and the symbol next to them emphasize if the cells were desensitized (S_2/average(S_1)<1, symbol ↓), sensitized (S_2/average(S_1)>1, symbol ↑) or if the trains were equally effective (S_2/average(S_1)≈1, symbol ≈). The numbers after ± sign define 95% confidence interval. The graphical representation of S_2/average(S_1) and τ_2/average(τ_1), based on experimental uptake results in Fig 4, is in Fig 5.

A–The growth medium

	Half dose	Single dose	1 min delay	2 min delay	3 min delay
S_1	215.5 ± 7.5	354.8 ± 9.9	179.6 ± 14.2	197.4 ± 17.2	204.2 ± 8.2
S_2	/	/	265.9± 13.9	226.9 ± 12.5	207.6 ± 8.8
τ_1	65.91 ± 4.17	63.45± 3.33	44.02± 6.16	69.47± 10.07	46.13 ± 3.44
τ_2	/	/	48.37 ± 1.58	47.01± 3.25	37.76 ± 2.98
k	0.06664 ± 0.02	0.06825 ± 0.0267	0.1831 ± 0.0124	0.1234 ± 0.0339	0.1024 ± 0.0372
S_2/average(S_1)	/	/	**1.34 ± 0.18 ↑**	**1.14 ± 0.15↑**	**1.04 ± 0.13≈**
τ_2/average(τ_1)	/	/	0.86 ± 0.20	0.83 ± 0.20	0.67 ± 0.16
R^2	0.9954	0.9961	0.9998	0.9993	0.9991

B–The low-conductivity buffer

	Half dose	Single dose	1 min delay	2 min delay	3 min delay
S_1	516.9 ± 3.9	965.7 ± 1.7	516.9 ± 3.9[a]	516.9 ± 3.9[a]	445.4 ± 19.4
S_2	/	/	413.1 ± 4.9	269 ± 12.4	229.2 ± 10.7
τ_1	91.6 ± 2.66	82.78 ± 0.6	91.6 ± 2.66[a]	91.6 ± 2.66[a]	86.7 ± 4.97
τ_2	/	/	51.58 ± 3.15	65.11 ± 3.40	44.95 ± 3.65
k	0	0	0	0.0985 ± 0.0293	0.1512 ± 0.0556
S_2/average(S_1)	/	/	**0.86 ± 0.04 ↓**	**0.56 ± 0.03↓**	**0.48 ± 0.03↓**
τ_2/average(τ_1)	/	/	0.58 ± 0.05	0.73 ± 0.06	0.50 ± 0.05
R^2	0.9962	0.9997	0.9980	0.9994	0.9996

C–The hyperosmotic buffer

	Half dose	Single dose	3 min delay
S_1	191 ± 2.4	387.7 ± 4.5	155.8 ± 27.3
S_2	/	/	86.76 ± 10.28
τ_1	161.1 ± 5.3	117.8 ± 4.5	124.8 ± 21.2
τ_2	/	/	69.63 ± 12.46
k	0	0	0.01741 ± 0.0662
S_2/average(S_1)	/	/	**0.50 ± 0.08 ↓**
τ_2/average(τ_1)	/	/	0.49 ± 0.10
R^2	0.9977	0.9958	0.9992

D–The high-conductivity buffer

	Single dose	3 min delay
S_1	681.2 ± 9.1	369.8 ± 31.4
S_2	/	379.8 ± 8.6
τ_1	57.54 ± 1.54	122.2 ± 11.7
τ_2	/	36.68 ± 1.34
k	0.4366 ± 0.0255	0.2719 ± 0.0623
S_2/average(S_1)	/	**1.03 ± 0.09 ≈**
τ_2/average(τ_1)	/	0.30 ± 0.10
R^2	0.9992	0.9999

E–The buffer with calcium

	Single dose[b]	3 min delay
S_1	1129 ± 432	365.6 ± 22.4
S_2	/	386.1 ± 22
τ_1	144 ± 55.9	79.36 ± 11

(Continued)

122

Table 3. (*Continued*)

τ_2	/	69.86 ± 5.54
k	0	0
S_2/average(S_1)	/	**1.06 ± 0.88 ≈**
τ_2/average(τ_1)	/	0.88 ± 0.14
R^2	0.9705	0.9974

[a] The values for the S_1 and τ_1 were taken from the results of fitting Eq 2 to the results of the half dose (2nd column) where the plateau of fluorescence was already reached, and the first order shape was clear.

[b] Here, the first order model was not appropriate since the 95% confidence interval was very large. These parameters do not influence the results of the analysis since the ratios were not calculated from the single dose parameters.

doi:10.1371/journal.pone.0159434.t003

error of curve fitting. The error of curve fitting was more noticeable if the delay between two pulse trains was short and the first-order shape of the uptake curve was not very clear. Therefore, in order to decrease the error we presented results by normalizing the S_2 and τ_2 to the average values of S_1 and τ_1 for each buffer separately. In the cell (de)sensitization definition, 'kt' was not included, since we assumed this additional process present from the beginning of the measurement.

Results

First, experiments were performed with a fixed inter-train delay (3 min) in five electroporation buffers. Results are presented in Cell sensitization in different buffers section. Second, different inter-train delays were tested in the growth medium and the low-conductivity buffer. These two buffers were chosen as a representative for the cell sensitization and cell desensitization effect. Results are presented in Cell sensitization with different delays section. The time dynamics of propidium uptake in the growth medium, the low-conductivity, the hyperosmotic, the high-conductivity buffer, and the buffer with calcium are shown in Fig 4A, 4B, 4C, 4D and 4E, respectively. The observations on higher or lower uptake as a response to the first or second train are based on fitting Eqs 1 and 2 to the experimental results. One of the fitted curves is plotted in Fig 3 where the parameters S_1, S_2, t_{delay}, τ_1, and τ_2 are shown. In Table 3, the optimal values of parameters and the calculated ratios of S_2/S_1 and τ_2/τ_1 are presented. If $S_2/S_1 > 1$, cells were assumed sensitized, if $S_2/S_1 < 1$, they were assumed desensitized, and if $S_2/S_1 \approx 1$ the trains were assumed equally effective. The final level of fluorescence was irrelevant in our definition of cell sensitization. In Fig 5A, there is the graphical representation of the ratios in the growth medium, the low-conductivity, the hyperosmotic, the high-conductivity buffer, and the buffer with calcium at fixed 3 minute inter-train delay. In Fig 5B, ratios for the growth medium, and in Fig 5C for the low-conductivity buffer at different delays are shown.

Cell sensitization in different buffers

In the growth medium, the total uptake after a split dose protocol (i.e. 4+4 pulses) was higher than after a single dose protocol (i.e. eight pulses) at 1 minute delay (Fig 4A). The second train contributed more to the total fluorescence (Fig 5A), i.e. cell sensitization was present. The value of k was similar for the single and the half dose, but it was much higher for the split dose. There was a gradual uptake of propidium even 8 minutes after the pulses ($k > 0$).

In the low-conductivity buffer, the split dose protocol resulted in lower final fluorescence than the single dose protocol (Fig 4B). In the split dose protocol, the uptake due to the second train was lower than due to the first train (Fig 5A), i.e. cell sensitization was not present. On
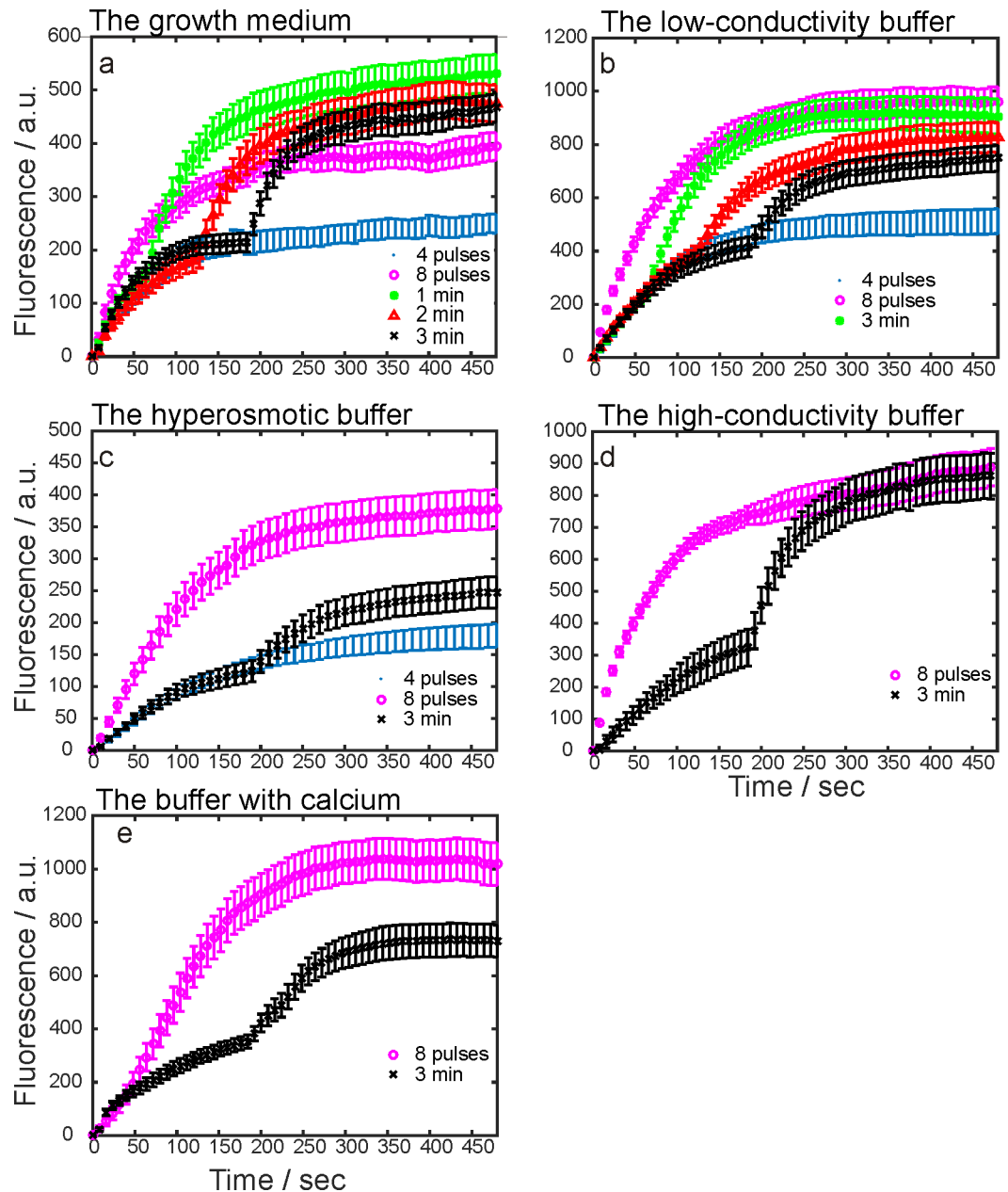
123

Fig 4. Measured fluorescence due to the propidium uptake in the growth medium and four different electroporation buffers. Propidium uptake was detected by fluorescence microscopy. On the *y*-axis, there are the average experimental values in arbitrary units ± standard error. On the *x*-axis, there is the time in seconds. (a), the growth medium; (b), the low-conductivity; (c) the hyperosmotic; (d), the high-conductivity buffer, (e) the buffer with calcium. The exposure times were different among the electroporation buffers.

doi:10.1371/journal.pone.0159434.g004

the contrary, cell desensitization was present. The value of k was 0 for single, half dose and 1 minute delay.

In the hyperosmotic buffer, the cells were exposed to half, single and split dose with 3 minute delay ([Fig 4C](#)). The split dose was less effective than the single dose. The uptake due to the second pulse train was lower than the uptake due to the first train ([Fig 5C](#)), i.e. cell desensitization was present. The parameter k was more than 0 only in the split dose protocol, and it was
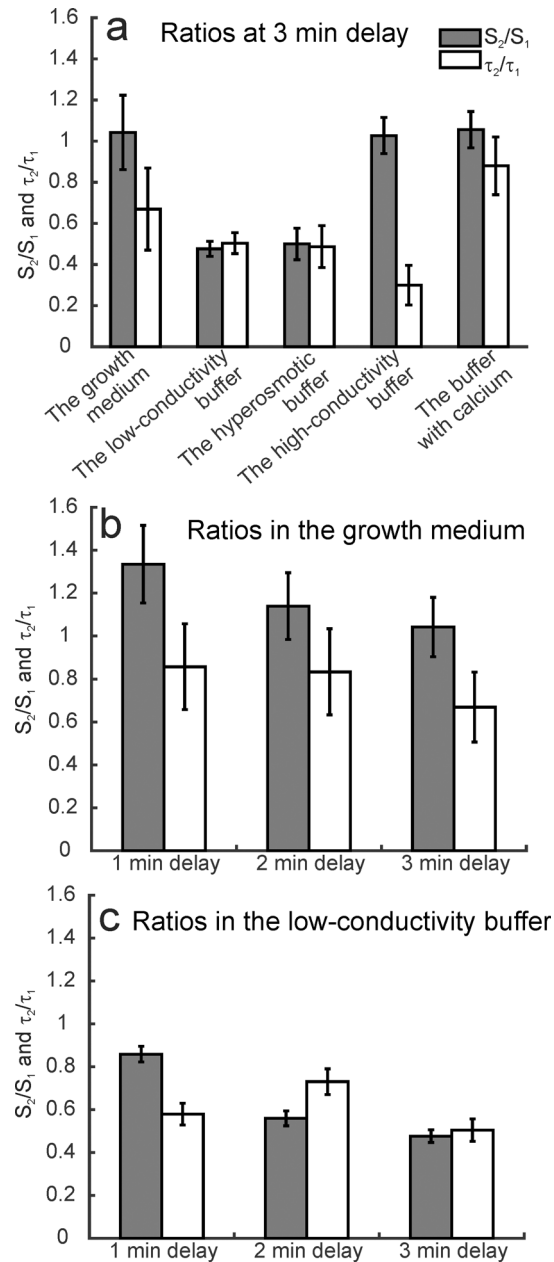
Fig 5. Graphical representation of the ratio of parameters S_2/S_1 and τ_2/τ_1. A first order model (Eqs 1 and 2) was fitted to the experimental results. S_2 and τ_2 were normalized to the average value of S_1 or τ_1, calculated from parameters of the half dose and the split doses with different delays. (a) The ratios at 3 minute delay between the trains in all buffers. (b) The ratios in the growth medium at 1, 2 or 3 minute delay. (c) The ratios in the low-conductivity buffer at 1, 2 and 3 minute delay. The bars at 3 minute delay in (b) and (c) represent the same results as the growth medium and the low-conductivity buffer bars in (c) to enable easier comparison of the ratios between the buffers. Error bars represent the 95% confidence interval.

doi:10.1371/journal.pone.0159434.g005

10-times smaller than in the low-conductivity buffer (the same exposure time allows us to make the comparison).

In the high-conductivity buffer, the cells were exposed to the single and split dose with 3 minute delay (Fig 4D). The uptake due to the second train was similar to the uptake due to the first train (Fig 5C), i.e. cell sensitization was not present. The uptake due to the split dose was
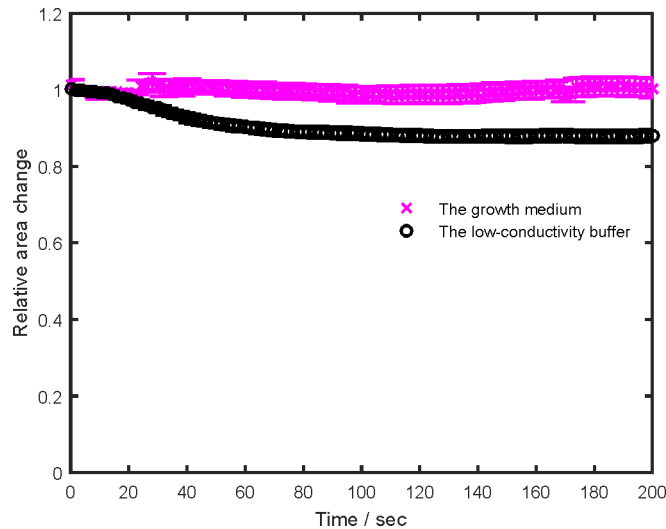
Fig 6. Cell size change dynamics in the growth medium and the low-conductivity buffer. Symbols denote the average ± standard error. The relative change was determined as a ratio of the cell cross-section after and before the pulses. The upper magenta curve–the growth medium; the lower black curve–the low-conductivity buffer.

doi:10.1371/journal.pone.0159434.g006

twice the uptake due to the half dose (determined by extrapolation). The k after the single dose was higher than after the split dose.

In the buffer with added calcium, the final uptake due to the single dose was higher than due to the split dose ([Fig 4E](#)). However, the uptake due to the second train was similar to the uptake due to the first train, i.e. cell sensitization was not present ([Fig 5A](#)). The value of k was 0 for the split and single dose.

The values of τ after the second pulse train were lower than after the first pulse train in the growth medium and all electroporation buffers, i.e. the resealing after the second pulse train was faster than after the first train ([Table 3](#)). The values of τ after the first train were the lowest in the growth medium (44–69 s^{-1}) and then they increased in the order: the buffer with added calcium (69–79 s^{-1}), the low-conductivity (86–91 s^{-1}), the high-conductivity (122 s^{-1}), and the hyperosmotic buffer (124–161 s^{-1}).

In the growth medium and the low-conductivity buffer, we also determined the cell size change after four 100 μs pulses (the half dose) ([Fig 6](#)). Cell size change was proposed as a possible mechanism of cell sensitization [24]. In the growth medium, the cell cross-section did not change much. In the low-conductivity buffer, it decreased. In the low-conductivity buffer, the dynamics of cell size change was different from the dynamics of the fluorescence change due to the second train ([Fig 4C](#)). The uptake due to the second train was lower at 3 than at 2 minute delay while the cell cross-section did not change from the first minute until the end of the measurement.

Cell sensitization with different delays

In the growth medium and the low-conductivity buffer, additional experiments with 1 and 2 minutes delay between the trains were performed ([Fig 4A and 4B](#)). In the growth medium, the cell sensitization decreased with increasing inter-train delay ([Fig 5B](#)). At 3 minute delay, there was no cell sensitization; the fluorescence was a sum of the separate contributions of the pulse trains. The parameter k decreased with an increasing inter-train delay as well. In the low-conductivity buffer, we observed cell 'desensitization' ($S_2/S_1 < 1$) which increased with increasing delay. The value of k was zero for single, half dose, and 1 minute delay.

126

Discussion

Cell sensitization was not present in all tested electroporation buffers as determined by the propidium uptake measurements. In the growth medium, the split dose was more efficient than the single dose at all delays, but the cells were sensitized by the first train only at 1 min. In other buffers, the split dose was similarly (the high-conductivity buffer, and the buffer with calcium), or less effective (the low-conductivity, and the hyperosmotic buffer) than the single dose. In these buffers, thus cell sensitization was not present. After pulse application, different processes are triggered in the cells or on their membranes. These processes apparently depend also on the electroporation buffer composition and influence the response of the cells to the electric pulses. The sum of these processes determines whether the cells will be sensitized, desensitized or the trains will be equally effective. In our study, if $S_2/S_1>1$, cells were assumed sensitized, if $S_2/S_1<1$, they were assumed desensitized, and if $S_2/S_1\approx1$ the trains were assumed equally effective. Cell sensitization, assessed by the uptake of different molecules or by survival after a single or a split dose protocol, was observed when applying pulses in the growth medium [24,25,28,30], in electroporation buffers [24,25,43], in three-dimensional cell cultures [29], and *in vivo* [26,27]. Our results in the growth medium are in agreement with them, but the results in the other buffers are not.

With our definition of cell sensitization (higher uptake due to the second than due to the first pulse train), the sensitizing effect was observed only at 1 minute delay in the growth medium (Fig 5B). However, the final level of fluorescence in the growth medium was still higher when applying the split dose than when the single dose with all delays tested (1, 2 or 3 min). In previously published studies, the higher final fluorescence of the split than of the single dose was already considered cell sensitization. There, cells were assumed sensitized if the split dose caused higher uptake or lower survival than the single dose. With their definition, in our experiments in the growth medium, all delays would be considered as cell sensitizing although the second pulse train did not cause higher uptake than the first pulse train, i.e. the cells were not sensitized during the inter-train delay.

Pulse splitting in different buffers

In the growth medium, cell sensitization was present, and the split dose was more effective (Figs 4A and 5A) than the single dose. The reason could be higher membrane damage due to the first pulse train than in other tested buffers which rendered cells more sensitive to the subsequent pulses. With increasing delay, the damage was repaired, and cell sensitization ceased. In other studies [24–27,30], the cell sensitization was present at longer delays. The possible explanations are: 1) They assessed cell sensitization as the efficiency of the split *vs* single dose. In our experiments, the final value of the fluorescence was higher when applying the split dose, although separate contributions to the final fluorescence of the two trains were equal. 2) They damaged the membrane more by applying more pulses of higher electric field. Since higher electric fields cause higher cell sensitization [30], they could also cause longer cell sensitization. 3) Our experiments were performed at 37°C where the membrane resealing is faster [44] while their experiments were performed at room temperature.

In the low-conductivity buffer, there were protecting processes happening which take more than 3 minutes to finish since the effect of 'desensitization' was still present with 3 minutes delay. The time dynamics of propidium uptake was different than in the growth medium which indicates that different mechanisms are involved. In the hyperosmotic buffer, the second train of the split dose was even less effective than in the low-conductivity buffer. Since one of the differences between these buffers was sucrose concentration, we can assume that it has an important role, as discussed in the following paragraphs. In the high-conductivity buffer, split

127

and single dose caused similar final fluorescence (Fig 4G). Although sucrose inhibited cell sensitization, its absence did not cause it.

Time constant τ describes the time dynamics of the membrane resealing. Membrane resealing is affected by several parameters. It was slower when the membrane was oxidized [45] and faster at higher temperatures [44], lower sucrose concentration [46], and in the presence of low Ca^{2+} concentrations [42]. The cell membrane resealing depended on calcium, which had to be present in low concentrations when the cells were damaged either chemically, mechanically or electrically [42,47–49]. The increased intracellular calcium concentration after electroporation served as a stress indicator that triggered the membrane resealing process in the form of endo- [49], and exocytosis [47,48]. In the growth medium and the buffer with calcium, there were low concentrations of Ca^{2+} present and τ was lower than in other buffers (faster resealing), probably due to Ca^{2+} facilitated membrane resealing. Even when calcium was not added, it was still present during electroporation. First, calcium is present in the intracellular storages [50]. Second, even if it is not added to the buffer, there is some free calcium which comes from the glass or impurities in the chemicals, as measured in [45] for the low-conductivity buffer. Interestingly, in [47], the resealing after a second membrane disruption was much faster than after the first one. Authors suggested that initial wound was healed by exocytosis of the vesicles from the endocytic compartment while the second wound resealed faster since Golgi apparatus (responsible for a formation of new vesicles) had already been activated by an increased Ca^{2+} influx. The role of Golgi apparatus is in agreement with our results since the resealing constant τ after the second pulse train was lower (faster resealing) than after the first one in all electroporation buffers (Table 3). Parameter τ decreased with increasing delay since there was more time for the activation of the Golgi apparatus. The resealing speed after the half and the single dose was very similar in all tested buffers, contrary to what was observed by Rols and Teissié [51]. However, they applied more pulses (10 or 20 as opposed to 4 or 8 in our study) of higher intensity (1.2 kV/cm as opposed to 0.75 kV/cm in our study) which caused more pronounced membrane damage and difference in the resealing speed.

Parameter k describes the additional uptake process on a longer time scale. A higher value of k indicates either higher final fluorescence or faster resealing since $k = \frac{s}{\tau}$, as derived in the S1 Appendix. Thus, k depends on the final fluorescence and inversely depends of the resealing time constant. In the growth medium, this additional process was always present. The value of k decreased with an increasing delay, which suggests that either 1) the fluorescence due to the additional process was decreasing or 2) its resealing speed was increasing. The decrease in the final fluorescence could be caused by the decreasing membrane permeabilization between the trains. The second train caused less damage, and the additional uptake was lower than at shorter delays. In the low-conductivity buffer, the additional process of linear propidium uptake was not always present. The trend of k was different than in the growth medium. With increasing delay, the final fluorescence of the additional process was increasing since slower resealing is not likely (longer delay should decrease the resealing time). When the additional process was not present, it finished too fast or was too small to be observed. With longer delays, the additional process was visible because it was not finished yet. Parameter k does not reflect the binding delay of propidium after it enters the cells since it binds in microseconds [52].

In [43] pulses were split into two trains, and propidium or Yo-Pro-1 uptakes were measured. Interestingly, under the same pulse parameters, there was a large cell sensitization effect present with propidium, but much smaller with Yo-Pro-1 [53]. Apparently, different dyes give different uptake results under the same conditions. Although pulses in the nanosecond range were applied, the observation is interesting also for the microsecond pulses since there are reports on cell sensitization with nanosecond [24] as well as with microsecond [25–27,30] pulses.

128

Possible mechanisms of cell (de)sensitization

Increasing sucrose concentration caused among others an increase in osmotic pressure which decreased the size or density of the permeabilizing structures in the membrane, slower membrane resealing [46] and stabilization of cell membrane [54]. Similarly, trehalose (a disaccharide similar to the sucrose) had a protective and stabilizing role [55,56]. Our results are in agreement with slower membrane resealing observation since τ increased with increasing sucrose concentration. Higher sucrose concentration also caused lower fluorescence due to the second pulse train—the cells were protected by a still unknown mechanism which is also in agreement with the protective role of the sucrose. When the sucrose was replaced by NaCl, the pulse trains were equally effective. Sucrose inhibits cell sensitization, but its absence does not facilitate it.

The electrical conductivity of the growth medium and the high-conductivity buffer was in the same range. In the high-conductivity buffer, there was no cell sensitization, while in the growth medium, cell sensitization was observed. Since a similar electrical conductivity induces a different cell response, it is considered not to be responsible for cell sensitization.

In [35], authors ascribed cell sensitization to the higher efficiency of lower pulse repetition frequencies. Applying pulses on a permeabilized cell membrane is less effective because the existing conducting structures prevent the establishment of an additional transmembrane potential, which they call 'cell desensitization'. (The expression was used in a different sense than in our paper.) Assuming that cell sensitization is a consequence of repetition frequency effect, one cannot explain such different behaviors in different buffers. Their explanation of cell sensitization effect is thus unlikely.

Extended pore opening times have also been proposed among possible mechanisms [26,27]. The duration of all the protocols was the same; the membrane resealing was in the same time range. Thus, the pore opening times were also of approximately the same duration. The extended pore opening time does not explain cell sensitization.

Cell size change after electroporation occurs due to the colloid osmotic pressure [57,58]. Electric pulses of different parameters cause different extent of cell permeability, and the cell membrane becomes permeable to small molecules but not to large ones. The colloid osmotic pressure drives the influx of water and small solutes in the cell, and the cell swells [2]. Molecules, larger than the pores, balance colloid osmolality and stop cell swelling [58]. Increased/decreased cell size could cause higher/lower induced transmembrane voltage according to the Schwann equation. Cell size was measured via visible cross-section. In the growth medium, the cell size did not increase and thus cannot be the reason for cell sensitization. In the low-conductivity buffer, the cells shrunk. Cell desensitization could in part be explained by cell shrinking and lower induced transmembrane voltage. However, cell shrinking cannot be the only reason since the time dynamics of the uptake due to the second train and the cross-section change were different.

Cell sensitization has been observed in several cell lines and *in vivo*. In our experiments, we used Chinese hamster ovary cells. Since in this cell line cell sensitization either was [25] or was not present, it does not depend only on the cell line. It is possible that even in the growth medium cell sensitization would not be present in certain cell lines; however this remains to be further investigated.

The cytoskeleton is damaged by electric pulses [59–61] and there were different observations made (e.g. damaged cytoskeleton does not influence electroporation [62,63], it increases permeabilization [28], it increases the survival [62], it changes the resealing dynamics [61]). Cytoskeleton disruption has also been connected to cell swelling [60]. In [28], the disruption of the cytoskeleton rendered cells more sensitive to electric pulses. However, the repair of the

cytoskeleton is in the range of hours [59], but the cell sensitization dynamics in our experiments was in the range of minutes. The cytoskeleton disruption is not a likely explanation for cell sensitization.

The concentration of calcium we used in our buffer with calcium was similar as in the HAM-F12 growth medium. In the buffer with calcium, cells were more sensitive to the second pulse train than in the low-conductivity buffer. However, this was due to the lack of sucrose in the buffer with calcium. In the high-conductivity buffer where there is no calcium, the ratio S_2/S_1 was 1.03 and in the buffer with calcium, it was 1.06. In both buffers, the first and the second pulse train were equally effective. It is possible that higher calcium concentrations would cause cell sensitization but they could also lower cell viability [64]. Namely, electroporation with 1 mM calcium already decreased survival of various cell lines to 20–40% [65].

In the literature, also other explanations for cell sensitization were suggested: ATP leakage, membrane oxidation, and reduced membrane line tension. The investigation of these factors is beyond the scope of our current study. Our study opens many more questions which deserve being investigated in future: the mechanism of sucrose's protection of the membrane, the effect of different pulse parameters (duration and the number of pulses, electric field).

Modeling of cell electroporation is very useful since it allows us to describe cell responses, make predictions about effects of electric pulses on the cells, decrease the number of experiments needed, and help us to understand what is happening [37,39,66–68]. However, until also biological effects are included in the models, they will have a limited power and will not correctly predict the outcome in certain cases.

Cell sensitization has also been observed *in vivo* by the delayed tumor growth, enhancement of tumor necrosis and perfusion defects [26,27]. The growth medium is an approximation of the *in vivo* extracellular fluid. The mechanism(s) for cell sensitization *in vitro* and *in vivo* could be similar. There are, however, many more factors *in vivo*–cell crowding, blood supply, immune system, electric field shielding.

Conclusions

Cell sensitization seems to be a buffer dependent phenomenon. In the growth medium, still unknown processes were triggered by the pulse application and rendered cells more susceptible to electric pulses. In the low-conductivity and hyperosmotic buffer, a protective effect of the sucrose and cell shrinking caused cell 'desensitization'. In the high-conductivity buffer, there was no cell 'desensitization', probably due to the lack of sucrose. There was also no cell sensitization present since the cell 'sensitizing' processes from the growth medium were missing. The exact mechanism of cell sensitization has still to be determined; however we believe we shed additional light on the existing hypotheses and discarded some of them. The effect of pulse repetition frequency [35], cell size change, cytoskeleton disruption [24] and calcium influx [24] seem unlikely explanations. Based on our results, there are different sensitizing and desensitizing mechanisms present and competing at the same time, and the outcome depends on their overall contributions.

Supporting Information

S1 Appendix. Derivation of the first-order uptake equation.
(DOCX)

Acknowledgments

130

Author Contributions

Conceived and designed the experiments: JD DM ONP AGP. Performed the experiments: JD. Analyzed the data: JD DM. Wrote the paper: DM. Interpreted the results: JD DM ONP AGP.

References

1. Kotnik T, Kramar P, Pucihar G, Miklavč D, Tarek M. Cell membrane electroporation- Part 1: The phenomenon. IEEE Electr Insul Mag. 2012; 28: 14–23. doi: 10.1109/MEI.2012.6268438

2. Tsong TY. Electroporation of Cell Membranes. Biophys J. 1991; 60: 297–306. PMID: 1912274

3. Edhemović I, Brecelj E, Gasljević G, Marolt Mušič M, Gorjup V, Mali B, et al. Intraoperative electrochemotherapy of colorectal liver metastases: Electrochemotherapy of Liver Metastases. J Surg Oncol. 2014; 110: 320–327. doi: 10.1002/jso.23625 PMID: 24782355

4. Granata V, Fusco R, Piccirillo M, Palaia R, Petrillo A, Lastoria S, et al. Electrochemotherapy in locally advanced pancreatic cancer: Preliminary results. Int J Surg. 2015; 18: 230–236. doi: 10.1016/j.ijsu.2015.04.055 PMID: 25917204

5. Miklavčič D, Mali B, Kos B, Heller R, Serša G. Electrochemotherapy: from the drawing board into medical practice. Biomed Eng OnLine. 2014; 13: 29. doi: 10.1186/1475-925X-13-29 PMID: 24621079

6. Čemažar M, Ambrožič Avgustin J, Pavlin D, Serša G, Poli A, Krhac Levačič A, et al. Efficacy and safety of electrochemotherapy combined with peritumoral IL-12 gene electrotransfer of canine mast cell tumours: Electrochemotherapy and IL-12 for mast cell tumours. Vet Comp Oncol. 2016; n/a-n/a. doi: 10.1111/vco.12208

7. Davalos RV, Mir LM, Rubinsky B. Tissue Ablation with Irreversible Electroporation. Ann Biomed Eng. 2005; 33: 223–231. doi: 10.1007/s10439-005-8981-8 PMID: 15771276

8. Jiang C, Davalos RV, Bischof JC. A Review of Basic to Clinical Studies of Irreversible Electroporation Therapy. IEEE Trans Biomed Eng. 2015; 62: 4–20. doi: 10.1109/TBME.2014.2367543 PMID: 25389236

9. Al-Sakere B, André F, Bernat C, Connault E, Opolon P, Davalos RV, et al. Tumor Ablation with Irreversible Electroporation. Isalan M, editor. PLoS ONE. 2007; 2: e1135. doi: 10.1371/journal.pone.0001135 PMID: 17989772

10. Daud AI, DeConti RC, Andrews S, Urbas P, Riker AI, Sondak VK, et al. Phase I trial of interleukin-12 plasmid electroporation in patients with metastatic melanoma. J Clin Oncol. 2008; 26: 5896–5903. doi: 10.1200/JCO.2007.15.6794 PMID: 19029422

11. Heller LC, Heller R. Electroporation gene therapy preclinical and clinical trials for melanoma. Curr Gene Ther. 2010; 10: 312–317. PMID: 20557286

12. Calvet CY, André FM, Mir LM. Dual therapeutic benefit of electroporation-mediated DNA vaccination in vivo: Enhanced gene transfer and adjuvant activity. OncoImmunology. 2014; 3: e28540. doi: 10.4161/onci.28540 PMID: 25050220

13. Rosazza C, Haberl Meglič S, Zumbusch A, Rols M-P, Miklavčič D. Gene Electrotransfer: A Mechanistic Perspective. Curr Gene Ther. 2016; 16: 98–129. PMID: 27029943

14. Denet A-R, Vanbever R, Préat V. Skin electroporation for transdermal and topical delivery. Adv Drug Deliv Rev. 2004; 56: 659–674. doi: 10.1016/j.addr.2003.10.027 PMID: 15019751

15. Yarmush ML, Golberg A, Serša G, Kotnik T, Miklavčič D. Electroporation-Based Technologies for Medicine: Principles, Applications, and Challenges. Annu Rev Biomed Eng. 2014; 16: 295–320. doi: 10.1146/annurev-bioeng-071813-104622 PMID: 24905876

16. Zorec B, Préat V, Miklavčič D, Pavšelj N. Active enhancement methods for intra- and transdermal drug delivery: a review. Zdr Vestn. 2013; 82: 339–56.

17. Kotnik T, Frey W, Sack M, Haberl Meglič S, Peterka M, Miklavčič D. Electroporation-based applications in biotechnology. Trends Biotechnol. 2015; doi: 10.1016/j.tibtech.2015.06.002

18. Mahnič-Kalamiza S, Vorobiev E, Miklavčič D. Electroporation in food processing and biorefinery. J Membr Biol. 2014; 247: 1279–1304. doi: 10.1007/s00232-014-9737-x PMID: 25287023

19. Sack M, Sigler J, Frenzel S, Eing C, Arnold J, Michelberger T, et al. Research on Industrial-Scale Electroporation Devices Fostering the Extraction of Substances from Biological Tissue. Food Eng Rev. 2010; 2: 147–156. doi: 10.1007/s12393-010-9017-1

131

20. Toepfl S. Pulsed electric field food processing–industrial equipment design and commercial applications. Stewart Postharvest Rev. 2012; 8: 1–7. doi: 10.2212/spr.2012.2.4

21. Mali B, Miklavčič D, Campana LG, Čemažar M, Serša G, Snoj M, et al. Tumor size and effectiveness of electrochemotherapy. Radiol Oncol. 2013; 47: 32–41. doi: 10.2478/raon-2013-0002 PMID: 23450195

22. Županič A, Miklavčič D. Tissue heating during tumor ablation with irreversible electroporation. Elektrotehniški Vestn Engl Ed. 2011; 78: 42–47.

23. Kos B, Voigt P, Miklavčič D, Moche M. Careful treatment planning enables safe ablation of liver tumors adjacent to major blood vessels by percutaneous irreversible electroporation (IRE). Radiol Oncol. 2015; 49. doi: 10.1515/raon-2015-0031

24. Pakhomova ON, Gregory BW, Khorokhorina VA, Bowman AM, Xiao S, Pakhomov AG. Electroporation-Induced Electrosensitization. Launikonis B, editor. PLoS ONE. 2011; 6: e17100. doi: 10.1371/journal.pone.0017100 PMID: 21347394

25. Pakhomova ON, Gregory BW, Pakhomov AG. Facilitation of electroporative drug uptake and cell killing by electrosensitization. J Cell Mol Med. 2013; 17: 154–159. doi: 10.1111/j.1582-4934.2012.01658.x PMID: 23305510

26. Jiang C, Shao Q, Bischof J. Pulse Timing During Irreversible Electroporation Achieves Enhanced Destruction in a Hindlimb Model of Cancer. Ann Biomed Eng. 2015; 43: 887–895. doi: 10.1007/s10439-014-1133-2 PMID: 25269611

27. Jiang C, Qin Z, Bischof J. Membrane-Targeting Approaches for Enhanced Cancer Cell Destruction with Irreversible Electroporation. Ann Biomed Eng. 2014; 42: 193–204. doi: 10.1007/s10439-013-0882-7 PMID: 23949655

28. Thompson GL, Roth C, Tolstykh G, Kuipers M, Ibey BL. Disruption of the actin cortex contributes to susceptibility of mammalian cells to nanosecond pulsed electric fields. Bioelectromagnetics. 2014; 35: 262–272. doi: 10.1002/bem.21845 PMID: 24619788

29. Muratori C, Pakhomov AG, Xiao S, Pakhomova ON. Electrosensitization assists cell ablation by nanosecond pulsed electric field in 3D cultures. Sci Rep. 2016; 6: 23225. doi: 10.1038/srep23225 PMID: 26987779

30. Dermol J, Pakhomova ON, Xiao S, Pakhomov AG, Miklavčič D. Cell Sensitization is Induced by a Wide Range of Permeabilizing Electric Fields. In: Jarm T, Kramar P, editors. 1st World Congress on Electroporation and Pulsed Electric Fields in Biology, Medicine and Food & Environmental Technologies. Singapore: Springer Singapore; 2016. pp. 163–166. Available: http://link.springer.com/10.1007/978-981-287-817-5_36

31. Demiryurek Y, Nickaeen M, Zheng M, Yu M, Zahn JD, Shreiber DI, et al. Transport, resealing, and reporation dynamics of two-pulse electroporation-mediated molecular delivery. Biochim Biophys Acta BBA—Biomembr. 2015; 1848: 1706–1714. doi: 10.1016/j.bbamem.2015.04.007

32. Mir LM, Gehl J, Serša G, Collins CG, Garbay J-R, Billard V, et al. Standard operating procedures of the electrochemotherapy: Instructions for the use of bleomycin or cisplatin administered either systemically or locally and electric pulses delivered by the CliniporatorTM by means of invasive or non-invasive electrodes. Eur J Cancer Suppl. 2006; 4: 14–25.

33. Marty M, Serša G, Garbay JR, Gehl J, Collins CG, Snoj M, et al. Electrochemotherapy–An easy, highly effective and safe treatment of cutaneous and subcutaneous metastases: Results of ESOPE (European Standard Operating Procedures of Electrochemotherapy) study. Eur J Cancer Suppl. 2006; 4: 3–13. doi: 10.1016/j.ejcsup.2006.08.002

34. Reberšek M, Miklavčič D, Bertacchini C, Sack M. Cell membrane electroporation-Part 3: the equipment. IEEE Electr Insul Mag. 2014; 30: 8–18. doi: 10.1109/MEI.2014.6804737

35. Silve A, Guimerà Brunet A, Al-Sakere B, Ivorra A, Mir LM. Comparison of the effects of the repetition rate between microsecond and nanosecond pulses: electropermeabilization-induced electro-desensitization? Biochim Biophys Acta. 2014; 1840: 2139–2151. doi: 10.1016/j.bbagen.2014.02.011 PMID: 24589913

36. Silve A, Leray I, Poignard C, Mir LM. Impact of external medium conductivity on cell membrane electropermeabilization by microsecond and nanosecond electric pulses. Sci Rep. 2016; 6: 19957. doi: 10.1038/srep19957 PMID: 26829153

37. Miklavčič D, Towhidi L. Numerical study of the electroporation pulse shape effect on molecular uptake of biological cells. Radiol Oncol. 2010; 44. doi: 10.2478/v10019-010-0002-3

38. Prausnitz MR, Lau BS, Milano CD, Conner S, Langer R, Weaver JC. A quantitative study of electroporation showing a plateau in net molecular transport. Biophys J. 1993; 65: 414–422. doi: 10.1016/S0006-3495(93)81081-6 PMID: 7690262

39. Son R, Gowrishankar T, Smith K, Weaver J. Modeling a conventional electroporation pulse train: Decreased pore number, cumulative calcium transportand an example of electrosensitization. IEEE Trans Biomed Eng. 2015; 1–1. doi: 10.1109/TBME.2015.2466234

132

40. Ušaj M, Trontelj K, Hudej R, Kandušer M, Miklavčič D. Cell size dynamics and viability of cells exposed to hypotonic treatment and electroporation for electrofusion optimization. Radiol Oncol. 2009; 43. doi: 10.2478/v10019-009-0017-9

41. Mazères S, Šel D, Golzio M, Pucihar G, Tamzali Y, Miklavčič D, et al. Non invasive contact electrodes for in vivo localized cutaneous electropulsation and associated drug and nucleic acid delivery. J Controlled Release. 2009; 134: 125–131. doi: 10.1016/j.jconrel.2008.11.003

42. Djuzenova CS, Zimmermann U, Frank H, Sukhorukov VL, Richter E, Fuhr G. Effect of medium conductivity and composition on the uptake of propidium iodide into electropermeabilized myeloma cells. Biochim Biophys Acta BBA—Biomembr. 1996; 1284: 143–152. doi: 10.1016/S0005-2736(96)00119-8

43. Gianulis EC, Pakhomov AG. Gadolinium modifies the cell membrane to inhibit permeabilization by nanosecond electric pulses. Arch Biochem Biophys. 2015; 570: 1–7. doi: 10.1016/j.abb.2015.02.013 PMID: 25707556

44. Saulis G, Venslauskas MS, Naktinis J. Kinetics of pore resealing in cell membranes after electroporation. J Electroanal Chem Interfacial Electrochem. 1991; 321: 1–13. doi: 10.1016/0022-0728(91)85564-6

45. Gabriel B, Teissié J. Generation of reactive-oxygen species induced by electropermeabilization of Chinese hamster ovary cells and their consequence on cell viability. Eur J Biochem FEBS. 1994; 223: 25–33.

46. Rols MP, Teissié J. Modulation of electrically induced permeabilization and fusion of Chinese hamster ovary cells by osmotic pressure. Biochemistry (Mosc). 1990; 29: 4561–4567.

47. Togo T, Alderton JM, Bi GQ, Steinhardt RA. The mechanism of facilitated cell membrane resealing. J Cell Sci. 1999; 112 (Pt 5): 719–731. PMID: 9973606

48. Huynh C, Roth D, Ward DM, Kaplan J, Andrews NW. Defective lysosomal exocytosis and plasma membrane repair in Chediak-Higashi/beige cells. Proc Natl Acad Sci. 2004; 101: 16795–16800. doi: 10.1073/pnas.0405905101 PMID: 15557559

49. Idone V, Tam C, Goss JW, Toomre D, Pypaert M, Andrews NW. Repair of injured plasma membrane by rapid Ca2+-dependent endocytosis. J Cell Biol. 2008; 180: 905–914. doi: 10.1083/jcb.200708010 PMID: 18316410

50. Alberts B, editor. Molecular biology of the cell. 4th ed. New York: Garland Science; 2002.

51. Rols MP, Teissié J. Electropermeabilization of mammalian cells. Quantitative analysis of the phenomenon. Biophys J. 1990; 58: 1089–1098. doi: 10.1016/S0006-3495(90)82451-6 PMID: 2291935

52. Pucihar G, Kotnik T, Miklavčič D, Teissié J. Kinetics of Transmembrane Transport of Small Molecules into Electropermeabilized Cells. Biophys J. 2008; 95: 2837–2848. doi: 10.1529/biophysj.108.135541 PMID: 18539632

53. Bowman AM, Nesin OM, Pakhomova ON, Pakhomov AG. Analysis of Plasma Membrane Integrity by Fluorescent Detection of Tl+ Uptake. J Membr Biol. 2010; 236: 15–26. doi: 10.1007/s00232-010-9269-y PMID: 20623351

54. Wang H, Griffiths MW. Mg2+-free buffer elevates transformation efficiency of Vibrio parahaemolyticus by electroporation. Lett Appl Microbiol. 2009; 48: 349–354. doi: 10.1111/j.1472-765X.2008.02531.x PMID: 19207855

55. Shirakashi R, Köstner CM, Müller KJ, Kürschner M, Zimmermann U, Sukhorukov VL. Intracellular Delivery of Trehalose into Mammalian Cells by Electropermeabilization. J Membr Biol. 2002; 189: 45–54. doi: 10.1007/s00232-002-1003-y PMID: 12202951

56. Pereira CS, Hünenberger PH. Interaction of the Sugars Trehalose, Maltose and Glucose with a Phospholipid Bilayer: A Comparative Molecular Dynamics Study. J Phys Chem B. 2006; 110: 15572–15581. doi: 10.1021/jp060789l PMID: 16884281

57. Nesin OM, Pakhomova ON, Xiao S, Pakhomov AG. Manipulation of cell volume and membrane pore comparison following single cell permeabilization with 60- and 600-ns electric pulses. Biochim Biophys Acta BBA—Biomembr. 2011; 1808: 792–801. doi: 10.1016/j.bbamem.2010.12.012

58. Kinosita K, Tsong TY. Formation and resealing of pores of controlled sizes in human erythrocyte membrane. Nature. 1977; 268: 438–441. doi: 10.1038/268438a0 PMID: 895849

59. Kanthou C, Kranjc S, Serša G, Tozer G, Županič A, Čemažar M. The endothelial cytoskeleton as a target of electroporation-based therapies. Mol Cancer Ther. 2006; 5: 3145–3152. doi: 10.1158/1535-7163.MCT-06-0410 PMID: 17172418

60. Pakhomov AG, Xiao S, Pakhomova ON, Semenov I, Kuipers MA, Ibey BL. Disassembly of actin structures by nanosecond pulsed electric field is a downstream effect of cell swelling. Bioelectrochemistry Amst Neth. 2014; 100: 88–95. doi: 10.1016/j.bioelechem.2014.01.004

133

61. Rols M-P, Teissié J. Experimental evidence for the involvement of the cytoskeleton in mammalian cell electropermeabilization. Biochim Biophys Acta BBA—Biomembr. 1992; 1111: 45–50. doi: 10.1016/0005-2736(92)90272-N

62. Xiao D, Tang L, Zeng C, Wang J, Luo X, Yao C, et al. Effect of actin cytoskeleton disruption on electric pulse-induced apoptosis and electroporation in tumour cells. Cell Biol Int. 2011; 35: 99–104. doi: 10.1042/CBI20100464 PMID: 20828369

63. Lin R, Chang DC, Lee Y-K. Single-cell electroendocytosis on a micro chip using in situ fluorescence microscopy. Biomed Microdevices. 2011; 13: 1063–1073. doi: 10.1007/s10544-011-9576-9 PMID: 21800146

64. Frandsen SK, Gibot L, Madi M, Gehl J, Rols M-P. Calcium Electroporation: Evidence for Differential Effects in Normal and Malignant Cell Lines, Evaluated in a 3D Spheroid Model. Rubinsky B, editor. PLOS ONE. 2015; 10: e0144028. doi: 10.1371/journal.pone.0144028 PMID: 26633834

65. Frandsen SK, Gissel H, Hojman P, Eriksen J, Gehl J. Calcium electroporation in three cell lines: a comparison of bleomycin and calcium, calcium compounds, and pulsing conditions. Biochim Biophys Acta BBA—Gen Subj. 2014; 1840: 1204–1208. doi: 10.1016/j.bbagen.2013.12.003

66. Dermol J, Miklavčič D. Mathematical Models Describing Chinese Hamster Ovary Cell Death Due to Electroporation In Vitro. J Membr Biol. 2015; 248: 865–881. doi: 10.1007/s00232-015-9825-6 PMID: 26223863

67. Dermol J, Miklavčič D. Predicting electroporation of cells in an inhomogeneous electric field based on mathematical modeling and experimental CHO-cell permeabilization to propidium iodide determination. Bioelectrochemistry. 2014; 100: 52–61. doi: 10.1016/j.bioelechem.2014.03.011 PMID: 24731594

68. Neu WK, Neu JC. Theory of Electroporation. In: Efimov IR, Kroll MW, Tchou PJ, editors. Cardiac Bioelectric Therapy. Boston, MA: Springer US; 2009. pp. 133–161. Available: http://link.springer.com/10.1007/978-0-387-79403-7_7

S1 Appendix: Derivation of the first-order uptake equation

We can follow a similar derivation as (Shirakashi et al. 2002) and assume that after a pulse application cell permeabilization decreases exponentially with time:

$$P(t) = P_0 \exp\left(-\frac{t}{\tau}\right),$$ (1)

where $P(t)$ means the permeability at time t, P_0 is the initial permeability at the end of the pulse and τ is the resealing constant. Flux through the electroporated membrane can be written as in (Miklavčič and Towhidi 2010):

$$j(t) = P_0 \exp\left(-\frac{t}{\tau}\right)(c_e - c_i) \approx P_0 \exp\left(-\frac{t}{\tau}\right)c_e,$$ (2)

where c_i means the internal and c_e the external concentration. We assume that all propidium in the cell binds to nucleic acids immediately and that the intracellular propidium concentration is 0 mM. Namely, in (Pucihar et al. 2008) it has been shown that the propidium signal starts to increase microseconds after the pulse start. In our experiments, we measured the uptake in the range of seconds, and we could neglect the time delay of propidium binding. Since in our experiments, we did not reach propidium saturation (the fluorescence value of the treated cells was below the maximal measured fluorescence of electroporated cells) we can assume that there was no unbound propidium in cells and thus the internal propidium concentration was 0 mM. The number of molecules N that enter the cells can be obtained by integration of j over time and permeabilized area ((Miklavčič and Towhidi 2010), Equation 9):

$$N(t) = P_0 \tau c_e A N_A \left(1 - \exp\left(-\frac{t}{\tau}\right)\right),$$ (3)

where A is the permeabilized area and N_A the Avogadro constant. By uniting τ, c_e, P_0, A and N_A into a constant C we obtain a first-order model:

$$N(t) = C\left(1 - \exp\left(-\frac{t}{\tau}\right)\right).$$ (4)

The fluorescence of propidium is linearly dependent on the number of the bound molecules below the saturation level (Kennedy et al. 2008). The constant C does not have any meaning; it is only a multiplicative factor and describes the plateau of the reached fluorescence. Thus, the fluorescence can be written as:

$$f(t) = S\left(1 - \exp\left(-\frac{t}{\tau}\right)\right),$$ (5)

where f signifies the fluorescence in dependence on time and S is constant. The expression (5) can be directly applied to our measurements.

The shape of the propidium uptake curves indicated that there is an additional process present that causes the linear uptake seen after the first order process is finished. If we assume that this process is also first-order and that its time constant is much larger than our observation time, we can use linear expansion and include the first two terms:

$$\exp(t) = 1 + \frac{t}{1!} + \frac{t^2}{2!} + \cdots = \sum_{n=0}^{\infty} \frac{t^n}{n!}. \tag{6}$$

We obtain an approximation of Equation (5):

$$f(t) = S\left(1 - \exp\left(-\frac{t}{\tau}\right)\right) \cong \frac{S}{\tau} t = kt, \tag{7}$$

where k equals the plateau of the process divided by the resealing constant.

1. Shirakashi R, Köstner CM, Müller KJ, Kürschner M, Zimmermann U, Sukhorukov VL. Intracellular Delivery of Trehalose into Mammalian Cells by Electropermeabilization. J Membr Biol. 2002;189: 45–54. doi:10.1007/s00232-002-1003-y
2. Miklavčič D, Towhidi L. Numerical study of the electroporation pulse shape effect on molecular uptake of biological cells. Radiol Oncol. 2010;44. doi:10.2478/v10019-010-0002-3
3. Pucihar G, Kotnik T, Miklavčič D, Teissié J. Kinetics of Transmembrane Transport of Small Molecules into Electropermeabilized Cells. Biophys J. 2008;95: 2837–2848. doi:10.1529/biophysj.108.135541
4. Kennedy SM, Ji Z, Hedstrom JC, Booske JH, Hagness SC. Quantification of electroporative uptake kinetics and electric field heterogeneity effects in cells. Biophys J. 2008;94: 5018–5027. doi:10.1529/biophysj.106.103218

Paper 5

Title: **From cell to tissue properties – modelling skin electroporation with pore and local transport region formation**

Authors: Janja Dermol-Černe, Damijan Miklavčič

Publication: IEEE Transactions on Biomedical Engineering, vol. 65, no. 2, pp. 458-468, Feb. 2018.

DOI: 10.1109/TBME.2017.2773126

Impact factor: 3.577 (2016), 3.407 (5-year)

Quartile: Q1 (Biomedical Engineering)

Rank: 12/77 (Biomedical Engineering)

From Cell to Tissue Properties—Modeling Skin Electroporation With Pore and Local Transport Region Formation

Janja Dermol-Černe [ID] and Damijan Miklavčič [ID]

Abstract—**Current models of tissue electroporation either describe tissue with its bulk properties or include cell level properties, but model only a few cells of simple shapes in low-volume fractions or are in two dimensions. We constructed a three-dimensional model of realistically shaped cells in realistic volume fractions. By using a 'unit cell' model, the equivalent dielectric properties of whole tissue could be calculated. We calculated the dielectric properties of electroporated skin. We modeled electroporation of single cells by pore formation on keratinocytes and on the papillary dermis which gave dielectric properties of the electroporated epidermis and papillary dermis. During skin electroporation, local transport regions are formed in the stratum corneum. We modeled local transport regions and increase in their radii or density which affected the dielectric properties of the stratum corneum. The final model of skin electroporation accurately describes measured electric current and voltage drop on the skin during electroporation with long low-voltage pulses. The model also accurately describes voltage drop on the skin during electroporation with short high-voltage pulses. However, our results indicate that during application of short high-voltage pulses additional processes may occur which increase the electric current. Our model connects the processes occurring at the level of cell membranes (pore formation), at the level of a skin layer (formation of local transport region in the stratum corneum) with the tissue (skin layers) and even level of organs (skin). Using a similar approach, electroporation of any tissue can be modeled, if the morphology of the tissue is known.**

Index Terms—**Franz diffusion cell, local transport region, multiscale approach, numerical modeling, pore formation, skin electroporation.**

I. INTRODUCTION

ELECTROPORATION is a physical way of disturbing cell membrane with the application of short, high-voltage pulses leading to increase in its permeability to different molecules (reversible electroporation) and to achieve cell death (IRE - irreversible electroporation) [1], [2]. Electroporation or pulsed electric field treatment is used in biotechnology [3], food-processing [4], [5] and medicine [6], e.g., gene electrotransfer [7], [8], DNA vaccination [9], [10], transdermal drug delivery [11], [12], IRE as an ablation technique [13], [14] and electrochemotherapy [15], [16].

Transdermal drug delivery is easy to conduct, non-invasive, quick and it avoids gastro-intestinal degradation. Skin is also a barrier not many drugs can penetrate, and various enhancement methods are used to improve drug delivery, electroporation being one of them [12]. However, skin electroporation is a complex phenomenon and still not well understood. It is believed that electric pulses cause the formation of regions of an increased electrical conductivity through which the transport occurs – i.e., local transport regions (LTRs). The density of the LTRs increases with increasing voltage while their size increases with increasing pulse duration [17]–[22].

Models of tissue electroporation enhance our understanding as they offer a concise description using mathematical and physical laws. The current tissue models are of two types – they model tissue as a bulk [23]–[26] while only few model tissues' microscopic structure [27]–[31]. The bulk tissue models describe the electric field distribution as a function of tissue properties, applied voltage and the geometry of the electrodes but assume that the tissue is homogeneous. For each tissue type, the critical electric field for electroporation or cell death must be experimentally determined or described with statistical models [32]–[34]. The models with included microstructure are in 2D or 3D. The 2D models include sampling the tissue with Cartesian transport lattices [30], [31], [35], describing it with the equivalent circuit [36], [37], or modeling it with the Voronoi network [29]. The 2D models disregard the geometry of the cells and cannot model different cell density which significantly alters the equivalent dielectric properties, the induced transmembrane voltage and electroporation [38]. In 3D, tissue was modeled as an infinite lattice [39], [40] or randomly distributed spherical cells of different sizes [28]. The volume fraction maximally achievable by face-centered cube or hexagonal close-packed lattices is 77% which is lower than the volume fractions we encounter in most tissues (e.g., 83% in the epidermis, 91% in the stratum corneum, 85% in the muscle tissue, 80% in the hypodermis [41]). Furthermore, cells were not of realistic shapes although it was shown that cell shapes also affects the dielectric properties [42]. An improvement was a model of spinach leaf which also

included the size and shape of the cells; however, only a small part was modeled [27], and a generalization to the whole leaf is questionable. The model by Huclova *et al*. [42] also models single cells but offers a more realistic description since cells can be of different shapes, sizes, and densities. Moreover, also tissue heterogeneity and anisotropy can be described which most of the current models cannot. The dielectric properties of cells are generalized to tissues as their equivalent dielectric properties. Numerical calculation is reduced to tissue level, and much larger geometry than a single cell can be modeled. The latter model describes the behaviour of cells in the linear range but has a potential to include also nonlinear behaviour, i.e., electroporation.

In the field of skin electroporation, only a few models exist [20], [43]–[48] and they mostly belong to the group of bulk tissue models and for the values of dielectric properties of separate layers take rough approximations or even model several layers with the same values. The values of the dielectric properties of the electroporated layers are also rough approximations [44]. Some models include the formation of the local transport regions [43], [46], [48] but are focused only on the stratum corneum and do not include pore formation in the membranes of the cells in lower layers. In the equivalent circuit of the skin [47], the information on the geometry of the cells is lost, and the resistance of the elements is determined by experimental measurements which vary between systems.

Our aim was thus to start from the microscopic scale to obtain a bulk model of skin electroporation. We started with the model by Huclova *et al*. [41] which has several advantages (possibility to model real shapes and densities of cells, heterogeneity and anisotropy). We modeled the change in dielectric parameters of skin during electroporation and validated our model with current-voltage measurements. We modeled pore formation in cell membranes and local transport region formation in the stratum corneum. We modeled the skin's dielectric properties after two protocols which varied in voltage and pulse duration – long low-voltage pulses (LV protocol) and short high-voltage pulses (HV protocol) [49]. We achieved good agreement with measurements of LV protocol by including LTR formation in the stratum corneum, change in electrical conductivity of the deeper skin layers due to cell membrane electroporation and electrode polarisation. During HV protocol the modeled voltage drop on the skin matched the measurements well; however, the current deviated for 50%. Also, the modeled density of the LTRs in the HV protocol was much higher than the experimentally determined values, which indicates that during the HV protocol additional processes may occur which are not yet identified and were thus not included in our model. The advantage of our approach is that it is not limited only to skin electroporation, but electroporation of any tissue can be modeled provided the geometric and dielectric properties of cells constituting the tissue are known.

II. METHODS

A. Experimental Work

For fitting and validation of our model, we used experimental results from [49]. In short, 350 μm thick dermatomed porcine ear skin was put between the donor and receiver chamber of the Franz diffusion cell. Porcine ear skin is similar to the human skin regarding layers' thickness, number of hairs, their size and extension depth [50]. Two Pt electrodes were positioned 0.2 cm above and 0.5 cm below the skin. Long low-voltage (3×45 V pulses of 250 ms duration, 100 ms pause – LV protocol) or short high-voltage pulses (3×500 V pulses of 500 μs duration, 500 μs pause – HV protocol) were delivered to the skin. The delivered voltage, the voltage on the skin and current were measured.

According to the model [41], the dermatomed skin consists of four layers: the stratum corneum, the epidermis, the papillary dermis, and the upper vessel plexus.

B. Construction of the Model

The model of the skin before electroporation was constructed according to [41]. The modeling in our study aimed to add electroporation to the model by Huclova *et al*. The main steps in our 'upgraded' model are described by Fig. 1. We manually changed (i.e., optimized) the parameters in the local transport region model and the electroporation in a unit cell model. We obtained equivalent dielectric properties of separate layers and introduced them into the Franz diffusion cell model. We applied voltage to the Franz diffusion cell model and calculated the electric current and the voltage drop on the skin. We compared the simulated values with the measured ones and changed the parameters in the local transport region model and electroporation in a unit cell model until the measured and simulated values matched. Values of dielectric and geometric parameters, used in the final model, are referred to as 'optimized values' although they could be only a local optimal values and not global.

The numerical calculations were done in Comsol Multiphysics (v5.3, Stockholm, Sweden) in 3D unless noted otherwise. All models were remeshed until there was a negligible difference in the modeled voltage drop on the skin with further remeshing. In all models, electric currents physics was used which calculates the electric potential in a subdomain by

$$-\nabla \left(\sigma \nabla \mathrm{V} \right) - \nabla \mathrm{j} \omega \varepsilon \nabla \mathrm{V} = 0 \qquad (1)$$

where σ denotes the electric conductivity, ε the relative permittivity of the subdomain. jω in the frequency domain is equivalent to time differentiation in the time domain. Cell membrane was modeled by boundary condition distributed impedance, given by

$$n \cdot J = \frac{1}{d_m} \left(\sigma_m + j \omega \varepsilon \right) \left(V - V_{\mathrm{ref}} \right) \qquad (2)$$

where d_m denotes the membrane thickness, ε its dielectric permittivity, σ_m its electrical conductivity, V_{ref} is the electric potential on the exterior side of the boundary, n is the unit vector normal to the boundary surface, J is the electric current density.

1) The Model of Dielectric Properties Without Electroporation: We constructed the model as described in [41]. For more detail on initial geometric and dielectric properties of the cells and settings of the numerical solver, we refer the reader to [41]. The authors modeled full thickness skin and also included layers which were not included in the dermatomed skin from our experiments. Initially, we modeled all layers for validation of our model, but for modeling electroporation, only the stratum
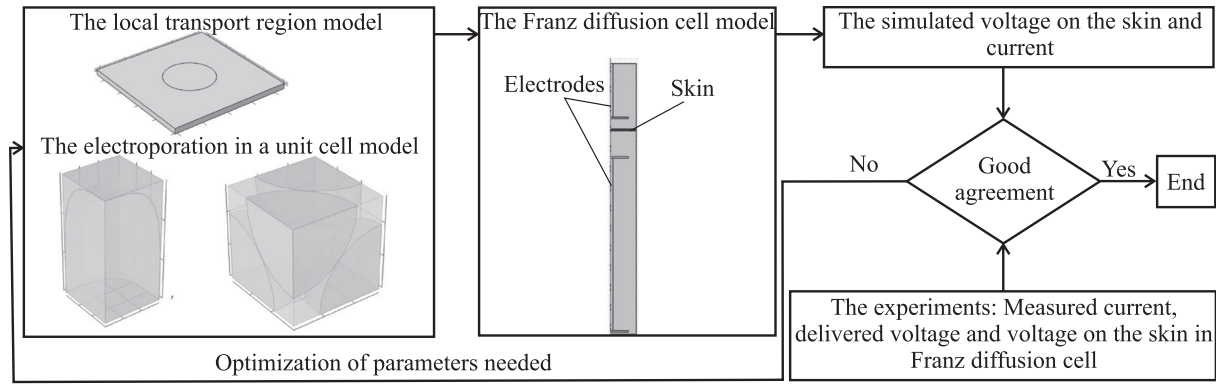
Fig. 1. Optimization scheme used in obtaining the parameters of the skin electroporation model. The parameters of the local transport region model and the electroporation in a unit cell model were changed and introduced into the Franz diffusion cell model. In the Franz diffusion cell model, we simulated the current through the Franz diffusion cell and voltage drop on the skin. Results of the simulation were compared to the results of the experiments. We varied the parameters of the models until the simulated and measured values matched.

corneum, epidermis, papillary dermis, and upper vessel plexus were modeled. Briefly, the skin was divided into separate layers, based on their morphology. In each layer, a typical biological cell (i.e., corneocyte, keratinocyte,) or a typical structure (i.e., blood vessels, collagen fibres) were identified. For the calculation of equivalent dielectric properties, either analytical or numerical method was applied. When the particles were embedded in the extracellular fluid in a low volume fraction ($<80\%$) the analytical Hanai-Bruggeman equation was used in Matlab R2015b (Mathworks, USA) which was calculated much faster than the numerical method. The papillary dermis was modeled as 40 μm spheres in 0.74 volume fraction and the upper vessel plexus as x-axis oriented cylinders with diameter 50 μm in volume fraction 0.3. Layers of higher volume fractions were modeled numerically. A unit cell was constructed for each cell layer. A biological cell in a unit cell was modeled via the 'superformula', imported into the Comsol and scaled to achieve the correct sizes and volume fractions. These were (in x-, y- and z-direction with corresponding volume fraction) for the corneocyte: (40 μm, 40 μm, 0.8 μm, 0.85) and the keratinocyte: (5.97 μm, 5.97 μm, 11.95 μm, 0.8). Several unit cells together could describe the morphology of the entire layer. Stratum corneum was modeled with corneocyte, epidermis with keratinocyte and subcutaneous tissue with adipocyte. In Fig. 2, the corneocyte, the keratinocyte and the papillary dermis (used with the Krassowska asymptotic equation) are shown. The opposite boundaries of the unit cell were exposed to a sinusoidal voltage, and via the admittance, the frequency dependent dielectric properties were calculated (ε^*). Other outer boundaries were set to insulation. The process was repeated in all three axes to obtain the dielectric tensor ($\bar{\bar{\varepsilon}}^*$). From $\bar{\bar{\varepsilon}}^*$, the electrical conductivity and relative permittivity were calculated and inserted in the Franz diffusion cell model as properties of separate layers. We used the frequency domain study, the direct PARDISO solver and the physics controlled mesh with finer or extra fine element size.

2) The Model of Dielectric Properties With Electroporation: We added skin electroporation to the model by Huclova *et al.* [41]. We modeled pore formation on the level of single cells as well as local transport region formation in stratum
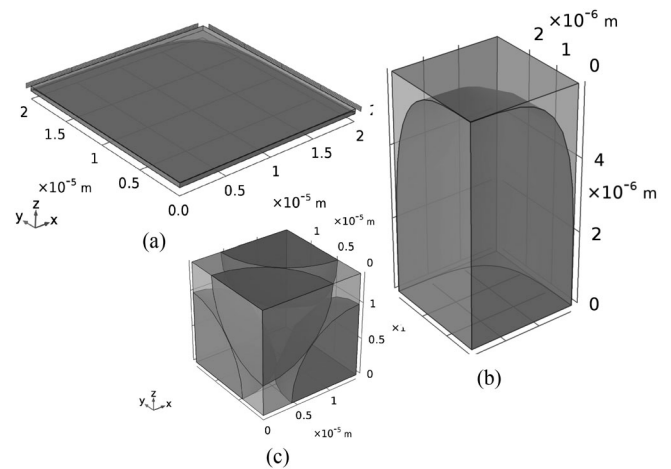
Fig. 2. The geometry of the (a) corneocyte, (b) keratinocyte. Due to the symmetry, only one-eighth was modeled. (c) Spheres in papillary dermis were arranged in the face-centered cubic arrangement and could not be described by including only one cell in the unit cell. Thus, for unit cell, we used a geometry which could periodically describe the geometry of the papillary dermis.

corneum. The pore formation was modeled on the keratinocytes and papillary dermis. The local transport region formation was modeled in the stratum corneum. The upper vessel plexus was assumed not be electroporated.

a) The Model of Pore Formation: Pore formation was included with Krassowska's asymptotic equation [51], [52]. We modeled pore formation on the keratinocytes [Fig. 2(b)] and spheres in the papillary dermis, [Fig. 2(c)]. The Krassowska's asymptotic equation cannot be analytically modeled, and thus we used the papillary dermis unit cell [Fig. 2(c)] and not the Hanai-Bruggeman equation. Papillary dermis was modeled as spheres in the face-centered cubic arrangement in volume fraction 0.74. To include Krassowska's asymptotic equation, we used the Weak Form Boundary Partial Differential Equation interface with

$$\frac{dN}{dt} = \alpha e^{\left(\frac{ITV}{Vep}\right)^2} \left(1 - \frac{N}{N_0} e^{-q\left(\frac{ITV}{Vep}\right)^2}\right), \qquad (3)$$

Symbol	Meaning	Value	Reference
ε_e	Dielectric permittivity of extracellular space (-)	80	[41]
σ_e	Electrical conductivity of extracellular space (S/m)	0.53	[41]
ε_m	Dielectric permittivity of cell membrane (-)	9.4	[41]
σ_{m0}	Initial electrical conductivity of cell membrane (S/m)	10^{-6}	[41]
ε_i	Dielectric permittivity of the intracellular space (-)	50	[41]
σ_i	Electrical conductivity of intracellular space (S/m)	0.12	[41]
d_m	Thickness of the cell membrane (nm)	7	[41]
V_{ep}	Electroporation threshold (mV)	258	[52]
α	Electroporation parameter ($m^{-2}s^{-1}$)	10^9	[52]
q	Electroporation constant	2.46	[52]
N_0	Equilibrium pore density (m^{-2})	1.5×10^9	[52]
R_p	Pore radius (nm)	0.75	[52]
V_{rest}	Resting membrane voltage (mV)	-50	[52]
σ_p	Pore electrical conductivity (S/m)	$\frac{\sigma_e - \sigma_i}{\ln(\frac{\sigma_e}{\sigma_i})}$	[52]
σ_m	Electrical conductivity of the electroporated cell membrane (S/m)	$\sigma_{m0} + \sigma_{ep}$	[52]

Fig. 3. Geometry of the local transport region (LTR) embedded in the stratum corneum (SC). The cylinder is the LTR. The outer region is the SC, unaffected by electric pulses. The image represents the size and density of the LTR at the end of low-voltage protocol at t = 1 s (a_{LV} was 443 μm and r_{LV} was 90 μm).

Symbol	Meaning	Value	Reference/method
ε_{LTR} (x, y, z)	Dielectric permittivity of the LTR (-)	x and y: 6.97×10^4, z: 5.46×10^2	Calculated with a unit cell with unelectroporated corneocyte
σ_{LTR} (isotropic)	Electrical conductivity of the LTR (S/m)	0.7	Optimized*
ε_{SC} (x, y, z)	Dielectric permittivity of the SC (-)	x and y: 6.97×10^4, z: 5.46×10^2	Calculated with a unit cell with unelectroporated corneocyte
σ_{SC} (x, y, z)	Electrical conductivity of the SC (S/m)	x and y: 1.38×10^{-2}, z: 2.29×10^{-4}	Calculated with a unit cell with unelectroporated corneocyte
r_{LV}	Radius of the LTR during LV protocol	Fig. 5(a)	[49]
r_{HV}	Radius of the LTR during HV protocol (μm)	10	[49]
a_{LV}	Length of the unit cell during LV protocol (μm)	443	[49]
a_{HV}	Length of the unit cell during LV protocol (μm)	177, 130, 100, 80, 60, 40, 30 (density in Fig. 6(a))	Optimized*
h_{LTR}	Height of the LTR (μm)	20	The same as the SC height
h_{SC}	Height of the SC (μm)	20	[41], [49], [50]

SC denotes stratum corneum and LTR local transport region.
*Optimization was done by comparing measured and simulated current and voltage drop on the skin.

where N denotes the density of the pores in the membrane, and N_0 in the unelectroporated membrane, *ITV* the induced transmembrane voltage, α, q, V_{ep} describe the characteristics of the electroporation process [51], [52], and t is time. The pore formation caused an increase in electrical conductivity of the cell membrane:

$$\sigma_{ep} = N \frac{2\pi r_p^2 \sigma_p d_m}{\pi r_p + 2d_m}, \qquad (4)$$

where r_p and σ_p were the radius and the internal electrical conductivity of a single pore, respectively, and d_m is the cell membrane thickness. The values of the parameters are in Table I. Increasing voltages were applied to the opposite boundaries of the unit cell in the *z*-direction. With increasing voltages, the density of the pores increased and consequently the induced transmembrane voltage. Dielectric tensor was calculated via the applied voltage and the current flowing through the unit cell. In the experiments, the pulses were applied in the *z*-direction, and pore formation was therefore primarily in the *z*-direction. Electrical conductivity in *x*- and *y*-directions and the relative permittivity in all three directions (*x, y, z*) were assumed unchanged and set to the unelectroporated values. We used the time domain study, the direct PARDISO solver and the physics controlled mesh with finer or extra fine element size.

b) The Model of the Local Transport Region Formation: The effect of electric pulses on the stratum corneum was modeled via local transport region (LTR) formation. The LTR was modeled as a cylinder in a unit cell (Fig. 3). We chose the size of the LTR as stated it [49] and adapted the density by changing the width and depth of the unit cell. In LV protocol, the LTR's diameter was chosen according to [49] and in HV protocol its density was adapted. Also here, we applied voltage on opposite boundaries in *x*- or *z*-direction, and via the electric

current calculated the dielectric tensor. Due to the symmetry, the properties in the *x*- and *y*-axis were the same. The geometric and dielectric properties of the stratum corneum and the LTR are in Table II. The dielectric properties of the electroporated stratum corneum were calculated under DC conditions since the applied pulses in LV and HV protocol were relatively long and the capacitive properties could be neglected. The size of the local transport region was taken from [49] and slightly adapted as we took into account that between pulses the LTRs could partially reseal which allowed a better description of our experimental data. We used frequency domain study, the direct PARDISO solver and the physics-controlled mesh with extra fine element size.
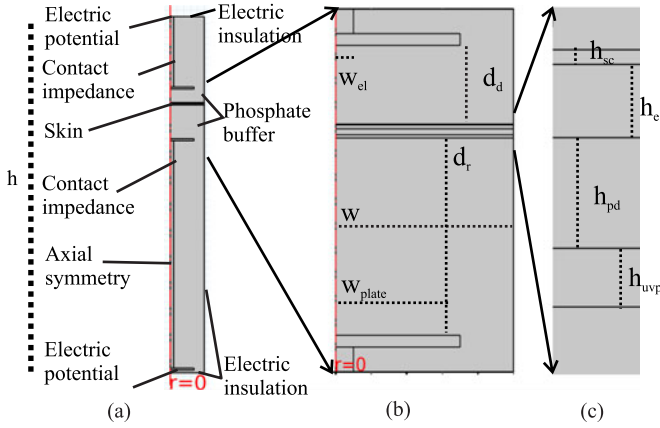
Fig. 4. Geometry of the Franz diffusion cell with marked boundary conditions and geometry. (a) the whole model, (b) zoomed to the area between the electrodes and (c) zoomed to the skin.

c) The Model of Franz Diffusion Cell: The Franz diffusion cell model was built according to the measurements and the data in [49]. In Comsol, we used 2D axisymmetric geometry. Although the properties of the skin were anisotropic, there was only 3% difference in the 2D and 3D calculation. However, the 3D calculation took approximately 6 hours and the 2D 1 minute. The boundary conditions and the geometric parameters of the Franz diffusion cell model are marked in Fig. 4. Between the electrodes, there was skin, immersed in phosphate buffer. On top of the electrodes, we applied the measured square voltage pulses. The other boundaries of the electrodes were assigned contact impedance to model the impedance of the double layer, formed at the electrode-liquid interface:

$$n \cdot J_1 = \frac{1}{\rho} (V_1 - V_2) \tag{5a}$$

$$n \cdot J_1 = \frac{1}{\rho} (V_1 - V_2) \tag{5b}$$

where ρ denotes the surface resistance and V_1 and V_2 are the voltages on each side of the boundary, n is the unit vector normal to the boundary surface, J is the electric current density. Properties of the stratum corneum were obtained from the model of the local transport region, properties of the epidermis from the unit cell of the keratinocyte and applied Krassowska's equation, properties of the papillary dermis from the unit cell of the spheres in the papillary dermis and applied Krassowska's asymptotic equation. We used the physics-controlled mesh with normal element size, time domain study and a direct MUMPS solver.

III. RESULTS

After choosing the size [49] [LV protocol – Fig. 5(a)] and adapting the density [HV protocol – Fig. 6(a)] of the local transport regions (LTRs) we obtained the corresponding equivalent electrical conductivity [Fig. 5(b) LV protocol and Fig. 6(b) HV protocol] and relative permittivity [Fig. 5(c) LV protocol and Fig. 6(c) HV protocol]. Fig. 5 thus shows results for the LV protocol – in Fig. 5(a) we can see how the radius of the LTR changed

during the treatment, in Fig. 5(b) the change in the equivalent electrical conductivity and Fig. 5(c) in equivalent relative permittivity in all three directions (x, y, and z). Fig. 6 shows results for the HV protocol – on Fig. 6(a) we can see how the density of LTRs changed during the treatment, in Fig. 6(b) the change in the equivalent electrical conductivity and Fig. 6(c) in equivalent relative permittivity in all three directions (x, y, and z).

Fig. 7 shows the electrical conductivity of lower layers (papillary dermis and epidermis) as calculated using the Krassowska's asymptotic equation. The electrical conductivity varies with different voltages on the boundary of the unit cell. Optimized values of the electrical conductivity were inserted in the Franz, diffusion model. Figs. 8 and 9 show the final results of our model – the simulated values of the voltage on the skin and the current and are compared with the measured values. In the LV protocol (Fig. 8) the simulated and measured values of the voltage drop on the skin [Fig. 8(a)] and the current [Fig. 8(b)] matched well while in the HV protocol [Fig. 9] the voltage drop on the skin corresponded well [Fig. 9(a)], but the current did not [Fig. 9(b)]. The simulated current underestimated the actual measurement for approximately 50%.

IV. DISCUSSION

A. Experimental Considerations

In the stratum corneum (SC), the local transport regions (LTRs) were formed. In the epidermis (E) and papillary dermis (PD), cell electroporation occurred as SC resistance decreased due to LTR formation, and consequently, electric field increased also in the lower layers. Electric pulses increase the permeability of blood vessels and induce vascular lock [55], [56]. However, we assumed there was no electroporation in the upper vessel plexus (UVP) as it is a layer of blood vessels and even if we assumed electroporation to occur there is a lack of experimental data on its dielectric properties after electroporation.

Change in dielectric properties of tissues can be used to describe and understand processes happening during electroporation. For assessing skin permeability, electric measurements were used before [17], [57]–[60]. Dielectric properties can be measured by dielectric spectroscopy [61], current-voltage measurements during electroporation [62], electric impedance tomography [63], and magnetic resonance electric impedance tomography [64]. The efficiency of electroporation can be monitored by measurements of the change in electrical conductivity [25], [65], [66]. When measuring dielectric properties of tissues, secondary effects can affect measurements – such as swelling of cells [67], forming of edema [65], loss of ions from the cells [62], vascular lock [55]. Thus, for the validation of our model, we used current-voltage measurements during pulse application when the secondary effects can still be largely neglected.

Skin hydration and the electrical conductivity of the liquid in which the skin is immersed was shown to have a large effect on skin impedance [68]. In our experiments, the dermatomed skin was well hydrated as it was immersed in phosphate buffer. We took hydration into account by increasing the electrical conductivity of LTRs to 0.7 S/m. This conductivity is in the same range as in [43] but is much higher than the electrical conductivity of
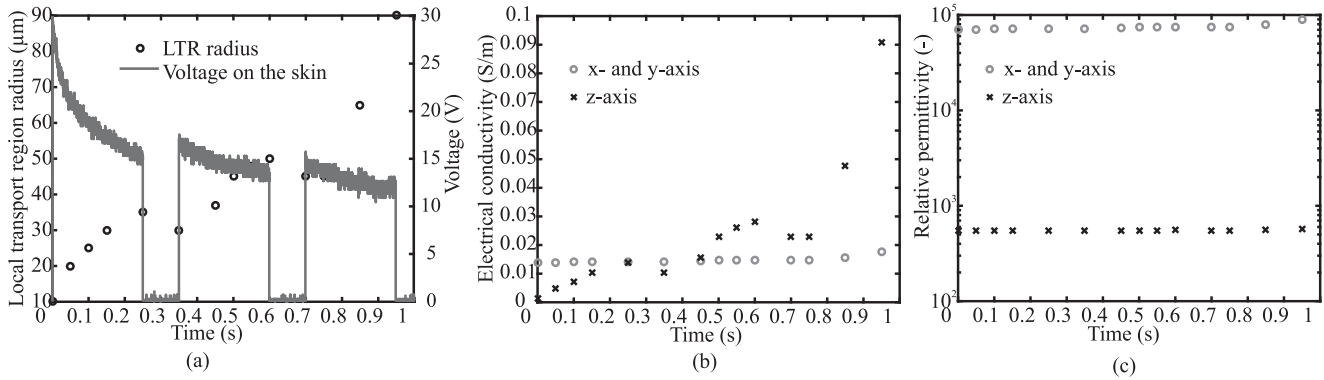
Fig. 5. Dynamics of local transport region (LTR) during low-voltage (LV) protocol. (a) LTR size and the corresponding voltage on the skin, (b) electrical conductivity and (c) relative permittivity change. The obtained values were then taken as equivalent dielectric properties of the whole stratum corneum. The axes correspond to the coordinate system in Fig. 3.
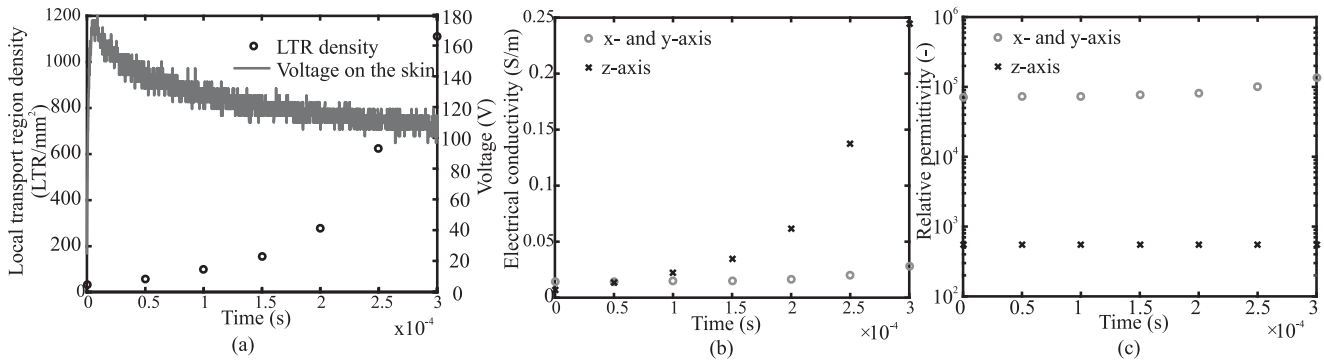
Fig. 6. Dynamics of local transport region (LTR) during high-voltage (HV) protocol. (a) LTR density and the corresponding voltage on the skin, (b) electrical conductivity and (c) relative permittivity change. The obtained values were then taken as equivalent dielectric properties of the whole stratum corneum. Please, notice the time-scale which is only 300 μs although the whole treatment took 2.5 ms. We assumed that all changes in the LTR density occur during the first pulse and afterwards there was no resealing or increasing of the LTR density. The axes correspond to the coordinate system in Fig. 3.
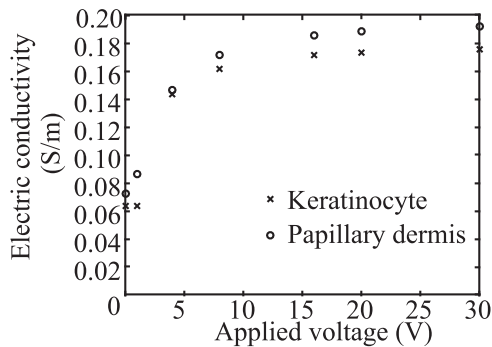
Fig. 7. Electrical conductivity as a function of voltage, applied to a unit cell of a keratinocyte or papillary dermis. Even before pulse formation, the unit cell has a certain conductivity which then increases as a function of applied voltage.

melted lipids (0.05 S/m [49]) which is relevant in the case of dry skin.

We assumed that the relative permittivity of the epidermis, papillary dermis and upper vessel plexus do not change due to electroporation since the applied pulses were long and the capacitive component of the layers at low frequencies is approximated

with an open circuit. The change in relative permittivity of the stratum corneum was based on the change in the geometry of the LTR.

The buffer used in the donor compartment was phosphate buffer, and in the receiver, it was phosphate buffered saline. They varied in the ionic composition and pH, but their electrical conductivity was the same (1 S/m). For our model, only the dielectric properties were important, and we modeled liquid in the donor and receiver compartment as the same buffer.

B. Pore Formation in Keratinocytes and Papillary Dermis

The Krassowska's asymptotic equation describes how the density of the pores changes as a function of applied voltage and time. It is a simplification of a theory of pore formation as it assumes all pores in the cell membrane are of the same size which is a justified approximation only for short nanosecond pulses. During longer pulses, the pores start to grow. For inclusion of an increase in pore radius, creation of stable macropores should be modeled [69], but the inclusion is computationally demanding. Therefore, we decided to calculate the change of electrical conductivity in the first few nanoseconds by Krassowska's asymptotic equation. As the sampling period of the current and voltage
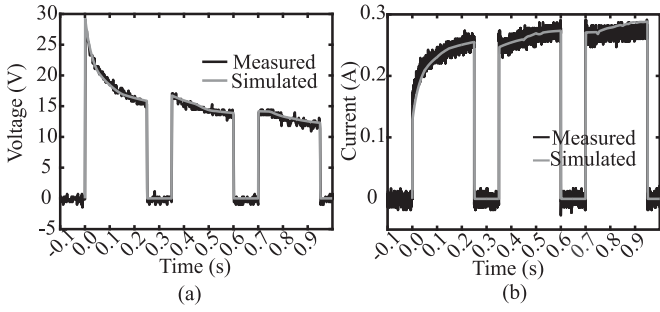
Fig. 8.   Measured and simulated (a) voltage on the skin and (b) current through the system during LV protocol.
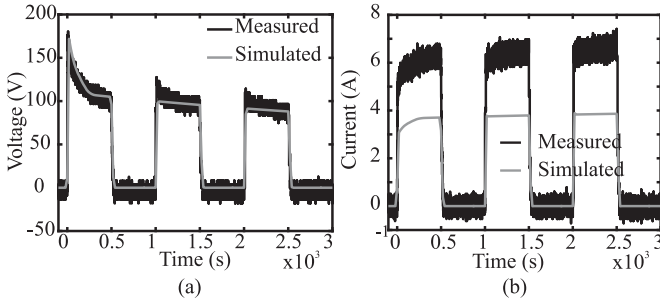
Fig. 9.   Measured and simulated (a) voltage on the skin and (b) current through the system during HV protocol.

measurements was much longer than nanoseconds, we assumed that the electrical conductivity of the papillary dermis and the epidermis changed immediately when the pulse was applied. We calculated the dielectric properties at $t = 0\,\mathrm{s}$ by the Krassowska's asymptotic equation. To avoid modeling pore growth, we simplified our model and adapted the bulk electrical conductivity of separate layers at the end of pulse application. The dielectric properties during pulse application were determined by interpolation between $t = 0\,\mathrm{s}$ and $t = 1\,\mathrm{s}$ (LV protocol) or $t = 2.5\,\mathrm{ms}$ (HV protocol). The changes in electrical conductivity of lower layers (papillary dermis and epidermis) had to be included; otherwise we could not describe the experimental measurements.

The initial electrical conductivity of the epidermis and papillary dermis was for the LV protocol approximated with Krassowska's equation when 0.07 V or 0.08 V were applied to the unit cell which corresponds to 69 mV or 71 mV of induced transmembrane voltage for corneocyte and papillary dermis, respectively. The initial electrical conductivity of the epidermis and papillary dermis was for the HV protocol approximated with Krassowska's equation when 3 V were applied to the unit cell which corresponds to 1.14 V or 1.24 V of induced membrane voltage for corneocyte and papillary dermis, respectively. The initial theoretical voltage drop at t = 0 s on the epidermis and papillary dermis was determined by treating skin as a voltage divider (right part of Fig. 10) on which there was a 30 V [LV protocol – initial peak of Fig. 8(a)] or 180 V [HV protocol – initial peak on Fig. 9(a)] voltage drop. Taking into account the geometry (thickness of layers, area 0.785 cm^2 [49], size of unit cells and corresponding number of unit cells in z-direction) and
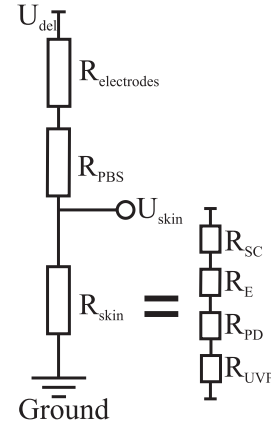

Fig. 10.   The equivalent circuit of the Franz diffusion cell. The electrode polarisation is represented only by resistance. Since we are delivering relatively long pulses, the capacitance due to a double layer which is in parallel with $R_{\mathrm{electrodes}}$, could be approximated as an open circuit and thus neglected. R_{skin} is represented by separate resistances of each layer. The voltage drop on the skin is thus distributed among R_{SC}, R_{E}, R_{PD} and R_{UVP}, according to the thickness and electric conductivity of each layer.

initial electrical conductivity of each layer before electroporation in z-direction (SC: 2.29×10^{-4} S/m, E: 6.36×10^{-2} S/m, PD: 7.19×10^{-2} S/m, UVP: 3.85×10^{-1} S/m) we calculated the resistance of each layer and a corresponding voltage drop on each layer. This calculated voltage drop was then used in the Krassowska's asymptotic model.

With HV protocol, the initial theoretical voltage drop on the epidermis and papillary dermis was 0.4 V, but a good agreement between measurements and model was achieved with 3 V. The initial electrical conductivity was thus higher than theoretically predicted. Higher initial electrical conductivity indicates that some defects were formed in the stratum corneum quickly and lower layers were exposed to a higher voltage than predicted.

In HV pulses, the change in electrical conductivity was the largest during the first pulse, and it changed only slightly during the following two pulses. Between pulses, there was some decrease in electrical conductivity present which indicates resealing of the cell membranes as defects in the stratum corneum were reported to reseal on a timescale of ms - hours [22].

C. Local Transport Region Formation in the Stratum Corneum

It was shown that short high-voltage pulses increase the density of the local transport regions (LTRs) while low-voltage long pulses increase the size of LTRs by Joule heating and lipid melting around the pre-existing defects [17]–[22]. The radius of the LTR during LV protocol increased from 10 μm to 90 μm and was taken from [49] and the values are within the ranges reported by [21], [22]. We assumed that LTRs reseal to some extent between pulses [Fig. 6(a)] although as with the HV protocol, it is possible that cells in the lower layers resealed as well. Since the pause during LV protocol was longer than during HV protocol (100 ms vs 500 μs), we modeled LTR resealing instead of corneocyte or papillary dermis resealing. The time course of recovery in skin electroporation ranges from a few ms up to

several hours [22]. Thus, we assumed that it is possible that LTR radii slightly decrease during the pause between pulses. Still, this is only an assumption – the increase in the resistance of the skin could as well be a consequence of resealing of the pores in the membranes of the cells in the lower layers. We have added the resealing in our model, and by doing so, we were able to describe the measurements of voltage and current more accurately.

The increase in electrical conductivity of SC during HV protocol was modeled by an increase in density of the LTRs while their radii stayed the same (10 μm). The modeled density of the LTR-s was high (up to 1200 LTRs/mm^2) in comparison to previously published studies ([43] and the references therein) (up to 9 LTR/mm^2). We tried decreasing the density of the LTRs down to the reported values, but the modeled voltage on the skin was 2-times higher than measured which indicates that with lower LTR density the predicted electrical conductivity of the skin is too low. Even with increasing the electrical conductivity of epidermis and papillary dermis to 1 S/m (electrical conductivity of the phosphate buffer), the voltage on the skin did not decrease enough to obtain voltage on the skin that would correspond to the measured values. This indicates that LTR density is most probably higher than expected.

D. Measurements and Simulation in the Franz Diffusion Cell

An equivalent circuit can represent the Franz diffusion cell (Fig. 10), where $R_{\text{electrodes}}$, R_{PBS} and R_{skin} denote the resistance of the double layer on the electrodes, phosphate buffer and skin, respectively. U_{del} is the voltage, delivered to the electrodes, and U_{skin} the voltage, measured on the skin. The double layer acts as an additional resistance in parallel to capacitance [53]. Since our pulses were relatively long, we assumed the capacitance as an open circuit, and only the resistance $R_{\text{electrodes}}$ was included in the equivalent circuit (Fig. 10). This additional resistance caused a drop of voltage on the electrodes, and the sample received less voltage than what was delivered to electrodes. In the case of LV protocol, the voltage drop on electrodes was significant in comparison to the applied voltage and voltage drop on the skin (around 1 V on the electrodes with delivered 45 V and 12–30 V on the skin). In the case of HV protocol, the voltage drop on the electrodes did not influence the results but was included for consistency. $R_{\text{electrodes}}$, R_{PBS}, U_{del}, and U_{skin} were known, which means that according to the voltage divider, R_{skin} is already determined:

$$R_{\text{skin}} = \frac{U_{\text{skin}} \left(R_{\text{electrodes}} + R_{PBS} \right)}{U_{\text{del}} - U_{\text{skin}}} \qquad (6)$$

The simulated voltage drop on the skin and current through the system after the LV protocol corresponded well with the measurements (Fig. 8). The fitting was obtained by adapting the electrical conductivities of separate layers until a good agreement was obtained between simulated and measured values. Taking into account that in LV protocol, the simulated and measured current match [Fig. 8(b)], our model was thus additionally validated.
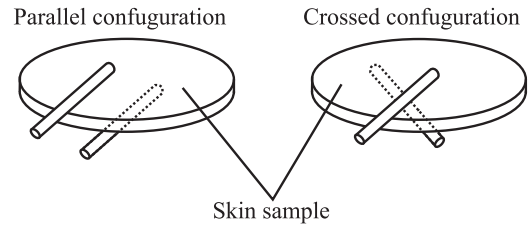
Fig. 11. Position of the measuring Cu electrodes. When in parallel, the electrodes were not directly one on top of another as they would squeeze the skin and change the thickness of the skin. When the electrodes were crossed, there was a preferential path for electric current.

In HV protocol, however, when we achieved a good agreement between simulated and measured voltage drop on the skin, the simulated and measured current did not match [Fig. 9(b)]. One possibility is additional processes, e.g., introduced by measuring Cu electrodes. Namely, when measuring the voltage drop on the skin, the Cu electrodes were in contact with skin. The electrodes were put on the skin between the donor and receiver part of the Franz diffusion chamber in two possible configurations: parallel and crossed (Fig. 11) (M. Reberšek, personal communication). Unfortunately, the exact position of the measuring electrodes was not noted during experiments and is thus not known. Crossed configuration introduced a preferential path for electric current since Cu is much more conductive than PBS or skin. It possible that there was localised heating and discharges present which caused the current to increase significantly, locally thus contributing to the overall current measured, but not causing a detectable voltage drop.

The shape of the voltage and current measurements reflects the different phenomena occurring during electroporation. The initial voltage drop and increase in current in the first few milliseconds is due to LTR formation in the stratum corneum. The emergence of LTRs increases the electric conductivity, but with increasing the radius of the LTRs, the effect slowly reaches a plateau. With decreasing resistance of the SC, the electric field increases in the lower layers of the skin. The prolonged decrease in voltage and increase in current is due to a slow but constant increase in the electric conductivity of lower layers due to pore formation in the cell membranes of the cells in the lower layers, i.e., electroporation.

From Table III we can see that HV protocol increased the electrical conductivity of all layers more than the LV protocol. In LV protocol, the delivered voltage was 45 V, and on the skin, it was 12 V–30 V (26%–66% of the delivered voltage). In HV protocol, the delivered voltage was 500 V, and on the skin, it was 100 V–180 V (20%–36% of the delivered voltage), which is much less than what was delivered to the skin in the LV protocol.

When electrodes are immersed in liquid, a double layer is formed at the electrode-liquid interface. The surface resistance due to the double layer changes with current density, electrode material, ions in the liquid. Interestingly, although it can significantly change the voltage the cells and tissues are exposed to, it is included only in a few models [70]. We used the values

TABLE III
GEOMETRIC AND DIELECTRIC PARAMETERS OF THE FRANZ DIFFUSION CELL MODEL, THEIR MEANING, VALUE AND REFERENCE

Parameter	Meaning	Value	Reference/Method
w	Radius of the skin sample (cm)	0.5	[49]
h_{sc}	Height of SC (μm)	20	[41], [49], [50]
h_e	Height of E (μm)	100	[41]
h_{pd}	Height of PD (μm)	140	[41]
h_{uvp}	Height of UVP (μm)	80	[41]
d_d	Distance between electrode in the donor solution and skin (cm)	0.2	[49]
d_r	Distance between electrode in the receiver solution and skin (cm)	0.5	[49]
T	Temperature of the FDC (°C)	37	[49]
w_{plate}	Radius of the plate on the electrode (mm)	3.5	[49]
w_{el}	Radius of the electrode (mm)	0.5	[49]
h	Height of the FDC (cm)	5.255	Measured
ρ_s	Surface resistance (Ωcm^2)	3.03	[53]
ε_{PBS}	Dielectric permittivity of the PBS(-)	80	[52]
σ_{PBS}	Electric conductivity of the PBS (S/m)	1	[49]
σ_{el}	Electric conductivity of the Pt electrodes (S/m)	9.43×10^6	[54]
$\varepsilon_{SC, LV}$ (x, y, z)	Dielectric permittivity of the SC after LV protocol (-)	Fig. 5(c)	Optimized*
$\sigma_{SC, LV}$ (x, y, z)	Electric conductivity of the SC after LV protocol (S/m)	Fig. 5(b)	Optimized*
$\varepsilon_{SC, HV}$ (x, y, z)	Dielectric permittivity of the SC after HV protocol (-)	Fig. 6(c)	Optimized*
$\sigma_{SC, HV}$ (x, y, z)	Electrical conductivity of the SC after HV protocol (S/m)	Fig. 6(b)	Optimized*
ε_E (x, y, z)	Dielectric permittivity of the E (-)	x and y: 4.83×10^3, z: 1.52×10^4	The unit-cell model with keratinocyte
$\sigma_{E, LV}$ (x, y, z)	Electrical conductivity of the E after LV protocol (S/m)	x and y: 5.82×10^{-2}, z: 6.36×10^{-2} at $t = 0$ and 7.69×10^{-2} at $t = 1$ s	Optimized*
$\sigma_{E, HV}$ (x, y, z)	Electrical conductivity of the E after HV protocol (S/m)	x and y: 5.82×10^{-2}, z: 0.12 at $t = 0$ and 0.17 at $t = 2.5$ ms	Optimized*
ε_{PD} (isotropic)	Dielectric permittivity of the PD (-)	1.62×10^4	The Hanai-Bruggeman equation
$\sigma_{PD, LV}$ (isotropic)	Electrical conductivity of the PD after LV protocol (S/m)	0.086 at $t = 0$, 0.096 at $t = 1$ s	Optimized*
$\sigma_{PD, HV}$ (isotropic)	Electrical conductivity of the PD after HV protocol (S/m)	0.13 at $t = 0$, 0.18 at t = 2.5 ms	Optimized*
ε_{UVP} (x, y, z)	Dielectric permittivity of the UVP (-)	x: 4.92×10^4, y and z: 6.40×10^4	The Hanai-Bruggeman equation
σ_{UVP} (x, y, z)	Electrical conductivity of the UVP (S/m)	0.42, 0.39, 0.39	The Hanai-Bruggeman equation

(x, y and z) denote the anisotropic properties in x-, y- and z-direction. SC denotes stratum corneum, E epidermis, PD papillary dermis, UVP upper vessel plexus, PBS phosphate buffer, and FDC the Franz diffusion cell. Dielectric permittivity of material was not relevant as it did not influence the results since the pulses were relatively long.
*Optimization was done by comparing measured and simulated current and voltage drop on the skin.

from a study [53] where they used Pt electrodes. However, they measured resistance in saline instead of phosphate buffer, and their electrodes were smaller, which could affect the results. More concerning is that they delivered much lower voltage than the voltage delivered in our experiments. The chemistry of high voltage pulses delivered to an electrolyte is still not well understood [71], with few studies focusing on the release of metal from electrodes [72] and possible reactions happening on or near the electrodes [73], [74].

The drawback of our model is that there are several combinations of parameters which can offer good agreement with the current and voltage measurements – e.g., we could change the dynamics of local transport region formation and describe the exponential decrease of voltage drop on the skin with different dynamics of change of electrical conductivity of lower layers. We could compensate for the different geometry of the LTRs with a different electric conductivity of the LTR. The model, obtained in this study, is not trying to replicate the experimental results precisely but serves as a proof of principle how cell level electroporation can be expanded to tissue level electroporation. For a more precise determination of parameters, more experiments and electrical measurements are needed as the values of several parameters are currently only estimated (for example, dielectric properties of separate layers during electroporation).

The advantage of using our model is that we can use it to describe any tissue with any resolution we want, we can include blood vessels, lymphatic system, different types of cells in a tissue etc. The only requirement is that the geometric and dielectric properties of the tissues' microstructure are known. When generalizing the properties to a tissue level, the computations are quick and enable inclusion of other physical phenomena – for example, heating or chemical reactions.

V. CONCLUSION

Our model connects the processes occurring at the level of cell membranes (pore formation), and at the level of a skin layer (formation of local transport region in the stratum corneum), with the level of tissue (skin layers) and even level of organs (skin). It enables description and prediction of changes in dielectric properties of tissue while taking into account microstructure and processes on a much smaller scale and simultaneously keeping the computational times reasonable. Not just skin but any other tissue could be described similarly, as long as its microstructure is known. Our model thus offers a step forward in modeling of electroporation at different spatial scales.

REFERENCES

[1] T. Kotnik *et al.*, "Cell membrane electroporation- Part 1: The phenomenon," *IEEE Elect. Insul. Mag.*, vol. 28, no. 5, pp. 14–23, Sep./Oct. 2012.

[2] T. Y. Tsong, "Electroporation of cell membranes," *Biophys. J.*, vol. 60, no. 2, pp. 297–306, Aug. 1991.

[3] T. Kotnik *et al.*, "Electroporation-based applications in biotechnology," *Trends Biotechnol.*, vol. 33, no. 8, pp. 480–488, Jun. 2015.

[4] S. Mahnič-Kalamiza *et al.*, "Electroporation in food processing and biorefinery," *J. Membrane Biol.*, vol. 247, no. 12, pp. 1279–1304, Dec. 2014.

[5] S. Toepfl *et al.*, "Overview of pulsed electric fields processing for food," in *Emerging Technologies for Food Processing*, Amsterdam, The Netherlands: Elsevier, 2014, pp. 93–114.

[6] M. L. Yarmush *et al.*, "Electroporation-Based technologies for medicine: Principles, applications, and challenges," *Annu. Rev. Biomed. Eng.*, vol. 16, no. 1, pp. 295–320, Jul. 2014.

[7] A. I. Daud *et al.*, "Phase I trial of interleukin-12 plasmid electroporation in patients with metastatic melanoma," *J. Clin. Oncol.*, vol. 26, no. 36, pp. 5896–5903, 2008.

[8] R. Heller and L. C. Heller, "Gene electrotransfer clinical trials," in *Advances in Genetics*, Amsterdam, The Netherlands: Elsevier, 2015, vol. 89, pp. 235–262.

[9] C. L. Trimble *et al.*, "Safety, efficacy, and immunogenicity of VGX-3100, a therapeutic synthetic DNA vaccine targeting human papillomavirus 16 and 18 E6 and E7 proteins for cervical intraepithelial neoplasia 2/3: a randomised, double-blind, placebo-controlled phase 2b trial," *The Lancet*, vol. 386, no. 10008, pp. 2078–2088, Nov. 2015.

[10] S. Vasan *et al.*, "In Vivo electroporation enhances the immunogenicity of an HIV-1 DNA vaccine candidate in healthy volunteers," *PLoS ONE*, vol. 6, no. 5, May 2011, Art. no. e19252.

[11] A. -R. Denet *et al.*, "Skin electroporation for transdermal and topical delivery," *Adv. Drug Del. Rev.*, vol. 56, no. 5, pp. 659–674, Mar. 2004.

[12] B. Zorec *et al.*, "Active enhancement methods for intra- and transdermal drug delivery: A review," *Zdravniski Vestnik*, vol. 82, no. 5, pp. 339–56, 2013.

[13] C. Jiang *et al.*, "A review of basic to clinical studies of irreversible electroporation therapy," *IEEE Trans. Biomed. Eng.*, vol. 62, no. 1, pp. 4–20, Jan. 2015.

[14] H. J. Scheffer *et al.*, "Irreversible electroporation for nonthermal tumor ablation in the clinical setting: A systematic review of safety and efficacy," *J. Vascular Interventional Radiol.*, vol. 25, no. 7, pp. 997–1011, Jul. 2014.

[15] B. Mali *et al.*, "Antitumor effectiveness of electrochemo-therapy: A systematic review and meta-analysis," *Eur. J. Surg. Oncol.*, vol. 39, pp. 4–16, 2013.

[16] D. Miklavčič *et al.*, "Electrochemotherapy: From the drawing board into medical practice," *Biomed. Eng. OnLine*, vol. 13, no. 1, p. 29, 2014.

[17] R. Vanbever *et al.*, "Comparison of the effects of short, high-voltage and long, medium-voltage pulses on skin electrical and transport properties," *J. Controlled Release*, vol. 60, no. 1, pp. 35–47, Jun. 1999.

[18] M. R. Prausnitz *et al.*, "Imaging regions of transport across human stratum corneum during High-Voltage and Low-Voltage exposures," *J. Pharm. Sci.*, vol. 85, no. 12, pp. 1363–1370, Dec. 1996.

[19] U. F. Pliquett *et al.*, "Local transport regions (LTRs) in human stratum corneum due to long and short 'high voltage' pulses," *Bioelectrochem. Bioenergetics*, vol. 47, no. 1, pp. 151–161, Nov. 1998.

[20] J. C. Weaver *et al.*, "Theory of electrical creation of aqueous pathways across skin transport barriers," *Adv. Drug Del. Rev.*, vol. 35, no. 1, pp. 21–39, Jan. 1999.

[21] U. F. Pliquett *et al.*, "Imaging of fluorescent molecule and small ion transport through human stratum corneum during high voltage pulsing: Localized transport regions are involved," *Biophys. Chem.*, vol. 58, no. 1/2, pp. 185–204, Jan. 1996.

[22] T. R. Gowrishankar *et al.*, "Changes in skin structure and electrical properties following high voltage exposure," *Ann. New York Acad. Sci.*, vol. 888, pp. 183–194, Oct. 1999.

[23] D. Šel *et al.*, "Sequential finite element model of tissue electropermeabilization," *IEEE Trans. Biomed. Eng.*, vol. 52, no. 5, pp. 816–827, May 2005.

[24] S. Čorović *et al.*, "In Vivo muscle electroporation threshold determination: realistic numerical models and In Vivo experiments," *J. Membrane Biol.*, vol. 245, no. 9, pp. 509–520, Sep. 2012.

[25] R. E. Neal 2nd *et al.*, "Experimental characterization and numerical modeling of tissue electrical conductivity during pulsed electric fields for irreversible electroporation treatment planning," *IEEE Trans. Biomed. Eng.*, vol. 59, no. 4, pp. 1076–1085, Apr. 2012.

[26] N. Pavšelj and D. Miklavčič, "Numerical modeling in electroporation-based biomedical applications," *Radiol. Oncol.*, vol. 42, no. 3, pp. 159–168, 2008.

[27] K. Dymek *et al.*, "Modeling electroporation of the non-treated and vacuum impregnated heterogeneous tissue of spinach leaves," *Innov. Food Sci. Emerging Technol.*, vol. 29, pp. 55–64, May 2015.

[28] M. Essone Mezeme *et al.*, "A numerical analysis of multicellular environment for modeling tissue electroporation," *Appl. Phys. Lett.*, vol. 100, no. 14, 2012, Art. no. 143701.

[29] R. P. Joshi *et al.*, "Model assessment of cell membrane breakdown in clusters and tissues under High-Intensity electric pulsing," *IEEE Trans. Plasma Sci.*, vol. 36, no. 4, pp. 1680–1688, Aug. 2008.

[30] D. A. Stewart Jr. *et al.*, Cylindrical cell membranes in uniform applied electric fields: Validation of a transport lattice method," *IEEE Trans. Biomed. Eng.*, vol. 52, no. 10, pp. 1643–1653, Oct. 2005.

[31] T. R. Gowrishankar and J. C. Weaver, "An approach to electrical modeling of single and multiple cells," in *Proc. Nat. Acad. Sci.*, Mar. 2003, vol. 100, no. 6, pp. 3203–3208.

[32] J. Dermol and D. Miklavčič, "Predicting electroporation of cells in an inhomogeneous electric field based on mathematical modeling and experimental CHO-cell permeabilization to propidium iodide determination," *Bioelectrochemistry*, vol. 100, pp. 52–61, Dec. 2014.

[33] J. Dermol and D. Miklavčič, "Mathematical models describing chinese hamster ovary cell death due to electroporation in vitro," *J. Membrane Biol.*, vol. 248, no. 5, pp. 865–881, Oct. 2015.

[34] A. Golberg and B. Rubinsky, "A statistical model for multidimensional irreversible electroporation cell death in tissue," *Biomed. Eng. OnLine*, vol. 9, no. 1, p. 13, 2010.

[35] A. T. Esser *et al.*, "Towards solid tumor treatment by nanosecond pulsed electric fields," *Technol. Cancer Res. Treatment*, vol. 8, no. 4, pp. 289–306, Aug. 2009.

[36] A. Ramos, "Effect of the electroporation in the field calculation in biological tissues," *Artif. Organs*, vol. 29, no. 6, pp. 510–513, Jun. 2005.

[37] A. Ramos *et al.*, "A new computational approach for electrical analysis of biological tissues," *Bioelectrochemistry*, vol. 59, no. 1/2, pp. 73–84, Apr. 2003.

[38] R. Susil *et al.*, "Electric field induced transmembrane potential depends on cell density and organization," *Electro- Magnetobiol.*, vol. 17, no. 3, pp. 391–399, 1998.

[39] A. Ramos, "Improved numerical approach for electrical modeling of biological cell clusters," *Med. Biol. Eng. Comput.*, vol. 48, no. 4, pp. 311–319, Apr. 2010.

[40] M. Pavlin *et al.*, "Dependence of induced transmembrane potential on cell density, arrangement, and cell position inside a cell system," *IEEE Trans. Biomed. Eng.*, vol. 49, no. 6, pp. 605–612, Jun. 2002.

[41] S. Huclova *et al.*, "Modelling and validation of dielectric properties of human skin in the MHz region focusing on skin layer morphology and material composition," *J. Phys. Appl. Phys.*, vol. 45, no. 2, Jan. 2012, Art. no. 025301.

[42] S. Huclova *et al.*, "Modelling effective dielectric properties of materials containing diverse types of biological cells," *J. Phys. Appl. Phys.*, vol. 43, no. 36, Sep. 2010, Art. no. 365405.

[43] N. Pavšelj and D. Miklavčič, "Numerical models of skin electropermeabilization taking into account conductivity changes and the presence of local transport regions," *IEEE Trans. Plasma Sci.*, vol. 36, no. 4, pp. 1650–1658, Aug. 2008.

[44] N. Pavšelj *et al.*, "A numerical model of skin electropermeabilization based on In Vivo experiments," *Ann. Biomed. Eng.*, vol. 35, no. 12, pp. 2138–2144, Nov. 2007.

[45] S. Becker *et al.*, "Transdermal transport pathway creation: Electroporation pulse order," *Math. Biosci.*, vol. 257, pp. 60–68, Nov. 2014.

[46] S. M. Becker and A. V. Kuznetsov, "Local temperature rises influence in vivo electroporation pore development: A numerical stratum corneum lipid phase transition model," *J. Biomech. Eng.*, vol. 129, no. 5, pp. 712–721, 2007.

[47] Y. A. Chizmadzhev *et al.*, "Electrical properties of skin at moderate voltages: contribution of appendageal macropores," *Biophys. J.*, vol. 74, no. 2, pp. 843–856, Feb. 1998.

[48] S. Becker, "Transport modeling of skin electroporation and the thermal behavior of the stratum corneum," *Int. J. Thermal Sci.*, vol. 54, pp. 48–61, Apr. 2012.

[49] B. Zorec *et al.*, Skin electroporation for transdermal drug delivery: The influence of the order of different square wave electric pulses," *Int. J. Pharmaceutics*, vol. 457, no. 1, pp. 214–223, Nov. 2013.

[50] U. Jacobi *et al.*, "Porcine ear skin: An in vitro model for human skin," *Skin Res. Technol.*, vol. 13, no. 1, pp. 19–24, Feb. 2007.

[51] J. C. Neu and W. Krassowska, "Asymptotic model of electroporation," *Phys. Rev. E*, vol. 59, no. 3, pp. 3471–3482, Mar. 1999.

[52] L. Rems *et al.*, "Cell electrofusion using nanosecond electric pulses," *Sci. Rep.*, vol. 3, 2013, Art. no. 3382.

[53] S. Mayer *et al.*, "Faradic resistance of the electrode/electrolyte interface," *Med. Biol. Eng. Comput.*, vol. 30, no. 5, pp. 538–542, Sep. 1992.

[54] R. A. Serway, *Principles of Physics*, 2nd ed. Fort Worth, TX, USA: Saunders, 1998.

[55] G. Serša *et al.*, "Vascular disrupting action of electroporation and electrochemotherapy with bleomycin in murine sarcoma," *Brit. J. Cancer*, vol. 98, no. 2, pp. 388–398, Jan. 2008.

[56] N. Dujardin *et al.*, "In vivo assessment of skin electroporation using square wave pulses," *J. Controlled Release.*, vol. 79, no. 1–3, pp. 219–227, Feb. 2002.

[57] S. A. Gallo *et al.*, Characterization of electric-pulse-induced permeabilization of porcine skin using surface electrodes," *Biophys. J.*, vol. 72, no. 6, pp. 2805–2811, Jun. 1997.

[58] U. Pliquett and C. Gusbeth, "Surface area involved in transdermal transport of charged species due to skin electroporation," *Bioelectrochemistry*, vol. 65, no. 1, pp. 27–32, Dec. 2004.

[59] U. Pliquett and M. R. Prausnitz, "Electrical impedance spectroscopy for rapid and noninvasive analysis of skin electroporation," *Methods Mol. Med.*, vol. 37, pp. 377–406, 2000.

[60] U. Pliquett, "Mechanistic studies of molecular transdermal transport due to skin electroporation," *Adv. Drug Del. Rev.*, vol. 35, no. 1, pp. 41–60, Jan. 1999.

[61] J. Zhuang and J. F. Kolb, "Time domain dielectric spectroscopy of nanosecond pulsed electric field induced changes in dielectric properties of pig whole blood," *Bioelectrochemistry*, vol. 103, pp. 28–33, Jun. 2015.

[62] M. Pavlin *et al.*, "Effect of cell electroporation on the conductivity of a cell suspension," *Biophys. J.*, vol. 88, no. 6, pp. 4378–4390, Jun. 2005.

[63] Y. Granot and B. Rubinsky, "Methods of optimization of electrical impedance tomography for imaging tissue electroporation," *Physiol. Meas.*, vol. 28, no. 10, pp. 1135–1147, Oct. 2007.

[64] M. Kranjc *et al.*, "Magnetic resonance electrical impedance tomography for measuring electrical conductivity during electroporation," *Physiol. Meas.*, vol. 35, no. 6, pp. 985–996, Jun. 2014.

[65] A. Ivorra *et al.*, "In vivo electrical conductivity measurements during and after tumor electroporation: Conductivity changes reflect the treatment outcome," *Phys. Med. Biol.*, vol. 54, no. 19, pp. 5949–5963, Oct. 2009.

[66] D. Cukjati *et al.*, "Real time electroporation control for accurate and safe in vivo non-viral gene therapy," *Bioelectrochemistry*, vol. 70, no. 2, pp. 501–507, May 2007.

[67] M. B. Sano *et al.*, "Towards the creation of decellularized organ constructs using irreversible electroporation and active mechanical perfusion," *Biomed. Eng. OnLine*, vol. 9, no. 1, p. 83, 2010.

[68] L. Davies *et al.*, "Modelling the effect of hydration on skin conductivity," *Skin Res. Technol.*, no. 23, pp. 363–368, 2016.

[69] K. C. Smith *et al.*, "Model of creation and evolution of stable electropores for DNA delivery," *Biophys. J.*, vol. 86, no. 5, pp. 2813–2826, May 2004.

[70] D. Šel *et al.*, "Finite-element modeling of needle electrodes in tissue from the perspective of frequent model computation," *IEEE Trans. Biomed. Eng.*, vol. 50, no. 11, pp. 1221–1232, Nov. 2003.

[71] D. E. Chafai *et al.*, "Assessment of the electrochemical effects of pulsed electric fields in a biological cell suspension," *Bioelectrochemistry*, vol. 106, pp. 249–257, Dec. 2015.

[72] R. Rodaite-Riseviciene *et al.*, "Release of iron ions from the stainless steel anode occurring during High-Voltage pulses and its consequences for cell electroporation technology," *IEEE Trans. Plasma Sci.*, vol. 42, no. 1, pp. 249–254, Jan. 2014.

[73] G. Saulis *et al.*, "Electrochemical processes during High-Voltage electric pulses and their importance in food processing technology," in *Advances in Food Biotechnology*, R. V. Rai, Ed. Chichester, U.K.: Wiley, 2015, pp. 575–592.

[74] G. Pataro *et al.*, "On the modelling of the electrochemical phenomena at the electrode-solution interface of a PEF treatment chamber: Effect of electrical parameters and chemical composition of model liquid food," *J. Food Eng.*, vol. 165, pp. 45–51, Nov. 2015.

Paper 6

Title: **Connecting the in vitro and in vivo experiments in electrochemotherapy: Modelling cisplatin transport in mouse melanoma using the dual-porosity**

Authors: Janja Dermol-Černe, Janja Vidmar, Janez Ščančar, Katja Uršič, Gregor Serša, Damijan Miklavčič

Paper 6

Title: **Connecting the in vitro and in vivo experiments in electrochemotherapy: Modelling cisplatin transport in mouse melanoma using the dual-porosity**

Connecting the in vitro and in vivo experiments in electrochemotherapy: Modeling cisplatin transport in mouse melanoma using the dual-porosity model

Janja Dermol-Černe[1], Janja Vidmar[2], Janez Ščančar[2], Katja Uršič[3], Gregor Serša[3,4], Damijan Miklavčič[1]

[1]University of Ljubljana, Faculty of Electrical Engineering, Tržaška cesta 25, 1000 Ljubljana, Slovenia

[2]Jozef Stefan Institute, Department of Environmental Sciences, Jamova cesta 39, 1000 Ljubljana, Slovenia

[3]Institute of Oncology Ljubljana, Department of Experimental Oncology, Zaloška cesta 2, 1000 Ljubljana, Slovenia

[4]University of Ljubljana, Faculty of Health Sciences, Zdravstvena pot 5, 1000 Ljubljana

Corresponding author: Damijan Miklavčič (Damijan.miklavcic@fe.uni-lj.si)

Declarations of interest: none

Abstract

In electrochemotherapy two conditions have to be met to be successful – the electric field of sufficient amplitude and sufficient uptake of chemotherapeutics in the tumor. Current treatment plans only take into account critical electric field to achieve cell membrane permeabilization. However, permeabilization alone does not guarantee uptake of chemotherapeutics and consequently successful treatment. In our study, we described the transport of cisplatin in vivo based on experiments performed in vitro. In vitro, a spectrum of parameters can be explored without ethical issues. In the experimental part of our study, we performed in vitro and in vivo experiments. Mouse melanoma B16-F1 cell suspension and inoculated B16-F10 tumors were exposed to electric pulses in the presence of chemotherapeutic cisplatin. The uptake of cisplatin was measured by inductively coupled plasma mass spectrometry. In the modeling part of our study, we modeled the transport with the dual-porosity model which is based on the diffusion equation, connects pore formation with membrane permeability, and includes transport between several compartments. In our case, there were three compartments - tumor cells, interstitial fraction and peritumoral region. Our hypothesis was that in vitro permeability coefficient can be introduced in vivo, as long as tumor physiology is taken into account. A transformation from in vitro to in vivo was possible by introducing a transformation coefficient which takes into account in vivo characteristics, i.e., smaller available area of the plasma membrane for transport due to cell density, and presence of cell-matrix in vivo, reducing drug mobility. Our model offers a step forward to connecting transport models at the cell level to the tissue level.

Keywords: electrochemotherapy, drug delivery, transport, modelling, dual-porosity model

1. Introduction

When biological cells are exposed to short high-voltage pulses, the permeability of the cell membrane increases, presumably due to pore formation following electroporation. As a result, membrane-impermeant molecules can pass the membrane [1–4], presumably through newly formed pores. If cells recover, it is called reversible electroporation. If the damage is too severe and cells die, it is called irreversible electroporation. Electroporation is used in biotechnology [5], food processing [6,7] and medicine [8,9], e.g. electrochemotherapy [10], gene electrotransfer [11,12], irreversible electroporation as an ablation technique [13,14] and transdermal drug delivery [15,16].

In electrochemotherapy transport of chemotherapeutics is critical for a successful treatment. In standard electrochemotherapy treatment, after intravenous or intratumoral injection of chemotherapeutic delivered electric pulses enhance the uptake of chemotherapeutics into tumor cells [17–19]. In electrochemotherapy, chemotherapeutics cisplatin and bleomycin are commonly used as described in the Standard Operating Procedures [18]. Starting in the late 1980s [20–22] with preclinical experiments, followed by clinical studies [23,24], intratumoral injection of cisplatin was introduced into the Standard Operating Procedures of the electrochemotherapy [18] and is now a well-established therapy in clinics across Europe [10]. Because the mass of cisplatin can be determined relatively easy, we used cisplatin in our study. Cisplatin enters cells by passive (diffusion) as well as active (endocytosis, pinocytosis, macrocytosis, membrane transporters) mechanisms [25–27]. Tumor cells can become resistant to cisplatin due to several mechanisms; modified

transport or detoxification, or increased DNA damage repair [27]. However, if the mechanism of resistance depends on membrane restriction of cisplatin uptake or increased pumping out of the cell, the resistant and non-resistant cells responded similarly to electroporation in vitro [28]. The situation in vivo was different, as electroporation was more effective on parental than cisplatin-resistant tumors, and it can only be hypothesized that additional factors could be present. Cisplatin is known to have negative side effects, among them nephrotoxicity, ototoxicity, nausea, depending on the cisplatin concentration and administration of the drug [29]. When injected, it accumulates in different organs (blood, liver, kidneys, and brain) [30]. Thus, electrochemotherapy offers a possibility to deliver lower dose than in chemotherapy while increasing local effectiveness. When treating patients with electrochemotherapy, we can follow standard operating procedures where electrode geometry, parameters of electric pulses and chemotherapeutic dose are predefined [18]. When tumors are outside the standard parameters, we can use variable electrode configuration [31]. With variable electrode configuration, we need a treatment plan where the position of the electrodes and electric pulse parameters are optimized to offer sufficient tumor coverage with above-threshold electric field [32–36]. Current treatment planning procedure could be upgraded by introducing a model of transport to the treatment plan. In this case, the spatially and temporally dependent number of intracellular cisplatin molecules could be predicted. Number of bleomycin molecules which must enter the cell to cause cell death has already been determined to be a few thousand [37]. If a similar dependency, i.e., a necessary number of molecules for cell death, would also be revealed for cisplatin, treatment efficacy could be more precisely predicted.

Usually, experiments are first performed in vitro and then translated to the in vivo environment. However, it is difficult to compare the transport during electroporation in vivo and in vitro. In in vitro experiments with single cell suspensions, the solute surrounds the cells, and the transport of solute occurs via diffusion. Solute can pass cell membrane where the membrane is permeabilized. The transport in the extracellular space is not limited. If there is enough of solute in the extracellular space, the transport stops when a cell membrane reseals after electroporation. The transport through the membrane can be directly linked to the cell membrane permeability [38]. In vivo, the initial solute concentration varies spatially. All the solute available can enter cells before the membrane reseals and although cell membrane is still permeable, it does not enter cells anymore, i.e., the extracellular compartment can be locally depleted. The transport of solute occurs via diffusion and convection [39]. Cells are close together which decreases the possible area for the uptake and decreases the induced transmembrane voltage due to electric field shielding [40]. Already in spheroids, it was shown that transport of small molecules was spatially heterogeneous, cells inside the spheroid contained less of solute than cells at the rim of the spheroid due to established concentration gradient [39,41]. Electric pulses cause vasoconstriction [42] which limits the transport of solute in or out of a tumor and prolongs the exposure of the tumor to chemotherapeutic. In a tumor, increased interstitial pressure, heterogeneous perfusion, defective lymphatic circulation, binding of the drug to non-target molecules and metabolism additionally affect the transport [43–45].

Modeling is advantageous since it decreases the number of necessary experiments and facilitates understanding of the underlying processes. Several models of the increased uptake of molecules after electroporation exist. For example, statistical models which describe the data well but do not include

specific transport mechanisms [46], the kinetic scheme of electroporation [47,48], (electro)diffusion through a permeable membrane or a single pore [49–53] and pharmacokinetic models [54,55]. We decided to use the dual-porosity model [38,56] which is based on the diffusion equation, connects pore formation with membrane permeability, and includes transport between several compartments – in our case between intracellular space, interstitial tumor fraction and peritumoral environment, and can also include thermal relations [57].

In our study, we focused on the electrochemotherapy and modeling of the drug transport after delivery of electric pulses, i.e., electroporation. Our hypothesis was that in vitro membrane permeability coefficients can be used to predict the transport of cisplatin in in vivo experiments. We used cisplatin as its intracellular mass can be determined via measuring the mass of Pt by inductively coupled plasma mass spectrometry [58] which is a very sensitive and precise method. We exposed suspension of mouse melanoma cells to electric pulses in the presence of chemotherapeutic cisplatin and measured the intracellular mass of Pt. We used the dual-porosity model to calculate the in vitro permeability coefficient as a function of pulse number and electric field. We performed in vivo experiments on mouse melanoma tumors and measured the intracellular and extracellular Pt mass, the mass of Pt in the serum, the mass of Pt bound to DNA and components other than DNA (i.e., proteins and lipids). We built a 3D numerical model of a tumor and by using the in vitro permeability coefficient predicted the mass of Pt in a tumor. A transformation from in vitro to in vivo was possible by introducing a transformation coefficient which takes into account the smaller available area of cell membrane for transport due to cell density, and presence of cell-matrix in vivo. Our model can describe the amount of intracellular Pt and Pt in the interstitial fraction after electroporation. We offer a step forward in connecting the transport at the cell level (in vitro) with the tissue level (in vivo) which could be eventually used in treatment planning.

2. Materials and Methods

2.1. In vitro experiments

2.1.1 Cell preparation

Mouse skin melanoma cell line B16-F1 was grown until 80% confluency in an incubator (Kambič, Slovenia) at 37°C and humidified 5% CO_2 in Dulbecco's Modified Eagle's Medium (DMEM, cat. no. D5671, 13.77 mS/cm 317-351 mOs/kg). The cell line was tested to be mycobacterium free. DMEM was supplemented with 10% fetal bovine serum (cat. no. F7524), 2 mM L-glutamine (cat. no. G7513) and antibiotics (50 μg/mL gentamycin (cat. no. G1397), 1 U/mL penicillin-streptomycin (cat. no. P11-010, PAA, Austria)) and was in this composition also used as electroporation buffer and for dilution of the samples.

The cell suspension was prepared by detaching the cells by 10x trypsin-EDTA (cat. no T4174), diluted 1:9 in Hank's basal salt solution (cat. no. H4641). Trypsin was inactivated with the DMEM containing 10% fetal bovine serum. For electroporation, cells were centrifuged (5 min, 180g, 21°C) and resuspended in

DMEM containing 10% fetal bovine serum at concentration 2.2×10^7 cells/mL. The chemicals were from Sigma Aldrich, Germany, unless noted otherwise.

2.1.2. Cell electroporation

The 3.3 mM stock cisplatin (Accord Healthcare, Poland) was diluted in 0.9% NaCl and prepared fresh for each experiment. Right before experiments, 120 µL of cell suspension was mixed with required quantity of cisplatin to achieve the desired concentration (usually 100 µM, unless noted otherwise). 60 µL of the cell suspension was transferred between the 2 mm stainless-steel electrodes [59], and pulses were delivered with a commercially available BetaTech electroporator (Electro cell B10, BetaTech, France). We varied the pulse number (1, 4, 8, 16, 32, 64) and the electric field (0.4 kV/cm, 0.6 kV/cm, 0.8 kV/cm, 1.0 kV/cm, 1.2 kV/cm) while pulse duration was 100 µs and repetition frequency 1 Hz. The remaining 60 µl was used as a control and was transferred between the electrodes, but no pulses were delivered. 50 µl of the treated and control sample was transferred to 15 mL centrifuge tubes. 10 min after pulse delivery (unless noted otherwise), the samples were diluted 40x in full DMEM and vortexed. Samples were then centrifuged (5 min, 900g, 21 °C) and the supernatant was separated from the pellet. Until the Pt mass measurements the samples were stored at -20 °C.

The following parameters were tested during establishment of our protocol: 1) the effect of extracellular cisplatin (1 µM, 5 µM, 10 µM, 20 µM, 50 µM, 100 µM, 200 µM, 330 µM) on the intracellular Pt mass, 2) time interval (5 min, 10 min or 20 min) between pulse delivery and dilution on the intracellular Pt mass, 3) the binding of cisplatin to proteins from fetal bovine serum by using DMEM with or without fetal bovine serum as the electroporation buffer, 4) we also determined the resealing time by adding 100 µM cisplatin 2 min, 5 min, 10 min and 20 min after pulse delivery. In the experiments mentioned in this paragraph, 8x100 µs pulses at 1.0 kV/cm and 1 Hz repetition frequency were delivered.

2.1.3. Cell death - Irreversible electroporation

Survival after electroporation (without cisplatin) was assessed with two different assays. Short-term irreversible electroporation was measured 1h after the treatment on flow cytometer by the propidium iodide uptake. The long-term irreversible electroporation was measured 24h after the treatment by a metabolic assay. Cells were prepared the same way as described under Cell preparation. Electroporation was performed as described in Cell electroporation section, but we added 0.9% NaCl instead of cisplatin.

2.2.3.1. Short-term irreversible electroporation

After application of electric pulses, cells were incubated at 37 °C for 30 min. During these 30 min cells resealed. We added propidium iodide (Life Technologies, USA) in final concentration 136 µM. As reversibly electroporated cells were already resealed, only irreversibly electroporated cells stained. After 5 min in the propidium iodide, we measured fluorescence on the flow cytometer (Attune NxT; Life Technologies, USA). Cells were excited with a blue laser at 488 nm, the emitted fluorescence was detected through a 574/26 nm band-pass filter, and 20.000 events were acquired. Two distinct peaks were formed on the histogram of fluorescence and percentage of dead cells was determined with Attune NxT software (Life Technologies, USA).

2.2.3.2. Long-term irreversible electroporation

Long-term death was assessed 24h after electroporation with the MTS test (CellTiter 96® AQueous One Solution Cell Proliferation Assay (MTS), Promega, USA). 20.000 cells per well were transferred into in a 96-well plate in triplicates and then incubated for 24 hr. 20 μL of the MTS was added per well, and after 2 hours at 37 °C, the absorbance at 490 nm was measured with a spectrofluorometer (Tecan Infinite 200; Tecan, Austria).

2.2.4. Statistical Analysis

The statistical analysis was performed in SigmaPlot (v11.0, Systat Software, USA). We performed the t-test when the normality test passed, or the Mann-Whitney rank sum test when the normality test failed.

2.2. In vivo experiments

2.2.1. Animals

Eight-week-old female C57Bl/6 mice (Envigo Laboratories, Udine, Italy) were used in experiments. At the beginning of the experiments, their body weight was between 18 and 20 g. All procedures were performed in compliance with the guidelines for animal experiments of the EU Directives, the permission of the Ministry of Agriculture and the Environment of the Republic of Slovenia (Permission No. U34401-1/2015/16), which was provided based on the approval of the National Ethics Committee for Experiments on Laboratory Animals. Mice were kept in a specific pathogen-free environment with 12-hour light/dark cycles at 20–24 °C with 55% ± 10% relative humidity and given food and water ad libitum.

2.2.2. Treatment and sample collection protocol

One day before the experiment, mice were shaved on their right flanks. Tumors were induced in the right flanks of the non-anesthetized mice with subcutaneous inoculations of 10^6 B16-F10 melanoma cell suspensions in 100 μL of a physiological solution prepared from cell culture in vitro. The treatment was performed when tumors reached volumes of 35–40 mm^3, which was 6-7 days after inoculation. Tumor volume was measured using a Vernier Caliper. The tumor volume was calculated using the following formula:

$$V=\pi \times e_1 \times e_2 \times e_3 \div 6; \tag{1}$$

where e_1, e_2, and e_3 are three orthogonal diameters of the tumor [60]. During the treatment, mice were under isoflurane (Izofluran Torrex para 250 ml, Chiesi Slovenia, Ljubljana, Slovenia) anesthesia. To obtain precise application of electroporation mice were initially anesthetized with inhalation anesthesia in the induction chamber with 2% (v/v) of isoflurane in pure oxygen and afterward, the mouse muzzle was placed under inhalation tube to keep mice anesthetized during the experiment. In experiments from [60], mice were randomly divided into three experimental groups, consisting of three animals per group. The three groups were: 1) control group, where we intratumorally injected 80 μL of physiological solution, 2) cisplatin group, where we injected 80 μL of cisplatin (40 μg of cisplatin) and 3) cisplatin and electroporation group, i.e. electrochemotherapy, where we injected 80 μL of cisplatin (40 μg of cisplatin) and after 2 minutes delivered electric pulses. Pt mass in these three groups was determined 60 minutes after injection as described in [60].

In the scope of this paper, additional two groups were used with three mice per group. The treatment consisted of an intratumoral injection of 80 µL cisplatin (40 µg of cisplatin). After two minutes, tumors were excised, removed from the overlaying skin and weighted. The blood was collected from the intraorbital sinus using glass capillary tubes. In the first group, we measured Pt in a whole tumor, and in the second group, Pt in several tumor compartments (serum, single cell suspension, extracellular matrix, DNA) [60]. For total tumor Pt content detection, tumors were frozen at -20 °C until the analysis.

2.3. Platinum measurements

For Pt determination inductively coupled plasma mass spectrometry (ICP-MS) was used.

2.3.1. Sample digestion

All dilutions of the samples were made with ultrapure water (18.2 MΩ cm) obtained from a Direct-Q 5 Ultrapure water system (Merck Millipore, USA). Nitric acid (65 % HNO_3) and hydrogen peroxide (30 % H_2O_2) were obtained by Merck Millipore, USA.

Samples of cell pellet were digested with 200 µL of concentrated nitric acid, 200 µL of concentrated hydrogen peroxide and heated overnight at 90°C in the heating oven (Binder GmbH, Tuttlingen, Germany). After the digestion, the samples were filled up to 5 mL with MilliQ water and measured by ICP-MS.

Samples of supernatant fluid were digested with one mL of concentrated nitric acid, one mL of concentrated hydrogen peroxide and heated overnight at 90°C in the heating oven. After the digestion, the samples were filled up to 10 mL with MilliQ water and 2.5-times diluted before ICP-MS measurements.

Samples from the in vivo experiments were digested at 90 °C for approximately 36 h in 0.2 to 2.0 mL of a mixture of concentrated nitric acid and hydrogen peroxide (1:1). After obtaining clear solutions, samples were adequately diluted with MilliQ water before ICP-MS measurements.

2.3.2. Inductively coupled plasma – mass spectrometry measurements

Mass concentrations of Pt in the digested samples were determined by the use of mass spectrometry with inductively coupled plasma (ICP-MS) against an external calibration curve using Ir as an internal standard. Calibration standard solutions of Pt were prepared from Pt stock solution (1000 µg Pt/mL in 8 % HCl), obtained from Merck (Darmstadt, Germany), and diluted in 2.6 % nitric acid. Experimental conditions for the ICP-MS instrument (Agilent 7900 ICP-MS instrument, Agilent Technologies, Tokyo, Japan), summarized in Table 1, were optimized for plasma robustness and adequate sensitivity.

For evaluation of the accuracy of the analytical method (digestion procedure and ICP-MS analysis), the same quantity of cell pellet was spiked with 20 µL of 500 ng/mL ionic Pt solution to reach final Pt concentration of 10 ng/sample, while the supernatant fluid was spiked with 20 µL of 50 µg/mL ionic Pt solution to reach final Pt concentration of 1000 ng/sample. Spiked samples were digested in the same way as described before. Recoveries (the ratio between the measured and expected Pt concentrations) were 101 ± 2 % (N=4) and 98 ± 1 % (N=4) for spiked cell pellets and spiked supernatant fluids, respectively.

Parameter	Type/Value

Sample introduction	
Nebulizer	Micromist
Spray chamber	Scott
Skimmer and sampler cone	Ni
Plasma condition	
Forward power	1550 W
Plasma gas flow	15.0 L min^{-1}
Carrier gas flow	1.05 L min^{-1}
Nebulizer pump	0.1 rps
Sample depth	8.0 mm
He gas flow	0 mL min^{-1}
Energy discrimination	5.0 V
Data acquisition parameters	
Isotopes monitored	^{195}Pt
Isotopes of internal standards	^{193}Ir

2.4. Modelling

2.4.1. In vitro

From the in vitro results, we calculated the coefficient membrane permeability to Pt (P). In vitro, the model of transport was relatively simple – the initial concentration of the extracellular cisplatin was the same for all the cells, there was enough of cisplatin so that we could consider the extracellular cisplatin concentration constant. The whole membrane was surrounded by cisplatin which could enter from all sides, depending on the permeability of the membrane. By changing the pulse number and voltage, we obtained the permeability coefficient as a function of pulse number and electric field intensity. Permeability coefficient was a direct measure of membrane permeability.

The resealing time constant was determined by describing the resealing data with a curve:

$$f(t) = C \exp\left(-\frac{t}{\tau}\right) \tag{2}$$

Where C denotes the intracellular Pt mass if cisplatin is present at the moment of pulse delivery, τ is the resealing time constant or time when 63% of the pores/defects are resealed [61], and t is the time elapsed since the end of pulse delivery.

In vitro, we used the dual-porosity model [38] to calculate the permeability coefficient. In Matlab (R2017a, Mathworks Inc., USA) we calculated the permeability coefficient (P) at t = 0 s which corresponds to P$_0$ by solving the differential equation:

$$\frac{\partial c_{int}}{\partial t} = P_0 \exp\left(-\frac{t}{\tau}\right)\frac{3}{R}(c_{int} - c_{ext}) \tag{3}$$

for the external concentration c$_{ext}$ (100 µM), the resealing constant τ (2.29 min), in vitro cell radius R (8.1 µm) [62], and initial conditions c_{int}(t=0s)=0 µM. The permeability coefficient was a function of time as the permeability decreased with time due to membrane resealing.

2.4.2. In vivo

Model of a tumor was constructed in Comsol Multiphysics® (v5.3, Comsol AB, Stockholm, Sweden). The tumor was modeled as a sphere with radius 2.03 mm which corresponds to 35 mm³, i.e., the average volume of a tumor when in vivo treatment was performed. Due to symmetry, we modeled only 1/8 of the tumor, i.e., one octant of the sphere. We used physics-controlled mesh with extra fine element size and confirmed that with decreasing element size, the calculated intra- and extracellular Pt mass did not change significantly. In Comsol, two equations were coupled and calculated in a whole tumor. In the intracellular space:

$$\frac{\partial c_{int}}{\partial t} = -\frac{3P(t)}{R}(c_{int} - c_{ext})k \tag{4}$$

And in the extracellular space:

$$\frac{\partial c_{ext}}{\partial t} = D_{cddp}\nabla^2 c_{ext} + \frac{3P(t)}{R}\frac{(1-f)}{f}(c_{int} - c_{ext})k \tag{5}$$

Where c_{int} and c_{ext} denote the intracellular and extracellular concentration, respectively, D_{cddp} is the diffusion coefficient of cisplatin in the extracellular tumor space, P is the permeability coefficient, time-dependent due to membrane resealing, R is the cell radius in vivo (6.25 µm) [63], f is the fraction of cells in a tumor (37%) [63,64], and k is the transformation coefficient which transforms the data from the in vitro to the in vivo conditions. The initial conditions were c$_{int}$(t=0)=0 mM and c$_{ext}$(t=0)=1.6 mM. P was determined from the in vitro experiments. The boundary conditions for the intracellular concentration were no flux on all boundaries and for extracellular concentration, no flux in the inner boundaries of a tumor and c_{ext}(r=2.03 mm)=0 mM at external boundaries.

In a model, we varied parameters k and D_{cddp} and calculated the intracellular and extracellular Pt mass for each combination of k and D_{cddp} when k was between 0 and 1 in steps of 0.2 and D_{cddp} was between 2 x10⁻⁸ cm²/s and 8x10⁻⁵ cm²/s in steps of 0.2 decades. Then, we determined a global minimum and sampled the space around it with higher resolution by changing k from 0.3 to 0.5 by 0.1 and D_{cddp} from 1.5x10⁻⁶ cm²/s to 2.5 x10⁻⁶ cm²/s by 0.1 decades. The final values of the parameters k and D_{cddp} were chosen as the values with which we achieved the best agreement with a measured mass of Pt in vivo and were the global minimum.

3. Results

3.1. In vitro experiments

First, we performed experiments to determine the effect of extracellular cisplatin concentration, incubation time, fetal bovine serum, and the resealing time on the Pt uptake. From Fig. 1 we can see that the

intracellular Pt mass was linearly dependent on the extracellular cisplatin concentration in control as well as in the electroporated cells. Thus, we decided to perform all subsequent experiments with 100 µM extracellular cisplatin and scaled our results to any concentration in the tested range. In Fig. 2 we can see that 5 min after pulse delivery we reach a plateau in the intracellular Pt mass. We thus decided to perform all subsequent experiments with 10 min incubation time after electroporation. Next, we tested whether the presence of serum in the electroporation medium affects cellular uptake of Pt (Fig 3). There was no statistical difference between the uptake with or without serum. In Fig. 4 we can see how the membranes resealed after pulse application. When describing the data with a first-order dynamics (Eq. (1)), we determined that the resealing time constant was 2.29 min. 10 min after pulse delivery was cell membrane resealed which corroborates results shown in Fig. 2.
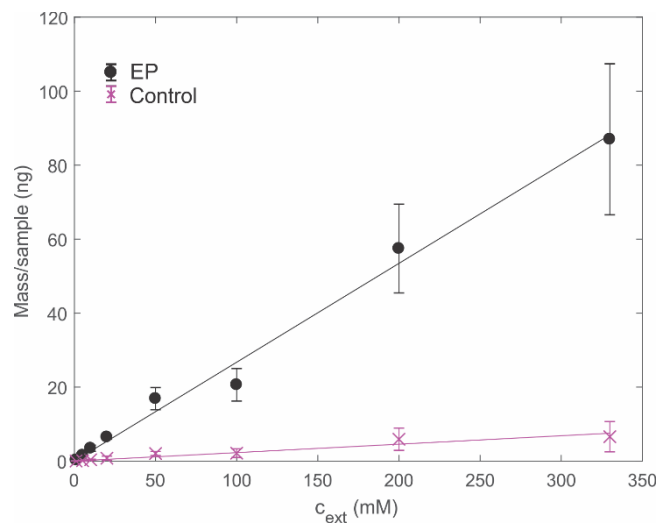
Fig. 1: Effect of extracellular cisplatin (C_{ext}) concentration on intracellular Pt mass when 8x100 µs pulses of 1 kV/cm were delivered at repetition frequency 1 Hz. The results could be described with a linear function $y = kc_{ext}$ with k and R^2 of 0.2672 and 0.99 for the treated and 0.0228 and 0.92 for the control cells, respectively. Mean ± standard deviation. Each data point was repeated 3-5 times. Except for 1 µM extracellular cisplatin where the measured values were below the detection threshold of 0.005 ng and we could not evaluate statistical significance, all electroporated samples were statistically different from the corresponding control samples (P<=0.03).
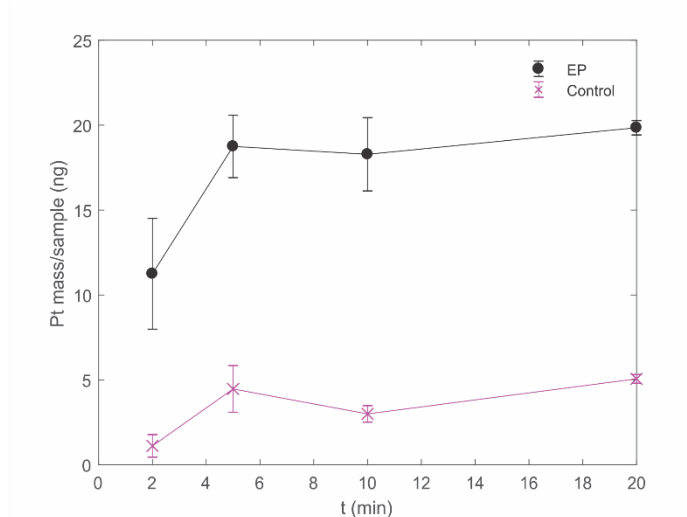
Fig. 2: Effect of incubation time after pulse application on the intracellular Pt mass *when 8x100 µs pulses of 1 kV/cm were delivered at repetition frequency 1 Hz and 100 µM extracellular cisplatin. Already 5 min after pulse delivery a plateau was reached. Mean ± standard deviation. Each data point was repeated 3-6 times. All treated samples were statistically different from the corresponding control (P<=0.001). There was a significant difference between 2 min and 5 min exposure of treated samples (P=0.02), other comparisons were not significant.*
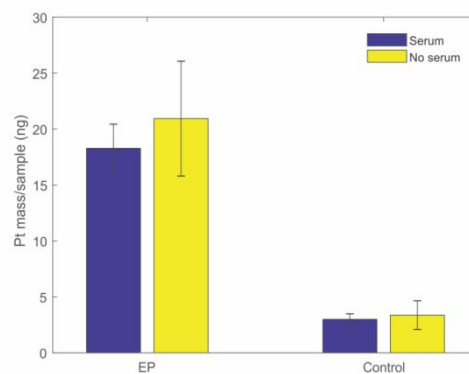
Fig. 3: Effect of the presence of serum in the electroporation medium on intracellular Pt mass*. There was no statistical difference in pulsed (P=0.652) and control (P=0.430) cells when serum was or was not present (t-test). Mean ± standard deviation. Each data point was repeated 3-5 times.*
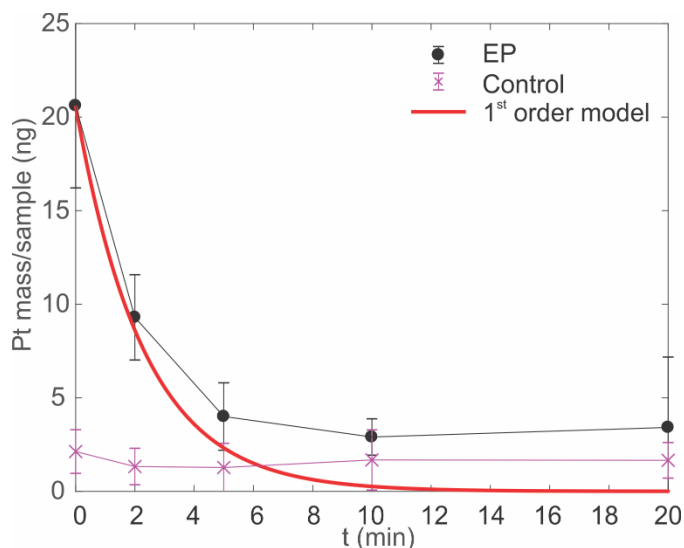
Fig. 4: Membrane resealing after 8x100 µs pulses of 1 kV/cm were delivered at repetition frequency 1 Hz and 100 µM cisplatin (mean ± standard deviation). Membrane resealed with a first-order dynamics with a time constant 2.29 min which is shown in red. Each data point was repeated 4-6 times. 2 and 5 min data point was statistically significantly different between electroporated and corresponding control samples (P<=0.001 for 2 min and P=0.045 for 5 min). There was also a statistical difference between 2 min and 5 min electroporated samples (P=0.002). All other comparisons were not significant.

In Fig. 5 intracellular Pt mass is shown as a function of pulse number and electric field intensity. We can see that the highest uptake was achieved with eight pulses of 1.2 kV/cm (35 ng of Pt per sample). With higher pulse number or higher electric field, the intracellular Pt mass decreased, most likely due to increased cell death. To explore hypothesis of cell death contribution, we also performed experiments evaluating cell death. Results are shown in Fig. 6 - in Fig. 6a is the short-term cell death measured by flow cytometry one hour after the treatment and in Fig. 6b is the metabolic activity measured by MTS assay 24 hours after the treatment. We can see that the results obtained with both assays correlate well. Survival starts to decrease at electric fields above 0.6 kV/cm for any pulse number tested. With 1, 4 or 8 pulses even at the highest electric fields, the survival was not yet affected. For calculating the permeability coefficients, we have to take into account cell death and correct the permeability coefficient.
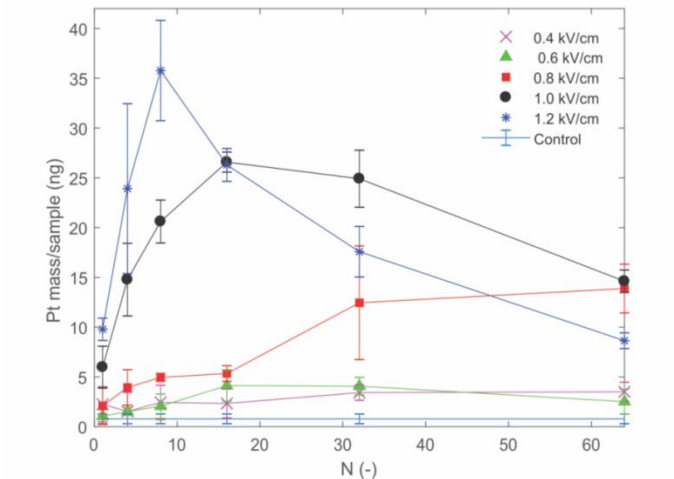
Fig. 5: Effect of number of pulses and the electric field on the intracellular Pt mass. 8x100 μs pulses of 1 kV/cm were delivered at repetition frequency 1 Hz (mean ± standard deviation). Each data point was repeated 3-5 times. Data points were compared to the control. Comparison was not significant for 0.4 kV/cm and 1, 4 or 32 pulses; for 0.6 kV/cm and 1, 4, 8 or 64 pulses, for 0.8 kV/cm and 1 or 4 pulses. All other data points were statistically significant (P<=0.05).
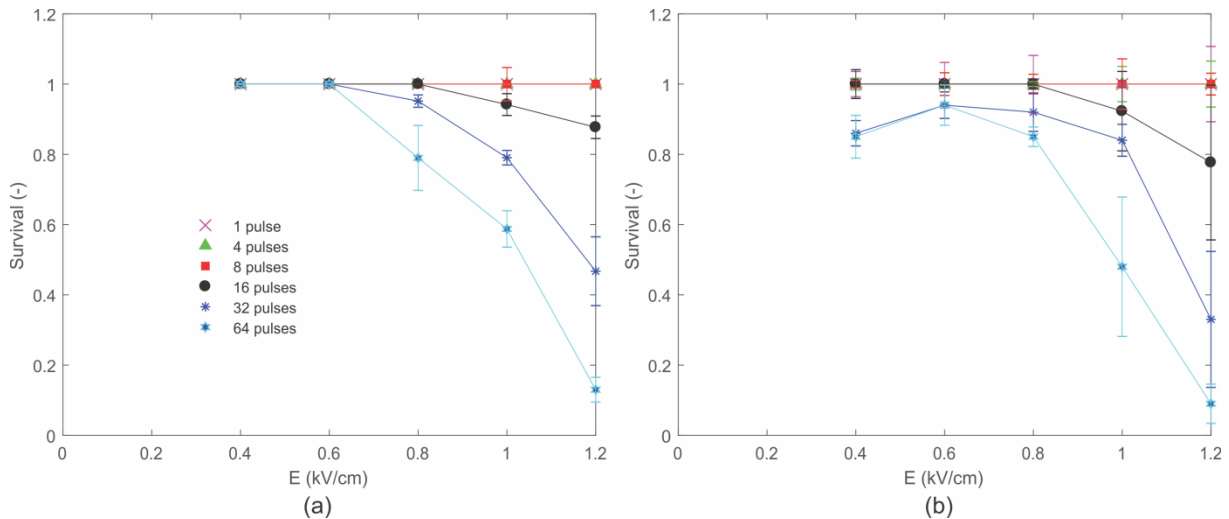
Fig. 6: Decrease in cell survival due to irreversible electroporation. (a) Survival determined by flow cytometry, one hour after electroporation and (b) by the MTS survival assay, 24 h after electroporation (mean ± standard deviation). The legend is valid for both figures. Each data point was repeated 3-6 times. In (a) the statistically significant points in comparison to the control were 0.8 kV/cm and 32 or 64 pulses, 1 kV/cm at 8, 16, 32 or 64 pulses and 1.2 kV/cm at 16, 32 or 64 pulses (P<=0.03). In (b) the statistically significant points in comparison to the control were 0.4 kV/cm at 8, 32 and 64 pulses, 0.8 kV/cm at 64 pulses, 1 kV/cm at 1, 32 or 64 pulses, 1.2 kV/cm at 8, 32 and 64 pulses (P<=0.03).

Due to increased cell membrane permeability, different molecules and ions can enter the cell in different concentrations, depending on their size, molecular weight and charge. Small molecules (several hundredths of Da) were shown to enter cells in 90-100% of their extracellular concentration [58]. In our experiments, we calculated intracellular cisplatin concentration in comparison to extracellular cisplatin concentration

(Fig. 7). We reached 80% of the extracellular concentration when 8 pulses of 1.2 kV/cm were applied (Fig. 7a). Lower cell membrane permeability or cell death decreased this percentage in case of other pulse parameters. We took cell death into account by normalizing the intracellular concentration to the survival as determined by flow cytometry and obtained graph in Fig. 7b. There we can see that we obtain uptake higher than 100% and is increasing with increasing electric field and pulse number.
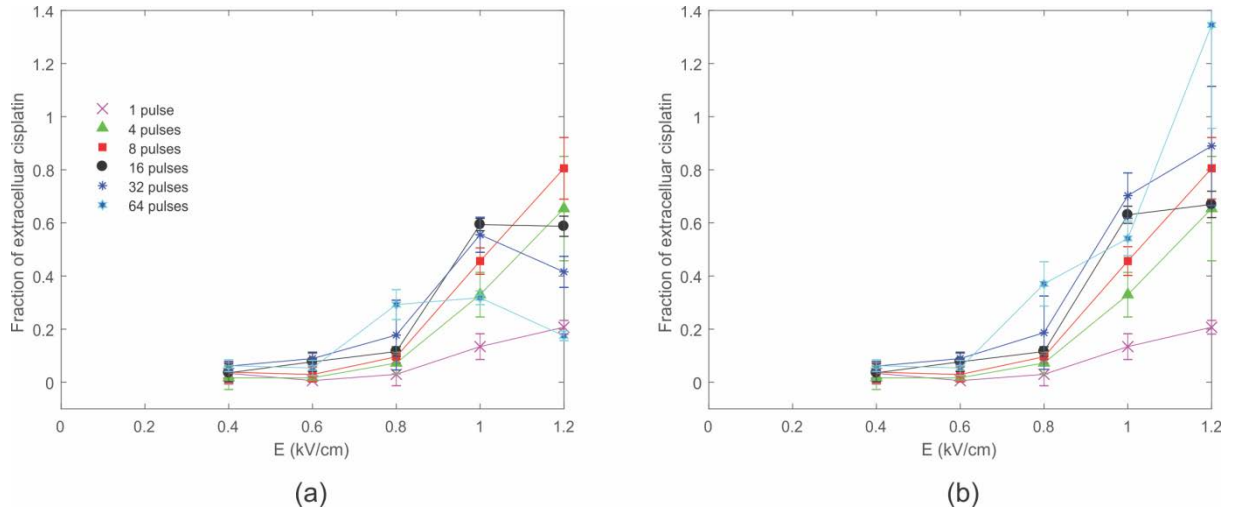
Fig. 7: The fraction of the extracellular Pt concentration, present in the intracellular compartment (mean ± standard deviation). a) Cell death was not taken into account, and the intracellular Pt concentration was almost 80% of the extracellular cisplatin concentration. b) Results of the uptake were corrected for cell death as determined by flow cytometry one hour after the treatment. The intracellular Pt concentration was almost 140% of the extracellular cisplatin concentration. The legend is valid for both figures.

3.2. In vivo experiments

We measured the intra- and extracellular Pt mass and by taking into account the size of cells and their volume fraction also calculated the intracellular and extracellular cisplatin concentration. The concentration is just an approximation since the concentration in the tissue/tumor is most likely inhomogeneous. Results are shown in Table 2.

Table 2: Intra- and extracellular Pt mass and the corresponding cisplatin concentration, based on the measured volume of each tumor at t=2 min after injection of cisplatin (initial conditions, time when electric pulses are applied) and at t=60 min after the therapy (cisplatin + electroporation). From the results at 60 min we subtracted the Pt in the control samples (without electroporation) to focus only on the transport due to electroporation.

	t = 0 min (Mean ± St. dev).	t = 60 min [60] (Mean ± St. dev.)
Intracellular Pt mass	17 ng ± 12 ng	67 ng ± 18 ng
Extracellular Pt mass	6431 ng ± 4681 ng	666 ng ± 104 ng
Intracellular cisplatin concentration	7 μM ± 5.5 μM	25 μM ± 10 μM

Extracellular cisplatin concentration	1600 μM ± 1200 μM	144 μM ±110 μM

3.3. Modeling

By using the dual-porosity model, we calculated the in vitro permeability coefficient. We also took into account that the permeability coefficient changes with time due to cell membrane resealing. We assumed that during resealing, the permeability of the plasma membrane decreases exponentially with time, which has been confirmed experimentally and by modeling in several studies [61,66,67]. Thus, the permeability coefficient also decreases exponentially with time. The resealing coefficient was obtained by fitting Eq. (2) to results, shown in Fig. 4 and optimizing the τ to obtain the highest R^2 value of the model. In Fig. 8a we can see the permeability coefficient P_0 at t=0 s, i.e., when electric pulses were applied and the cell membrane was fully permeabilized and in Fig. 8b, how the permeability coefficient changed with time.
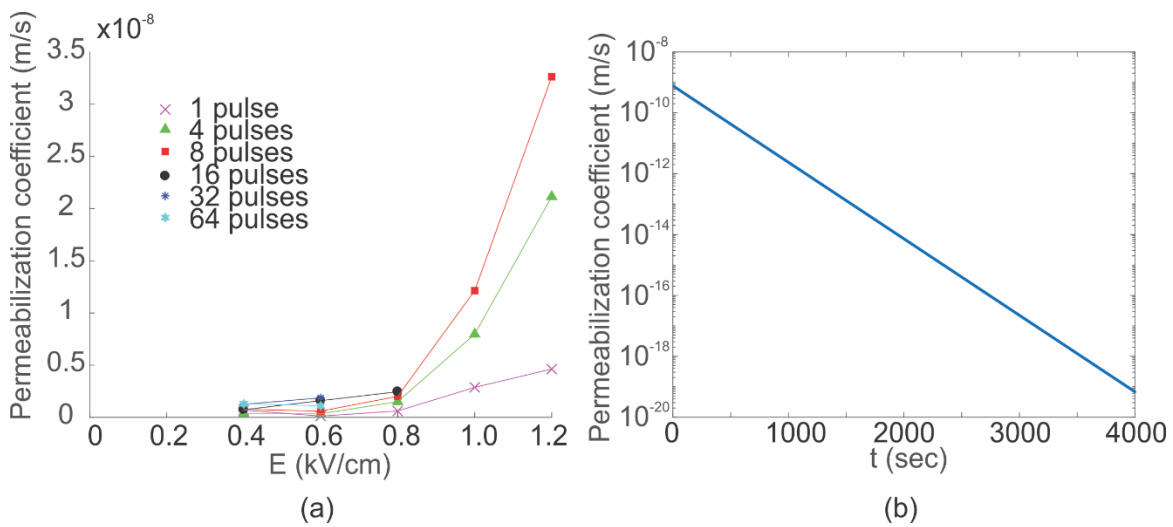
Fig. 8: The permeability coefficient at pulse application determined by the dual-porosity model [32] for all conditions, where survival was 100%. a) Permeability coefficient at t=0, i.e., just after exposure to electric pulses. b) Permeability coefficient as a function of time when 8x100 μs pulses were delivered at 0.4 kV/cm and 1 Hz repetition frequency on a semi-logarithmic scale. This was the permeability coefficient which was used in the in vivo model.

For the in vivo conditions, we modeled transport in a tumor modeled by a sphere consisting of intra- (tumor cells) and extracellular (interstitial fraction) space. In each compartment, the transport was described by the dual-porosity model. We determined the optimal diffusion coefficient to be 2.1×10^{-6} cm^2/s and the optimal transformation coefficient to be 0.3. We obtained temporal and spatial dynamics of Pt uptake in the intra- and extracellular environment. To compare results of the simulation with experimental results [60], we extracted from the model results one hour after pulse delivery. In the model, the Pt mass achieved plateau sooner since cell membrane resealed in 10 min (Fig. 4) but we simulated one hour more to be in the same time point as when tumors were excised.

The concentration of Pt in a tumor one hour after electroporation as calculated by the model was inhomogeneous with higher concentration in the center of a tumor and gradually decreasing to the rim of a

tumor, where concentration was 0 mM (Fig. 9). Therefore, we compared the mass of Pt which was calculated as an integral over the corresponding volume fraction to the measured Pt mass in the in vivo experiments.
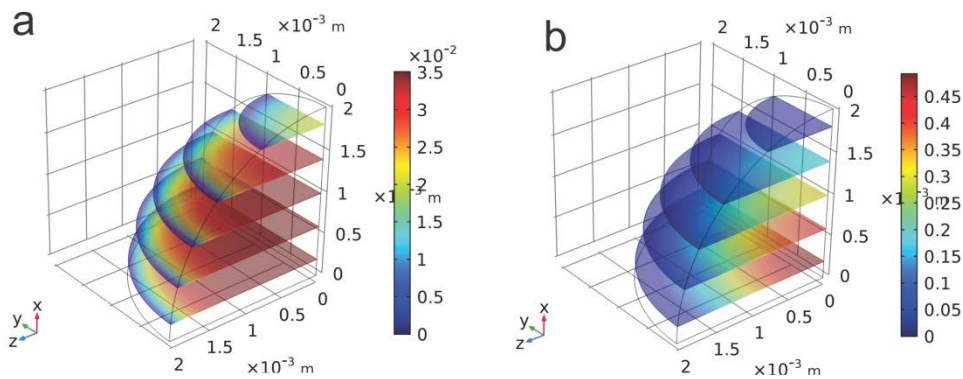
Fig 9: Modelled spatial dependency of Pt concentration 1 hour after pulse delivery in mol/m³. (a) Intra- and (b) extracellular Pt concentration. Spatial distribution is inhomogeneous in both cases.

Table 3: Experimentally determined and modelled mass of Pt in the intracellular and extracellular space of a tumor 1 hour after the treatment with electrochemotherapy [54].

	Experiments [60]	Model
Intracellular Pt mass	67 ng	65 ng
Extracellular Pt mass	666 ng	664 ng

4. Discussion

Our aim was to model the transport of chemotherapeutics in tumors based on experiments obtained on cell suspension. On cell suspension, experiments are easier to perform, there are no ethical issues, and a large spectrum of parameters can be explored. Our goal was to include a model of transport in treatment planning of electroporation-based medical treatments. In treatment planning of electrochemotherapy, a critical experimentally determined electric field of permeabilization [68,69] or statistical models [59,70] are used to determine which area will be permeabilized/affected and which not. Permeabilization alone, however, does not guarantee treatment efficacy [10]. For successful electrochemotherapy, a sufficient amount of chemotherapeutics has to enter tumor cells and bind to DNA (the main target of cisplatin) or target other molecules in the cell to prevent future cell division and cause cell death. Current treatment plans of electrochemotherapy lack a model of transport and drug uptake in a tumor and the cells. A number of internalized bleomycin has been correlated with the biological effect – few thousand bleomycin molecules cause mitotic death while several million molecules cause cell death similar to apoptosis [37,71]. A similar analysis could also be done for cisplatin.

In our paper, we connected the in vitro experiments with the in vivo experiments by the dual-porosity model. We accurately calculated the Pt mass in the intra- and extracellular tumor space by using in vitro

permeability coefficients. Our model could be used to predict treatment efficacy from a number of molecules delivered to cells as a function of the electric field in tissue.

4.1. Experimental part

In vitro, we used mouse melanoma B16-F1 cells and in vivo, tumor from mouse melanoma B16-F10 cells. B16-F1 and B16-F10 cells vary only in their metastatic potential. [72] In vitro, increased uptake of molecules after to electroporation is relatively easy to determine using fluorescent dyes and techniques like fluorescent microscopy, flow cytometry, spectrofluorometry [73]. In vivo, the increased uptake of molecules after electroporation is challenging to assess. ^{57}Co-bleomycin [74], ^{111}In-bleomycin [75], ^{99m}Tc-DTPA [76], ^{51}Cr-EDTA [77], gadolinium [78], lucifer yellow [79] and cisplatin [20,21,28,80–84] were used previously. Cisplatin is Pt-based chemotherapeutic. We can calculate the concentration of cisplatin by measuring Pt mass in a known volume. The mass of Pt can be measured precisely even for very low amounts by inductively coupled plasma mass spectrometry. As Pt mass is easily determined in vitro as well as in vivo, we used cisplatin in our study. Another possibility for Pt detection is attaching a contrasting agent as a ligand to the Pt.

Before exploring the parameter space by changing the number of applied electric pulses and electric field, we tested 1) at what extracellular cisplatin concentration we should perform the experiments, 2) if we could use the fetal bovine serum, 3) how long should we incubate cells after pulse delivery and 4) what was the effect of membrane resealing on intracellular Pt mass. 1) We determined that with increasing extracellular cisplatin concentration, also intracellular Pt mass increased. The dependency was linear which indicates that the increased uptake of molecules after electroporation was mostly diffusive and not electrophoretic or endocytic which is in accordance with an already published study [85]. We decided to perform experiments at 100 μM and because of the linear dependency results could be scaled to any concentration in the tested range. 100 μM concentration was used because it is in a similar range as in other in vitro studies [22,86–88] and higher cisplatin concentration caused higher intracellular Pt mass which enabled to more accurately distinguish between intracellular masses at similar pulse parameters. 2) Fetal bovine serum added to the growth medium consists mostly of proteins. Cisplatin unspecifically binds to proteins [58] and also to collagen [89] which represents 5-10% of the matrix. The time dynamics of cisplatin binding to proteins is in a range of hours [58,90,91]. Cisplatin, bound to proteins, is biologically inactive [92]. In vitro the binding of cisplatin to proteins in the fetal bovine serum in the first 10 minutes was negligible (Fig. 3). Because cisplatin was observed to bind to proteins in a time-range of hours-days, we did not include cisplatin binding in the tumor model. 3) When we tested the influence of incubation time after electric pulse application, we determined that a plateau is reached after 5 minutes (Fig. 2). Thus we decided to perform all our experiments 10 min after pulse application when the uptake due to electroporation ends. The reason for reaching a plateau could be that the increased uptake of molecules after electroporation is much faster than the passive diffusion or active mechanisms which exist in the cells. Namely, it was shown that without electroporation, intracellular cisplatin concentration increases in a time-range of hours, in vitro as well as in vivo [30,93] The additional mechanisms could contribute to a higher transport and increase in the uptake on a longer timescale. To focus only on the modeling uptake due to electroporation, we subtracted the mass of

the Pt in the control samples from the mass of Pt in treated samples when calculating the permeability coefficient and comparing the results of our model with the experiments.

Electrochemotherapy is usually performed with 8x100 µs pulses. However, we wanted our model to be valid in a larger parameter space, which would enable its use also with other pulse parameters. Thus, we applied from 1 to 64 pulses. With increasing pulse number and electric field the intracellular Pt mass increased with a peak at eight 100 µs pulses of 1.2 kV/cm (Fig. 5). We calculated the volume of all cells (≈2 mm^3) in a sample and using the measured Pt mass in the cells calculated the intracellular Pt concentration. We determined that the intracellular Pt concentration is up to 80% of the extracellular cisplatin concentration (Fig. 7a). The high percentage is in agreement with the mass of the cisplatin (300 g/mol) [65]. With some parameters of electric pulses, we were already irreversibly electroporating cells (Fig. 6) which also affected the uptake. The uptake was decreased as can be observed in the shape of the curves in Fig. 5, i.e., we reach maximum at lower pulse number (eight pulses at 1.2 kV/cm or 16 pulses at 1.0 kV/cm) and then with increasing pulse number the uptake decreases. We normalized the percentage of intracellular cisplatin concentration to survival and obtained values higher than 100% (Fig. 7b) which indicates that either 1) cisplatin binds to DNA and concentration gradient increases, 2) cell death was not the only reason for decreased uptake, 3) some other cell death assay would be more suitable, 4) active mechanisms additionally transport cisplatin into cells. We determined that eight pulses are the optimal number to be delivered which is consistent with the standard electrochemotherapy protocol [18]. For our in vivo model, we only used the permeability coefficient when the survival was 100%.

In the in vivo experiments, we injected 26 µg of Pt by intratumoral injection of 80 µl of cisplatin in 35 mm^3 tumors. The volume of injection was twice the volume of a tumor because we reused the data from [60] to follow the 3Rs of the animal experiments [94]. Most of the injected Pt was not measured. When a tumor was excised 2 min after cisplatin injection, we determined that 27 % of the injected Pt was still present in a tumor and the serum. A part of cisplatin was lost due to lower tumor volume than injection volume and due to washout of cisplatin from the tumor. When a tumor was excised after 1 hour, we determined that in a tumor and serum there was 2% of the injected Pt in the control samples (cisplatin injection, no electroporation) and 7 % in the treated (cisplatin injection and electroporation) samples. Thus, in vivo, the majority of cisplatin was unaccounted for. Part of cisplatin was lost due to the used methodology (when the tumor was mechanically disintegrated and during blood collection). Part of cisplatin could accumulate in different organs and cause unwanted side effects [95].

4.2. Modelling part

Our model is based on a hypothesis that cell permeability in vitro and in vivo is similar when cells are exposed to the same induced transmembrane voltage. However, the transport in vivo is decreased in comparison to the transport in vitro due to the hindered transport of molecules in the in vivo environment due to the cell matrix, the lower diffusion coefficient of molecules in the interstitial space and close cell contacts. The transformation of the transport model from the in vitro to the in vivo environment is challenging. We can use the in vitro permeability coefficient in the in vivo model, as long as we take into account the geometric characteristics of tissue (cell volume fraction, cell matrix volume fraction, cell size).

We took the characteristics into account by decreasing the transport by the transformation coefficient. In our model, we assume that the transformation coefficient is a function of tissue morphology and decreases with increasing cell volume fraction and matrix volume fraction. It remains to be tested if the transformation coefficient can be used over several values of parameters and if transformation coefficient is a function of experimental conditions (e.g., tumor cell volume fraction) [63].

Our initial conditions of the in vivo model were homogeneously distributed 1.6 mM cisplatin in the tumor interstitial fraction. Initial cisplatin concentration was determined from experiments by excising tumors 2 min after cisplatin injection when usually electric pulses were applied. According to our calculations, the initial cisplatin concentration in a tumor (1.6 mM) was similar to the concentration injected (1.65 mM), which means that by injecting cisplatin we washed out the interstitial fluid and replaced it with cisplatin. Thus, part of cisplatin volume was lost due to washout from the tumor, but the remaining cisplatin was not diluted in the interstitial fraction, and it remained in (almost) initial concentration. Initial cisplatin distribution was determined from the literature [21,96]. Solutes are washed out relatively quickly from small tumors and with some delay from larger tumors [96]. In [21] it was determined that electrochemotherapy treatment was most efficient when electric pulses were delivered 0-5 min after intratumoral cisplatin injection. This time scale indicates that in the first 5 minutes after intratumoral injection the cisplatin distribution in a tumor is approximately homogeneous and not yet washed out of a tumor. 0-5 minutes was a similar time range as used in our experiments (2 min) implying that approximating the initial cisplatin distribution in the model as homogeneous is justified. In future, for experimental determination of initial cisplatin distribution, a technique like imaging mass cytometry could be used [89]. 60 minutes after the treatment, the cisplatin concentration was the highest in the center of the tumor, which corresponds to previously published data – in [79] a fluorescent dye was injected, and in the tissue sections it can be seen that the highest concentration of the dye was in the middle of the sample.

We modeled the tumor as a symmetrical sphere, thus decreasing the complexity of the model and time of calculation, which was justifiable because mouse melanomas used in our experiments were spherical due to a localized injection during inoculation. However, our model also supports also other geometries, the only adaptations required would be those of the geometry and the mesh.

The volume fraction of cells in a tumor was calculated by the method presented in [64] - the surface fraction of cells determined on a slice is a good approximation of volume fraction. We used experimental data [63] where the volume fraction of cells and cell matrix and cell size in B16-F1 mouse melanoma tumors were assessed. We calculated cell volume fraction of 37% in tumors. Since a tumor has a high cellular fraction in comparison to our in vitro results, we took that into account. The high volume fraction of cells decreased the induced transmembrane voltage due to electric field shielding [40]. Considering the calculations in [97,98] we can determine that the induced transmembrane voltage in cells in vivo is 76-88% of the one induced on a single spherical cell. The average radius of cells in vivo was determined to be 6.25 μm [63] which is less than the average in vitro radius of 8.1±1.1 μm [62] which means that according to Schwann equation, the induced transmembrane on the cells in vivo is 77% of the in vitro induced transmembrane voltage. Taking into account the decrease in induced transmembrane voltage due to cell proximity and smaller cells in vivo, under the same external electric field, the induced transmembrane

voltage is approximately 60% of the one induced on cells in vitro. The voltage-to-distance ratio delivered to a tumor by parallel plate electrodes was 1.3 kV/cm. It was numerically determined that the electric field in a tumor was inhomogeneous [36], and in the center of a tumor, it was 0.6 kV/cm. Taking into account the lower induced transmembrane voltage on the cells in vivo, the conditions in vivo correspond to when 0.34-0.4 kV/cm is delivered in vitro. Thus, the in vitro permeability coefficient when eight 100 μs, 0.4 kV/cm at 1 Hz was used in the tumor model. We also took into account cell resealing after pulse application and the decrease in cell permeability coefficient. From the in vitro results, we determined the time constant of resealing was 2.29 min which is in agreement with the in vivo data (Fig. 2 in [21]). When eight pulses at 0.4 kV/cm were delivered the survival was still 100% (Fig. 6) and thus there was no need for permeability coefficient correction. The calculated value of 0.4 kV/cm is in agreement with the literature where 0.4 kV/cm is usually assumed to be a threshold of electroporation for a tumor [79,99].

In tumors, the transport differs from normal tissues, as tumors have an abnormal vasculature and increased interstitial pressure which facilitates cisplatin loss [100,101]. In the interstitial space, two mechanisms of transport are present – diffusion and convection. The diffusion in tissues is lower than in water as tissue structures obstruct the transport. In the literature, values of diffusion coefficient for cisplatin or similar molecules are reported in the range of $0.1\text{-}0.7\text{x}10^{-6}$ cm^2/s [102–104] which is less than the value we determined in our model ($2.1\text{x}10^{-6}$ cm^2/s). Electric pulses cause a vascular lock which is present in the time range of hours, although blood flow is to some extent restored in first 15 minutes [42]. It is possible that the diffusion constant in our study is higher because a part of the transport out of a tumor was due to convection, while we limited our analysis to diffusion. However, convection introduces a new unknown parameter (velocity) in the model, and here we decided to model the transport as only diffusive. Also, vasoconstriction due to electric pulses decreases convective transport from the tumor. In future, the convective transport could be included, but experimental data are first needed.

All models include simplifications. The following are simplifications we made in our model. We assumed that the electric field in a tumor was homogeneous although in reality, it is inhomogeneous [36,79]. We approximated initial cisplatin distribution in the tumor as homogeneous and the cisplatin concentration at the external border of a tumor to be 0 mM, although in reality there is a smooth transition in the concentration between intra- and extratumoral cisplatin. Our model was tested on one type of a tumor, and more in vivo experiments are needed, preferably with several different tumor types to increase the validity of the model. Our current hypothesis is that different tumor types will differ in the diffusion coefficient for cisplatin and the transformation coefficient in the interstitial tumor fraction depending on the volume fraction of cells in the tumor, both decreasing with the increased volume fraction of cells in the tumor. Additionally, different sizes and volume fractions of cells in different tumors affect the induced transmembrane voltage [97,98]. Permeability coefficient for different tumor types should be calculated from the experiments on corresponding cell types in vitro as different cells exhibit different sensitivity to electric pulses [105]. We have applied electric pulses in vivo at only one pulse number and electric field. Thus our model is valid at 1.3 kV/cm voltage over the distance, 8x100 μs pulses between the electrodes and should in future be tested with more parameters in vivo. Our model is valid for transport of small molecules in the range of several hundred Da. For gene electrotherapy where large plasmids have to pass the cell

membrane, a different approach would need to be used as the mechanisms governing the transport of large molecules [106] are different from mechanisms governing the transport of small molecules [50,54,85]. Also, the mobility of large molecules such as plasmids in the tissue is smaller than the mobility of small molecules like cisplatin [43]. We assumed that the resealing time in vitro and in vivo is similar, as was suggested by comparing our in vitro data to the in vivo already published study [21]. The difference in the resealing would influence the time dependency of the permeability coefficient. The size of the cells in vitro is statistically distributed [54] which could in future be included in the calculation of the permeability coefficient.

There are several possible upgrades to our model. We could include kinetics of the binding of cisplatin to the DNA and resulting cell death as was previously described at a cell level [107–110]. We modeled intratumoral cisplatin delivery as suggested in Standard Operating procedures of electrochemotherapy [18]. However, for our model to be useful for intravenous (i.v.) drug delivery, additional steps would have to be performed to determine the initial spatial drug concentration in the tumor. In the i.v. delivery the drug has to overcome several obstacles before entering the tumor – it has to extravasate from the blood vessels, reach the tumor, overcome the increased interstitial pressure and distribute throughout the interstitial tumor fraction [100]. With our model, we could predict not only the intracellular cisplatin concentration but also cell death as a function of the electric field in the tissue and injected cisplatin dose. We would need to additionally determine the sufficient amount of molecules in the cell to achieve cell death, and then predict the apoptotic or necrotic area of the tumor.

5. Conclusion

Electrochemotherapy is a combination of delivering chemotherapeutics and electric pulses to efficiently treat tumors. To predict the treatment outcome or optimize the position of the electrodes, we first calculate the electric field distribution. We use the critical electric field for reversible electroporation to determine reversibly electroporated area, i.e., the area where electrochemotherapy would be efficient. In the paper, we introduced a model of drug transport that described the transport of cisplatin after intratumoral injection and application of electric pulses in subcutaneous melanoma tumor. We modeled the transport of chemotherapeutic between several compartments – tumor cells, interstitial tumor fraction, and peritumoral environment using the dual-porosity model. We described the uptake of cisplatin in vivo by using the permeability coefficient from in vitro experiments. By optimizing the parameters of the treatment in vitro, a large spectrum of parameters could be easily tested, and a number of experiments on animals could be reduced. We offer a step forward in bridging the models at the cell level (in vitro) and the models at the tissue level (in vivo). By incorporating the analysis of transport into treatment planning of electrochemotherapy, the precision of the outcome could be increased taking into account the cell-level mechanisms of electroporation.

Acknowledgements

References

[1] T. Kotnik, P. Kramar, G. Pucihar, D. Miklavčič, M. Tarek, Cell membrane electroporation- Part 1: The phenomenon, IEEE Electr. Insul. Mag. 28 (2012) 14–23. doi:10.1109/MEI.2012.6268438.

[2] T.Y. Tsong, Electroporation of cell membranes, Biophys. J. 60 (1991) 297–306. doi:10.1016/S0006-3495(91)82054-9.

[3] J.C. Weaver, Electroporation of cells and tissues, IEEE Trans. Plasma Sci. 28 (2000) 24–33. doi:10.1109/27.842820.

[4] L. Rems, D. Miklavčič, Tutorial: Electroporation of cells in complex materials and tissue, J. Appl. Phys. 119 (2016) 201101. doi:10.1063/1.4949264.

[5] T. Kotnik, W. Frey, M. Sack, S. Haberl Meglič, M. Peterka, D. Miklavčič, Electroporation-based applications in biotechnology, Trends Biotechnol. (2015). doi:10.1016/j.tibtech.2015.06.002.

[6] S. Mahnič-Kalamiza, E. Vorobiev, D. Miklavčič, Electroporation in food processing and biorefinery, J. Membr. Biol. 247 (2014) 1279–1304.

[7] J. Blahovec, E. Vorobiev, N. Lebovka, Pulsed Electric Fields Pretreatments for the Cooking of Foods, Food Eng. Rev. 9 (2017) 226–236. doi:10.1007/s12393-017-9170-x.

[8] M.L. Yarmush, A. Golberg, G. Serša, T. Kotnik, D. Miklavčič, Electroporation-Based Technologies for Medicine: Principles, Applications, and Challenges, Annu. Rev. Biomed. Eng. 16 (2014) 295–320. doi:10.1146/annurev-bioeng-071813-104622.

[9] D. Miklavčič, R.V. Davalos, Electrochemotherapy (ECT) and irreversible electroporation (IRE) -advanced techniques for treating deep-seated tumors based on electroporation, Biomed. Eng. OnLine. 14 (2015) I1. doi:10.1186/1475-925X-14-S3-I1.

[10] D. Miklavčič, B. Mali, B. Kos, R. Heller, G. Serša, Electrochemotherapy: from the drawing board into medical practice, Biomed. Eng. OnLine. 13 (2014) 29. doi:10.1186/1475-925X-13-29.

[11] R. Heller, L.C. Heller, Gene Electrotransfer Clinical Trials, in: Adv. Genet., Elsevier, 2015: pp. 235–262. http://linkinghub.elsevier.com/retrieve/pii/S0065266014000078 (accessed January 26, 2016).

[12] S. Vasan, A. Hurley, S.J. Schlesinger, D. Hannaman, D.F. Gardiner, D.P. Dugin, M. Boente-Carrera, R. Vittorino, M. Caskey, J. Andersen, Y. Huang, J.H. Cox, T. Tarragona-Fiol, D.K. Gill, H. Cheeseman, L. Clark, L. Dally, C. Smith, C. Schmidt, H.H. Park, J.T. Kopycinski, J. Gilmour, P. Fast, R. Bernard, D.D. Ho, In Vivo Electroporation Enhances the Immunogenicity of an HIV-1 DNA Vaccine Candidate in Healthy Volunteers, PLoS ONE. 6 (2011) e19252. doi:10.1371/journal.pone.0019252.

[13] C. Jiang, R.V. Davalos, J.C. Bischof, A Review of Basic to Clinical Studies of Irreversible Electroporation Therapy, IEEE Trans. Biomed. Eng. 62 (2015) 4–20. doi:10.1109/TBME.2014.2367543.

[14] R.V. Davalos, L.M. Mir, B. Rubinsky, Tissue Ablation with Irreversible Electroporation, Ann. Biomed. Eng. 33 (2005) 223–231. doi:10.1007/s10439-005-8981-8.

[15] B. Zorec, V. Préat, D. Miklavčič, N. Pavšelj, Active enhancement methods for intra- and transdermal drug delivery: a review., Zdr. Vestn. 82 (2013) 339–56.

[16] N. Dujardin, E. Staes, Y. Kalia, P. Clarys, R. Guy, V. Préat, In vivo assessment of skin electroporation using square wave pulses, J. Controlled Release. 79 (2002) 219–227.

[17] M. Marty, G. Serša, J.R. Garbay, J. Gehl, C.G. Collins, M. Snoj, V. Billard, P.F. Geertsen, J.O. Larkin, D. Miklavčič, I. Pavlović, S.M. Paulin-Košir, M. Čemažar, N. Morsli, D.M. Soden, Z. Rudolf, C. Robert, G.C. O'Sullivan, L.M. Mir, Electrochemotherapy – An easy, highly effective and safe treatment of cutaneous and subcutaneous metastases: Results of ESOPE (European Standard Operating Procedures of Electrochemotherapy) study, Eur. J. Cancer Suppl. 4 (2006) 3–13. doi:10.1016/j.ejcsup.2006.08.002.

[18] L.M. Mir, J. Gehl, G. Serša, C.G. Collins, J.-R. Garbay, V. Billard, P.F. Geertsen, Z. Rudolf, G.C. O'Sullivan, M. Marty, Standard operating procedures of the electrochemotherapy: Instructions for the use of bleomycin or cisplatin administered either systemically or locally and electric pulses delivered by the CliniporatorTM by means of invasive or non-invasive electrodes, Eur. J. Cancer Suppl. 4 (2006) 14–25.

[19] J.-M. Escoffre, M.-P. Rols, Electrochemotherapy: progress and prospects, Curr. Pharm. Des. 18 (2012) 3406–3415.

[20] J.E. Melvik, E.O. Pettersen, P.B. Gordon, P.O. Seglen, Increase in cis-dichlorodiammineplatinum (II) cytotoxicity upon reversible electropermeabilization of the plasma membrane in cultured human NHIK 3025 cells, Eur. J. Cancer Clin. Oncol. 22 (1986) 1523–1530.

[21] M. Čemažar, R. Milačič, D. Miklavčič, V. Dolzan, G. Serša, Intratumoral cisplatin administration in electrochemotherapy: antitumor effectiveness, sequence dependence and platinum content, Anticancer. Drugs. 9 (1998) 525–530. doi:10.1097/00001813-199807000-00002.

[22] G. Serša, M. Čemažar, D. Miklavčič, Antitumor effectiveness of electrochemotherapy with cis-diamminedichloroplatinum(II) in mice, Cancer Res. 55 (1995) 3450–3455.

[23] G. Serša, B. Štabuc, M. Čemažar, D. Miklavčič, Z. Rudolf, Electrochemotherapy with cisplatin: clinical experience in malignant melanoma patients, Clin. Cancer Res. Off. J. Am. Assoc. Cancer Res. 6 (2000) 863–867.

[24] G. Serša, B. Štabuc, M. Čemažar, B. Jančar, D. Miklavčič, Z. Rudolf, Electrochemotherapy with cisplatin: potentiation of local cisplatin antitumour effectiveness by application of electric pulses in cancer patients, Eur. J. Cancer. 34 (1998) 1213–1218. doi:10.1016/S0959-8049(98)00025-2.

[25] S. Spreckelmeyer, C. Orvig, A. Casini, Cellular Transport Mechanisms of Cytotoxic Metallodrugs: An Overview beyond Cisplatin, Molecules. 19 (2014) 15584–15610. doi:10.3390/molecules191015584.

[26] D. Gately, S. Howell, Cellular accumulation of the anticancer agent cisplatin: A review, Br. J. Cancer. 67 (1993) 1171–1176. doi:10.1038/bjc.1993.221.

[27] D.-W. Shen, L.M. Pouliot, M.D. Hall, M.M. Gottesman, Cisplatin Resistance: A Cellular Self-Defense Mechanism Resulting from Multiple Epigenetic and Genetic Changes, Pharmacol. Rev. 64 (2012) 706–721. doi:10.1124/pr.111.005637.

[28]   M. Čemažar, D. Miklavčič, L.. Mir, J. Belehradek, M. Bonnay, D. Fourcault, G. Serša, Electrochemotherapy of tumours resistant to cisplatin, Eur. J. Cancer. 37 (2001) 1166–1172. doi:10.1016/S0959-8049(01)00091-0.

[29]   A.-M. Florea, D. Büsselberg, Cisplatin as an Anti-Tumor Drug: Cellular Mechanisms of Activity, Drug Resistance and Induced Side Effects, Cancers. 3 (2011) 1351–1371. doi:10.3390/cancers3011351.

[30]   A. Johnsson, C. Olsson, O. Nygren, M. Nilsson, B. Seiving, E. Cavallin-Stahl, Pharmacokinetics and tissue distribution of cisplatin in nude mice: platinum levels and cisplatin-DNA adducts, Cancer Chemother. Pharmacol. 37 (1995) 23–31. doi:10.1007/BF00685625.

[31]   D. Miklavčič, G. Serša, E. Brecelj, J. Gehl, D. Soden, G. Bianchi, P. Ruggieri, C.R. Rossi, L.G. Campana, T. Jarm, Electrochemotherapy: technological advancements for efficient electroporation-based treatment of internal tumors, Med. Biol. Eng. Comput. 50 (2012) 1213–1225. doi:10.1007/s11517-012-0991-8.

[32]   D. Pavliha, B. Kos, A. Županič, M. Marčan, G. Serša, D. Miklavčič, Patient-specific treatment planning of electrochemotherapy: Procedure design and possible pitfalls, Bioelectrochemistry. 87 (2012) 265–273.

[33]   P.A. Garcia, B. Kos, J.H. Rossmeisl, D. Pavliha, D. Miklavčič, R.V. Davalos, Predictive therapeutic planning for irreversible electroporation treatment of spontaneous malignant glioma, Med. Phys. 44 (2017) 4968–4980. doi:10.1002/mp.12401.

[34]   I. Edhemović, E. Brecelj, G. Gasljevič, M. Marolt Mušič, V. Gorjup, B. Mali, T. Jarm, B. Kos, D. Pavliha, B. Grčar Kuzmanov, M. Čemažar, M. Snoj, D. Miklavčič, E.M. Gadžijev, G. Serša, Intraoperative electrochemotherapy of colorectal liver metastases: Electrochemotherapy of Liver Metastases, J. Surg. Oncol. 110 (2014) 320–327.

[35]   A. Županič, B. Kos, D. Miklavčič, Treatment planning of electroporation-based medical interventions: electrochemotherapy, gene electrotransfer and irreversible electroporation, Phys. Med. Biol. 57 (2012) 5425–5440. doi:10.1088/0031-9155/57/17/5425.

[36]   D. Miklavčič, S. Čorović, G. Pucihar, N. Pavšelj, Importance of tumour coverage by sufficiently high local electric field for effective electrochemotherapy, Eur. J. Cancer Suppl. 4 (2006) 45–51. doi:10.1016/j.ejcsup.2006.08.006.

[37]   O. Tounekti, G. Pron, J. Belehradek, L.M. Mir, Bleomycin, an apoptosis-mimetic drug that induces two types of cell death depending on the number of molecules internalized, Cancer Res. 53 (1993) 5462–5469.

[38]   S. Mahnič-Kalamiza, D. Miklavčič, E. Vorobiev, Dual-porosity model of solute diffusion in biological tissue modified by electroporation, Biochim. Biophys. Acta BBA - Biomembr. 1838 (2014) 1950–1966. doi:10.1016/j.bbamem.2014.03.004.

[39]   P.J. Canatella, M.M. Black, D.M. Bonnichsen, C. McKenna, M.R. Prausnitz, Tissue electroporation: quantification and analysis of heterogeneous transport in multicellular environments, Biophys. J. 86 (2004) 3260–3268. doi:10.1016/S0006-3495(04)74374-X.

[40]   G. Pucihar, T. Kotnik, J. Teissié, D. Miklavčič, Electropermeabilization of dense cell suspensions, Eur. Biophys. J. 36 (2007) 172–185.

[41]   L. Gibot, L. Wasungu, J. Teissié, M.-P. Rols, Antitumor drug delivery in multicellular spheroids by electropermeabilization, J. Controlled Release. 167 (2013) 138–147. doi:10.1016/j.jconrel.2013.01.021.

[42]   G. Serša, T. Jarm, T. Kotnik, A. Coer, M. Podkrajsek, M. Šentjurc, D. Miklavčič, M. Kadivec, S. Kranjc, A. Secerov, M. Čemažar, Vascular disrupting action of electroporation and electrochemotherapy with bleomycin in murine sarcoma, Br. J. Cancer. 98 (2008) 388–398. doi:10.1038/sj.bjc.6604168.

[43]   L.T. Baxter, R.K. Jain, Transport of fluid and macromolecules in tumors. I. Role of interstitial pressure and convection, Microvasc. Res. 37 (1989) 77–104. doi:10.1016/0026-2862(89)90074-5.

[44]   L.T. Baxter, R.K. Jain, Transport of fluid and macromolecules in tumors. II. Role of heterogeneous perfusion and lymphatics, Microvasc. Res. 40 (1990) 246–263. doi:10.1016/0026-2862(90)90023-K.

[45]   L.T. Baxter, R.K. Jain, Transport of fluid and macromolecules in tumors: III. Role of binding and metabolism, Microvasc. Res. 41 (1991) 5–23. doi:10.1016/0026-2862(91)90003-T.

[46]   P.J. Canatella, M.R. Prausnitz, Prediction and optimization of gene transfection and drug delivery by electroporation, Gene Ther. 8 (2001) 1464–1469. doi:10.1038/sj.gt.3301547.

[47]   E. Neumann, K. Toensing, S. Kakorin, P. Budde, J. Frey, Mechanism of electroporative dye uptake by mouse B cells, Biophys. J. 74 (1998) 98–108. doi:10.1016/S0006-3495(98)77771-9.

[48]   D. Miklavčič, L. Towhidi, Numerical study of the electroporation pulse shape effect on molecular uptake of biological cells, Radiol. Oncol. 44 (2010). doi:10.2478/v10019-010-0002-3.

[49]   Y. Granot, B. Rubinsky, Mass transfer model for drug delivery in tissue cells with reversible electroporation, Int. J. Heat Mass Transf. 51 (2008) 5610–5616. doi:10.1016/j.ijheatmasstransfer.2008.04.041.

[50]   J. Li, H. Lin, Numerical simulation of molecular uptake via electroporation, Bioelectrochemistry. 82 (2011) 10–21. doi:10.1016/j.bioelechem.2011.04.006.

[51]   S. Movahed, D. Li, Electrokinetic transport through the nanopores in cell membrane during electroporation, J. Colloid Interface Sci. 369 (2012) 442–452. doi:10.1016/j.jcis.2011.12.039.

[52]   S. Movahed, D. Li, Electrokinetic transport of nanoparticles to opening of nanopores on cell membrane during electroporation, J. Nanoparticle Res. 15 (2013). doi:10.1007/s11051-013-1511-y.

[53]   K.C. Smith, J.C. Weaver, Transmembrane molecular transport during versus after extremely large, nanosecond electric pulses, Biochem. Biophys. Res. Commun. 412 (2011) 8–12. doi:10.1016/j.bbrc.2011.06.171.

[54]   M. Puc, T. Kotnik, L.M. Mir, D. Miklavčič, Quantitative model of small molecules uptake after in vitro cell electropermeabilization, Bioelectrochemistry. 60 (2003) 1–10.

[55]   A. Agarwal, M. Wang, J. Olofsson, O. Orwar, S.G. Weber, Control of the Release of Freely Diffusing Molecules in Single-Cell Electroporation, Anal. Chem. 81 (2009) 8001–8008. doi:10.1021/ac9010292.

[56]   S. Mahnič-Kalamiza, D. Miklavčič, E. Vorobiev, Dual-porosity model of mass transport in electroporated biological tissue: Simulations and experimental work for model validation, Innov. Food Sci. Emerg. Technol. 29 (2015) 41–54. doi:10.1016/j.ifset.2014.09.011.

[57]   S. Mahnič-Kalamiza, N. Poklar Ulrih, E. Vorobiev, D. Miklavčič, A comprehensive theoretical study of thermal relations in plant tissue following electroporation, Int. J. Heat Mass Transf. 111 (2017) 150–162. doi:10.1016/j.ijheatmasstransfer.2017.03.119.

[58]   A. Martinčič, M. Čemažar, G. Serša, V. Kovač, R. Milačič, J. Ščančar, A novel method for speciation of Pt in human serum incubated with cisplatin, oxaliplatin and carboplatin by conjoint liquid chromatography on monolithic disks with UV and ICP-MS detection, Talanta. 116 (2013) 141–148. doi:10.1016/j.talanta.2013.05.016.

[59]   J. Dermol, D. Miklavčič, Mathematical Models Describing Chinese Hamster Ovary Cell Death Due to Electroporation In Vitro, J. Membr. Biol. 248 (2015) 865–881. doi:10.1007/s00232-015-9825-6.

[60]   K. Uršič, Š. Kos, U. Kamenšek, M. Čemažar, J. Ščančar, S. Bucek, S. Kranjc, B. Starešinič, G. Serša, Comparable effectiveness and immunomodulatory actions of oxaliplatin and cisplatin in electrochemotherapy of murine melanoma, Bioelectrochemistry. 119 (2018) 161–171. doi:10.1016/j.bioelechem.2017.09.009.

[61]   J. Dermol, O.N. Pakhomova, A.G. Pakhomov, D. Miklavčič, Cell Electrosensitization Exists Only in Certain Electroporation Buffers, PLOS ONE. 11 (2016) e0159434. doi:10.1371/journal.pone.0159434.

[62]   M. Ušaj, K. Trontelj, D. Miklavčič, M. Kandušer, Cell-cell electrofusion: optimization of electric field amplitude and hypotonic treatment for mouse melanoma (B16-F1) and Chinese Hamster ovary (CHO) cells, J. Membr. Biol. 236 (2010) 107–116. doi:10.1007/s00232-010-9272-3.

[63]   S. Mesojednik, D. Pavlin, G. Sersa, A. Coer, S. Kranjc, A. Grosel, G. Tevz, M. Cemazar, The effect of the histological properties of tumors on transfection efficiency of electrically assisted gene delivery to solid tumors in mice, Gene Ther. 14 (2007) 1261–1269. doi:10.1038/sj.gt.3302989.

[64]   G.A. Meek, H.Y. Elder, Analytical and Quantitative Methods in Microscopy, CUP Archive, 1977.

[65]   A. Maček Lebar, G. Serša, M. Čemažar, D. Miklavčič, Elektroporacija Electroporation, Med. Razgledi. (1998) 339–354.

[66]   R. Shirakashi, V.L. Sukhorukov, I. Tanasawa, U. Zimmermann, Measurement of the permeability and resealing time constant of the electroporated mammalian cell membranes, Int. J. Heat Mass Transf. 47 (2004) 4517–4524. doi:10.1016/j.ijheatmasstransfer.2004.04.007.

[67]   C.S. Djuzenova, U. Zimmermann, H. Frank, V.L. Sukhorukov, E. Richter, G. Fuhr, Effect of medium conductivity and composition on the uptake of propidium iodide into electropermeabilized myeloma cells, Biochim. Biophys. Acta BBA - Biomembr. 1284 (1996) 143–152. doi:10.1016/S0005-2736(96)00119-8.

[68]   S. Čorović, L.M. Mir, D. Miklavčič, In Vivo Muscle Electroporation Threshold Determination: Realistic Numerical Models and In Vivo Experiments, J. Membr. Biol. 245 (2012) 509–520. doi:10.1007/s00232-012-9432-8.

[69]   D. Šel, A.M. Lebar, D. Miklavčič, Feasibility of Employing Model-Based Optimization of Pulse Amplitude and Electrode Distance for Effective Tumor Electropermeabilization, IEEE Trans. Biomed. Eng. 54 (2007) 773–781. doi:10.1109/TBME.2006.889196.

[70]   J. Dermol, D. Miklavčič, Predicting electroporation of cells in an inhomogeneous electric field based on mathematical modeling and experimental CHO-cell permeabilization to propidium iodide determination, Bioelectrochemistry. 100 (2014) 52–61. doi:10.1016/j.bioelechem.2014.03.011.

[71]   O. Tounekti, A. Kenani, N. Foray, S. Orlowski, Ll.M. Mir, The ratio of single- to double-strand DNA breaks and their absolute values determine cell death pathway, Br. J. Cancer. 84 (2001) 1272–1279.

[72]   G. Poste, J. Doll, I.R. Hart, I.J. Fidler, In vitro selection of murine B16 melanoma variants with enhanced tissue-invasive properties, Cancer Res. 40 (1980) 1636–1644.

[73]   T.B. Napotnik, D. Miklavčič, In vitro electroporation detection methods – An overview, Bioelectrochemistry. (2017). doi:10.1016/j.bioelechem.2017.12.005.

[74]   J. Belehradek, S. Orlowski, L.H. Ramirez, G. Pron, B. Poddevin, L.M. Mir, Electropermeabilization of cells in tissues assessed by the qualitative and quantitative electroloading of bleomycin, Biochim. Biophys. Acta. 1190 (1994) 155–163.

[75]   P.E. Engström, B.R.R. Persson, L.G. Salford, Dynamic gamma camera studies of –bleomycin complex in normal and glioma bearing rats after in vivo electropermeabilization using exponential high-voltage pulses, Bioelectrochem. Bioenerg. 46 (1998) 241–248. doi:10.1016/S0302-4598(98)00141-X.

[76]   G. Grafström, P. Engström, L.G. Salford, B.R.R. Persson, 99mTc-DTPA uptake and electrical impedance measurements in verification of in vivo electropermeabilization efficiency in rat muscle, Cancer Biother. Radiopharm. 21 (2006) 623–635. doi:10.1089/cbr.2006.21.623.

[77]   D. Batiuškaitė, D. Cukjati, L.M. Mir, Comparison of in vivo electropermeabilization of normal and malignant tissue using the 51Cr-EDTA uptake test, Biologija. 2003 (2003) 45–47.

[78]   P.A. Garcia, J.H. Rossmeisl, J.L. Robertson, J.D. Olson, A.J. Johnson, T.L. Ellis, R.V. Davalos, 7.0-T Magnetic Resonance Imaging Characterization of Acute Blood-Brain-Barrier Disruption Achieved with Intracranial Irreversible Electroporation, PLoS ONE. 7 (2012) e50482. doi:10.1371/journal.pone.0050482.

[79]   M. Kranjc, B. Markelc, F. Bajd, M. Čemažar, I. Serša, T. Blagus, D. Miklavčič, In Situ Monitoring of Electric Field Distribution in Mouse Tumor during Electroporation, Radiology. 274 (2015) 115–123. doi:10.1148/radiol.14140311.

[80]   G. Serša, S. Kranjc, J. Ščančar, M. Kržan, M. Čemažar, Electrochemotherapy of Mouse Sarcoma Tumors Using Electric Pulse Trains with Repetition Frequencies of 1 Hz and 5 kHz, J. Membr. Biol. 236 (2010) 155–162. doi:10.1007/s00232-010-9268-z.

[81]   M. Ogihara, O. Yamaguchi, Potentiation of effects of anticancer agents by local electric pulses in murine bladder cancer, Urol. Res. 28 (2000) 391–397.

[82]   M. Čemažar, D. Miklavčič, J. Ščančar, V. Dolžan, R. Golouh, G. Serša, Increased platinum accumulation in SA-1 tumour cells after in vivo electrochemotherapy with cisplatin, Br. J. Cancer. 79 (1999) 1386–1391. doi:10.1038/sj.bjc.6690222.

[83]   M. Čemažar, V. Todorović, J. Ščančar, U. Lampreht, M. Štimac, U. Kamenšek, S. Kranjc, A. Coer, G. Serša, Adjuvant TNF-α therapy to electrochemotherapy with intravenous cisplatin in murine sarcoma exerts synergistic antitumor effectiveness, Radiol. Oncol. 49 (2015) 32–40. doi:10.1515/raon-2015-0005.

[84]   R. Hudej, D. Miklavčič, M. Čemažar, V. Todorović, G. Serša, A. Bergamo, G. Sava, A. Martinčič, J. Ščančar, B.K. Keppler, I. Turel, Modulation of Activity of Known Cytotoxic Ruthenium(III) Compound (KP418) with Hampered Transmembrane Transport in Electrochemotherapy In Vitro and In Vivo, J. Membr. Biol. 247 (2014) 1239–1251. doi:10.1007/s00232-014-9696-2.

[85]   G. Pucihar, T. Kotnik, D. Miklavčič, J. Teissié, Kinetics of Transmembrane Transport of Small Molecules into Electropermeabilized Cells, Biophys. J. 95 (2008) 2837–2848. doi:10.1529/biophysj.108.135541.

[86]   J. Gehl, T. Skovsgaard, L.M. Mir, Enhancement of cytotoxicity by electropermeabilization: an improved method for screening drugs, Anticancer. Drugs. 9 (1998) 319–325.

[87]   V. Todorović, G. Serša, K. Flisar, M. Čemažar, Enhanced cytotoxicity of bleomycin and cisplatin after electroporation in murine colorectal carcinoma cells, Radiol. Oncol. 43 (2009). doi:10.2478/v10019-009-0037-5.

[88]   J.L. Vásquez, P. Ibsen, H. Lindberg, J. Gehl, In Vitro and In Vivo Experiments on Electrochemotherapy for Bladder Cancer, J. Urol. 193 (2015) 1009–1015. doi:10.1016/j.juro.2014.09.039.

[89]   Q. Chang, O.I. Ornatsky, I. Siddiqui, R. Straus, V.I. Baranov, D.W. Hedley, Biodistribution of cisplatin revealed by imaging mass cytometry identifies extensive collagen binding in tumor and normal tissues, Sci. Rep. 6 (2016). doi:10.1038/srep36641.

[90]   W.J.F. van der Vijgh, I. Klein, Protein binding of five platinum compounds: Comparison of two ultrafiltration systems, Cancer Chemother. Pharmacol. 18 (1986) 129–132. doi:10.1007/BF00262281.

[91]   J.E. Melvik, J.M. Dornish, E.O. Pettersen, The binding of cis-dichlorodiammineplatinum(II) to extracellular and intracellular compounds in relation to drug uptake and cytotoxicity in vitro, Br. J. Cancer. 66 (1992) 260–265. doi:10.1038/bjc.1992.254.

[92]   K. Takahashi, T. Seki, K. Nishikawa, S. Minamide, M. Iwabuchi, M. Ono, S. Nagamine, H. Horinishi, Antitumor activity and toxicity of serum protein-bound platinum formed from cisplatin, Jpn. J. Cancer Res. Gann. 76 (1985) 68–74.

[93]   P.A. Andrews, S. Velury, S.C. Mann, S.B. Howell, cis-Diamminedichloroplatinum(II) accumulation in sensitive and resistant human ovarian carcinoma cells, Cancer Res. 48 (1988) 68–73.

[94]   P. Workman, E.O. Aboagye, F. Balkwill, A. Balmain, G. Bruder, D.J. Chaplin, J.A. Double, J. Everitt, D.A.H. Farningham, M.J. Glennie, L.R. Kelland, V. Robinson, I.J. Stratford, G.M. Tozer, S. Watson, S.R. Wedge, S.A. Eccles, Guidelines for the welfare and use of animals in cancer research, Br. J. Cancer. 102 (2010) 1555–1577. doi:10.1038/sj.bjc.6605642.

[95]   S.M. Sancho-Martínez, L. Prieto-García, M. Prieto, J.M. López-Novoa, F.J. López-Hernández, Subcellular targets of cisplatin cytotoxicity: An integrated view, Pharmacol. Ther. 136 (2012) 35–55. doi:10.1016/j.pharmthera.2012.07.003.

[96]   M. Nishikawa, M. Hashida, Pharmacokinetics of anticancer drugs, plasmid DNA, and their delivery systems in tissue-isolated perfused tumors, Adv. Drug Deliv. Rev. 40 (1999) 19–37. doi:10.1016/S0169-409X(99)00038-1.

[97]   M. Pavlin, N. Pavšelj, D. Miklavčič, Dependence of induced transmembrane potential on cell density, arrangement, and cell position inside a cell system, IEEE Trans. Biomed. Eng. 49 (2002) 605–612. doi:10.1109/TBME.2002.1001975.

[98]   M. Essone Mezeme, G. Pucihar, M. Pavlin, C. Brosseau, D. Miklavčič, A numerical analysis of multicellular environment for modeling tissue electroporation, Appl. Phys. Lett. 100 (2012) 143701. doi:10.1063/1.3700727.

[99]   D. Miklavčič, M. Snoj, A. Županič, B. Kos, M. Čemažar, M. Kropivnik, M. Bračko, T. Pečnik, E.M. Gadžijev, G. Serša, Towards treatment planning and treatment of deep-seated solid tumors by electrochemotherapy, Biomed. Eng. OnLine. 9 (2010) 10. doi:10.1186/1475-925X-9-10.

[100]   A.I. Minchinton, I.F. Tannock, Drug penetration in solid tumours, Nat. Rev. Cancer. 6 (2006) 583–592. doi:10.1038/nrc1893.

[101]   J. Pušenjak, D. Miklavčič, Modeling of interstitial fluid pressure in solid tumor, Simul. Pract. Theory. 8 (2000) 17–24.

[102]   L.J. Nugent, R.K. Jain, Extravascular diffusion in normal and neoplastic tissues, Cancer Res. 44 (1984) 238–244.

[103]   P.F. Morrison, R.L. Dedrick, Transport of Cisplatin in Rat Brain Following Microinfusion: an Analysis, J. Pharm. Sci. 75 (1986) 120–128. doi:10.1002/jps.2600750204.

[104]   G.M. Thurber, R. Weissleder, A Systems Approach for Tumor Pharmacokinetics, PLoS ONE. 6 (2011) e24696. doi:10.1371/journal.pone.0024696.

[105]   M. Čemažar, T. Jarm, D. Miklavčič, A. Maček Lebar, A. Ihan, N.A. Kopitar, G. Serša, Effect of electric-field intensity on electropermeabilization and electrosensitivity of various tumor-cell lines in vitro, Electro- Magnetobiology. 17 (1998) 263–272.

[106]   C. Rosazza, S. Haberl Meglič, A. Zumbusch, M.-P. Rols, D. Miklavčič, Gene Electrotransfer: A Mechanistic Perspective, Curr. Gene Ther. 16 (2016) 98–129. doi:10.2174/1566523216666160331130040.

[107]   V. Sresht, J.R. Bellare, S.K. Gupta, Modeling the Cytotoxicity of Cisplatin, Ind. Eng. Chem. Res. 50 (2011) 12872–12880. doi:10.1021/ie102360e.

[108]   J.-Y. Hong, G.-H. Kim, J.-W. Kim, S.-S. Kwon, E.F. Sato, K.-H. Cho, E. Shim, Computational modeling of apoptotic signaling pathways induced by cisplatin, BMC Syst. Biol. 6 (2012) 122. doi:10.1186/1752-0509-6-122.

[109]   A.W. El-Kareh, T.W. Secomb, A Mathematical Model for Cisplatin Cellular Pharmacodynamics, Neoplasia. 5 (2003) 161–169. doi:10.1016/S1476-5586(03)80008-8.

[110]   P.D. Sadowitz, B.A. Hubbard, J.C. Dabrowiak, J. Goodisman, K.A. Tacka, M.K. Aktas, M.J. Cunningham, R.L. Dubowy, A.-K. Souid, Kinetics of cisplatin binding to cellular DNA and modulations by thiol-blocking agents and thiol drugs, Drug Metab. Dispos. Biol. Fate Chem. 30 (2002) 183–190.

Conclusions and future work

In the scope of this doctoral dissertation, we have modeled electroporation at the level of single cells and the level of tissues. At the level of single cells, experiments are relatively easy to perform, and a large spectrum of parameters can be explored without ethical issues which are present in animal experiments (Workman et al. 2010). However, not many models include single-cell properties in the bulk tissue models. Our aim was to use results of cell level in vitro experiments to establish models which can be then used to model electroporation in vivo.

First, we have employed mathematical models of cell membrane permeability and cell death to describe results of in vitro experiments on cell suspensions and cell monolayers. We concluded that several models describe the experimental data well. Our optimized Peleg-Fermi model of cell death was already used on tissues with good accuracy of prediction (Kranjc et al. 2017). In the survival models, the models approach survival zero but never reach it. It remains to be established how low the survival has to be to achieve a complete response. The last few remaining cells in electrochemotherapy as well as in ablation with irreversible electroporation are shown to be eradicated by the immune system (Neal et al. 2013; Serša et al. 2015).

We analyzed the time-dynamics of the dye uptake into cells after electroporation. We could describe the uptake with the first-order model which corresponded to the dynamics of pore resealing in the cell membrane. In several studies, speed of resealing was assessed and it was determined that it was in the range of minutes in the in vitro as well as in the in vivo experiments, which was in agreement with our experimental data (Kinosita and Tsong 1977; Saulis et al. 1991; Čemažar et al. 1998; Shirakashi et al. 2004; Kandušer et al. 2006; Demiryurek et al. 2015).

In electroporation of excitable tissues, we can trigger action potential and thus muscle contraction and pain. We determined experimental strength-duration curve for excitable and non-excitable cell lines and modeled it with the phenomenological Lapicque curve and the Hodgkin-Huxley model. In future, it should be established to what extent the in vitro determined strength-duration curve correlates to the in vivo muscle contractions and pain sensation. When using strength-duration curves to predict action potential in excitable cells, we have to take into account that for a while after the pulses cells are not able to trigger an action potential. In future, a model describing the time between delivered electric pulses and action potential could be determined. There are even studies which showed that high-voltage electric pulses could cause damage to membrane proteins like voltage-gated channels (Chen et al. 2006b; Azan et al. 2017). The protein conformational changes that open and close the channel gate take place on the order of a hundred times per second, i.e., in the range of milliseconds (Gadsby 2009). It is interesting that nanosecond pulses are even able to trigger an action potential (Pakhomov et al. 2017) as they are much shorter than the time needed for conformational changes of voltage-gated channels. The models of excitability were determined phenomenologically in the range of physiologically possible transmembrane voltages. However, electroporation increases the transmembrane voltage more which is thus outside the range of the physiological values. It should be established to what extent the current excitability models are valid in the range of high transmembrane voltages (several hundreds of millivolts).

Second, we have modeled the change in dielectric properties of tissues by modeling pore formation in cell membranes and local transport region formation in the stratum corneum. In future, a similar model could also be built for other tissues and validated with current-voltage measurements. For example, this could be done for electroporation of liver metastases or muscles. A possible upgrade of the model is to model also change in pore radii during pulses. Namely, with the asymptotic equation of pore formation, we assume that all pores are of the same radii and only their density changes. We could use a method described in (Smith et al. 2004) and model also change in pore radii. In this way, the change in of dielectric properties of skin layers would not be determined based on the best agreement with the measurements, but it would be based on mechanisms of electroporation. We achieved good agreement with current-voltage measurements when long low-voltage pulses were applied. However, when short high-voltage pulses were applied the modeled current deviated 50% from the measured one. In experiments, additional current component appeared which could not be explained by the formation of the local transport regions. Even if we assumed that the whole stratum corneum was one big local transport region or that the whole stratum corneum was substituted with the electroporation buffer, the simulated current through the skin was lower than the measured one, and simulated voltage drop on skin was too low as the conductivity of skin was too high. When measuring voltage drop on the skin two thin copper wires were used, one on each side of the skin. Copper wires created a preferential high-conductivity path for the electric current because they were much more conductive than the electroporation buffer or the skin. Thus, electric current could locally increase and contribute to the measured current, but it would not affect voltage drop on the skin. In future, also electrochemistry happening during electroporation should be evaluated. During electroporation pH changes, metal is released from the electrodes. We can see bubble formation, which could be a consequence of local water evaporation or chemical reactions and formation of different gases. We could also include thermal effects. Because of Joule heating the temperature increases and consequently, electric conductivity also increases. In our model, heating was included indirectly, through the increase of radii of local transport regions, which occurs due to lipid melting in the stratum corneum. In future, also melting of lipids could be included in our model of local transport region formation (Becker and Kuznetsov 2007; Becker 2012; Becker et al. 2014). Currently, we have taken the values of radii of local transport regions directly from (Zorec et al. 2013a), we have only added a slight decrease in radii during the pause between pulses, which described the experimental data better.

In the model, we have estimated the induced transmembrane voltage by treating the skin as a voltage divider and taking into account the thickness of one layer and size of cells in that layer. However, the induced transmembrane voltage is decreased due to close cell connections and electric field shielding. It is possible that we overestimated the change in conductivity of lower layers and underestimated the conductivity of local transport regions or their size and density. The change in the electric conductivity of skin layers influences the electric field distribution and vice versa which could also introduce errors in our modeling.

Third, we have modeled transport of small molecule in tumor during electroporation. Our model is valid for small molecules in the range of cisplatin size (300 g/mol). It was shown that larger molecules pass cell membrane with more difficulty than small molecules when electric pulses of the same parameters are

applied (Maček Lebar et al. 1998). The first reason could be lower diffusion coefficient of larger molecules in the tumor interstitial fraction than of smaller molecules. Also, larger molecules enter cells predominantly by electrophoresis while small molecules enter cells predominantly by diffusion (Pucihar et al. 2008). Larger molecules, i.e., DNA, enter cells in several steps (Rosazza et al. 2016). Currently, in the model, we assume that all the transport is due to diffusion, which is not necessarily always valid. Due to increased interstitial pressure in the tumor (Baxter and Jain 1989; Boucher et al. 1990; Pušenjak and Miklavčič 2000), convection mediated washout of drugs from the tumors is elevated. In the case of systemic drug administration, this translates to the hindered entrance of drugs into the tumor. In the case of intratumoral drug administration, which was employed in our in vivo experiments, this translates to increase in the washout of the drug from the tumor. We found several velocities of the convective transport in the literature (Ning et al. 1999). However, they did not correspond to our measurements of intracellular platinum mass before pulse application and one hour after it. By inserting existing velocities from the literature in our numerical model, all cisplatin was washed out in a few minutes. In future, the convective transport in the mouse melanoma tumor needs to be evaluated. Our model was tested on only one tumor type. It is known that different tumors have a different cell and matrix volume fractions (Mesojednik et al. 2007). Different volume fractions influenced the diffusion coefficient of molecules in the tumor and the surface of the cell membranes, available for the transport. In future, or model could be tested with different tumor types. We could evaluate if transformation coefficient could be predicted from the tumor morphology. I believe that such a transformation should exist – higher cell and matrix volume fractions in tumor should be reflected in lower mobility of chemotherapeutic in the tumor and the cells and consequently, in lower transformation coefficient. Another question is whether transformation coefficient depends on parameters of electric pulses. Currently, we have tested our model at single pulse parameters in vivo. More experiments are needed to test our model in wider parameter space and determine the functional dependency of the transformation coefficient.

When delivering chemotherapeutic intratumorally, we avoid several steps in chemotherapeutic transport, when it is delivered systemically. In systemic administration, the drug must first enter the bloodstream and distribute through the vascular compartment, transport across the microvascular wall and then through the interstitial fraction (Jain 1999; Jang et al. 2003). In a tumor, increased interstitial pressure decreases drug transport into the tumor and facilitates drug washout from the tumor. In our model, we took into account intratumoral delivery of cisplatin where we made a justified assumption of initial homogeneous distribution of cisplatin in high concentration. If chemotherapeutic were delivered systemically, we would need to additionally calculate initial conditions of cisplatin concentration in a tumor.

In the in vitro experiments, all cisplatin was accounted for. In the in vivo experiments, we injected 26 µg of platinum by intratumoral injection of 80 µl in 35 mm³ tumors. The volume of injection was two-times the volume of a tumor because we reused the data from (Uršič et al. 2018). Most of the injected platinum was not measured. When a tumor was excised 2 min after cisplatin injection, we determined that 27 % of the injected platinum was still present in a tumor and the serum. A part of cisplatin was lost due to lower tumor volume than injection volume and due to washout of cisplatin from the tumor. When a tumor was excised after 1 hour, we determined that in a tumor and serum there was 2% of the injected platinum (control

samples - cisplatin injection, no electroporation) and 7 % in the treated (cisplatin injection and electroporation) samples. Thus, in vivo, the majority of cisplatin was unaccounted for. Part of cisplatin was lost when the tumor was mechanically disintegrated and during blood collection. Part of cisplatin could accumulate in different organs and cause unwanted side effects (Sancho-Martínez et al. 2012). In future, it should be established if injecting a lower volume of cisplatin could maintain high treatment efficacy while decreasing unwanted side effects. In the literature, it was observed that changing the volume of injection did not affect treatment efficacy (Wang 2006; Frandsen et al. 2017) which was also in agreement with our results. Namely, although almost 70% of the injected cisplatin volume was lost already when injecting cisplatin, the remaining cisplatin in the tumor was in high concentration, and consequently, the concentration gradient was high.

Number of bleomycin molecules necessary to cause cell death was determined in (Tounekti et al. 1993; Tounekti et al. 2001). A similar analysis should also be done for cisplatin as it would allow us to optimize treatment parameters to achieve a high enough intracellular cisplatin concentration. The inductively coupled plasma – mass spectrometry enables precise measurements of platinum mass in the cells. We could also perform experiments evaluating cell death (e.g., by the clonogenic assay) at the same pulse parameters used in the measurements of the platinum uptake. Then, we could link the survival and transport and determine the necessary number of cisplatin molecules to cause cell death. Namely, the complete tumor eradication is our final goal in electrochemotherapy, and our model of the cisplatin transport is a step forward in achieving more precise prediction of cell death.

Electroporation results in an increase of membrane electric conductivity and permeability, which can be understood as two separate phenomena (Miklavčič and Towhidi 2010; Leguèbe et al. 2014). The initial idea was to connect membrane conductivity and permeability in one model. However, this idea was deemed difficult to achieve. Already in the initial experiments, we determined that when exposing cells to electric pulses in buffers which varied in their ionic composition but were of similar electric conductivity much different time dynamics of a dye uptake was measured (Dermol et al. 2016). It was observed as well that electroporation buffer conductivity did not affect cell sensitization (Gianulis et al. 2018). A similar electric conductivity of a buffer would indicate similar induced transmembrane voltage and thus similar pore density. In future, it would be interesting to determine what is the connection between cell membrane conductivity and permeability or if permeability is largely influenced by biological processes happening in a cell. The electric conductivity of cell membrane namely decreases relatively fast after pulse application, while the transport lasts for several minutes or even hours if cells are left to reseal at lower temperatures (Saulis et al. 1991). Another possible explanation of prolonged transport is the oxidative damage caused to the cell membrane by electric pulses (Benov et al. 1994; Gabriel and Teissié 1995; Maccarrone et al. 1995; Pakhomova et al. 2012). Oxidative damage disturbs the lipid bilayer and increases membrane permeability.

One of the main problems when modeling electroporation is the lack of measurements and experimental data, e.g., electric conductivity of the local transport regions, the convective transport in the tumors, the initial drug distribution prior to electroporation treatment, electric conductivity of separate skin layers before and after electroporation, the change in local transport region radii as a function of pulse duration and electric field. The models describing electroporation are namely very complex and have a large number

of parameters whose values are only estimated. When establishing and optimizing models of electroporation, we can thus in many cases determine only local optimal values of parameters and not necessarily global optimal values, as we determined in (Dermol-Černe and Miklavčič 2018).

In future, we aim to use the presented models in the treatment planning of electroporation-based treatments. When optimizing electrode geometry and pulse parameters, currently we aim to reach a high-enough experimentally determined critical electric field. We could first introduce the statistical models of cell death and permeability. Later, we could aim to achieve a high-enough intracellular cisplatin concentration or even number of molecules to cause cell death. We could decrease muscle contractions and pain which would shorten and simplify the treatment. We could add measurement of the electric field in the tissue (Kranjc et al. 2014; Kranjc et al. 2015) and change the pulse parameters in real-time while delivering electric pulses to more precisely know the expected outcome.

In my opinion, natural sciences cannot exist without models which describe the processes, predict the behavior of biological systems, offer insights into biological processes and their connections, and decrease number of needed experiments. In this thesis, I have tried to unveil a small part of knowledge in the field of electroporation. With the knowledge I have gained in the process of model development, even more questions exist now than there did when I first started working on my Ph.D. and they should be answered in future.

Original Scientific Contributions

Mathematical modeling of cell membrane permeability and cell death

We used mathematical models to describe and predict cell membrane permeability and depolarization and cell death in vitro. First, we made an overview of the existing models. The existing models are mostly phenomenological and do not include any electroporation mechanisms. Only a few models of cell membrane permeability exist. On the contrary, there are many models of cell death because they are being used for prediction of the efficacy of pulsed electric field assisted food pasteurization and sterilization. The parameters of the models were optimized using experimental results. Cell membrane permeability and depolarization were assessed by fluorescent dyes, and spectrofluorometric measurements and fluorescent microscopy and cell death was assessed by metabolic activity test and clonogenic assay. The experiments were performed on attached monolayers and cell suspensions. Our in vitro data was described well with several different models. An easy transformation from cell level to tissue level was not possible – each model had to be optimized separately for each tissue type, and thus their predictive power was limited.

The transition between single-cell models and the tissue models, where the realistic three-dimensional skin model is presented with the model of electroporation of all components and essential layers of the skin

Electroporation changes dielectric properties of tissues which can be assessed by different measuring methods. We built a three-dimensional skin model by taking into account geometry of single cells. Each cell was representative of the whole layer – corneocytes of the stratum corneum, keratinocytes of the epidermis and lipid spheres of the papillary dermis. We modeled dielectric properties of each layer analytically by the Hanai-Bruggeman formula or numerically, by a 'unit cell' to obtain a bulk skin model. We added electroporation with long low-voltage or short high-voltage pulses to our model. We modeled formation and growth of local transport regions in the stratum corneum. By asymptotic pore equation we modeled pore formation on membranes of the cells of the lower layers. We accurately described current-voltage measurements of skin electroporation. Our method can be used to determine the change in dielectric properties due to electroporation of any tissue, as long as the geometric and the dielectric properties of cells constituting the tissue are known.

Mathematical modeling of transport of small molecules (chemotherapeutic) across the cell membrane using the dual porosity model

For efficient electrochemotherapy treatment, a sufficient uptake of chemotherapeutic in the tumor cells has to be achieved to cause cell death. We accurately described the uptake of cisplatin by the tumor cells in the mouse melanoma tumors. We performed experiments in vitro and measured the mass of the intracellular platinum by the inductively coupled plasma – mass spectrometry. With the dual porosity model, we calculated the permeability coefficient as a function of pulse number and electric field. We have built a 3D tumor model where we described the transport of cisplatin between several compartments - tumor cells, interstitial tumor fraction, and peritumoral environment. We determined that in vitro permeability coefficient could be used to model uptake of cisplatin in vivo. However, in vivo, the transport was slower due to close cell connections, smaller available membrane area for transport and presence of cell matrix.

These differences between in vivo and in vitro were taken into account by a transformation coefficient, which is most likely a function of tumor morphology. Our model can be in future used in treatment planning of electrochemotherapy.

References

Abidor IG, Arakelyan VB, Chernomordik LV, Chizmadzhev YA, Pastushenko VF, Tarasevich MR (1979) 246 - Electric breakdown of bilayer lipid membranes I. The main experimental facts and their qualitative discussion. Bioelectrochem Bioenerg 6:37–52 . doi: 10.1016/0302-4598(79)85005-9

Abidor IG, Barbul AI, Zhelev DV, Doinov P, Bandrina IN, Osipova EM, Sukharev SI (1993) Electrical properties of cell pellets and cell electrofusion in a centrifuge. Biochim Biophys Acta 1152:207–218

Agarwal A, Wang M, Olofsson J, Orwar O, Weber SG (2009) Control of the Release of Freely Diffusing Molecules in Single-Cell Electroporation. Anal Chem 81:8001–8008 . doi: 10.1021/ac9010292

Agerholm-Larsen B, Iversen HK, Ibsen P, Moller JM, Mahmood F, Jensen KS, Gehl J (2011) Preclinical Validation of Electrochemotherapy as an Effective Treatment for Brain Tumors. Cancer Res 71:3753–3762 . doi: 10.1158/0008-5472.CAN-11-0451

Aihara H, Miyazaki J (1998) Gene transfer into muscle by electroporation in vivo. Nat Biotechnol 16:867–870 . doi: 10.1038/nbt0998-867

Alberts B, Bray D, Hopkin K, Johnson AD, Johnson A, Lewis J, Raff M, Roberts K, Walter P (2009) Essential Cell Biology, 3 edition. Garland Science, New York

Antov Y, Barbul A, Mantsur H, Korenstein R (2005) Electroendocytosis: Exposure of Cells to Pulsed Low Electric Fields Enhances Adsorption and Uptake of Macromolecules. Biophys J 88:2206–2223 . doi: 10.1529/biophysj.104.051268

Arena CB, Davalos RV (2012) Advances in Therapeutic Electroporation to Mitigate Muscle Contractions. J Membr Sci Technol 02: . doi: 10.4172/2155-9589.1000e102

Arena CB, Sano MB, Rylander MN, Davalos RV (2011) Theoretical Considerations of Tissue Electroporation With High-Frequency Bipolar Pulses. IEEE Trans Biomed Eng 58:1474–1482 . doi: 10.1109/TBME.2010.2102021

Argus F, Boyd B, Becker SM (2017) Electroporation of tissue and cells: A three-equation model of drug delivery. Comput Biol Med 84:226–234 . doi: 10.1016/j.compbiomed.2017.04.001

Asami K (2002) Characterization of heterogeneous systems by dielectric spectroscopy. Prog Polym Sci 27:1617–1659 . doi: 10.1016/S0079-6700(02)00015-1

Azan A, Untereiner V, Descamps L, Merla C, Gobinet C, Breton M, Piot O, Mir LM (2017) Comprehensive Characterization of the Interaction between Pulsed Electric Fields and Live Cells by Confocal Raman Microspectroscopy. Anal Chem 89:10790–10797 . doi: 10.1021/acs.analchem.7b02079

Ball C, Thomson KR, Kavnoudias H (2010) Irreversible Electroporation: A New Challenge in "Out of Operating Theater" Anesthesia. Anesth Analg 110:1305–1309 . doi: 10.1213/ANE.0b013e3181d27b30

Barnes FS, Greenebaum B (eds) (2006) Handbook of Biological Effects of Electromagnetic Fields, Third Edition - 2 Volume Set, 3 edition. CRC Press, Boca Raton, FL

Batiuškaitė D, Cukjati D, Mir LM (2003) Comparison of in vivo electropermeabilization of normal and malignant tissue using the 51Cr-EDTA uptake test. Biologija 2003:45–47

Baxter DF, Kirk M, Garcia AF, Raimondi A, Holmqvist MH, Flint KK, Bojanic D, Distefano PS, Curtis R, Xie Y (2002) A novel membrane potential-sensitive fluorescent dye improves cell-based assays for ion channels. J Biomol Screen 7:79–85 . doi: 10.1177/108705710200700110

References

Baxter LT, Jain RK (1989) Transport of fluid and macromolecules in tumors. I. Role of interstitial pressure and convection. Microvasc Res 37:77–104 . doi: 10.1016/0026-2862(89)90074-5

Baxter LT, Jain RK (1990) Transport of fluid and macromolecules in tumors. II. Role of heterogeneous perfusion and lymphatics. Microvasc Res 40:246–263 . doi: 10.1016/0026-2862(90)90023-K

Baxter LT, Jain RK (1991) Transport of fluid and macromolecules in tumors: III. Role of binding and metabolism. Microvasc Res 41:5–23 . doi: 10.1016/0026-2862(91)90003-T

Becker S (2012) Transport modeling of skin electroporation and the thermal behavior of the stratum corneum. Int J Therm Sci 54:48–61 . doi: 10.1016/j.ijthermalsci.2011.10.022

Becker S, Zorec B, Miklavčič D, Pavšelj N (2014) Transdermal transport pathway creation: Electroporation pulse order. Math Biosci 257:60–68 . doi: 10.1016/j.mbs.2014.07.001

Becker SM, Kuznetsov AV (2007) Local Temperature Rises Influence In Vivo Electroporation Pore Development: A Numerical Stratum Corneum Lipid Phase Transition Model. J Biomech Eng 129:712 . doi: 10.1115/1.2768380

Becker SM, Kuznetsov AV (eds) (2013) Transport in biological media. Elsevier Science, Amsterdam

Belehradek J, Orlowski S, Ramirez LH, Pron G, Poddevin B, Mir LM (1994) Electropermeabilization of cells in tissues assessed by the qualitative and quantitative electroloading of bleomycin. Biochim Biophys Acta 1190:155–163

Benov LC, Antonov PA, Ribarov SR (1994) Oxidative damage of the membrane lipids after electroporation. Gen Physiol Biophys 13:85–97

Bianchi G, Campanacci L, Ronchetti M, Donati D (2016) Electrochemotherapy in the Treatment of Bone Metastases: A Phase II Trial. World J Surg 40:3088–3094 . doi: 10.1007/s00268-016-3627-6

Blahovec J, Vorobiev E, Lebovka N (2017) Pulsed Electric Fields Pretreatments for the Cooking of Foods. Food Eng Rev 9:226–236 . doi: 10.1007/s12393-017-9170-x

Blumrosen G, Abazari A, Golberg A, Yarmush ML, Toner M (2016) Single-step electrical field strength screening to determine electroporation induced transmembrane transport parameters. Biochim Biophys Acta 1858:2041–2049 . doi: 10.1016/j.bbamem.2016.05.022

Böckmann RA, de Groot BL, Kakorin S, Neumann E, Grubmüller H (2008) Kinetics, statistics, and energetics of lipid membrane electroporation studied by molecular dynamics simulations. Biophys J 95:1837–1850 . doi: 10.1529/biophysj.108.129437

Boinagrov D, Loudin J, Palanker D (2010) Strength-Duration Relationship for Extracellular Neural Stimulation: Numerical and Analytical Models. J Neurophysiol 104:2236–2248 . doi: 10.1152/jn.00343.2010

Boucher Y, Baxter LT, Jain RK (1990) Interstitial pressure gradients in tissue-isolated and subcutaneous tumors: implications for therapy. Cancer Res 50:4478–4484

Boyd B, Becker S (2015) Modeling of In Vivo Tissue Electroporation and Cellular Uptake Enhancement. IFAC-Pap 48:255–260 . doi: 10.1016/j.ifacol.2015.10.148

Breton M, Delemotte L, Silve A, Mir LM, Tarek M (2012) Transport of siRNA through Lipid Membranes Driven by Nanosecond Electric Pulses: An Experimental and Computational Study. J Am Chem Soc 134:13938–13941 . doi: 10.1021/ja3052365

Bulysheva AA, Hargrave B, Burcus N, Lundberg CG, Murray L, Heller R (2016) Vascular endothelial growth factor-A gene electrotransfer promotes angiogenesis in a porcine model of cardiac ischemia. Gene Ther 23:649–656 . doi: 10.1038/gt.2016.35

Cadossi R, Ronchetti M, Cadossi M (2014) Locally enhanced chemotherapy by electroporation: clinical experiences and perspective of use of electrochemotherapy. Future Oncol Lond Engl 10:877–890 . doi: 10.2217/fon.13.235

Calmels L, Al-Sakere B, Ruaud J-P, Leroy-Willig A, Mir LM (2012) In vivo MRI follow-up of murine tumors treated by electrochemotherapy and other electroporation-based treatments. Technol Cancer Res Treat 11:561–570

Calvet CY, André FM, Mir LM (2014) Dual therapeutic benefit of electroporation-mediated DNA vaccination in vivo: Enhanced gene transfer and adjuvant activity. OncoImmunology 3:e28540 . doi: 10.4161/onci.28540

Campana LG, Mali B, Serša G, Valpione S, Giorgi CA, Strojan P, Miklavčič D, Rossi CR (2014) Electrochemotherapy in non-melanoma head and neck cancers: a retrospective analysis of the treated cases. Br J Oral Maxillofac Surg 52:957–964 . doi: 10.1016/j.bjoms.2014.08.004

Canatella PJ, Black MM, Bonnichsen DM, McKenna C, Prausnitz MR (2004) Tissue electroporation: quantification and analysis of heterogeneous transport in multicellular environments. Biophys J 86:3260–3268 . doi: 10.1016/S0006-3495(04)74374-X

Canatella PJ, Prausnitz MR (2001) Prediction and optimization of gene transfection and drug delivery by electroporation. Gene Ther 8:1464–1469 . doi: 10.1038/sj.gt.3301547

Cannon R, Ellis S, Hayes D, Narayanan G, Martin RCG (2013) Safety and early efficacy of irreversible electroporation for hepatic tumors in proximity to vital structures. J Surg Oncol 107:544–549 . doi: 10.1002/jso.23280

Casciola M, Bonhenry D, Liberti M, Apollonio F, Tarek M (2014) A molecular dynamic study of cholesterol rich lipid membranes: comparison of electroporation protocols. Bioelectrochemistry 100:11–17 . doi: 10.1016/j.bioelechem.2014.03.009

Casciola M, Kasimova MA, Rems L, Zullino S, Apollonio F, Tarek M (2016) Properties of lipid electropores I: Molecular dynamics simulations of stabilized pores by constant charge imbalance. Bioelectrochemistry 109:108–116 . doi: 10.1016/j.bioelechem.2016.01.006

Casciola M, Tarek M (2016) A molecular insight into the electro-transfer of small molecules through electropores driven by electric fields. Biochim Biophys Acta BBA - Biomembr 1858:2278–2289 . doi: 10.1016/j.bbamem.2016.03.022

Casciola M, Xiao S, Pakhomov AG (2017) Damage-free peripheral nerve stimulation by 12-ns pulsed electric field. Sci Rep 7:10453 . doi: 10.1038/s41598-017-10282-5

Čemažar M, Miklavčič D, Mir L., Belehradek J, Bonnay M, Fourcault D, Serša G (2001) Electrochemotherapy of tumours resistant to cisplatin. Eur J Cancer 37:1166–1172 . doi: 10.1016/S0959-8049(01)00091-0

Čemažar M, Miklavčič D, Ščančar J, Dolžan V, Golouh R, Serša G (1999) Increased platinum accumulation in SA-1 tumour cells after in vivo electrochemotherapy with cisplatin. Br J Cancer 79:1386–1391 . doi: 10.1038/sj.bjc.6690222

Čemažar M, Milačič R, Miklavčič D, Dolzan V, Serša G (1998) Intratumoral cisplatin administration in electrochemotherapy: antitumor effectiveness, sequence dependence and platinum content. Anticancer Drugs 9:525–530 . doi: 10.1097/00001813-199807000-00002

Čemažar M, Todorovič V, Ščančar J, Lampreht U, Štimac M, Kamenšek U, Kranjc S, Coer A, Serša G (2015) Adjuvant TNF-α therapy to electrochemotherapy with intravenous cisplatin in murine sarcoma exerts synergistic antitumor effectiveness. Radiol Oncol 49:32–40 . doi: 10.1515/raon-2015-0005

Chalermchat Y, Malangone L, Dejmek P (2010) Electropermeabilization of apple tissue: Effect of cell size, cell size distribution and cell orientation. Biosyst Eng 105:357–366 . doi: 10.1016/j.biosystemseng.2009.12.006

Chen C, Evans JA, Robinson MP, Smye SW, O'Toole P (2010) Electroporation of cells using EM induction of ac fields by a magnetic stimulator. Phys Med Biol 55:1219–1229 . doi: 10.1088/0031-9155/55/4/021

Chen C, Smye SW, Robinson MP, Evans JA (2006a) Membrane electroporation theories: a review. Med Biol Eng Comput 44:5–14 . doi: 10.1007/s11517-005-0020-2

Chen W, Zhongsheng Z, Lee RC (2006b) Supramembrane potential-induced electroconformational changes in sodium channel proteins: a potential mechanism involved in electric injury. Burns J Int Soc Burn Inj 32:52–59 . doi: 10.1016/j.burns.2005.08.008

Chizmadzhev YA, Indenbom AV, Kuzmin PI, Galichenko SV, Weaver JC, Potts RO (1998) Electrical properties of skin at moderate voltages: contribution of appendageal macropores. Biophys J 74:843–856 . doi: 10.1016/S0006-3495(98)74008-1

Čorović S, Mir LM, Miklavčič D (2012) In Vivo Muscle Electroporation Threshold Determination: Realistic Numerical Models and In Vivo Experiments. J Membr Biol 245:509–520 . doi: 10.1007/s00232-012-9432-8

Čorović S, Pavlin M, Miklavčič D (2007) Analytical and numerical quantification and comparison of the local electric field in the tissue for different electrode configurations. Biomed Eng OnLine 6:37

Čorović S, Županič A, Kranjc S, Al Sakere B, Leroy-Willig A, Mir LM, Miklavčič D (2010) The influence of skeletal muscle anisotropy on electroporation: in vivo study and numerical modeling. Med Biol Eng Comput 48:637–648 . doi: 10.1007/s11517-010-0614-1

Cukjati D, Batiuskaite D, André F, Miklavčič D, Mir LM (2007) Real time electroporation control for accurate and safe in vivo non-viral gene therapy. Bioelectrochemistry 70:501–507 . doi: 10.1016/j.bioelechem.2006.11.001

Daud AI, DeConti RC, Andrews S, Urbas P, Riker AI, Sondak VK, Munster PN, Sullivan DM, Ugen KE, Messina JL, Heller R (2008) Phase I trial of interleukin-12 plasmid electroporation in patients with metastatic melanoma. J Clin Oncol 26:5896–5903

Davalos RV, Mir LM, Rubinsky B (2005) Tissue Ablation with Irreversible Electroporation. Ann Biomed Eng 33:223–231 . doi: 10.1007/s10439-005-8981-8

Davalos RV, Otten DM, Mir LM, Rubinsky B (2004) Electrical Impedance Tomography for Imaging Tissue Electroporation. IEEE Trans Biomed Eng 51:761–767 . doi: 10.1109/TBME.2004.824148

Davalos RV, Rubinsky B, Otten DM (2002) A feasibility study for electrical impedance tomography as a means to monitor tissue electroporation for molecular medicine. IEEE Trans Biomed Eng 49:400–403 . doi: 10.1109/10.991168

Dean DA, Ramanathan T, Machado D, Sundararajan R (2008) Electrical impedance spectroscopy study of biological tissues. J Electrost 66:165–177 . doi: 10.1016/j.elstat.2007.11.005

Delemotte L, Tarek M (2012) Molecular dynamics simulations of lipid membrane electroporation. J Membr Biol 245:531–543 . doi: 10.1007/s00232-012-9434-6

Demiryurek Y, Nickaeen M, Zheng M, Yu M, Zahn JD, Shreiber DI, Lin H, Shan JW (2015) Transport, resealing, and re-poration dynamics of two-pulse electroporation-mediated molecular delivery. Biochim Biophys Acta BBA - Biomembr 1848:1706–1714 . doi: 10.1016/j.bbamem.2015.04.007

Denet A-R, Vanbever R, Préat V (2004) Skin electroporation for transdermal and topical delivery. Adv Drug Deliv Rev 56:659–674 . doi: 10.1016/j.addr.2003.10.027

Deodhar A, Dickfeld T, Single GW, Hamilton WC, Thornton RH, Sofocleous CT, Maybody M, Gónen M, Rubinsky B, Solomon SB (2011a) Irreversible electroporation near the heart: ventricular arrhythmias can be prevented with ECG synchronization. AJR Am J Roentgenol 196:W330-335 . doi: 10.2214/AJR.10.4490

Deodhar A, Monette S, Single GW, Hamilton WC, Thornton R, Maybody M, Coleman JA, Solomon SB (2011b) Renal Tissue Ablation With Irreversible Electroporation: Preliminary Results in a Porcine Model. Urology 77:754–760 . doi: 10.1016/j.urology.2010.08.036

Dermol J (2014) Matematično modeliranje permeabilizacije celične membrane in preživetja celic. Magistrsko delo, Fakulteta za elektrotehniko, Univerza v Ljubljani

Dermol J, Miklavčič D (2015) Mathematical Models Describing Chinese Hamster Ovary Cell Death Due to Electroporation In Vitro. J Membr Biol 248:865–881 . doi: 10.1007/s00232-015-9825-6

Dermol J, Miklavčič D (2014) Predicting electroporation of cells in an inhomogeneous electric field based on mathematical modeling and experimental CHO-cell permeabilization to propidium iodide determination. Bioelectrochemistry 100:52–61 . doi: 10.1016/j.bioelechem.2014.03.011

Dermol J, Miklavčič D (2016) Mathematical Models Describing Cell Death Due to Electroporation. In: Miklavčič D (ed) Handbook of Electroporation. Springer International Publishing, Cham, pp 1–20

Dermol J, Pakhomova ON, Pakhomov AG, Miklavčič D (2016) Cell Electrosensitization Exists Only in Certain Electroporation Buffers. PLOS ONE 11:e0159434 . doi: 10.1371/journal.pone.0159434

Dermol-Černe J, Miklavčič D (2018) From Cell to Tissue Properties—Modeling Skin Electroporation With Pore and Local Transport Region Formation. IEEE Trans Biomed Eng 65:458–468 . doi: 10.1109/TBME.2017.2773126

Dermol-Černe J, Miklavčič D, Reberšek M, Mekuč P, Bardet SM, Burke R, Arnaud-Cormos D, Leveque P, O'Connor RP (2018) Plasma membrane depolarization and permeabilization due to electric pulses in cell lines of different excitability. Bioelectrochemistry. 122:103-114 . doi: 10.1016/j.bioelechem.2018.03.011

Dovgan B, Barlič A, Knežević M, Miklavčič D (2017) Cryopreservation of Human Adipose-Derived Stem Cells in Combination with Trehalose and Reversible Electroporation. J Membr Biol. 250:1-9 . doi: 10.1007/s00232-016-9916-z

Dymek K, Dejmek P, Galindo FG (2014) Influence of Pulsed Electric Field Protocols on the Reversible Permeabilization of Rucola Leaves. Food Bioprocess Technol 7:761–773 . doi: 10.1007/s11947-013-1067-y

Dymek K, Rems L, Zorec B, Dejmek P, Galindo FG, Miklavčič D (2015) Modeling electroporation of the non-treated and vacuum impregnated heterogeneous tissue of spinach leaves. Innov Food Sci Emerg Technol 29:55–64 . doi: 10.1016/j.ifset.2014.08.006

Edhemović I, Brecelj E, Gasljevič G, Marolt Mušič M, Gorjup V, Mali B, Jarm T, Kos B, Pavliha D, Grčar Kuzmanov B, Čemažar M, Snoj M, Miklavčič D, Gadžijev EM, Serša G (2014) Intraoperative electrochemotherapy of colorectal liver metastases: Electrochemotherapy of Liver Metastases. J Surg Oncol 110:320–327

Engström PE, Persson BRR, Salford LG (1998) Dynamic gamma camera studies of –bleomycin complex in normal and glioma bearing rats after in vivo electropermeabilization using exponential high-voltage pulses. Bioelectrochem Bioenerg 46:241–248 . doi: 10.1016/S0302-4598(98)00141-X

Esser AT, Smith KC, Gowrishankar TR, Weaver JC (2007) Towards Solid Tumor Treatment by Irreversible Electroporation: Intrinsic Redistribution of Fields and Currents in Tissue. Technol Cancer Res Treat 6:261–273 . doi: 10.1177/153303460700600402

Esser AT, Smith KC, Gowrishankar TR, Weaver JC (2009) Towards solid tumor treatment by nanosecond pulsed electric fields. Technol Cancer Res Treat 8:289–306

Essone Mezeme M, Kranjc M, Bajd F, Serša I, Brosseau C, Miklavčič D (2012a) Assessing how electroporation affects the effective conductivity tensor of biological tissues. Appl Phys Lett 101:213702 . doi: 10.1063/1.4767450

Essone Mezeme M, Pucihar G, Pavlin M, Brosseau C, Miklavčič D (2012b) A numerical analysis of multicellular environment for modeling tissue electroporation. Appl Phys Lett 100:143701 . doi: 10.1063/1.3700727

Frandsen SK, Gibot L, Madi M, Gehl J, Rols M-P (2015) Calcium Electroporation: Evidence for Differential Effects in Normal and Malignant Cell Lines, Evaluated in a 3D Spheroid Model. PLOS ONE 10:e0144028 . doi: 10.1371/journal.pone.0144028

Frandsen SK, Krüger MB, Mangalanathan UM, Tramm T, Mahmood F, Novak I, Gehl J (2017) Normal and Malignant Cells Exhibit Differential Responses to Calcium Electroporation. Cancer Res 77:4389–4401 . doi: 10.1158/0008-5472.CAN-16-1611

Frandsen SK, McNeil AK, Novak I, McNeil PL, Gehl J (2016) Difference in Membrane Repair Capacity Between Cancer Cell Lines and a Normal Cell Line. J Membr Biol 249:569–576 . doi: 10.1007/s00232-016-9910-5

Franken NAP, Rodermond HM, Stap J, Haveman J, van Bree C (2006) Clonogenic assay of cells in vitro. Nat Protoc 1:2315–2319

Gabriel B, Teissié J (1995) Spatial compartmentation and time resolution of photooxidation of a cell membrane probe in electropermeabilized Chinese hamster ovary cells. Eur J Biochem FEBS 228:710–718

Gabriel C, Gabriel S, Corthout E (1996a) The dielectric properties of biological tissues: I. Literature survey. Phys Med Biol 41:2231–2249

Gabriel S, Lau RW, Gabriel C (1996b) The dielectric properties of biological tissues: II. Measurements in the frequency range 10 Hz to 20 GHz. Phys Med Biol 41:2251–2269

Gabriel S, Lau RW, Gabriel C (1996c) The dielectric properties of biological tissues: III. Parametric models for the dielectric spectrum of tissues. Phys Med Biol 41:2271–2293

Gadsby DC (2009) Ion channels versus ion pumps: the principal difference, in principle. Nat Rev Mol Cell Biol 10:344–352 . doi: 10.1038/nrm2668

Galindo FG, Dymek K (2016) Pulsed Electric Fields in Combination with Vacuum Impregnation for Improving Freezing Tolerance of Vegetables. In: Miklavcic D (ed) Handbook of Electroporation. Springer International Publishing, Cham, pp 1–17

Garcia PA, Davalos RV, Miklavčič D (2014) A Numerical Investigation of the Electric and Thermal Cell Kill Distributions in Electroporation-Based Therapies in Tissue. PLoS ONE 9:e103083 . doi: 10.1371/journal.pone.0103083

Garcia PA, Rossmeisl JH, Neal RE, Ellis TL, Olson JD, Henao-Guerrero N, Robertson J, Davalos RV (2010) Intracranial Nonthermal Irreversible Electroporation: In Vivo Analysis. J Membr Biol 236:127–136 . doi: 10.1007/s00232-010-9284-z

Garcia PA, Rossmeisl JH, Robertson JL, Olson JD, Johnson AJ, Ellis TL, Davalos RV (2012) 7.0-T Magnetic Resonance Imaging Characterization of Acute Blood-Brain-Barrier Disruption Achieved with Intracranial Irreversible Electroporation. PLoS ONE 7:e50482 . doi: 10.1371/journal.pone.0050482

García-Sánchez T, Azan A, Leray I, Rosell-Ferrer J, Bragós R, Mir LlM (2015) Interpulse multifrequency electrical impedance measurements during electroporation of adherent differentiated myotubes. Bioelectrochemistry 105:123–135 . doi: 10.1016/j.bioelechem.2015.05.018

Garner AL, Chen G, Chen N, Sridhara V, Kolb JF, Swanson RJ, Beebe SJ, Joshi RP, Schoenbach KH (2007) Ultrashort electric pulse induced changes in cellular dielectric properties. Biochem Biophys Res Commun 362:139–144 . doi: 10.1016/j.bbrc.2007.07.159

Gasbarrini A, Campos WK, Campanacci L, Boriani S (2015) Electrochemotherapy to Metastatic Spinal Melanoma: A Novel Treatment of Spinal Metastasis? SPINE 40:E1340–E1346 . doi: 10.1097/BRS.0000000000001125

Geeraerd AH, Herremans CH, Van Impe JF (2000) Structural model requirements to describe microbial inactivation during a mild heat treatment. Int J Food Microbiol 59:185–209 . doi: 10.1016/S0168-1605(00)00362-7

Ghosh PM, Keese CR, Giaever I (1993) Monitoring electropermeabilization in the plasma membrane of adherent mammalian cells. Biophys J 64:1602–1609 . doi: 10.1016/S0006-3495(93)81531-5

Gianulis EC, Casciola M, Xiao S, Pakhomova ON, Pakhomov AG (2018) Electropermeabilization by uni- or bipolar nanosecond electric pulses: The impact of extracellular conductivity. Bioelectrochemistry 119:10–19 . doi: 10.1016/j.bioelechem.2017.08.005

Gibot L, Wasungu L, Teissié J, Rols M-P (2013) Antitumor drug delivery in multicellular spheroids by electropermeabilization. J Controlled Release 167:138–147 . doi: 10.1016/j.jconrel.2013.01.021

Gielis J (2003) A generic geometric transformation that unifies a wide range of natural and abstract shapes. Am J Bot 90:333–338 . doi: 10.3732/ajb.90.3.333

Golberg A, Bruinsma BG, Uygun BE, Yarmush ML (2015) Tissue heterogeneity in structure and conductivity contribute to cell survival during irreversible electroporation ablation by "electric field sinks." Sci Rep 5:8485 . doi: 10.1038/srep08485

Golberg A, Rubinsky B (2012) Towards Electroporation Based Treatment Planning Considering Electric Field Induced Muscle Contractions. Technol Cancer Res Treat 11:189–201 . doi: 10.7785/tcrt.2012.500249

Golberg A, Rubinsky B (2010) A statistical model for multidimensional irreversible electroporation cell death in tissue. Biomed Eng OnLine 9:13 . doi: 10.1186/1475-925X-9-13

Golberg A, Sack M, Teissie J, Pataro G, Pliquett U, Saulis G, Stefan T, Miklavcic D, Vorobiev E, Frey W (2016) Energy-efficient biomass processing with pulsed electric fields for bioeconomy and sustainable development. Biotechnol Biofuels 9: . doi: 10.1186/s13068-016-0508-z

Golzio M, Teissié J, Rols MP (2002) Direct visualization at the single-cell level of electrically mediated gene delivery. Proc Natl Acad Sci 99:1292–1297 . doi: 10.1073/pnas.022646499

Gothelf A, Gehl J (2012) What you always needed to know about electroporation based DNA vaccines. Hum Vaccines Immunother 8:1694–1702 . doi: 10.4161/hv.22062

Gowrishankar TR, Herndon TO, Vaughan TE, Weaver JC (1999a) Spatially constrained localized transport regions due to skin electroporation. J Controlled Release 60:101–110 . doi: 10.1016/S0168-3659(99)00064-4

References

Gowrishankar TR, Pliquett U, Weaver JC (1999b) Changes in skin structure and electrical properties following high voltage exposure. Ann N Y Acad Sci 888:183–194

Gowrishankar TR, Weaver JC (2003) An approach to electrical modeling of single and multiple cells. Proc Natl Acad Sci 100:3203–3208 . doi: 10.1073/pnas.0636434100

Gowrishankar TR, Weaver JC (2006) Electrical behavior and pore accumulation in a multicellular model for conventional and supra-electroporation. Biochem Biophys Res Commun 349:643–653 . doi: 10.1016/j.bbrc.2006.08.097

Grafström G, Engström P, Salford LG, Persson BRR (2006) 99mTc-DTPA uptake and electrical impedance measurements in verification of in vivo electropermeabilization efficiency in rat muscle. Cancer Biother Radiopharm 21:623–635 . doi: 10.1089/cbr.2006.21.623

Granot Y, Rubinsky B (2007) Methods of optimization of electrical impedance tomography for imaging tissue electroporation. Physiol Meas 28:1135–1147 . doi: 10.1088/0967-3334/28/10/001

Granot Y, Rubinsky B (2008) Mass transfer model for drug delivery in tissue cells with reversible electroporation. Int J Heat Mass Transf 51:5610–5616 . doi: 10.1016/j.ijheatmasstransfer.2008.04.041

Griese T, Kakorin S, Neumann E (2002) Conductometric and electrooptic relaxation spectrometry of lipid vesicle electroporation at high fields. Phys Chem Chem Phys 4:1217–1227 . doi: 10.1039/b108193b

Grimnes S, Martinsen ØG (2008) Bioimpedance and bioelectricity basics, 2nd ed. Academic Press, London

Haberl S, Jarc M, Štrancar A, Peterka M, Hodžić D, Miklavčič D (2013a) Comparison of Alkaline Lysis with Electroextraction and Optimization of Electric Pulses to Extract Plasmid DNA from Escherichia coli. J Membr Biol. doi: 10.1007/s00232-013-9580-5

Haberl S, Miklavčič D, Serša G, Frey W, Rubinsky B (2013b) Cell membrane electroporation – Part 2: The applications. Electr Insul Mag IEEE 29:29–37

Hall SK, Ooi EH, Payne SJ (2014) A mathematical framework for minimally invasive tumor ablation therapies. Crit Rev Biomed Eng 42:383–417

Hargrave B, Downey H, Strange R, Murray L, Cinnamond C, Lundberg C, Israel A, Chen Y-J, Marshall W, Heller R (2013) Electroporation-mediated gene transfer directly to the swine heart. Gene Ther 20:151–157 . doi: 10.1038/gt.2012.15

Hargrave B, Strange R, Navare S, Stratton M, Burcus N, Murray L, Lundberg C, Bulysheva A, Li F, Heller R (2014) Gene Electro Transfer of Plasmid Encoding Vascular Endothelial Growth Factor for Enhanced Expression and Perfusion in the Ischemic Swine Heart. PLoS ONE 9:e115235 . doi: 10.1371/journal.pone.0115235

Heller R, Heller LC (2015) Gene Electrotransfer Clinical Trials. In: Advances in Genetics. Elsevier, pp 235–262

Hibino M, Shigemori M, Itoh H, Nagayama K, Kinosita K (1991) Membrane conductance of an electroporated cell analyzed by submicrosecond imaging of transmembrane potential. Biophys J 59:209–220 . doi: 10.1016/S0006-3495(91)82212-3

Huang K, Tian H, Gai L, Wang J (2012) A review of kinetic models for inactivating microorganisms and enzymes by pulsed electric field processing. J Food Eng 111:191–207 . doi: 10.1016/j.jfoodeng.2012.02.007

Huclova S, Baumann D, Talary MS, Fröhlich J (2011) Sensitivity and specificity analysis of fringing-field dielectric spectroscopy applied to a multi-layer system modelling the human skin. Phys Med Biol 56:7777–7793 . doi: 10.1088/0031-9155/56/24/007

Huclova S, Erni D, Fröhlich J (2010) Modelling effective dielectric properties of materials containing diverse types of biological cells. J Phys Appl Phys 43:365405 . doi: 10.1088/0022-3727/43/36/365405

Huclova S, Erni D, Fröhlich J (2012) Modelling and validation of dielectric properties of human skin in the MHz region focusing on skin layer morphology and material composition. J Phys Appl Phys 45:025301 . doi: 10.1088/0022-3727/45/2/025301

Hudej R, Miklavčič D, Čemažar M, Todorovič V, Serša G, Bergamo A, Sava G, Martinčič A, Ščančar J, Keppler BK, Turel I (2014) Modulation of Activity of Known Cytotoxic Ruthenium(III) Compound (KP418) with Hampered Transmembrane Transport in Electrochemotherapy In Vitro and In Vivo. J Membr Biol 247:1239–1251 . doi: 10.1007/s00232-014-9696-2

Hülsheger H, Niemann EG (1980) Lethal effects of high-voltage pulses on E. coli K12. Radiat Environ Biophys 18:281–288

Hülsheger H, Potel J, Niemann EG (1981) Killing of bacteria with electric pulses of high field strength. Radiat Environ Biophys 20:53–65

Ivorra A, Al-Sakere B, Rubinsky B, Mir LM (2009) In vivo electrical conductivity measurements during and after tumor electroporation: conductivity changes reflect the treatment outcome. Phys Med Biol 54:5949–5963 . doi: 10.1088/0031-9155/54/19/019

Ivorra A, Rubinsky B (2007) In vivo electrical impedance measurements during and after electroporation of rat liver. Bioelectrochemistry 70:287–295 . doi: 10.1016/j.bioelechem.2006.10.005

Jain RK (1999) Transport of Molecules, Particles, and Cells in Solid Tumors. Annu Rev Biomed Eng 1:241–263 . doi: 10.1146/annurev.bioeng.1.1.241

Jang SH, Wientjes MG, Lu D, Au JLS (2003) Drug delivery and transport to solid tumors. Pharm Res 20:1337–1350

Jiang C, Davalos RV, Bischof JC (2015a) A Review of Basic to Clinical Studies of Irreversible Electroporation Therapy. IEEE Trans Biomed Eng 62:4–20 . doi: 10.1109/TBME.2014.2367543

Jiang C, Qin Z, Bischof J (2014) Membrane-Targeting Approaches for Enhanced Cancer Cell Destruction with Irreversible Electroporation. Ann Biomed Eng 42:193–204 . doi: 10.1007/s10439-013-0882-7

Jiang C, Shao Q, Bischof J (2015b) Pulse Timing During Irreversible Electroporation Achieves Enhanced Destruction in a Hindlimb Model of Cancer. Ann Biomed Eng 43:887–895 . doi: 10.1007/s10439-014-1133-2

Jiang N, Cooper BY (2011) Frequency-dependent interaction of ultrashort E-fields with nociceptor membranes and proteins. Bioelectromagnetics 32:148–163 . doi: 10.1002/bem.20620

José A, Sobrevals L, Ivorra A, Fillat C (2012) Irreversible electroporation shows efficacy against pancreatic carcinoma without systemic toxicity in mouse models. Cancer Lett 317:16–23 . doi: 10.1016/j.canlet.2011.11.004

Joshi RP, Mishra A, Schoenbach KH (2008) Model Assessment of Cell Membrane Breakdown in Clusters and Tissues Under High-Intensity Electric Pulsing. IEEE Trans Plasma Sci 36:1680–1688 . doi: 10.1109/TPS.2008.917307

Kandušer M, Šentjurc M, Miklavčič D (2006) Cell membrane fluidity related to electroporation and resealing. Eur Biophys J 35:196–204 . doi: 10.1007/s00249-005-0021-y

Kardos TJ, Rabussay DP (2012) Contactless magneto-permeabilization for intracellular plasmid DNA delivery in-vivo. Hum Vaccines Immunother 8:1707–1713 . doi: 10.4161/hv.21576

Kennedy SM, Ji Z, Hedstrom JC, Booske JH, Hagness SC (2008) Quantification of electroporative uptake kinetics and electric field heterogeneity effects in cells. Biophys J 94:5018–5027 . doi: 10.1529/biophysj.106.103218

Kinosita K, Tsong TY (1977) Formation and resealing of pores of controlled sizes in human erythrocyte membrane. Nature 268:438–441 . doi: 10.1038/268438a0

Kirsch SA, Böckmann RA (2015) Membrane pore formation in atomistic and coarse-grained simulations. Biochim Biophys Acta BBA - Biomembr. doi: 10.1016/j.bbamem.2015.12.031

Kos B, Županič A, Kotnik T, Snoj M, Serša G, Miklavčič D (2010) Robustness of Treatment Planning for Electrochemotherapy of Deep-Seated Tumors. J Membr Biol 236:147–153

Kotnik T, Frey W, Sack M, Haberl Meglič S, Peterka M, Miklavčič D (2015) Electroporation-based applications in biotechnology. Trends Biotechnol. doi: 10.1016/j.tibtech.2015.06.002

Kotnik T, Kramar P, Pucihar G, Miklavčič D, Tarek M (2012) Cell membrane electroporation- Part 1: The phenomenon. IEEE Electr Insul Mag 28:14–23 . doi: 10.1109/MEI.2012.6268438

Kotnik T, Miklavčič D (2000a) Theoretical evaluation of the distributed power dissipation in biological cells exposed to electric fields. Bioelectromagnetics 21:385–394

Kotnik T, Miklavčič D (2000b) Analytical Description of Transmembrane Voltage Induced by Electric Fields on Spheroidal Cells. Biophys J 79:670–679 . doi: 10.1016/S0006-3495(00)76325-9

Kotnik T, Miklavčič D (2006) Theoretical Evaluation of Voltage Inducement on Internal Membranes of Biological Cells Exposed to Electric Fields. Biophys J 90:480–491 . doi: 10.1529/biophysj.105.070771

Kotnik T, Miklavcic D, Mir LM (2001) Cell membrane electropermeabilization by symmetrical bipolar rectangular pulses. Part II. Reduced electrolytic contamination. Bioelectrochemistry Amst Neth 54:91–95

Kotnik T, Miklavčič D, Slivnik T (1998) Time course of transmembrane voltage induced by time-varying electric fields—a method for theoretical analysis and its application. Bioelectrochem Bioenerg 45:3–16 . doi: 10.1016/S0302-4598(97)00093-7

Kotnik T, Pucihar G, Miklavčič D (2010) Induced transmembrane voltage and its correlation with electroporation-mediated molecular transport. J Membr Biol 236:3–13 . doi: 10.1007/s00232-010-9279-9

Kranjc M, Bajd F, Serša I, Miklavčič D (2014) Magnetic resonance electrical impedance tomography for measuring electrical conductivity during electroporation. Physiol Meas 35:985–996

Kranjc M, Kranjc S, Bajd F, Serša G, Serša I, Miklavčič D (2017) Predicting irreversible electroporation-induced tissue damage by means of magnetic resonance electrical impedance tomography. Sci Rep 7:10323 . doi: 10.1038/s41598-017-10846-5

Kranjc M, Markelc B, Bajd F, Čemažar M, Serša I, Blagus T, Miklavčič D (2015) In Situ Monitoring of Electric Field Distribution in Mouse Tumor during Electroporation. Radiology 274:115–123 . doi: 10.1148/radiol.14140311

Kranjc S, Kranjc M, Ščančar J, Jelenc J, Serša G, Miklavčič D (2016) Electrochemotherapy by pulsed electromagnetic field treatment (PEMF) in mouse melanoma B16F10 in vivo. Radiol Oncol 50:39–48

Laird AK (1964) Dynamics of Tumour Growth. Br J Cancer 18:490–502

Lavee J, Onik G, Mikus P, Rubinsky B (2007) A Novel Nonthermal Energy Source for Surgical Epicardial Atrial Ablation: Irreversible Electroporation. Heart Surg Forum 10:E162–E167 . doi: 10.1532/HSF98.20061202

Leguèbe M, Silve A, Mir LM, Poignard C (2014) Conducting and permeable states of cell membrane submitted to high voltage pulses: Mathematical and numerical studies validated by the experiments. J Theor Biol 360:83–94 . doi: 10.1016/j.jtbi.2014.06.027

Levin M, Stevenson CG (2012) Regulation of Cell Behavior and Tissue Patterning by Bioelectrical Signals: Challenges and Opportunities for Biomedical Engineering. Annu Rev Biomed Eng 14:295–323 . doi: 10.1146/annurev-bioeng-071811-150114

Li J, Lin H (2011) Numerical simulation of molecular uptake via electroporation. Bioelectrochemistry 82:10–21 . doi: 10.1016/j.bioelechem.2011.04.006

Li J, Tan W, Yu M, Lin H (2013) The effect of extracellular conductivity on electroporation-mediated molecular delivery. Biochim Biophys Acta BBA - Biomembr 1828:461–470 . doi: 10.1016/j.bbamem.2012.08.014

Li W, Fan Q, Ji Z, Qiu X, Li Z (2011) The Effects of Irreversible Electroporation (IRE) on Nerves. PLoS ONE 6:e18831 . doi: 10.1371/journal.pone.0018831

Linnert M, Iversen HK, Gehl J (2012) Multiple brain metastases - current management and perspectives for treatment with electrochemotherapy. Radiol Oncol 46: . doi: 10.2478/v10019-012-0042-y

Lyu T, Wang X, Su Z, Shangguan J, Sun C, Figini M, Wang J, Yaghmai V, Larson AC, Zhang Z (2017) Irreversible electroporation in primary and metastatic hepatic malignancies: A review. Medicine (Baltimore) 96:e6386 . doi: 10.1097/MD.0000000000006386

Maccarrone M, Bladergroen MR, Rosato N, Agro AF (1995) Role of Lipid Peroxidation in Electroporation-Induced Cell Permeability. Biochem Biophys Res Commun 209:417–425 . doi: 10.1006/bbrc.1995.1519

Maček Lebar A, Miklavčič D (2001) Cell electropermeabilization to small molecules in vitro: control by pulse parameters. Radiol Oncol 35:193–202

Maček Lebar A, Serša G, Čemažar M, Miklavčič D (1998) Elektroporacija Electroporation. Med Razgledi 339–354

Mahnič-Kalamiza S, Miklavčič D, Vorobiev E (2014a) Dual-porosity model of solute diffusion in biological tissue modified by electroporation. Biochim Biophys Acta BBA - Biomembr 1838:1950–1966 . doi: 10.1016/j.bbamem.2014.03.004

Mahnič-Kalamiza S, Miklavčič D, Vorobiev E (2015) Dual-porosity model of mass transport in electroporated biological tissue: Simulations and experimental work for model validation. Innov Food Sci Emerg Technol 29:41–54 . doi: 10.1016/j.ifset.2014.09.011

Mahnič-Kalamiza S, Poklar Ulrih N, Vorobiev E, Miklavčič D (2017) A comprehensive theoretical study of thermal relations in plant tissue following electroporation. Int J Heat Mass Transf 111:150–162 . doi: 10.1016/j.ijheatmasstransfer.2017.03.119

Mahnič-Kalamiza S, Vorobiev E (2014) Dual-porosity model of liquid extraction by pressing from biological tissue modified by electroporation. J Food Eng 137:76–87 . doi: 10.1016/j.jfoodeng.2014.03.035

Mahnič-Kalamiza S, Vorobiev E, Miklavčič D (2014b) Electroporation in food processing and biorefinery. J Membr Biol 247:1279–1304

Mali B, Gorjup V, Edhemovic I, Brecelj E, Cemazar M, Sersa G, Strazisar B, Miklavcic D, Jarm T (2015) Electrochemotherapy of colorectal liver metastases - an observational study of its effects on the electrocardiogram. Biomed Eng OnLine 14:S5 . doi: 10.1186/1475-925X-14-S3-S5

Mali B, Jarm T, Corovic S, Paulin-Kosir MS, Cemazar M, Sersa G, Miklavcic D (2008) The effect of electroporation pulses on functioning of the heart. Med Biol Eng Comput 46:745–757 . doi: 10.1007/s11517-008-0346-7

Mali B, Jarm T, Snoj M, Serša G, Miklavčič D (2013) Antitumor effectiveness of electrochemo-therapy: A systematic review and meta-analysis. Eur J Surg Oncol 39:4–16

Marty M, Serša G, Garbay JR, Gehl J, Collins CG, Snoj M, Billard V, Geertsen PF, Larkin JO, Miklavčič D, Pavlović I, Paulin-Košir SM, Čemažar M, Morsli N, Soden DM, Rudolf Z, Robert C, O'Sullivan GC, Mir LM (2006) Electrochemotherapy – An easy, highly effective and safe treatment of cutaneous and subcutaneous metastases: Results of ESOPE (European Standard Operating Procedures of Electrochemotherapy) study. Eur J Cancer Suppl 4:3–13 . doi: 10.1016/j.ejcsup.2006.08.002

Meek GA, Elder HY (1977) Analytical and Quantitative Methods in Microscopy. CUP Archive

Meir A, Rubinsky B (2014) Electrical impedance tomographic imaging of a single cell electroporation. Biomed Microdevices 16:427–437 . doi: 10.1007/s10544-014-9845-5

Melvik JE, Pettersen EO, Gordon PB, Seglen PO (1986) Increase in cis-dichlorodiammineplatinum (II) cytotoxicity upon reversible electropermeabilization of the plasma membrane in cultured human NHIK 3025 cells. Eur J Cancer Clin Oncol 22:1523–1530

Mercadal B, Arena CB, Davalos RV, Ivorra A (2017) Avoiding nerve stimulation in irreversible electroporation: a numerical modeling study. Phys Med Biol. doi: 10.1088/1361-6560/aa8c53

Mesojednik S, Pavlin D, Sersa G, Coer A, Kranjc S, Grosel A, Tevz G, Cemazar M (2007) The effect of the histological properties of tumors on transfection efficiency of electrically assisted gene delivery to solid tumors in mice. Gene Ther 14:1261–1269 . doi: 10.1038/sj.gt.3302989

Miklavčič D, Čorović S, Pucihar G, Pavšelj N (2006a) Importance of tumour coverage by sufficiently high local electric field for effective electrochemotherapy. Eur J Cancer Suppl 4:45–51 . doi: 10.1016/j.ejcsup.2006.08.006

Miklavčič D, Davalos RV (2015) Electrochemotherapy (ECT) and irreversible electroporation (IRE) - advanced techniques for treating deep-seated tumors based on electroporation. Biomed Eng OnLine 14:I1 . doi: 10.1186/1475-925X-14-S3-I1

Miklavčič D, Mali B, Kos B, Heller R, Serša G (2014) Electrochemotherapy: from the drawing board into medical practice. Biomed Eng OnLine 13:29 . doi: 10.1186/1475-925X-13-29

Miklavčič D, Pavšelj N, Hart FX (2006b) Electric Properties of Tissues. In: Akay M (ed) Wiley Encyclopedia of Biomedical Engineering. John Wiley & Sons, Inc., Hoboken, NJ, USA

Miklavčič D, Pucihar G, Pavlovec M, Ribarič S, Mali M, Maček-Lebar A, Petkovšek M, Nastran J, Kranjc S, Čemažar M, Serša G (2005) The effect of high frequency electric pulses on muscle contractions and antitumor efficiency in vivo for a potential use in clinical electrochemotherapy. Bioelectrochemistry 65:121–128 . doi: 10.1016/j.bioelechem.2004.07.004

Miklavčič D, Šemrov D, Mekid H, Mir LM (2000) A validated model of in vivo electric field distribution in tissues for electrochemotherapy and for DNA electrotransfer for gene therapy. Biochim Biophys Acta 1523:73–83

Miklavčič D, Serša G, Brecelj E, Gehl J, Soden D, Bianchi G, Ruggieri P, Rossi CR, Campana LG, Jarm T (2012) Electrochemotherapy: technological advancements for efficient electroporation-based

treatment of internal tumors. Med Biol Eng Comput 50:1213–1225 . doi: 10.1007/s11517-012-0991-8

Miklavčič D, Snoj M, Županič A, Kos B, Čemažar M, Kropivnik M, Bračko M, Pečnik T, Gadžijev EM, Serša G (2010) Towards treatment planning and treatment of deep-seated solid tumors by electrochemotherapy. Biomed Eng OnLine 9:10 . doi: 10.1186/1475-925X-9-10

Miklavčič D, Towhidi L (2010) Numerical study of the electroporation pulse shape effect on molecular uptake of biological cells. Radiol Oncol 44: . doi: 10.2478/v10019-010-0002-3

Mir LM (2006) Bases and rationale of the electrochemotherapy. Eur J Cancer Suppl 4:38–44 . doi: 10.1016/j.ejcsup.2006.08.005

Mir LM, Gehl J, Serša G, Collins CG, Garbay J-R, Billard V, Geertsen PF, Rudolf Z, O'Sullivan GC, Marty M (2006) Standard operating procedures of the electrochemotherapy: Instructions for the use of bleomycin or cisplatin administered either systemically or locally and electric pulses delivered by the CliniporatorTM by means of invasive or non-invasive electrodes. Eur J Cancer Suppl 4:14–25

Movahed S, Li D (2012) Electrokinetic transport through the nanopores in cell membrane during electroporation. J Colloid Interface Sci 369:442–452 . doi: 10.1016/j.jcis.2011.12.039

Movahed S, Li D (2013) Electrokinetic transport of nanoparticles to opening of nanopores on cell membrane during electroporation. J Nanoparticle Res 15: . doi: 10.1007/s11051-013-1511-y

Müller KJ, Horbaschek M, Lucas K, Zimmermann U, Sukhorukov VL (2003) Electrotransfection of anchorage-dependent mammalian cells. Exp Cell Res 288:344–353

Muratori C, Pakhomov AG, Heller L, Casciola M, Gianulis E, Grigoryev S, Xiao S, Pakhomova ON (2017) Electrosensitization Increases Antitumor Effectiveness of Nanosecond Pulsed Electric Fields In Vivo. Technol Cancer Res Treat 153303461771239 . doi: 10.1177/1533034617712397

Muratori C, Pakhomov AG, Xiao S, Pakhomova ON (2016) Electrosensitization assists cell ablation by nanosecond pulsed electric field in 3D cultures. Sci Rep 6:23225 . doi: 10.1038/srep23225

Napotnik TB, Miklavčič D (2017) In vitro electroporation detection methods – An overview. Bioelechemistry. doi: 10.1016/j.bioelechem.2017.12.005

Neal RE, Garcia PA, Robertson JL, Davalos RV (2012) Experimental Characterization and Numerical Modeling of Tissue Electrical Conductivity during Pulsed Electric Fields for Irreversible Electroporation Treatment Planning. IEEE Trans Biomed Eng 59:1076–1085

Neal RE, Millar JL, Kavnoudias H, Royce P, Rosenfeldt F, Pham A, Smith R, Davalos RV, Thomson KR (2014) In vivo characterization and numerical simulation of prostate properties for non-thermal irreversible electroporation ablation: Characterized and Simulated Prostate IRE. The Prostate 74:458–468 . doi: 10.1002/pros.22760

Neal RE, Rossmeisl JH, Robertson JL, Arena CB, Davis EM, Singh RN, Stallings J, Davalos RV (2013) Improved local and systemic anti-tumor efficacy for irreversible electroporation in immunocompetent versus immunodeficient mice. PloS One 8:e64559 . doi: 10.1371/journal.pone.0064559

Nene D, Jiang N, Rau KK, Richardson M, Cooper BY (2006) Nociceptor activation and damage by pulsed E-fields. In: Shwaery GT, Blitch JG, Land C (eds). p 621904

Neu JC, Krassowska W (1999) Asymptotic model of electroporation. Phys Rev E 59:3471–3482 . doi: 10.1103/PhysRevE.59.3471

Neu JC, Smith KC, Krassowska W (2003) Electrical energy required to form large conducting pores. Bioelectrochemistry 60:107–114 . doi: 10.1016/S1567-5394(03)00051-3

Neu WK, Neu JC (2009) Theory of Electroporation. In: Efimov IR, Kroll MW, Tchou PJ (eds) Cardiac Bioelectric Therapy. Springer US, Boston, MA, pp 133–161

Neumann E, Toensing K, Kakorin S, Budde P, Frey J (1998) Mechanism of electroporative dye uptake by mouse B cells. Biophys J 74:98–108 . doi: 10.1016/S0006-3495(98)77771-9

Neven K, van Driel V, van Wessel H, van Es R, Doevendans PA, Wittkampf F (2014a) Myocardial Lesion Size After Epicardial Electroporation Catheter Ablation After Subxiphoid Puncture. Circ Arrhythm Electrophysiol 7:728–733 . doi: 10.1161/CIRCEP.114.001659

Neven K, van Driel V, van Wessel H, van Es R, Doevendans PA, Wittkampf F (2014b) Epicardial linear electroporation ablation and lesion size. Heart Rhythm 11:1465–1470 . doi: 10.1016/j.hrthm.2014.04.031

Ning S, Yu N, Brown DM, Kanekal S, Knox SJ (1999) Radiosensitization by intratumoral administration of cisplatin in a sustained-release drug delivery system. Radiother Oncol 50:215–223 . doi: 10.1016/S0167-8140(98)00134-0

Novickij V, Dermol J, Grainys A, Kranjc M, Miklavčič D (2017a) Membrane permeabilization of mammalian cells using bursts of high magnetic field pulses. PeerJ 5:e3267 . doi: 10.7717/peerj.3267

Novickij V, Girkontaite I, Zinkeviciene A, Svediene J, Lastauskiene E, Paskevicius A, Markovskaja S, Novickij J (2017b) Reversible Permeabilization of Cancer Cells by High Submicrosecond Magnetic Field. IEEE Trans Magn 1–1 . doi: 10.1109/TMAG.2017.2719699

Novickij V, Grainys A, Kucinskaite-Kodze I, Zvirbliene A, Novickij J (2015) Magneto-Permeabilization of Viable Cell Membrane Using High Pulsed Magnetic Field. IEEE Trans Magn 51:1–5 . doi: 10.1109/TMAG.2015.2439638

Oblak J, Križaj D, Amon S, Maček-Lebar A, Miklavčič D (2007) Feasibility study for cell electroporation detection and separation by means of dielectrophoresis. Bioelectrochemistry 71:164–171 . doi: 10.1016/j.bioelechem.2007.04.001

Ogihara M, Yamaguchi O (2000) Potentiation of effects of anticancer agents by local electric pulses in murine bladder cancer. Urol Res 28:391–397

Onik G, Mikus P, Rubinsky B (2007) Irreversible electroporation: implications for prostate ablation. Technol Cancer Res Treat 6:295–300

Pakhomov AG, Kolb JF, White JA, Joshi RP, Xiao S, Schoenbach KH (2007) Long-lasting plasma membrane permeabilization in mammalian cells by nanosecond pulsed electric field (nsPEF). Bioelectromagnetics 28:655–663 . doi: 10.1002/bem.20354

Pakhomov AG, Semenov I, Casciola M, Xiao S (2017) Neuronal excitation and permeabilization by 200-ns pulsed electric field: An optical membrane potential study with FluoVolt dye. Biochim Biophys Acta BBA - Biomembr 1859:1273–1281 . doi: 10.1016/j.bbamem.2017.04.016

Pakhomova ON, Gregory BW, Khorokhorina VA, Bowman AM, Xiao S, Pakhomov AG (2011) Electroporation-Induced Electrosensitization. PLoS ONE 6:e17100 . doi: 10.1371/journal.pone.0017100

Pakhomova ON, Gregory BW, Pakhomov AG (2013a) Facilitation of electroporative drug uptake and cell killing by electrosensitization. J Cell Mol Med 17:154–159

Pakhomova ON, Gregory BW, Semenov I, Pakhomov AG (2013b) Two Modes of Cell Death Caused by Exposure to Nanosecond Pulsed Electric Field. PLoS One 8:e70278 . doi: 10.1371/journal.pone.0070278

Pakhomova ON, Khorokhorina VA, Bowman AM, Rodaitė-Riševičienė R, Saulis G, Xiao S, Pakhomov AG (2012) Oxidative effects of nanosecond pulsed electric field exposure in cells and cell-free media. Arch Biochem Biophys 527:55–64 . doi: 10.1016/j.abb.2012.08.004

Pataro G, Barca GMJ, Donsì G, Ferrari G (2015a) On the modeling of electrochemical phenomena at the electrode-solution interface in a PEF treatment chamber: Methodological approach to describe the phenomenon of metal release. J Food Eng 165:34–44 . doi: 10.1016/j.jfoodeng.2015.05.009

Pataro G, Barca GMJ, Donsì G, Ferrari G (2015b) On the modelling of the electrochemical phenomena at the electrode-solution interface of a PEF treatment chamber: Effect of electrical parameters and chemical composition of model liquid food. J Food Eng 165:45–51 . doi: 10.1016/j.jfoodeng.2015.05.010

Pataro G, Barca GMJ, Pereira RN, Vicente AA, Teixeira JA, Ferrari G (2014) Quantification of metal release from stainless steel electrodes during conventional and pulsed ohmic heating. Innov Food Sci Emerg Technol 21:66–73 . doi: 10.1016/j.ifset.2013.11.009

Pavliha D, Kos B, Županič A, Marčan M, Serša G, Miklavčič D (2012) Patient-specific treatment planning of electrochemotherapy: Procedure design and possible pitfalls. Bioelectrochemistry 87:265–273

Pavliha D, Mušič MM, Serša G, Miklavčič D (2013) Electroporation-Based Treatment Planning for Deep-Seated Tumors Based on Automatic Liver Segmentation of MRI Images. PLoS ONE 8:e69068 . doi: 10.1371/journal.pone.0069068

Pavlin M, Kandušer M, Reberšek M, Pucihar G, Hart FX, Magjarevićcacute; R, Miklavčič D (2005) Effect of Cell Electroporation on the Conductivity of a Cell Suspension. Biophys J 88:4378–4390 . doi: 10.1529/biophysj.104.048975

Pavlin M, Kotnik T, Miklavčič D, Kramar P, Maček Lebar A (2008) Chapter Seven Electroporation of Planar Lipid Bilayers and Membranes. In: Advances in Planar Lipid Bilayers and Liposomes. Elsevier, pp 165–226

Pavlin M, Miklavčič D (2008) Theoretical and experimental analysis of conductivity, ion diffusion and molecular transport during cell electroporation — Relation between short-lived and long-lived pores. Bioelectrochemistry 74:38–46 . doi: 10.1016/j.bioelechem.2008.04.016

Pavlin M, Miklavčič D (2009) The Effective Conductivity and the Induced Transmembrane Potential in Dense Cell System Exposed to DC and AC Electric Fields. IEEE Trans Plasma Sci 37:99–106 . doi: 10.1109/TPS.2008.2005292

Pavlin M, Pavšelj N, Miklavčič D (2002) Dependence of induced transmembrane potential on cell density, arrangement, and cell position inside a cell system. IEEE Trans Biomed Eng 49:605–612 . doi: 10.1109/TBME.2002.1001975

Pavšelj N, Miklavčič D (2008a) Numerical Models of Skin Electropermeabilization Taking Into Account Conductivity Changes and the Presence of Local Transport Regions. IEEE Trans Plasma Sci 36:1650–1658 . doi: 10.1109/TPS.2008.928715

Pavšelj N, Miklavčič D (2008b) Numerical modeling in electroporation-based biomedical applications. Radiol Oncol 42:159–168

Pavšelj N, Préat V, Miklavčič D (2007) A Numerical Model of Skin Electropermeabilization Based on In Vivo Experiments. Ann Biomed Eng 35:2138–2144 . doi: 10.1007/s10439-007-9378-7

Peleg M (1995) A model of microbial survival after exposure to pulsed electric fields. J Sci Food Agric 67:93–99

Peleg M (2006) Advanced quantitative microbiology for foods and biosystems: models for predicting growth and inactivation. Taylor & Francis, Boca Raton

Peleg M, Penchina CM (2000) Modeling Microbial Survival during Exposure to a Lethal Agent with Varying Intensity. Crit Rev Food Sci Nutr 40:159–172 . doi: 10.1080/10408690091189301

Pethig R (1984) Dielectric Properties of Biological Materials: Biophysical and Medical Applications. IEEE Trans Electr Insul EI-19:453–474 . doi: 10.1109/TEI.1984.298769

Pethig R, Kell DB (1987) The passive electrical properties of biological systems: their significance in physiology, biophysics and biotechnology. Phys Med Biol 32:933–970

Pliquett F, Wunderlich S (1983) Relationship between cell parameters and pulse deformation due to these cells as well as its change after electrically induced membrane breakdown. Bioelectrochem Bioenerg 10:467–475 . doi: 10.1016/0302-4598(83)80073-7

Pliquett U, Langer R, Weaver JC (1995) Changes in the passive electrical properties of human stratum corneum due to electroporation. Biochim Biophys Acta BBA - Biomembr 1239:111–121 . doi: 10.1016/0005-2736(95)00139-T

Pliquett UF, Vanbever R, Preat V, Weaver JC (1998) Local transport regions (LTRs) in human stratum corneum due to long and short `high voltage' pulses. Bioelectrochem Bioenerg 47:151–161 . doi: 10.1016/S0302-4598(98)00180-9

Pliquett UF, Zewert TE, Chen T, Langer R, Weaver JC (1996) Imaging of fluorescent molecule and small ion transport through human stratum corneum during high voltage pulsing: localized transport regions are involved. Biophys Chem 58:185–204 . doi: 10.1016/0301-4622(95)00098-4

Prausnitz MR, Gimm JA, Guy RH, Langer R, Weaver JC, Cullander C (1996) Imaging Regions of Transport Across Human Stratum Corneum during High-Voltage and Low-Voltage Exposures. J Pharm Sci 85:1363–1370 . doi: 10.1021/js960020s

Puc M, Kotnik T, Mir LM, Miklavčič D (2003) Quantitative model of small molecules uptake after in vitro cell electropermeabilization. Bioelectrochemistry 60:1–10

Pucihar G, Kotnik T, Miklavčič D, Teissié J (2008) Kinetics of Transmembrane Transport of Small Molecules into Electropermeabilized Cells. Biophys J 95:2837–2848 . doi: 10.1529/biophysj.108.135541

Pucihar G, Kotnik T, Teissié J, Miklavčič D (2007) Electropermeabilization of dense cell suspensions. Eur Biophys J 36:172–185

Pucihar G, Kotnik T, Valič B, Miklavčič D (2006) Numerical determination of transmembrane voltage induced on irregularly shaped cells. Ann Biomed Eng 34:642–652 . doi: 10.1007/s10439-005-9076-2

Pucihar G, Krmelj J, Reberšek M, Napotnik T, Miklavčič D (2011) Equivalent Pulse Parameters for Electroporation. IEEE Trans Biomed Eng 58:3279–3288 . doi: 10.1109/TBME.2011.2167232

Pucihar G, Miklavčič D (2009) The influence of intracellular connections on the electric field induced membrane voltage and electroporation of cells in clusters. In: Dössel O, Schlegel WC (eds) World Congress on Medical Physics and Biomedical Engineering, September 7 - 12, 2009, Munich, Germany. Springer Berlin Heidelberg, Berlin, Heidelberg, pp 74–77

Puértolas E, López N, Condón S, Álvarez I, Raso J (2010) Potential applications of PEF to improve red wine quality. Trends Food Sci Technol 21:247–255 . doi: 10.1016/j.tifs.2010.02.002

Pušenjak J, Miklavčič D (2000) Modeling of interstitial fluid pressure in solid tumor. Simul Pract Theory 8:17–24

Ramos A (2005) Effect of the electroporation in the field calculation in biological tissues. Artif Organs 29:510–513 . doi: 10.1111/j.1525-1594.2005.29085.x

Ramos A (2010) Improved numerical approach for electrical modeling of biological cell clusters. Med Biol Eng Comput 48:311–319 . doi: 10.1007/s11517-010-0591-4

Ramos A, Raizer A, Marques JLB (2003) A new computational approach for electrical analysis of biological tissues. Bioelectrochemistry 59:73–84 . doi: 10.1016/S1567-5394(03)00004-5

Ramos C, Teissié J (2000) Electrofusion: A biophysical modification of cell membrane and a mechanism in exocytosis. Biochimie 82:511–518 . doi: 10.1016/S0300-9084(00)00200-5

Reigada R (2014) Electroporation of heterogeneous lipid membranes. Biochim Biophys Acta BBA - Biomembr 1838:814–821 . doi: 10.1016/j.bbamem.2013.10.008

Rems L, Miklavčič D (2016) Tutorial: Electroporation of cells in complex materials and tissue. J Appl Phys 119:201101 . doi: 10.1063/1.4949264

Rems L, Miklavčič D (2014) Različni modeli elektroporacije in transporta molekul prek celične membrane. Elektrotehniški Vestn 81:64–72

Rems L, Tarek M, Casciola M, Miklavčič D (2016) Properties of lipid electropores II: Comparison of continuum-level modeling of pore conductance to molecular dynamics simulations. Bioelectrochemistry 112:112–124 . doi: 10.1016/j.bioelechem.2016.03.005

Rems L, Ušaj M, Kandušer M, Reberšek M, Miklavčič D, Pucihar G (2013) Cell electrofusion using nanosecond electric pulses. Sci Rep 3: . doi: 10.1038/srep03382

Rols MP, Femenia P, Teissie J (1995) Long-Lived Macropinocytosis Takes Place in Electropermeabilized Mammalian Cells. Biochem Biophys Res Commun 208:26–35 . doi: 10.1006/bbrc.1995.1300

Roodenburg B, Morren J, Berg HE (Iekje), de Haan SWH (2005) Metal release in a stainless steel Pulsed Electric Field (PEF) system. Innov Food Sci Emerg Technol 6:327–336 . doi: 10.1016/j.ifset.2005.04.006

Rosazza C, Haberl Meglič S, Zumbusch A, Rols M-P, Miklavčič D (2016) Gene Electrotransfer: A Mechanistic Perspective. Curr Gene Ther 16:98–129 . doi: 10.2174/1566523216666160331130040

Rossmeisl JH, Garcia PA, Pancotto TE, Robertson JL, Henao-Guerrero N, Neal RE, Ellis TL, Davalos RV (2015) Safety and feasibility of the NanoKnife system for irreversible electroporation ablative treatment of canine spontaneous intracranial gliomas. J Neurosurg 123:1008–1025 . doi: 10.3171/2014.12.JNS141768

Rubinsky B, Onik G, Mikus P (2007) Irreversible Electroporation: a New Ablation Modality - Clinical Implications. Technol Cancer Res Treat 6:37–48

Sack M, Sigler J, Frenzel S, Eing C, Arnold J, Michelberger T, Frey W, Attmann F, Stukenbrock L, Müller G (2010) Research on Industrial-Scale Electroporation Devices Fostering the Extraction of Substances from Biological Tissue. Food Eng Rev 2:147–156 . doi: 10.1007/s12393-010-9017-1

Sadik MM, Li J, Shan JW, Shreiber DI, Lin H (2013) Quantification of propidium iodide delivery using millisecond electric pulses: experiments. Biochim Biophys Acta 1828:1322–1328 . doi: 10.1016/j.bbamem.2013.01.002

Sadik MM, Yu M, Zheng M, Zahn JD, Shan JW, Shreiber DI, Lin H (2014) Scaling Relationship and Optimization of Double-Pulse Electroporation. Biophys J 106:801–812 . doi: 10.1016/j.bpj.2013.12.045

Salford LG, Persson BRR, Brun A, Ceberg CP, Kongstad PC, Mir LM (1993) A New Brain Tumor Therapy Combining Bleomycin with in Vivo Electropermeabilization. Biochem Biophys Res Commun 194:938–943 . doi: 10.1006/bbrc.1993.1911

Salimi E, Thomson DJ, Bridges GE (2013) Membrane dielectric dispersion in nanosecond pulsed electroporation of biological cells. IEEE Trans Dielectr Electr Insul 20:1256–1265 . doi: 10.1109/TDEI.2013.6571442

Sancho-Martínez SM, Prieto-García L, Prieto M, López-Novoa JM, López-Hernández FJ (2012) Subcellular targets of cisplatin cytotoxicity: An integrated view. Pharmacol Ther 136:35–55 . doi: 10.1016/j.pharmthera.2012.07.003

Sano MB, Arena CB, Bittleman KR, DeWitt MR, Cho HJ, Szot CS, Saur D, Cissell JM, Robertson J, Lee YW, Davalos RV (2015) Bursts of Bipolar Microsecond Pulses Inhibit Tumor Growth. Sci Rep 5:14999 . doi: 10.1038/srep14999

Sano MB, Neal RE, Garcia PA, Gerber D, Robertson J, Davalos RV (2010) Towards the creation of decellularized organ constructs using irreversible electroporation and active mechanical perfusion. Biomed Eng OnLine 9:83 . doi: 10.1186/1475-925X-9-83

Santamaria F, Bower JM (2009) Hodgkin–Huxley Models. In: Encyclopedia of Neuroscience. Elsevier, pp 1173–1180

Saulis G, Venslauskas MS, Naktinis J (1991) Kinetics of pore resealing in cell membranes after electroporation. J Electroanal Chem Interfacial Electrochem 321:1–13 . doi: 10.1016/0022-0728(91)85564-6

Scheffer HJ, Nielsen K, de Jong MC, van Tilborg AA, Vieveen JM, Bouwman AR, Meijer S, van Kuijk C, van den Tol PM, Meijerink MR (2014a) Irreversible Electroporation for Nonthermal Tumor Ablation in the Clinical Setting: A Systematic Review of Safety and Efficacy. J Vasc Interv Radiol 25:997–1011 . doi: 10.1016/j.jvir.2014.01.028

Scheffer HJ, Nielsen K, van Tilborg A a. JM, Vieveen JM, Bouwman RA, Kazemier G, Niessen HWM, Meijer S, van Kuijk C, van den Tol MP, Meijerink MR (2014b) Ablation of colorectal liver metastases by irreversible electroporation: results of the COLDFIRE-I ablate-and-resect study. Eur Radiol 24:2467–2475 . doi: 10.1007/s00330-014-3259-x

Schmeer M, Seipp T, Pliquett U, Kakorin S, Neumann E (2004) Mechanism for the conductivity changes caused by membrane electroporation of CHO cell-pellets. Phys Chem Chem Phys 6:5564 . doi: 10.1039/b411037d

Schoellnast H, Monette S, Ezell PC, Deodhar A, Maybody M, Erinjeri JP, Stubblefield MD, Single GW, Hamilton WC, Solomon SB (2011) Acute and subacute effects of irreversible electroporation on nerves: experimental study in a pig model. Radiology 260:421–427 . doi: 10.1148/radiol.11103505

Schoenbach K, Joshi R, Beebe S, Baum C (2009) A scaling law for membrane permeabilization with nanopulses. IEEE Trans Dielectr Electr Insul 16:1224–1235 . doi: 10.1109/TDEI.2009.5293932

Šel D, Cukjati D, Batiuskaite D, Slivnik T, Mir LM, Miklavčič D (2005) Sequential Finite Element Model of Tissue Electropermeabilization. IEEE Trans Biomed Eng 52:816–827 . doi: 10.1109/TBME.2005.845212

Šel D, Mazères S, Teissié J, Miklavčič D (2003) Finite-element modeling of needle electrodes in tissue from the perspective of frequent model computation. IEEE Trans Biomed Eng 50:1221–1232 . doi: 10.1109/TBME.2003.818466

Serša G, Jarm T, Kotnik T, Coer A, Podkrajsek M, Šentjurc M, Miklavčič D, Kadivec M, Kranjc S, Secerov A, Čemažar M (2008) Vascular disrupting action of electroporation and electrochemotherapy with bleomycin in murine sarcoma. Br J Cancer 98:388–398 . doi: 10.1038/sj.bjc.6604168

Serša G, Kranjc S, Ščančar J, Kržan M, Čemažar M (2010) Electrochemotherapy of Mouse Sarcoma Tumors Using Electric Pulse Trains with Repetition Frequencies of 1 Hz and 5 kHz. J Membr Biol 236:155–162 . doi: 10.1007/s00232-010-9268-z

Serša G, Miklavčič D, Čemažar M, Belehradek J, Jarm T, Mir LM (1997) Electrochemotherapy with CDDP on LPB sarcoma: comparison of the anti-tumor effectiveness in immunocompetent and immunodeficient mice. Bioelectrochem Bioenerg 43:270–283

Serša G, Teissié J, Čemažar M, Signori E, Kamenšek U, Marshall G, Miklavčič D (2015) Electrochemotherapy of tumors as in situ vaccination boosted by immunogene electrotransfer. Cancer Immunol Immunother 64:1315–1327 . doi: 10.1007/s00262-015-1724-2

Sharabi S, Kos B, Last D, Guez D, Daniels D, Harnof S, Mardor Y, Miklavčič D (2016) A statistical model describing combined irreversible electroporation and electroporation-induced blood-brain barrier disruption. Radiol Oncol 50:28–38

Shirakashi R, Köstner CM, Müller KJ, Kürschner M, Zimmermann U, Sukhorukov VL (2002) Intracellular Delivery of Trehalose into Mammalian Cells by Electropermeabilization. J Membr Biol 189:45–54 . doi: 10.1007/s00232-002-1003-y

Shirakashi R, Sukhorukov VL, Tanasawa I, Zimmermann U (2004) Measurement of the permeability and resealing time constant of the electroporated mammalian cell membranes. Int J Heat Mass Transf 47:4517–4524 . doi: 10.1016/j.ijheatmasstransfer.2004.04.007

Smith KC, Neu JC, Krassowska W (2004) Model of Creation and Evolution of Stable Electropores for DNA Delivery. Biophys J 86:2813–2826 . doi: 10.1016/S0006-3495(04)74334-9

Smith KC, Son RS, Gowrishankar TR, Weaver JC (2014) Emergence of a large pore subpopulation during electroporating pulses. Bioelectrochemistry 100:3–10 . doi: 10.1016/j.bioelechem.2013.10.009

Smith KC, Weaver JC (2011) Transmembrane molecular transport during versus after extremely large, nanosecond electric pulses. Biochem Biophys Res Commun 412:8–12 . doi: 10.1016/j.bbrc.2011.06.171

Stewart Jr. DA, Gowrishankar TR, Smith KC, Weaver JC (2005) Cylindrical Cell Membranes in Uniform Applied Electric Fields: Validation of a Transport Lattice Method. IEEE Trans Biomed Eng 52:1643–1653 . doi: 10.1109/TBME.2005.856030

Stolwijk JA, Hartmann C, Balani P, Albermann S, Keese CR, Giaever I, Wegener J (2011) Impedance analysis of adherent cells after in situ electroporation: Non-invasive monitoring during intracellular manipulations. Biosens Bioelectron 26:4720–4727 . doi: 10.1016/j.bios.2011.05.033

Susil R, Šemrov D, Miklavčič D (1998) Electric field induced transmembrane potential depends on cell density and organization. Electro- Magnetobiology 17:391–399

Suzuki DOH, Ramos A, Ribeiro MCM, Cazarolli LH, Silva FRMB, Leite LD, Marques JLB (2011) Theoretical and Experimental Analysis of Electroporated Membrane Conductance in Cell Suspension. IEEE Trans Biomed Eng 58:3310–3318 . doi: 10.1109/TBME.2010.2103074

Sweeney DC, Reberšek M, Dermol J, Rems L, Miklavčič D, Davalos RV (2016) Quantification of cell membrane permeability induced by monopolar and high-frequency bipolar bursts of electrical pulses. Biochim Biophys Acta BBA - Biomembr 1858:2689–2698 . doi: 10.1016/j.bbamem.2016.06.024

Takahashi K, Seki T, Nishikawa K, Minamide S, Iwabuchi M, Ono M, Nagamine S, Horinishi H (1985) Antitumor activity and toxicity of serum protein-bound platinum formed from cisplatin. Jpn J Cancer Res Gann 76:68–74

Tieleman DP (2006) Computer simulations of transport through membranes: passive diffusion, pores, channels and transporters. Clin Exp Pharmacol Physiol 33:893–903 . doi: 10.1111/j.1440-1681.2006.04461.x

Ting F, Tran M, Böhm M, Siriwardana A, Van Leeuwen PJ, Haynes A-M, Delprado W, Shnier R, Stricker PD (2016) Focal irreversible electroporation for prostate cancer: functional outcomes and short-term oncological control. Prostate Cancer Prostatic Dis 19:46–52 . doi: 10.1038/pcan.2015.47

Toepfl S (2012) Pulsed electric field food processing –industrial equipment design and commercial applications. Stewart Postharvest Rev 8:1–7 . doi: 10.2212/spr.2012.2.4

Toepfl S, Siemer C, Saldaña-Navarro G, Heinz V (2014) Overview of Pulsed Electric Fields Processing for Food. In: Emerging Technologies for Food Processing. Elsevier, pp 93–114

Tounekti O, Kenani A, Foray N, Orlowski S, Mir LlM (2001) The ratio of single- to double-strand DNA breaks and their absolute values determine cell death pathway. Br J Cancer 84:1272–1279

Tounekti O, Pron G, Belehradek J, Mir LM (1993) Bleomycin, an apoptosis-mimetic drug that induces two types of cell death depending on the number of molecules internalized. Cancer Res 53:5462–5469

Towhidi L, Firoozabadi S, Mozdarani H, Miklavčič D (2012) Lucifer Yellow uptake by CHO cells exposed to magnetic and electric pulses. Radiol Oncol 46: . doi: 10.2478/v10019-012-0014-2

Towhidi L, Kotnik T, Pucihar G, Firoozabadi SMP, Mozdarani H, Miklavčič D (2008) Variability of the minimal transmembrane voltage resulting in detectable membrane electroporation. Electromagn Biol Med 27:372–385 . doi: 10.1080/15368370802394644

Trainito CI, Français O, Le Pioufle B (2015) Analysis of pulsed electric field effects on cellular tissue with Cole–Cole model: Monitoring permeabilization under inhomogeneous electrical field with bioimpedance parameter variations. Innov Food Sci Emerg Technol 29:193–200 . doi: 10.1016/j.ifset.2015.02.004

Trimble CL, Morrow MP, Kraynyak KA, Shen X, Dallas M, Yan J, Edwards L, Parker RL, Denny L, Giffear M, Brown AS, Marcozzi-Pierce K, Shah D, Slager AM, Sylvester AJ, Khan A, Broderick KE, Juba RJ, Herring TA, Boyer J, Lee J, Sardesai NY, Weiner DB, Bagarazzi ML (2015) Safety, efficacy, and immunogenicity of VGX-3100, a therapeutic synthetic DNA vaccine targeting human papillomavirus 16 and 18 E6 and E7 proteins for cervical intraepithelial neoplasia 2/3: a randomised, double-blind, placebo-controlled phase 2b trial. The Lancet 386:2078–2088 . doi: 10.1016/S0140-6736(15)00239-1

Trontelj K, Reberšek M, Kandušer M, Šerbec VČ, Šprohar M, Miklavčič D (2008) Optimization of bulk cell electrofusion in vitro for production of human–mouse heterohybridoma cells. Bioelectrochemistry 74:124–129 . doi: 10.1016/j.bioelechem.2008.06.003

Tschon M, Salamanna F, Ronchetti M, Cavani F, Gasbarrini A, Boriani S, Fini M (2015) Feasibility of Electroporation in Bone and in the Surrounding Clinically Relevant Structures: A Preclinical Investigation. Technol Cancer Res Treat. doi: 10.1177/1533034615604454

Tsong TY (1991) Electroporation of cell membranes. Biophys J 60:297–306 . doi: 10.1016/S0006-3495(91)82054-9

Ursic K, Kos Š, Kamenšek U, Čemažar M, Ščančar J, Bucek S, Kranjc S, Staresinic B, Serša G (2018) Comparable effectiveness and immunomodulatory actions of oxaliplatin and cisplatin in electrochemotherapy of murine melanoma. Bioelectrochemistry 119:161–171 . doi: 10.1016/j.bioelechem.2017.09.009

Ušaj M, Trontelj K, Miklavčič D, Kandušer M (2010) Cell-cell electrofusion: optimization of electric field amplitude and hypotonic treatment for mouse melanoma (B16-F1) and Chinese Hamster ovary (CHO) cells. J Membr Biol 236:107–116 . doi: 10.1007/s00232-010-9272-3

Valič B, Golzio M, Pavlin M, Schatz A, Faurie C, Gabriel B, Teissié J, Rols MP, Miklavčič D (2003) Effect of electric field induced transmembrane potential on spheroidal cells: theory and experiment. Eur Biophys J 519–528

Vanbever R, Pliquett UF, Préat V, Weaver JC (1999) Comparison of the effects of short, high-voltage and long, medium-voltage pulses on skin electrical and transport properties. J Controlled Release 60:35–47 . doi: 10.1016/S0168-3659(99)00018-8

Vasan S, Hurley A, Schlesinger SJ, Hannaman D, Gardiner DF, Dugin DP, Boente-Carrera M, Vittorino R, Caskey M, Andersen J, Huang Y, Cox JH, Tarragona-Fiol T, Gill DK, Cheeseman H, Clark L, Dally L, Smith C, Schmidt C, Park HH, Kopycinski JT, Gilmour J, Fast P, Bernard R, Ho DD (2011) In Vivo Electroporation Enhances the Immunogenicity of an HIV-1 DNA Vaccine Candidate in Healthy Volunteers. PLoS ONE 6:e19252 . doi: 10.1371/journal.pone.0019252

Wang Y (2006) Effects of rate, volume, and dose of intratumoral infusion on virus dissemination in local gene delivery. Mol Cancer Ther 5:362–366 . doi: 10.1158/1535-7163.MCT-05-0266

Weaver JC (1993) Electroporation: a general phenomenon for manipulating cells and tissues. J Cell Biochem 51:426–435

Weaver JC, Vaughan TE, Chizmadzhev Y (1999) Theory of electrical creation of aqueous pathways across skin transport barriers. Adv Drug Deliv Rev 35:21–39 . doi: 10.1016/S0169-409X(98)00061-1

Wegner LH (2015) The conductance of cellular membranes at supra-physiological voltages. Bioelectrochemistry 103:34–38 . doi: 10.1016/j.bioelechem.2014.08.005

Wegner LH, Frey W, Silve A (2015) Electroporation of DC-3F Cells Is a Dual Process. Biophys J 108:1660–1671 . doi: 10.1016/j.bpj.2015.01.038

Workman P, Aboagye EO, Balkwill F, Balmain A, Bruder G, Chaplin DJ, Double JA, Everitt J, Farningham DAH, Glennie MJ, Kelland LR, Robinson V, Stratford IJ, Tozer GM, Watson S, Wedge SR, Eccles SA (2010) Guidelines for the welfare and use of animals in cancer research. Br J Cancer 102:1555–1577 . doi: 10.1038/sj.bjc.6605642

Yarmush ML, Golberg A, Serša G, Kotnik T, Miklavčič D (2014) Electroporation-Based Technologies for Medicine: Principles, Applications, and Challenges. Annu Rev Biomed Eng 16:295–320 . doi: 10.1146/annurev-bioeng-071813-104622

Yoon J, Leblanc N, Zaklit J, Vernier PT, Chatterjee I, Craviso GL (2016) Enhanced Monitoring of Nanosecond Electric Pulse-Evoked Membrane Conductance Changes in Whole-Cell Patch Clamp Experiments. J Membr Biol 249:633–644 . doi: 10.1007/s00232-016-9902-5

Zaharoff DA, Henshaw JW, Mossop B, Yuan F (2008) Mechanistic Analysis of Electroporation-Induced Cellular Uptake of Macromolecules. Exp Biol Med 233:94–105 . doi: 10.3181/0704-RM-113

Zhuang J, Kolb JF (2015) Time domain dielectric spectroscopy of nanosecond pulsed electric field induced changes in dielectric properties of pig whole blood. Bioelectrochemistry 103:28–33 . doi: 10.1016/j.bioelechem.2014.08.009

Zhuang J, Ren W, Jing Y, Kolb JF (2012) Dielectric evolution of mammalian cell membranes after exposure to pulsed electric fields. IEEE Trans Dielectr Electr Insul 19:609–622 . doi: 10.1109/TDEI.2012.6180256

Zorec B, Becker S, Reberšek M, Miklavčič D, Pavšelj N (2013a) Skin electroporation for transdermal drug delivery: The influence of the order of different square wave electric pulses. Int J Pharm 457:214–223 . doi: 10.1016/j.ijpharm.2013.09.020

Zorec B, Préat V, Miklavčič D, Pavšelj N (2013b) Active enhancement methods for intra- and transdermal drug delivery: a review. Zdr Vestn 82:339–56

Županič A, Kos B, Miklavčič D (2012) Treatment planning of electroporation-based medical interventions: electrochemotherapy, gene electrotransfer and irreversible electroporation. Phys Med Biol 57:5425–5440 . doi: 10.1088/0031-9155/57/17/5425

Županič A, Ribarič S, Miklavčič D (2007) Increasing the repetition frequency of electric pulse delivery reduces unpleasant sensations that occur in electrochemotherapy. Neoplasma 54:246–250